



Laboratory Testing and Technical Assessments of Corrosion-Resistant Alloys for High-Pressure, High-Temperature Subsea Applications

Mechanical Property and Corrosion Performance Testing and Assessments of Nickel Alloys 725, 825, 945X, 955, and C22HS

Energy Systems and Nuclear Engineering Divisions

About Argonne National Laboratory

Argonne is a U.S. Department of Energy laboratory managed by UChicago Argonne, LLC under contract DE-AC02-06CH11357. The Laboratory's main facility is outside Chicago, at 9700 South Cass Avenue, Argonne, Illinois 60439. For information about Argonne and its pioneering science and technology programs, see www.anl.gov.

DOCUMENT AVAILABILITY

Online Access: U.S. Department of Energy (DOE) reports produced after 1991 and a growing number of pre-1991 documents are available free at OSTI.GOV (<http://www.osti.gov/>), a service of the US Dept. of Energy's Office of Scientific and Technical Information.

Reports not in digital format may be purchased by the public from the National Technical Information Service (NTIS):

U.S. Department of Commerce
National Technical Information Service
5301 Shawnee Rd
Alexandria, VA 22312
www.ntis.gov
Phone: (800) 553-NTIS (6847) or (703) 605-6000
Fax: (703) 605-6900
Email: orders@ntis.gov

Reports not in digital format are available to DOE and DOE contractors from the Office of Scientific and Technical Information (OSTI):

U.S. Department of Energy
Office of Scientific and Technical Information
P.O. Box 62
Oak Ridge, TN 37831-0062
www.osti.gov
Phone: (865) 576-8401
Fax: (865) 576-5728
Email: reports@osti.gov

Disclaimer

This report was prepared by Argonne National Laboratory (ANL) under contract to the Department of Energy (DOE) through an interagency agreement between the Department of Interior, Bureau of Safety and Environmental Enforcement (BSEE) and the DOE. The opinions, findings, conclusions, and recommendations expressed in the report are those of the authors and they do not necessarily reflect the views or policies of BSEE.

This report was prepared as an account of work sponsored by an agency of the United States Government. Neither the United States Government nor any agency thereof, nor UChicago Argonne, LLC, nor any of their employees or officers, makes any warranty, express or implied, or assumes any legal liability or responsibility for the accuracy, completeness, or usefulness of any information, apparatus, product, or process disclosed, or represents that its use would not infringe privately owned rights. Reference herein to any specific commercial product, process, or service by trade name, trademark, manufacturer, or otherwise, does not necessarily constitute or imply its endorsement, recommendation, or favoring by the United States Government or any agency thereof. The views and opinions of document authors expressed herein do not necessarily state or reflect those of the United States Government or any agency thereof, Argonne National Laboratory, or UChicago Argonne, LLC.

"THIS INFORMATION IS DISTRIBUTED SOLELY FOR THE PURPOSE OF PRE-DISSEMINATION PEER REVIEW UNDER APPLICABLE INFORMATION QUALITY GUIDELINES. IT HAS NOT BEEN FORMALLY DISSEMINATED BY THE BSEE. IT DOES NOT REPRESENT AND SHOULD NOT BE CONSTRUED TO REPRESENT ANY AGENCY DETERMINATION OR POLICY."

ANL-19/30

Laboratory Testing and Technical Assessments of Corrosion-Resistant Alloys for High-Pressure, High-Temperature Subsea Applications

*Mechanical Property and Corrosion Performance Testing and Assessments
of Nickel Alloys 725, 825, 945X, 955, and C22HS*

prepared by

Roy A. Lindley,¹ Bruce Miglin,² and Meimei Li¹

¹ Energy Systems and Nuclear Engineering Divisions, Argonne National Laboratory

² Adica, LLC

July 31, 2019

"THIS INFORMATION IS DISTRIBUTED SOLELY FOR THE PURPOSE OF PRE-DISSEMINATION PEER REVIEW UNDER APPLICABLE INFORMATION QUALITY GUIDELINES. IT HAS NOT BEEN FORMALLY DISSEMINATED BY THE BSEE. IT DOES NOT REPRESENT AND SHOULD NOT BE CONSTRUED TO REPRESENT ANY AGENCY DETERMINATION OR POLICY."

CONTENTS

LIST OF ACRONYMS AND ABBREVIATION NOTATIONS.....	ix
ACKNOWLEDGEMENTS.....	xi
EXECUTIVE SUMMARY	xiii
1 INTRODUCTION TO HPHT.....	1
1.1 HPHT Defined for Subsea Applications.....	1
1.2 HPHT Material Challenges.....	1
2 ENVIRONMENTAL TEST PROGRAM PURSUED	3
2.1 Modes of Materials Failure.....	3
2.2 Test Conditions	3
2.2.1 Overview and Objective	3
2.2.2 Seawater Environment Conditions	4
2.2.3 Sour Conditions	4
2.2.4 Temperature and Pressure.....	4
2.2.5 Test Durations.....	5
3 CORROSION RESISTANT ALLOYS FOR LABORATORY TESTING	6
3.1 Alloy Selection Rationale	6
3.2 Materials and Material Forms Acquired for Testing	7
4 OVERVIEW OF INDUSTRY LITERATURE ON CHARACTERISTICS OF CRA MATERIALS TESTED	9
4.1 Published Material Density and Melting Points	9
4.2 ASTM Specified Heat Treatments.....	9
4.3 Published Mechanical Properties.....	10
4.4 Published C-Ring Corrosion Test Data.....	13
5 CHEMICAL COMPOSITIONS (SPECIFICATIONS, VENDOR, AND ACTUALS) FOR MATERIALS TESTED.....	14
6 TEST METHODOLOGY AND SUMMARY OF TESTS PERFORMED.....	17
6.1 Test Methodologies.....	17
6.2 Summary of Testing Performed.....	18
7 MEASURED MECHANICAL PROPERTIES FOR TESTED MATERIALS (WESTMORELAND)	20

7.1 Mechanical Property Test Matrix	20
7.2 Mechanical Test Specimens.....	21
7.3 Tensile and Yield Strength Test Results.....	22
7.4 Charpy Results.....	24
7.5 Creep Testing.....	24
8 ENVIRONMENTALLY ASSISTED CRACKING RESULTS SUMMARY	
(DNV-GL).....	26
8.1 Test and Data Matrix	26
8.2 Environmental Crack Growth Rate Specimens	28
8.3 Summary of Environmental Crack Growth Test Results	29
8.4 Sour Production Environment.....	29
8.5 Seawater with Cathodic Protection Environment.....	29
8.6 Seawater Environment.....	31
8.7 Post-test Microscopy on DNV Samples (Argonne).....	34
8.7.1 Specimen Preparation	34
8.7.2 Precipitation Hardening Alloys (725, 945X, and 955)	35
8.7.3 Work Hardening Alloys (825 and C22HS).....	44
8.7.4 Microscopy Summary.....	47
9 C-Ring and Corrosion Rate Results Summary (HCS).....	49
9.1 Test and Data Matrix	49
9.2 Corrosion and C-Ring Test Specimens.....	50
9.3 Summary of HCS Results	52
9.4 Corrosion Coupon Surface Images (Argonne)	53
9.5 Microscopy Examinations of 945X C-Rings.....	64
9.5.1 Reason for Alloys Specific Examinations	64
9.5.2 Six- and 48-week Chemistry Comparison.....	64
9.5.3 SEM Images and Observations for 6- and 48-Week Exposures.....	65
9.5.4 SEM Results from 12-Week Exposure.....	67
9.5.5 SEM Results from 18-Week Exposure.....	71
9.5.6 Observations from 945X Electron Microscopy.....	77
10 GENERAL DISCUSSION AND INTERPRETATION OF RESULTS	78
10.1 Precipitation Hardening Alloys (725, 945X and 955).....	78
10.2 Work Hardening Alloys (825 and C22HS).....	79
11 CONCLUDING REMARKS.....	81
12 REFERENCES	82
APPENDIX A: Mechanical Property Test Reports	1
A.1 Mechanical Test Reports for Alloy 725.....	1

A.2 Mechanical Test Reports for Alloy 945X.....	7
A.3 Mechanical Test Reports for Alloy 955.....	14
A.4 Mechanical Test Reports for Alloy 825.....	19
A.5 Mechanical Test Reports for Alloy C22HS.....	26
A.6 Tensile Test Reports for All Alloys at 950°F.....	33
A.7 Creep Test Report Mechanical Test Reports for Alloy C22HS.....	36
APPENDIX B: Environmentally Assisted Cracking Data Report (DNV-GL).....	1
APPENDIX C: Corrosion Testing Report (Honeywell Corrosion Solutions).....	1

LIST OF TABLES

1 Notational Relative Cost for Various Types of Materials of Construction.....	2
2 Materials Supply Sources, Forms, and Hardness.....	8
3 Alloy Density and Melting Temperature Ranges in Literature.....	9
4 Recommended Heat Treatments as Appearing in Selected Standard’s Specifications.....	10
5 Mechanical Properties from Selected Specifications (Requirements) and Vendor Literature (Actual Advertised).....	11
6 NACE TMO177 Qualification Test Data for Alloys and High-Strength 718.....	13
7 Chemical Compositions-Specifications and Actuals for CRA Alloys Tested.....	15
8 Test Matrix—Numbers of Tests by Alloy and Summaries of Test Conditions for Mechanical Testing (Westmoreland).....	20
9 Results of Elevated Temperature Load Testing for Each Alloy.....	25
10 Test Data Matrix—Numbers of Datasets Obtained by Alloy and Summaries of Test Conditions for Environmentally Assisted Cracking Testing (DNV-GL).....	26
11 Critical Crevice Corrosion Temperature of Materials Tested in 3.5 wt% NaCl with +700 mV SCE.....	32
12 Etching Condition for Each Alloy.....	34
13 Test Matrix—Numbers of Tests by Alloy and Summaries of Test Conditions for C-Ring and Corrosion Testing (HCS) ^a	50
14 Chemistry Comparison for 6- and 48-Week C-Ring Sample 14149.....	64

LIST OF FIGURES

1 H2S Concentration vs. Pressure Illustrating Sour Conditions in Parts per Million (PPM).....	5
2 Tensile Specimen (ASTM E 8M)	21
3 Charpy Impact Specimen (ASTM E23).....	21
4 Average Tensile and Yield Strength.....	22
5 Average Elongation and Reduction in Area for Tensile Testing.....	23
6 Average Modulus.....	23
7 Average Charpy Energy (Ft-Lb _f) at 32°F and 73°F.....	24
8 Electrochemical Behavior Specimen Form with Crevice Formers.....	28
9 Compact Tension Specimen (ASTM E399)	28
10 Fatigue Crack Growth Rate vs. Loading Frequency in Simulated Seawater with Cathodic Protection.....	30
11 Static Crack Growth Rate of 955 in Simulated Seawater vs. Applied Potentials.....	31
12 CCT vs. PREN Values for Five Alloys	32
13 Cyclic Crack Growth Rate Versus Loading Frequency in Simulated Seawater for Five Alloys.....	33
14 Overview of the Crack Observed in the Tested Alloy 725 Specimen before Etching ...	35
15 Optical Image of the Cracked Alloy 725 Specimen	36
16 SEM Image Showing Grain Boundary Void Formation in Alloy 725	36
17 Optical Image of Alloy 945X Showing the Grain Structure and Cracking Behavior	37
18 SEM Images Revealing Slip Bands (indicated by arrows) Formed within Grains along the Crack in Alloy 945X	37
19 Optical Image Showing the Grain Structure and Cracking Behavior in Alloy 955.....	38
20 SEM Images of Alloy 955 after Etching.....	39

21 (a) TEM HAADF Image Showing Grain Boundary Precipitates; (b)–(f) EDS Elemental Mapping of Mo, Cr, S, Ti, and Nb in the Same Area in Alloy 725.....	40
22 (a) TEM HAADF Image Showing Precipitates at Grain Boundaries and within Grains; (b)–(f) EDS Elemental Mapping of Mo, Cr, S, Ti, and Nb in the Same Area of (a) in Alloy 725.....	40
23 (a) TEM HAADF Image Showing Nano-Sized Precipitates in the Matrix; (b)–(f) EDS Elemental Mapping of Ni, Cr, Ti, Nb, and Al in the Same Area of (a); (g) Bright-Field Image; (h) Dark-Field Image; and (i) Electron Diffraction Pattern Showing the Precipitates in the Matrix in Alloy 725.....	41
24 (a) TEM HAADF Image Showing Nano-Sized Precipitates in the Matrix; (b)–(f) EDS Elemental Mapping of Ni, Cr, Ti, Nb, and Al in the Same Area of (a); (g) Bright-Field Image; (h) Dark-Field Image; and (i) Electron Diffraction Pattern Showing the Precipitates in the Matrix in Alloy 945X.....	42
25 (a) TEM HAADF Image Showing Nano-Sized Precipitates within Grains; (b)–(f) EDS Elemental Mapping of Ni, Cr, Ti, Nb, and Al in the Same Area of (a); (g) Bright-Field Image; (h) Dark-Field Image; and (i) Electron Diffraction Pattern Showing the Precipitates within Grains in Alloy 955.....	43
26 (a) TEM HAADF Image Showing Grain Boundary Precipitates and (b)–(f) EDS Elemental Mapping of Mo, Cr, S, Ti, and Nb in the Same Area of (a) in Alloy 955.....	44
27 Cracks Developed in Alloy 825 During the SCC Test	45
28 SEM Images Showing the Slip Activities (indicated by arrows) along the Crack in Alloy 825.....	45
29 TEM Bright-Field Images Showing (a) the Grain Structure and (b) the Dislocation Density within the Grain in Alloy 825.	46
30 Overview of the Crack Developed During the SCC Test in Alloy C22HS	46
31 SEM Image Showing the Slip Activities (indicated by arrow) along the Crack in Alloy C22HS	47
32 TEM Bright-Field Images Showing the Microstructure of Alloy C22HS (a) Low-Magnification Image and (b) High-magnification Image.....	47
33 Exposure Coupon For Corrosion Rate Determinations	51
34 C-Ring Test Specimen Details.....	51
35 Galvanic C-Ring Test Specimen and Steel Contact Details	52

36	Plot of Average Corrosion Rate Under HPHT Conditions Versus Exposure Time	53
37	Alloy 725 Surface Images at Various Magnifications (Sample 8C).....	54
38	Alloy 945X Surface Images at Various Magnifications (Sample 8C).....	56
39	Alloy 955 Surface Images at Various Magnifications (Sample 8C).....	58
40	Alloy 825 Surface Images at Various Magnifications (Sample 8C).....	60
41	Alloy C22HS Surface Images at Various Magnifications (Sample 8C).....	62
42	SEM Images of 14149.1X (Coupon) from 6-Week Exposure.....	65
43	SEM Images of 14149.1R (C-Ring) from 6-Week Exposure.....	65
44	SEM Images of 14149.7C (Coupon) from 48-Week Exposure.....	66
45	SEM Images with EDS of 14149-7R (Ring) from 48-Week Exposure.....	67
46	SEM Images of the SCC C-Ring 14149.3R from 12-Week Exposure.....	68
47	SEM with EDS of the SCC C-Ring 14149.3R from 12-Week Exposure.....	69
48	Further EDS of the SCC C-Ring 14149.3R from 12-Week Exposure	70
49	SEM Images in Areas without Oxide Scale for 18-Week Exposure SCC C-Ring 14149.5R	72
50	EDS Mappings for Areas without Oxide Scale for 18-Week Exposure SCC C-Ring 14149.5R	73
51	SEM Images for Areas with Oxide Scale for 18-Week Exposure SCC C-Ring 14149.5R	74
52	EDS Mapping for Areas with Oxide Scale For 18-Week Exposure SCC C-Ring 14149.5R	76

LIST OF ACRONYMS AND ABBREVIATION NOTATIONS

API	American Petroleum Institute
ANSI	American National Standards Institute
Argonne	Argonne National Laboratory
ASTM	American Society for Testing and Materials
BS	British Standards
BSEE	Bureau of Safety and Environmental Enforcement, an agency within the U.S. Department of the Interior (DOI)
CCT	critical crevice temperature
CRA	corrosion-resistant alloy steel
DNV-GL	Det Norske Veritas and Germanischer Lloyd
DOE	U.S. Department of Energy
DOI	U.S. Department of the Interior
EAC	environmentally assisted cracking
EDS	energy dispersive (x-ray) spectroscopy
EUL	elongation under load
FFP	fit for purpose
GB	grain boundary
GCHC	galvanically coupled hydrogen cracking
GHSC	galvanic hydrogen stress cracking
HAADF	high-angle annular dark field
HCS	Honeywell Corrosion Solutions
HRC	hardness, Rockwell C scale
HS	???
in.	inch(es)
ISO	International Standards Organization
K	stress intensity
ΔK	change of K
ksi	1,000 pounds per square inch, stress or pressure
LMP	Larson-Miller parameter
m	meter(s)
MPa	megapascal(s)

NACE	National Association of Corrosion Engineers
PH	precipitation hardening
PPM	parts per million
PREN	pitting resistance equivalency number
R	ratio of maximum load to minimum load
SCC	stress corrosion cracking
SCE	saturated calomel electrode
SEM	scanning electron microscopy
SSC	sulfide stress cracking
TEM	transmission electron microscopy
UTS	ultimate tensile strength
YS	yield strength

ACKNOWLEDGEMENTS

The authors thank the Argonne technical editors, Carolyn Steele and Victoria Martin for their helpful suggestions and effort necessary to complete this report on relatively short notice. Andrew Dobosenski, an Argonne summer student intern, helped search literature for available materials properties. In addition, student interns Adam Popper, Nicole Duda, and Moath Sharayah provided assistance in data organization and formatting. Argonne summer interns complete two years of technical or engineering education at the College of DuPage, work at Argonne during the summers, and typically transfer their academic work to a major regional university to continue their technical studies.

Zuotao Zeng and Wei-Ying Chen are Argonne staff members working with Dr. M. Li. Zuotao was instrumental in completing metallography, SEM, and high-magnification surface imaging of corrosion coupons. Wei-Ying was responsible for TEM imaging. This scientific work included exposures and measurements from the Argonne Advanced Photon Source (APS).

Finally, the technical leads Ramgopal Thodla at DNV-GL and Peter Ellis at Honeywell Corrosion Solutions (HCS) and their technical staffs are recognized for their contracted laboratory work that resulted in much of the experimental information in this report. In addition, Argonne appreciates the assistance of Maurice Peltier of Aiken Engineering for coordinating the joint efforts of Westmoreland, the mechanical testing organization, as well as DNV-GL and HCS.

This page intentionally left blank.

EXECUTIVE SUMMARY

This report presents information gained from laboratory testing of mechanical properties, crack growth, corrosion rates and subsequent microscopy examinations of high-strength corrosion-resistant alloys (CRAs) 725, 825, 945X, 955, and C22HS. These high-nickel-content metals may be suitable for subsea equipment service associated with sour environments often encountered in high-pressure (15,000 psia) high-temperature (350°F min) oil and gas wells in the Gulf of Mexico. Each of these alloys were subjected to the same testing procedures for each type of test performed. Three of the alloys, 725, 945X and 955 are precipitation hardening alloys with similarities to 718, an alloy which has been used for some time in sour oil and gas wells. The remaining two, 825 and C22HS, are work hardening alloys. Together, the five alloys offer a range of possibilities in terms of product forms, availability, relative cost, technical performance and other attributes.

The particular alloys were selected since they represent a fairly wide spectrum of CRA materials often chosen for offshore applications. Applications for these materials include: cladding, flowlines, water injectors, well heads, and fasteners to name a few. The variation in alloy content for these materials results in a unit cost factor range of about four to five. In comparison to steel components, the cost factor can be as high as 25.

This laboratory testing program included potential exposure scenarios expected offshore: cold seawater exposure with and without imposed cathodic protection and high-pressure, high-temperature (HPHT) exposure to a sour environment for extended time periods. The testing used both self-loaded and dynamically loaded specimens in the environments of choice. It included investigations of corrosion rate over time, crevice and pitting corrosion, determination of crack growth rates, and effects of applied cathodic potentials. It also included post-test microscopy examinations. A brief investigation into higher temperature (i.e., 950°F) loading was performed to determine if any detrimental creep effects were noted.

All five of the materials behaved well in extended time sour autoclave tests simulating actual HPHT conditions. The failure of a pair of 945X specimens after a 6-week exposure was inconsistent with non-failure of the same material after 12, 18, and 48 weeks. Cathodic charging contributed to the fatigue crack growth of precipitation hardening alloys, especially 725, but had no effect on the work hardening alloys. None of the materials suffered significant pitting attack. The crevice corrosion observed can be understood in terms of the relative amounts of alloy content as quantified by the pitting resistance equivalent number (PREN). One elevated temperature failure occurred at 950°F for Alloy 825.

Lastly, there is most likely no single “right” materials choice for a particular offshore oil and gas production application. The prime selection criterion needs be that the potential materials candidates will be suitable for the foreseeable environments and loading conditions over the intended life of the component. One then needs to ensure that the materials can be delivered when they are needed and that they have the specified properties. One must also ensure that the delivered materials costs meet the financial constraints imposed on the project. This particular program has demonstrated that there could be many potential candidates that meet the technical needs. The other needs will depend on the particular offshore project.

1 INTRODUCTION TO HPHT

1.1 HPHT DEFINED FOR SUBSEA APPLICATIONS

The history of subsea oil and gas production has been one of more and more challenging operational conditions. These challenges have included increasing water depth, greater distances from topside structures, more severe environmental (i.e., chemical) conditions, higher pressures, and hotter conditions. These last two conditions of high pressure and high temperatures have given rise to the “HPHT” acronym. Within the HPHT vernacular, the HP portion typically means pressures of at least 15 ksi (103 MPa). Similarly, the HT portion typically means temperatures of at least 350°F (176°C). Different operating companies may have somewhat different values than these in mind when they talk about HPHT conditions, but in general, the 15 ksi, 350°F is a good baseline representation of the HPHT condition.

1.2 HPHT MATERIAL CHALLENGES

The material of choice for offshore construction is steel because of experience in its use and cost. Also, steel is readily available from many global sources. Indeed, when local-content requirements are imposed on international construction contracts, fulfilling this requirement with steel from domestic suppliers is one way to meet these contract terms. However, when environmental conditions are such that excessive corrosion of steel cannot be tolerated for particular applications, corrosion resistant alloys (CRAs) are then sought to meet the needs. The designation of CRA is somewhat misleading, because these materials do corrode but take long times and do so in a much more localized fashion such as pitting, crevice corrosion, hydrogen embrittlement, or cracking. These forms of corrosion can be of greater concern than the “rusting” of steel since they can cause failure of a component with very little mass loss of material and with very little prior warning if the progress of the localized corrosion process is not readily detectable. Thus, it is important to know if localized modes of corrosion occur with CRA/environmental combinations. NACE MR0175/ISO 15156 documents some safe environmental windows for CRA materials¹ in challenging environments.

For CRA materials as the alloy content increases, so, does the cost and the delivery time of the material. Table 1 provides a notional idea of the relative cost of generic CRA materials compared to steel. Depending on the product form, delivery times of these CRA alloys can be from months to a couple of years. Hence, it is quite understandable that the oil and gas industry specifies the use of CRA materials for only “as-needed” environmental conditions. It is also quite understandable why it is desirable to fully identify the environmental operational windows for CRAs and to safely select the most cost-effective material solution to the environmental need.

1

TABLE 1 Notational Relative Cost for Various Types of Materials of Construction

Material Type	Cost Relative to Steel
Carbon Steel	1
Martensitic Stainless Steel	3-4
Super Duplex Stainless Steel	6
Super Austenitics: Fe-Ni-Cr-Mo Alloys	7-10
High-Nickel Base Alloys	15-25

Use of CRAs for petroleum production became more common in the 1980s as the wells became more corrosive to steel because of greater amounts of acid gases. In particular, the production of carbon dioxide resulted in lower pH values and higher corrosion losses. Mitigation of high-corrosion losses of steel via active corrosion inhibition, although technically possible, was considered potentially unreliable for continuous use. This resulted in greater reliance on CRA materials to avoid premature failure from corrosion.

If the environmental conditions are deemed to be too corrosive for the use of steel, then a CRA material is chosen for the particular application. The choice of which CRA to use is based on several factors including failure resistance to the anticipated environment(s) and loading conditions, the availability of the material, and the life cycle cost. A risk assessment is often conducted to make sure that all failure modes have been identified and sufficiently addressed. Sometimes alloy performance can be found in open literature. Often, however, specific testing is required to evaluate materials performance in the suspected environment, especially if more than one material might be potential candidates for use.

The purpose of this report is to document a test program which evaluated the performance of five CRA materials based on testing and examining each similarly. The intended use of these alloys is subsea and/or severe downhole environments in particular HPHT conditions.

2 ENVIRONMENTAL TEST PROGRAM PURSUED

2.1 MODES OF MATERIALS FAILURE

Materials used in oil and gas production experience a whole spectrum of environmental and loading conditions. This is especially true in offshore conditions. Prudent design of structures and components incorporates information about how materials of construction perform in anticipated environments and under anticipated loadings. Corrosion resistant alloys inherently have low, but not zero corrosion rates. Hence, one property worth measuring is the general corrosion rate and to investigate whether the corrosion rate changes over time.

Since CRA materials have very low corrosion rates, other forms of corrosion are typically of more interest. These other forms include pitting and cracking. Both of these modes of degradation can lead to failure with very little mass loss of the material. Pitting can occur on broad exposed surfaces or might be restricted to creviced areas. Cracking modes are dependent on mechanical loads; and the form of cracking might be caused by a static load (stress corrosion cracking) or a dynamic load (corrosion fatigue). Cracking can be affected by environmental conditions which lead to very localized corrosion. Such environmental conditions can occur in oil and gas production under acidic situations. Sour wells can be of particular concern since these conditions can lead to hydrogen embrittlement of some construction materials. Thus, these localized forms of corrosion are important to evaluate and validate the choice of materials for given applications.

2.2 TEST CONDITIONS

2.2.1 Overview and Objective

A key objective of this test program is to compare the performance of five CRA materials when exposed to potential loading/environmental conditions that might occur during the production of hydrocarbons at an offshore location. Exact environmental conditions are unique for each specific location. However, types of operational conditions include down-hole well conditions, subsea conditions, and splash zone conditions, with the latter conditions often under cathodic protection. The intent of this study is to examine examples of these conditions. To do so, work was divided among four organizations based on capabilities. These organizations are: Westmoreland (specimen preparation and mechanical testing), DNV-GL (environment dynamic loading crack growth tests in simulated environments), Honeywell Corrosion Solutions (HCS) (corrosion rate and crack growth under high pressure and static load), and Argonne (metallography and microscopy).

2.2.2 Seawater Environment Conditions

Materials in offshore conditions are exposed to different seawater type environments. These environments can be from the ocean itself or from brine conditions that exist in the borehole of a drilled well. For seawater conditions, a concentration of 3.5% sodium chloride is typically used to simulate the environment. For those laboratory simulations, the pH of the test solution is set at a value of 4.0. For well conditions, brine concentrations of up to 20% NaCl are often used to simulate the severe chloride content found in some of these wells. High chloride content with high temperatures is especially aggressive to metal components in terms of general and localized corrosion processes.

2.2.3 Sour Conditions

The technical definition of sour conditions is prescribed by NACE MR0175/ISO 15156. This definition is given as not a concentration of hydrogen sulfide (H_2S) but rather as a partial pressure of H_2S . By the MR0175/ISO 15156 definition, sour conditions occur when the partial pressure of H_2S is equal to or greater than 0.05 psia. When this partial pressure value is reached (or exceeded), best practice is to use NACE qualified materials of construction.

Because sour conditions are defined by the partial pressure of H_2S , particularly challenging situations arise with high-pressure applications. The Figure 1 illustrates this point. Note, for example, that a 5,000 psi well reaches this so-called NACE limit with a 10 ppm concentration of H_2S , but at a 15,000 psi pressure, only 3.4 ppm H_2S is required. Hence, material selection for oil and gas production depends on knowing the operational pressure and the chemical components (and their concentrations) of the produced products over the entire intended design life.

2.2.4 Temperature and Pressure

The past operational limit for high-pressure offshore production equipment has been around 10,000 psi. Newer deep-water discoveries have pushed this value to about 15,000 psi and 350°F. These temperature and pressure values present economic challenges for materials of construction. The key for reliable component design in such pressure and temperature conditions is to find materials of construction that are both robust and yet affordable. It also is a benefit to the design team if they have more than one material and more than one supplier that can provide the properties needed for the given application. Temperature and pressure are addressed in C-Ring and corrosion coupon testing in autoclaves at HCS.

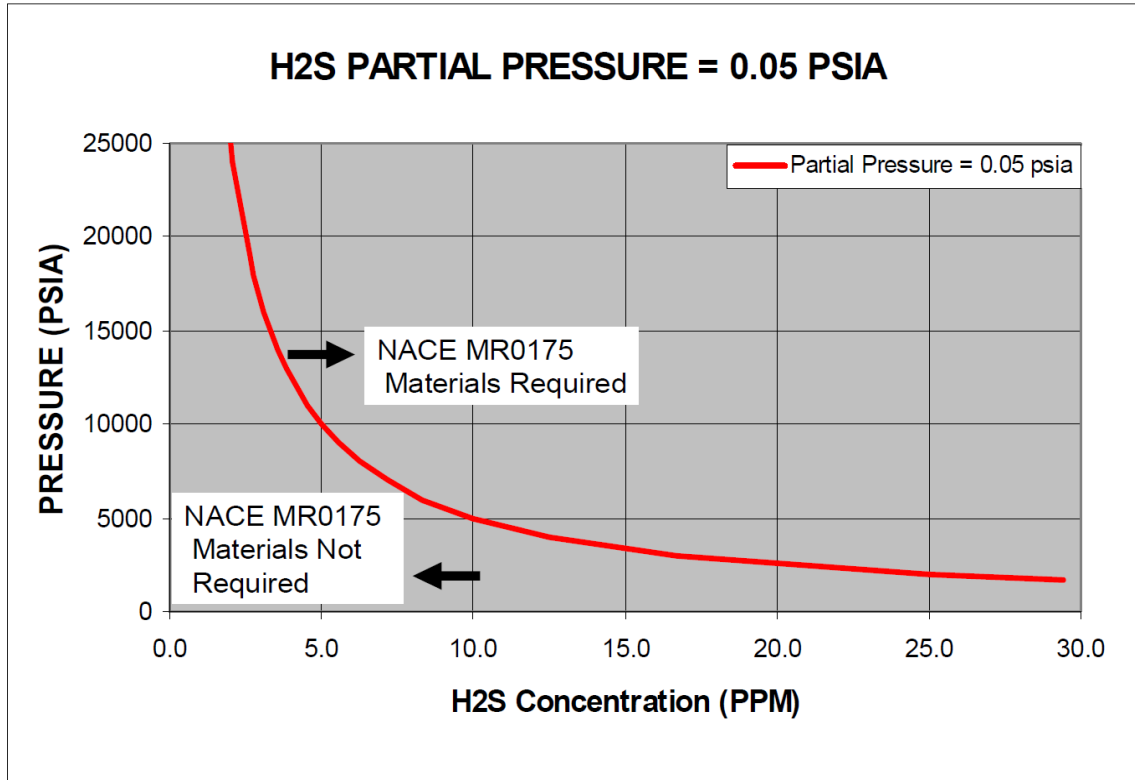


FIGURE 1 H2S Concentration vs. Pressure Illustrating Sour Conditions in Parts per Million (PPM)

2.2.5 Test Durations

Environmental test durations for materials are based on either industry standard practice or specific time periods set by a particular project need. The industry standard for sour conditions is NACE TM0177 which specifies 720 hours of test exposure. This 720-hour duration is a good “go by” when the test is such that no interruptions in exposure occur (i.e., set it up and leave it run). However, since CRA materials are inherently resistant, it is often good practice to run these types of exposures for as long as possible. For the high-pressure autoclave exposures in this program, time periods of 6, 12, 18, and 48 weeks were chosen. These periods correspond to 1008, 2016, 3024, and 8064 exposure hours respectively, with the longest exposure a factor of more than eight greater than the standard test duration.

For testing where dynamic loading occurs the test operator typically wants to get a stable crack growth rate and will adjust loading conditions (like min and max loads, loading wave form, and loading frequency) until a steady rate has occurred. This practice is based on user experience. It is particularly effective for comparison of materials’ performance.

3 CORROSION RESISTANT ALLOYS FOR LABORATORY TESTING

3.1 ALLOY SELECTION RATIONALE

Five CRA alloys were chosen for this laboratory test program. These materials were: Alloys 725, 825, 945X, 955 and C22HS. A brief description of each of these materials follows with typical uses and why the alloy was chosen for this testing program:

Alloy 725 (UNS N07725)

Description of Alloy: Alloy 725 is a precipitation hardening (PH) alloy. A PH alloy gains its strength from the formation of precipitates in the material upon particular heat treatments. Alloy 725 has a nominal composition that is 57Ni-22Cr-8.5Mo-3.5Nb.

Potential Offshore Uses: Downhole equipment for water injector wells.

Why Chosen for Consideration: Alloy 725 has a high alloy content. Because of this high alloy content, it will likely have a fairly good performance.

Alloy 825 (UNS N08825)

Description of Alloy: Alloy 825 is an Ni-Fe-Cr alloy with additions of Mo and Ti. It has good pitting and crevice corrosion resistance in chloride environments. The strength of the material is enhanced by cold working.

Potential Offshore Uses: Subsea flowlines, well heads, cladding for corrosion resistance

Why Chosen for Consideration: Alloy 825 is widely used in offshore oil and gas production applications.

Alloy 945X (UNS N09946)

Description of Alloy: Alloys 945X was developed to be an oil patch replacement material for Alloy 718. Alloy 945X is currently being used in 140 to 150 ksi strength grades. Alloy 945X, however, does not have the experience base as with 718. This alloy is precipitation hardening. Niobium, titanium and aluminum participate in the age hardening reaction that occurs during heat treatment. Their interaction forms gamma prime and gamma double prime precipitates, which strengthen the alloy. API Standard 6A-CRA details how 945 should be processed and gives property ranges. The more recent 945X (i.e., UNS N09946), however, is not detailed in that particular API document.

Potential Offshore Uses: The use of 945X would be the same as those for Alloy 718. These are: seal rings, fittings, small components, valve stems, subsurface safety valves, tubing hangers, and packers.

Why Chosen for Consideration: The alloy additions in this material clearly indicate different elemental proportions than the traditional industry workhorse, Alloy 718. In addition, 945X has a higher yield strength than does 718 (140 ksi versus 120 ksi).

Alloy 955 (UNS N09955)

Description of Alloy: This is a new PH alloy. This alloy has twice the Mo content as an alloy like 718 and thus should have better pitting and crevice corrosion resistance for use in hot chloride environments. As a PH alloy, it should also have good mechanical strength (yield strength in range of 130 ksi at 350°F)

Potential Offshore Uses: Downhole equipment for water injector wells.

Why Chosen for Consideration: In order to keep reservoir pressures high as they are depleted by oil production, a common technique offshore is to inject water into the oil depleting reservoir. Water injection utilizes seawater for that purpose. Injection of oxygenated seawater into a hot well is a challenge for the down-hole injector materials. Corrosion rates of steel would be prohibitively high; pitting of lean CRAs would lead to rapid failure.

Alloy C22HS (UNS N07022)

Description of Alloy: Alloy C22HS is available as a cold worked or as an age hardenable material. It is a nickel-based material with 21Cr-17Mo and minor additions of Co and W. Some recent publications have suggested that this material could be available at strength levels of 200 ksi. These publications also suggest that the material has good corrosion resistance to marine environments.

Potential Offshore Uses: Fasteners such as high-strength bolts

Why Chosen for Consideration: The high-strength nature of this material in conjunction with literature data showing good corrosion resistance suggest that this could be a good alloy for HPHT conditions. It also has been incorporated into the NACE MR0175/ISO 15156 document. The size limitations for production of this product are not known.

3.2 MATERIALS AND MATERIAL FORMS ACQUIRED FOR TESTING

Table 2 lists suppliers and acquisition information about the materials used for the testing programs described in this report. All test specimens were machined from this material and then provided to the organizations for their respective testing.

TABLE 2 Materials Supply Sources, Forms, and Hardness

Alloy	DNV- GL #	Heat #	Description	Source	Hardness (HRC)	Solutionizing	Heat Treatment
725	2810	Z0403-1	4.5-in. OD × 24-in. length	Special Quality Alloys, Inc.	38	1038C/2.06hr	738c/8.1 HR FC to 621C-hold for 8hr followed by air cool
945X	2805	XX5778RY11	4.00-in. OD × 24-in. length	Howco Metals Management, LLC	40.7	1038C/2hr	704C/ 8hr FC to 621C-hold for 8.5 hr followed by air cool
955	2808	VAR41519/ Heat 06930	8.00-in. OD × 7-in. length	Foroni S.p.A.	43		
825	2833	F06919	7.625-in. OD × 60-in. length	Special Quality Alloys, Inc			
C22HS	2785	2321-2-2505	2.25-in. OD × 60-in. length	Howco Metals Management, LLC	40		

4 OVERVIEW OF INDUSTRY LITERATURE ON CHARACTERISTICS OF CRA MATERIALS TESTED

A key purpose of this report is to provide technical data where each of the five candidate materials were exposed to the same testing methods, particular tests for all were performed by the same vendor, and limited to materials of potential value to the industry beyond Alloy 718. The following sections contain selected information available in open literature on the five materials tested and reported in this paper. For comparative purposes, Alloy 718H (high strength) is added because this is an alloy in current use and is a well-characterized material.

This test program used three test laboratories to complete the required work. As such, each laboratory tested the five CRA materials as machined specimens that were most appropriate for the particular test (or tests) conducted at each laboratory. In order to expedite and track the large number of specimens, all of the machining was performed at one location. All test specimens were machined at Westmoreland Mechanical Testing and Research. The appendices of this report include the formal reports of these testing efforts (mechanical testing at Westmoreland (Appendix A), environmental cracking under dynamic loading at DNV-GL (Appendix B), and stress cracking and corrosion under high pressure at HCS (Appendix C). Westmoreland data is certified test reports. The DNV-GL and HCS reports provide details on the specimens, procedures, and detailed testing results.

4.1 PUBLISHED MATERIAL DENSITY AND MELTING POINTS

Table 3 provides density and melting temperature ranges for the alloys tested and for 718H. All alloys have similar ranges, with the exception of C22HS, which has higher density.

TABLE 3 Alloy Density and Melting Temperature Ranges in Literature

Alloy (UNS)	Density (lb./in ³)	Melting Temperature Range, °F (°C)
725 (N07725) [8]	0.30	2,320–2,449 (1,271–1,343)
945X (N09945) [9]	0.298	2,323–2,424 (1,273–1,345) [3]
955 (N09955)	Not provided in corporate refs [5] and [4]	Not provided in corporate refs [5] and [4]
825 (N08825) [8]	0.294	2,500–2,550 (1,370–1,400)
C22HS (N07022) [10]	0.311	2,380–2,495 (1,304–1,368) [7]
718H (N07718) [8]	0.296	2,300–2,437 (1,260–1,336)

4.2 ASTM SPECIFIED HEAT TREATMENTS

Table 4 lists recommended heat treatments for the alloys studied as appearing in standard specifications.

TABLE 4 Recommended Heat Treatments as Appearing in Selected Standard’s Specifications

Alloy	Form/Service	Annealing	Solution	Stabilizing	Precipitation Hardening/ Heat Treatment
725 (N07725) [11] and [12]	Bars, forgings, forging stock for moderate or high- temperature service.	-	1900 ± 25F (1038 ± 14C), hold 0.5 min, and h hr max, cool at rate equivalent to air cool.	-	1350 ±25 (732 ±14C), hold at temperature for 5 to 8.5 hr, furnace cool to 1150F ±25F (621 ±14C), hold at temperature for 5 to 8.5 hr, air cool or faster.
945X (N09946 Type 1 shown) [9]	Welded precipitation hardenable or cold work nickel alloy tube.		1850 to 1950F (1010 to 1066C), air cool, or faster		1300 to 1350 F (704 to 732 C) for 6 to 8 hr, furnace cool at 50 to 100F (26 to 56C)/hr to 1125 to 1175F (607 to 365C), hold for 6 to 8 hr, air cool
C22HS (N07022, Type 1A or 1B) ^a [11]			1800 to 2100F (982- 1149C), hold 0.5 hr, 5 min minimum, rapid air cool or water quench		
C22HS (N07022, Type 2) ^b [11]			1800-2100F (982- 1149C),hold 0.5 hr, 5 min minimum, rapid air cool or water quench		1125 ± 25F (605 ± 14C), hold 10 hr, air cool
718H (N07718) [11]	Bars, forgings, forging stock for moderate or high- temperature service.	-	1700-1850F (924- 1010C) Hold ½ hour minimum , cool at rate equivalent to air cool or faster	-	1325±25F (718±14C), hold at temperature for 8 hr, furnace cool to 1150 ±25F (641±14C), hold until total precipitation heat treat time reaches 18 hr, air cool

^a For solution treated + cold worked material only, when specified (Table 4 in reference).

^b For solution treated + cold worked + precipitation hardened material only, when specified (Table 4).

4.3 PUBLISHED MECHANICAL PROPERTIES

Mechanical properties from a selection of sources appear in Table 5. These values are from ASTM specifications (denoted by “S” and blue shading) and vendor literature (denoted by “V” and yellow shading) and thus the standard’s values are minimums relative to advertised values. For most materials only a few of the possible conditions have been included because there are many permutations of product form, size, heat treatment, cold working, hot or cold rolled products, and measurement direction (longitudinal and transverse). Notably, there are numerous blanks and a significant number of footnotes in the table attributed to the types and completeness of information appearing in the sources.

TABLE 5 Mechanical Properties from Selected Specifications (Requirements) and Vendor Literature (Actual Advertised)

Alloy	Ref. Type	Form/Service (Heat Treatment)	Tensile Strength (ksi) ^a	Yield Strength (0.2% offset, ksi)	Elongation (in 2 in or 4 D %)	Reduct, in Area (%)	Hardness	Charpy (Lbr-Ft)	Young's Modulus (ksi)
725 (N07725) [11]	S	Solution + precipitation harden	150 min	120 min	20 min		43 HRC max		
725 (N07725) [13]	S	Plate (annealed)	150 min	120 min	20 min				
725 (N07725) [13]	S	Sheet (annealed)	150 min	120 min	20 min				
725 (N07725) [14]	S	Bar and wire (annealed)	110 min	45 min	30 min				
725 (N07725) ^b [1]	V	Round-Annealed	124.0	62.0	57		5 HRC		29.6 × 10 ³
	V	Round-Age hardened	180.0	133.0	30		36 HRC	68	29.6 × 10 ³
725 (N07725) ^c [1]	V	Round-Age hardened	180.0	131.0	31		36 HRC	97	29.6 × 10 ³
725 (N07725) [1]	V	Tube-Annealed	113.6	48.4	60		5 HRC		29.6 × 10 ³
		Tube-Age Hardened	183.9	133.6	27		39 HRC		29.6 × 10 ³
945X (N09946, Type 1) [9]	S	Solution anneal and precipitation hardened	165 min	140 min	18 min		42 HRC		
945X (N09946, Type 2) [9]	S	Solution anneal	100 min	65 min	30 min				
945X (N09946, Type 2) [9]	S	Solution anneal and precipitation hardened	165 min	140 min	18 min		42 HRC		
945X (N09946) ^d [3]	V	Not specified-heats used for SCC, SSC, and GHSC	170.7 avg	136.9 avg	25.4 avg	40.6 avg	38-41.2 HRC	47 ^e	29.4 × 10 ³
955 (N09955) [4]	V	120 Ksi, bar at mid radius of bar prolongations	168	136	36/ (54% reduction of area)		38 HRC (ASTM E18)		
955 (N09955) [4]	V	140ksi, bar and mid radius of bar prolongations	177	147	30/ (50% reduction of area)		40 HRC (ASTM E18)		
825 (N08825) [15]	S	Forgings	85 min	35 min	30 min				
825 (N08825) [16]	S	Hot rolled plate, cold rolled Plate, and rod and bar	85 min	35 min	30 min				
825 (N08825) [6]	V	Tubing-annealed	112	64	36				28.3 × 10 ³ (hot rolled and annealed plate)
		Tubing-cold drawn	145	129	15				
		Bar-annealed	100	47	45				
		Plate-annealed	96	49	45			79.0 (plate-longitudinal) 83.0 (plate-transverse)	

TABLE 5 (Cont.)

Alloy	Ref. Type	Form/Service (Heat Treatment)	Tensile Strength (ksi) ^a	Yield Strength (0.2% Offset, ksi)	Elongation (in 2 in or 4 D %)	Reduct, in Area (%)	Hardness	Charpy (Lbr-Ft)	Young's Modulus (ksi)
C22HS (N07022, Type 1A) [11]	S	Solution + cold worked	160 min	150 min	17 min	50 min	382 B max		
C22HS (N07022, Type 1B) [11]	S	Solution + cold worked	185 mi	180 min	13 min	30 min	425 B max		
C22HS (N07022, Type 2) [11]	S	Solution + cold worked + precipitation hardened	178 min	160 min	15 min	24 min	479 B max		
C22HS (N07022, Type 3) [11]	S	Solution + precipitation hardened	145 min	80 min	15 min	14 min	228 min		
C22HS (N07022) [7]	V	Standard annealed + age hardened		~100					
	V	Cold worked bar ^f	203.5	198	16.7	64,2	42 HRC ^g	146 ^h	
718H (N07718) [11]	S	Bars, forgings, forging stock for moderate or high-temperature service. (Solution-precipitation harden) ⁱ	185 ^j min	150 min	12 min		331 B min		
718H (N07718) [7]	V	Plate: Mill annealed + 1325F/8hr/ furnace cool to 1150F/8hr/air cool.	200.5	167.8	20.6				29 × 10 ³ (dynamic)
718H (N07718/ w.Nr. 2.4668) ^k [17]	V	Hot finished products (table 29 in reference) 8 in diam-18 hr heat treatment	209	183.5	17	32		13	

^a Unless specified otherwise, properties are at room temperature (68/70F).

^b Transverse specimens from hot-finished rounds of 4.0 to 7.5 in diameter. Mean values given from Special Metals brochure.

^c Longitudinal specimens from hot finished rods of 0.5 to 7.5 in diameter. Mean values given from Special Metals brochure.

^d Tensile, yield, elongation, and reduction in area represents average of three commercial heats used for NACE testing per MR0175/ISO 15156-3.

^e From annealed plus aged sample of 22 in diam rod at mid radius. Impact at 75°F.

^f Cold worked in the range of 43-47%

^g Cold worked 43-47% bar of tube.

^h 1 in diameter cold worked bar (44%)

ⁱ Values apply for tension specimens machined tangentially from near the center of large disk forgings of 50 in² in cross section or radially from rings 3 in or more in thickness.

^j Values apply for tension specimens machined tangentially from near the center of large disk forgings of 50 in² in cross section or radially from rings 3 in or more in thickness.

^k Note: this material is well characterized and reported for many different states, forms, finishings, and sizes beyond the excerpt given here.

4.4 PUBLISHED C-RING CORROSION TEST DATA

Room temperature test results in the literature for the selected alloys appears in Table 6. Information sources are identified in the alloy.

TABLE 6 NACE TMO177 Qualification Test Data for Alloys and High-Strength 718

Alloy	Material Condition	Test Temperature	Test Duration	YS (0.2% offset) ksi	% YS	Hardness	SSC Observed?
725 (N07725) ^a [1]	Age Hardened	70°F	30 d	117.6	100	37 HRc	No
	“	70°F	30 d	128.6	100	40 HRc	No
	“	70°F	30 d	130.8	100	41.5 HRc	No
	“	70°F	42 d	132.9	100	36 HRc	No
	“	70°F	30 d	133	100	39 HRc	No
945X (N09946) [3]	Age hardened (inferred in reference	75°F	30 d	136	90		No
	“	75°F	30 d	163	90		No
	“	75°F	30 d	163	90		No
	“	75°F	30 d	164	90		No
	“	75°F	30 d	164	90		No
	“	75°F	30 d	164	90		No
	“	75°F	30 d	169	90		No
	“	75°F	30 d	169	90		No
955 (N09955) Rep. Gr. 3 and Gr 3HS ^b	Age hardened round bar (8 and 10 in. diameter)	75°F	1 mo.	136 (6 in), 131 (8 in)			No ^c
	“	75°F	1 mo.	“			No
825 (N08825) [18]	Not specified	75°F	>1000 hr	160		38HRc	No (cracking)
C22HS	Cold worked- 3 heats coupled and not coupled to carbon steel ^d	TMO177 level II and III			100		Pass
718 (U ukn) [1]	Age Hardened	70°F	42	120	100	30	No
	“	70°F	42	130	100	37	No
	“	70°F	42	134	100	38.5	No
	“	70°F	42	139	100	38	No
	“	70°F	60	156	100	41	No

^a From Table 8 in reference-room temperature tests in 5% NaCl plus 0.5% acetic acid saturated with H₂S. All specimens were coupled to carbon steel.

^b From Table 21 of reference-room temperature at 5 w% NaCl, .5w% Acetic Acid, 14.5 psia H₂S partial pressure, TM0177-2004 Method A. Firsts listed test-no coupling to carbon steel, second test coupled to carbon steel.

^c Author notes there also was not weight loss after 20X optical examination for either test series.

^d 25% NaCl, 500 psi H₂S + 500 psi CO₂, 401 F, Test Level VII, elemental sulfur= 1 g/l and 5g/l with stirring.

5 CHEMICAL COMPOSITIONS (SPECIFICATIONS, VENDOR, AND ACTUALS) FOR MATERIALS TESTED

Chemical composition percentages for the CRA alloys tested appear in Table 7. Where available, values are provided as appearing in vendor literature and ASTM documents. For many elements, percentages are identical but there are a few instances where the vendor appears to deviate in some way. For example, for 945X, the phosphorus and chrome limits for the two specifications are different. For these two elements the actual content of the samples used was substantially below the highest allowable specification value. With minor exception in the case of 955 (for which there was not a standard specification available), all of the material samples used for testing complied with both specifications.

TABLE 7 Chemical Compositions-Specifications and Actuals for CRA Alloys Tested^a

UNS	725			945X			955		825		C22HS		
	N07725			N09945			N09955		N08825		N07022		
Element	Specif. (Vendor)	Specif. (ASTM)	Actual	Specif. (Vendor)	Specif. (ASTM)	Actual	Specif. (Vendor)	Actual	Specif. (Vendor)	Actual	Specif. (Vendor)	Specif. (ASTM)	Actual
C	0.03 max	0.03 max	0.015	0.005–0.04		0.011		0.015	0.05 max	0.01	0.01 max	0.010 max	0.003
Si	0.20 max		0.04	0.5 max		0.07		0.09	0.5 max	0.4	0.08 max	0.2 max	0.015
Mn	0.35 max	0.35 max	0.03	1.0 max	1.0 max	0.08		0.08	1.0 max	0.75	0.8 max	0.5 max	0.25
P	0.015 max	0.20 max	0.003	0.03 max	0.5 max	0.01		0.009		0.017		0.08 max	<0.01
S	0.010 max	0.015 max	0.0006	0.03 max	0.03 max	0.001		0.0002	0.03 max	0.0002		0.025 max	<0.001
Cr	19.0–22.5	19.0–22.5	20.7	19.5–23	23.5–25.5	20.8	21.8	21.6	19.5–23.5	22.35	21	20.0–21.4	20.5
Mo	7.0–9.5	7.00–9.50	8.01	3.0–4.0	3.0–4.0	3.26	5.87	5.9	2.5–3.5	3.08	17	15.5–17.4	16.6
Ni	55.0–59.0	55.0–59.0	57.5	45.0–55.0	45.0–55.0	53.3	57.8	57.4	38.0–46.0	38.37	Bal. ~58–62	Bal. ~55.76–64.5	61
Al	0.35 max	0.35 max	0.32	0.01–0.7	0.01–0.7	0.11	0.46	0.43	0.2 max	0.12	0.5 max	0.5 max	0.23
B			0.0035					0.0043			0.006 max	0.006 max	0.006
Co			0.05			0.3	0.12	0.01				1.0 max	<0.05
Cu			<0.01	1.5–3.0	1.5–3.0	1.99		0.037	1.5–3.0	1.86		0.5 max	
Nb	2.75–4.0	2.75–4.00	3.54	2.5–4.5	2.4–4.5	4.06	4.74	4.8					0.08
Pb			<0.00001			0							
Ti	1.0–1.7	1.00–1.70	1.56	0.5–2.5	0.5–2.5	1.52	0.85	0.86	.6-1.2	0.83			<0.01
Bi			0.0003										
Ca			0.0003			0.003							
Mg			<0.00005			0.0004							0.034
Se			<0.00005										
Ta			0.004			0.01							<0.1

TABLE 7 (Cont.)

UNS	725			945X			955		825		C22HS		
	N07725			N09945			N09955		N08825		N07022		
Element	Specif. (Vendor)	Specif. (ASTM)	Actual	Specif. (Vendor)	Specif. (ASTM)	Actual	Specif. (Vendor)	Actual	Specif. (Vendor)	Actual	Specif. (Vendor)	Specif. (ASTM)	Actual
Fe	Bal. ~2.5– 15.25	0.010 max	Bal	Bal. ~5.5– 27.9	0.03 max	14.4	8.19	8.7	22 min	32	2 max	0.015 max	1.1
Nb+Ta			3.544			4.06							0.18
W					Bal. ~3.24– 24.09						1 max	1.8 max	
V												0.8 max	

^a See table notes below for information sources. Actual values are from mill reports accompanying material received.

Table 7 notes: References for alloy 725- Vendor [1], ASTM [2]; 945X – Vendor [3], ASTM [2]; 955- Vendor [4] and [5]; 825-Vendor [6]; C22HS-Vendor ([7], ASTM [2]. All actual values are derived from table in HCS’s Report appearing in Appendix C (HCS) on 6 and 48 Week Testing.

6 TEST METHODOLOGY AND SUMMARY OF TESTS PERFORMED

6.1 TEST METHODOLOGIES

In general, two test methodologies are possible to evaluate the suitability of materials for intended applications: (1) standardized testing per industry agreed upon requirements; and (2) fit-for-purpose (FFP) testing, which is particularly tailored to meet known specific operational parameters of a given application.

The oil and gas (O&G) industry typically uses the most current version of ANSI/NACE TM0177 (Laboratory Testing of Metals for Resistance to Sulfide Stress Cracking and Stress Corrosion Cracking in H₂S Environments) when ordering materials that may experience sour service conditions. Among the cautions noted in the opening paragraph of this document is this statement: "This standard represents minimum requirements and should in no way be interpreted as a restriction on the use of better procedures or materials. Neither is this standard intended to apply in all cases relating to the subject." When materials are ordered from a supplier, part of the specification document often includes performance requirements that state, for example, "must pass TM0177 exposure testing." Hence, what the O&G industry collaboration that wrote this standard is saying is that specific heats of materials must pass this minimum standard if the customer requires it. Conformance with ANSI/NACE TM0177 is often seen as a quality control/quality assurance issue.

FFP testing most often pushes known or operational experience limits beyond standard conditions. Typical ANSI/NACE TM0177 testing is at ambient temperature and ambient pressure. However, so-called high-pressure, high-temperature (HPHT) conditions for oil and gas production can be at pressures around 15,000 psi and temperatures of about 350°F. Analytical methods can be used to extrapolate results from ambient conditions to HPHT conditions, but it is prudent to perform FFP tests at expected conditions to add this extra verification step.

In the current work directed by Argonne for BSEE, FFP testing was chosen in order to address "what-if" scenarios. For example, the test duration specified by the standard ANSI/NACE TM0177 testing is 720 hours (4.28 weeks). The FFP testing conducted at HCS was for 6, 12, 18, and 48 weeks. In addition, the pressure and temperature conditions at HCS were 15,000 psi and 350°F, much more severe than ambient conditions. These HCS tests went beyond the notional conditions required by ANSI/NACE TM0177 testing.

The environmental tests conducted at DNV-GL also addressed what-if scenarios. ANSI/NACE TM0177 has limited requirements for evaluating crack growth in sour environments. The testing there is for statically loaded test specimens. At the end of a test, one stress corrosion value per specimen is available. DNV-GL used dynamically loaded specimens, which allowed several values to be determined per specimen and also allowed for a determination of what happens to growing cracks as loads change. Specific standards that DNV-GL followed in their testing were: ASTM E647—Standard Test Method for Measurement of Fatigue Crack Growth Rates; and for exposure of specimens in an environment, ASTM E1681—

Standard Test Method for Determining Threshold Stress Intensity Factor for Environmentally Assisted Crack Growth of Metallic Materials.

In conclusion, testing materials to specific industry accepted standards are minimum requirements typically placed at the time of order. Passing these requirements is seen as passing quality control gates prior to being accepted by the buyer. The prudent material buyer will evaluate if the standard testing is "good enough" or if further testing is needed/desired. Further testing requirements might be imposed on the supplier (for added cost) or might be performed by the buyer at their own cost.

6.2 SUMMARY OF TESTING PERFORMED

In a laboratory environment, materials were subjected to a variety of test conditions and more detail is provided in the combination of the sections dedicated to testing by three entities and the Appendices A, B, and C. These tests, chosen per the above rationale, are:

- Standard ASTM mechanical tensile,
- Charpy impact,
- Creep,
- Crack growth as function of frequency in two environments (sour and seawater plus cathodic protection),
- Crack length as function of time in two environments (sour and seawater plus cathodic protection),
- Crack growth rate as function of time and potential,
- Critical crevice temperature (CCT),
- Corrosion coupon in high-pressure autoclave for four durations,
- C-ring stress corrosion cracking in high-pressure autoclave for four durations, and
- C-ring galvanic hydrogen stress corrosion cracking in high-pressure autoclave for four durations.²

² Test conducted at 350°F rather than low temperature defined by NACE MR0175/ISO 15156.

Raw data from the tensile and Charpy tests is found in Appendix A. These tests were conducted by Westmoreland. Environmental assisted cracking data and the accompanying report prepared by the performer, DNV-GL, are in Appendix B including added data supporting each table and graph in their report. HCS performed the autoclave testing with C-rings and an exposure coupon. Their report appears in Appendix C.

The following sections summarize the testing and results of each laboratory testing entity.

7 MEASURED MECHANICAL PROPERTIES FOR TESTED MATERIALS (WESTMORELAND)

In the interest of consistency Westmoreland machined test specimens for the mechanical tests as defined in Table 8, as well as those specimens used by DNV-GL and HCS. In addition to the machining, Westmoreland conducted all the mechanical testing and provided results to the other testing entities.

7.1 MECHANICAL PROPERTY TEST MATRIX

Table 8 lists the mechanical tests Westmoreland performed. The table summarizes conditions and lists the numbers of samples.

TABLE 8 Test Matrix—Numbers of Tests by Alloy and Summaries of Test Conditions for Mechanical Testing (Westmoreland)

Temperature	Alloy (UNS)				
	725 (N07725)	945x (N09946)	955 (N09955)	825 (N08825)	C22HS (N07022)
Mechanical Tests: Tensile (UTS), Yield Strength (0.2%), Yield Strength (0.2% Elongation under load-EUL), Elongation, Reduction in Area, Modulus, Ultimate load, 0.2% Yield load, Load (0.2% EUL w/stress stain curves-full and truncated at peak stress) with Tensile Test Article Dimensions (Original Diameter, Final Diameter, 4D Original Gage length, 4D Final Gage length, Original Area)					
Room Temperature ^a	3	3	3	3	3
350°F ^b	3	3	3	3	3
950°F ^c	1	1	1 ^d	1 ^e	1
Impact (Charpy-V Notch) ^f : Energy, Mills Lat. Exp, % Shear Fracture					
32°F	3	3	3	3	3
73°F	3	3	3	3	3
Creep Testing (1,000 hours at 83% YS)					
350°F	1	1	1	1	1
950°F	1	1	1	1	1

- ^a Tensile-related parameters at room temperature: ASTM E8-16a, 0.005 in./in./min. testing speed, extensometer travel exceeded; test continued as last stroke rate.
- ^b Tensile-related parameters at 350°F: ASTM E21-09, 30-min. soak time, 0.005 in./in./min., extensometer travel exceeded; test continued at last stroke rate.
- ^c Tensile-related parameters at 950°F: ASTM E21-17, soak time 30 min., 0.005 in./in./min., 0.05 in./min./in. (no 0.2% EUL and 0.2% EUL load values).
- ^d Incorrectly identified as Alloy 925 in Appendix A instead of the actual Alloy 955.
- ^e This value was higher than the values at lower temperatures; suspected to be recording or testing error.
- ^f Impact-related parameters: ASMT E23-16b.

7.2 MECHANICAL TEST SPECIMENS

Tensile Specimen (ASTM E 8M) as shown in Figure 2 was used to determine mechanical properties of materials. In addition, this type of specimen was used for 1,000-hour creep testing.

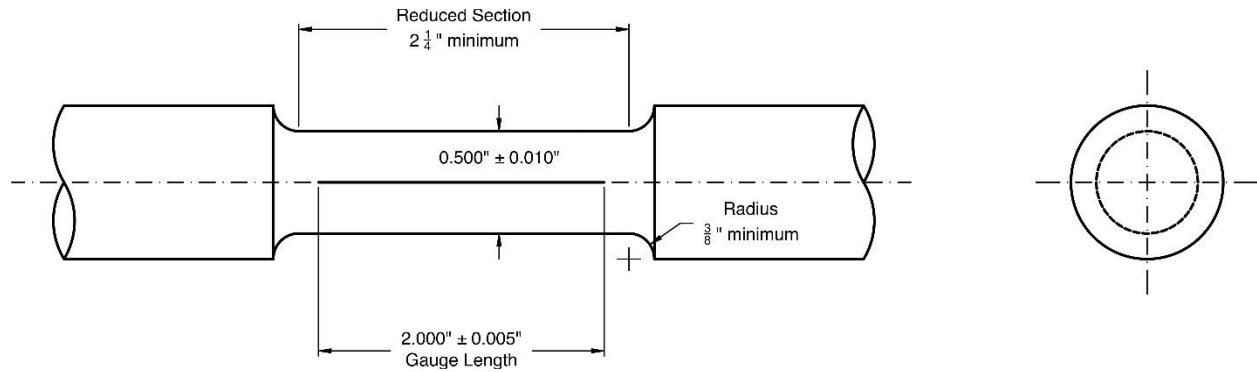


FIGURE 2 Tensile Specimen (ASTM E 8M)

Figure 3 shows the standard Charpy Impact Specimen (ASTM E23) used to get impact properties of materials (dimensions in mm).

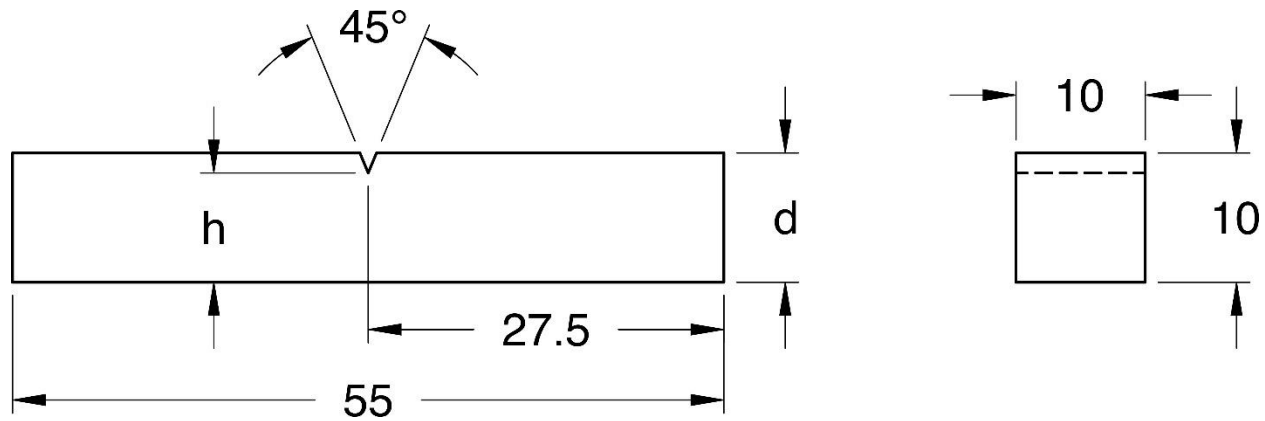


FIGURE 3 Charpy Impact Specimen (ASTM E23)

7.3 TENSILE AND YIELD STRENGTH TEST RESULTS

Tensile strength and yield strength (YS) were measured for all five alloys at room temperature, 350°F, and 950°F. Average tensile and YS results are shown in Figure 4 with corresponding elongation and reduction of area results shown in Figure 5. For room temperature and 350°F, data is based on three measurements and one test was done for each alloy at 950°F. Additional details about these tests appear in Appendix A in tabular form and, for room temperature and 350°F, in graphical form as individual stress-strain curves.

The three precipitation hardening (PH) alloys (725, 945X, and 955) have comparable strengths within only a few percent. Between, the two non-PH alloys, the C22HS has much higher tensile and yield strengths compared to Alloy 825. As shown in Figure 6, the modulus for the non-PH alloys remains higher at the upper temperatures in comparison to the particular PH alloys tested.

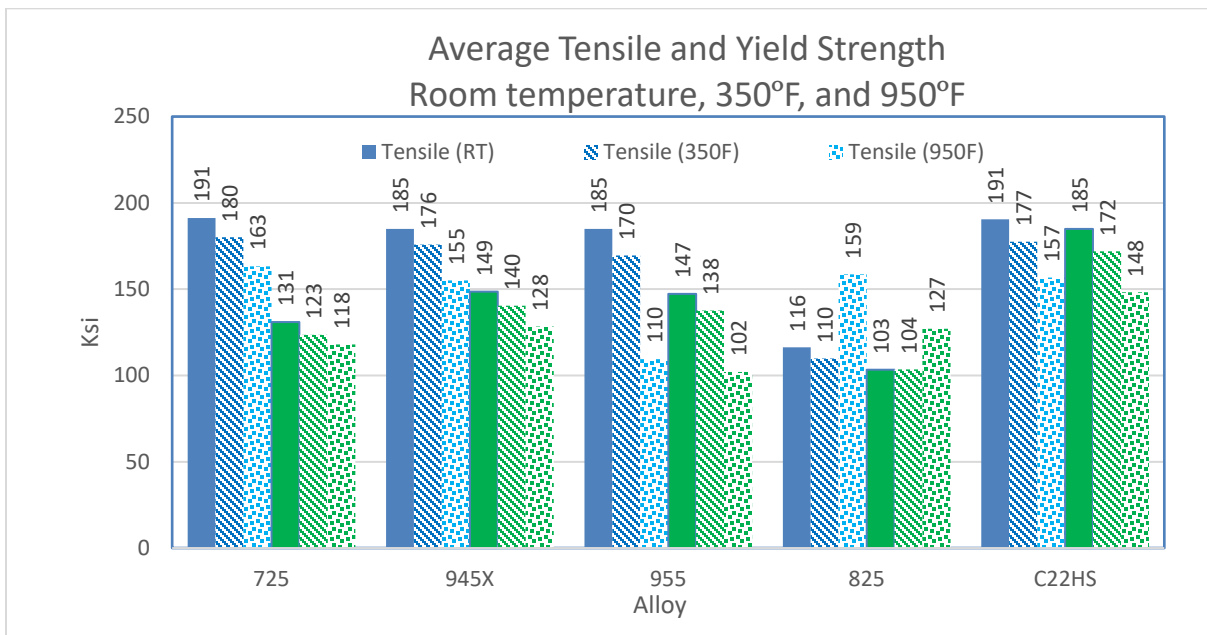


FIGURE 4 Average Tensile and Yield Strength

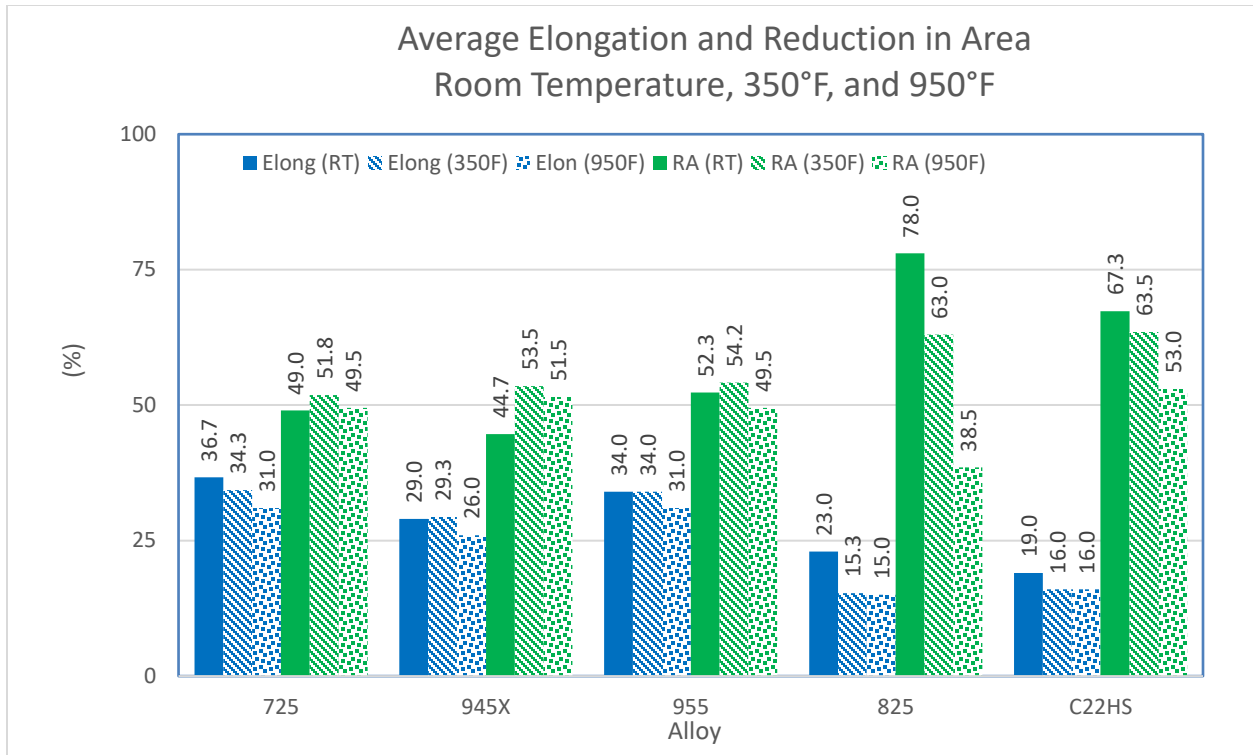


FIGURE 5 Average Elongation and Reduction in Area for Tensile Testing

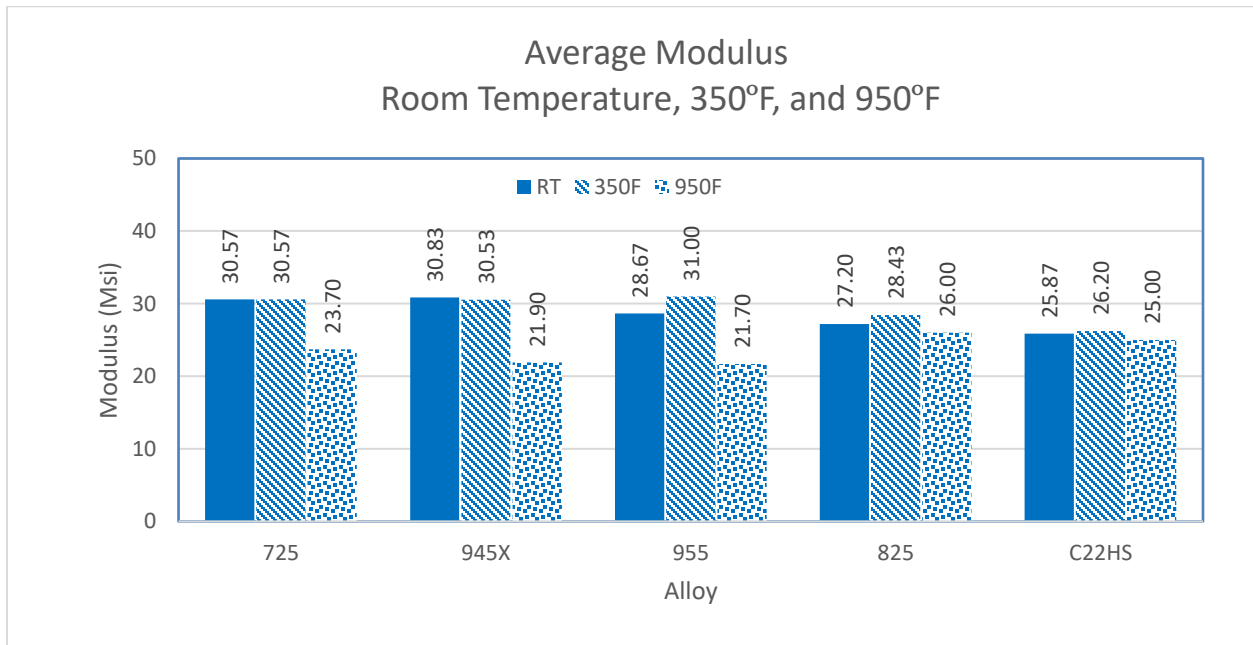


FIGURE 6 Average Modulus

7.4 CHARPY RESULTS

Charpy tests were conducted for all five alloys at 32°F and 73°F. Average Charpy results are shown in Figure 7. From data given in Appendix A, the averages are based on three tests for each alloy and temperature.

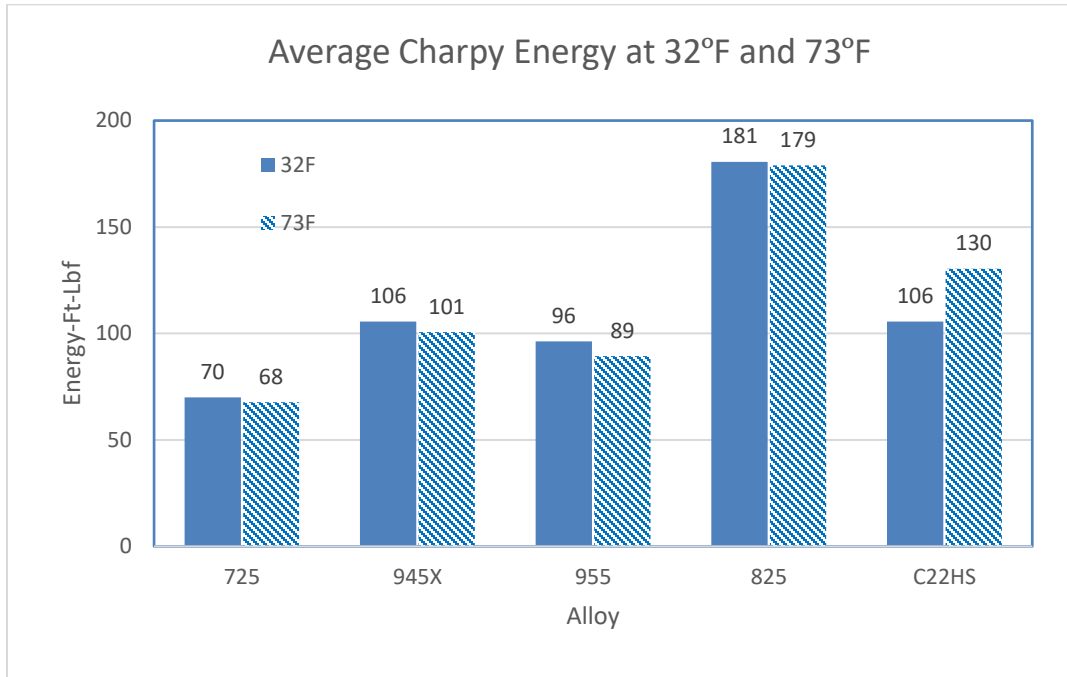


FIGURE 7 Average Charpy Energy (Ft-Lbf) at 32°F and 73°F

7.5 CREEP TESTING

Creep tests were conducted per ASTM E139-11 to see whether elevated temperature had any adverse effects on loaded specimens and whether this becomes a design concern for HPHT oil and gas. Since oil and gas environments do not experience the high temperatures a component might experience in a refinery, these tests were actually “low-temperature” creep to investigate this situation. Tests were conducted at two test temperatures (350 and 950°F) with a “run out” time of 1,000 hours. Run out means that the test has reached the pre-established time with no failure of the test specimen. The load on the specimens was 83% of the yield strength at the test temperature. Results are summarized in Table 9 and the certified data sheets can be found in Appendix A. For those cases without known concern for data integrity (825 at 950°F and 945X at 950°F), there were no failures.

There were some questions related to the loading of the 825 specimen (loaded at 106.5 ksi at 950°F, which is above the measured yield strength); and time constraints did not permit a retest. However, even if this failure was real (i.e., repeatable), a Larson-Miller analysis indicated that it would require about 20 years to failure for constant load at 750°F or about

4,000 years for constant load at 650°F, with both of these temperatures very extreme for offshore oil and gas production.

TABLE 9 Results of Elevated Temperature Load Testing for Each Alloy

Alloy	Temperature (°F)	Result
725	350	No failure
	950	No failure
945X	350	No failure
	950	Equipment malfunction
955	350	No failure
	950	No failure
C22HS	350	No failure
	950	No failure
825	350	No failure
	950	Failure at 46.5 hours

8 ENVIRONMENTALLY ASSISTED CRACKING RESULTS SUMMARY (DNV-GL)

Environmentally assisted cracking laboratory work was performed at DNV-GL as described and summarized in Table 10. Their entire report is included as Appendix B of this report. Some of the more relevant results are summarized and repeated in this section. Once DNV-GL completed experimental work Argonne began microscopy examination of these samples. This description of this microscopy appears in Section 8.7.

8.1 TEST AND DATA MATRIX

Table 10 lists the tests and data from work at DNV-GL.

TABLE 10 Test Data Matrix—Numbers of Datasets Obtained by Alloy and Summaries of Test Conditions for Environmentally Assisted Cracking Testing (DNV-GL)

Test Conditions	Alloy (UNS)				
	725 (N07725)	945x (N09946)	955 (N09955)	825 (N08825)	C22HS (N07022)
Crack Growth per Cycle as Function of Frequency (K controlled tests-compact tension specimens: 1 in. w × 0.5 in.)					
Sour Environment (Various ΔK and R combinations)					
350°F (2 at 400°F for Alloy 725 only), various ΔK and R ratio-1 sample for each condition	4 (DNV-GL Fig. 7)	4 (DNV-GL Fig. 9)	4 (DNV-GL Fig. 13)	4 (DNV-GL Fig. 15)	4 (DNV-GL Fig. 14)
Seawater with Cathodic Protection (Various ΔK and R combinations)					
40°F, all at -1,050 mV except two C22HS at -1,200 mV, hold periods, various ΔK and R ratio-1 sample for each condition	5 (NV-GL Fig. 17)	4 (DNV-GL Fig. 20)	4 (DNV-GL Fig. 26)	4 (DNV-GL Fig. 34)	4 (DNV-GL Fig. 32)
60°F, All at -1,050 mV, various ΔK and R ratio S-1 sample for each condition	2 (DNV-GL Fig. 36a, b)	2 (DNV-GL Fig. 36a, b)	2 (DNV-GL Fig. 36a, b)	2 (DNV-GL Fig. 36a, b)	2 (DNV-GL Fig. 36a, b)
Seawater under Open Circuit Conditions					
Range of frequencies	1 (DNV-GL Figs. 37a, 39)	1 (DNV-GL Figs. 37b, 39)	1 (DNV-GL Figs. 37c, 39)	1 (DNV-GL Figs. 38b, 39)	1 DNV-GL Figs. 38a, 39)

TABLE 10 (Cont.)

Test Conditions	Alloy (UNS)				
	725 (N07725)	945x (N09946)	955 (N09955)	825 (N08825)	C22HS (N07022)
Crack Length as Function of Time (sour environment-20 w% NaCl, 125 psia CO ₂ , 0.08 Psia H ₂ S, pH = 4.0)					
Sour Environment (various ΔK, R, and hold combinations)					
350°F except 400°F for 725	1 (DNV-GL Fig. 8)	3 (DNV-GL Figs. 10, 11, 12)			1 (DNV-GL Fig. 16)
Seawater with Cathodic Protection					
Various K and varying K situations	1 (DNV-GL Fig. 18)	2 (DNV-GL Figs. 21, 22, 24a, 24b)	1 (DNV-GL Figs. 26, 27)	1 (DNV-GL Figs. 34, 35)	1 (DNV-GL Fig. 33)
Function of applied potential		1 (DNV-GL Fig. 25)	2 (DNV-GL Figs. 28, 29)		
Crack Growth Rate as Function of K and Loading Mode					
Seawater with Cathodic Protection					
Decreasing and constant K	2 (DNV-GL Fig. 19)	4 (DNV-GL Figs. 20, 23)	1 (DNV-GL Fig. 31)		
Crack Growth Rate as Function of Potential (3.5 wt% NaCl, 40 F)					
Various K (88, 92.4, 70.2, and 66 mPa/√m)			3 (DNV-GL Fig. 29)		
CCT-ASTM G150 (3.5 wt% NaCl at +750 mV, seawater, 0.2°C/min. temperature ramp) (post-test images DNV-GL Fig. 5)	2 (DNV-GL Fig. 4d)	2 (DNV-GL Fig. 4b)	2 (DNV-GL Fig. 4c)	2 (DNV-GL Fig. 4a)	2 DNV-GL Fig. 4e)

8.2 ENVIRONMENTAL CRACK GROWTH RATE SPECIMENS

The specimen configuration shown in Figure 8 was used to evaluate electrochemical behavior of a creviced materials.

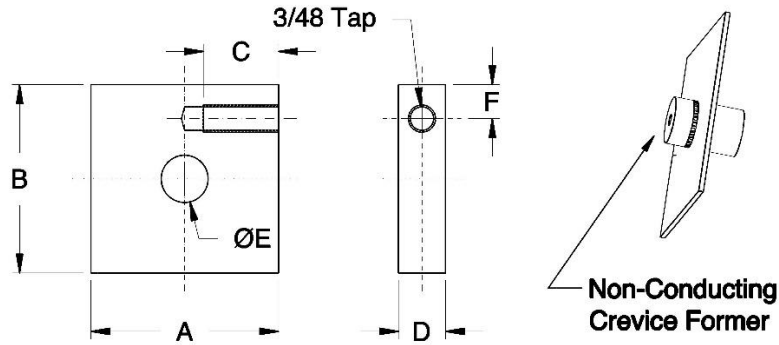


FIGURE 8 Electrochemical Behavior Specimen Form with Crevice Formers

The compact tension specimen (ASTM E399) shown in Figure 9 was used to determine if environmental cracking occurs under dynamic loading during an exposure test. For these tests, $w = 1.0$ in.

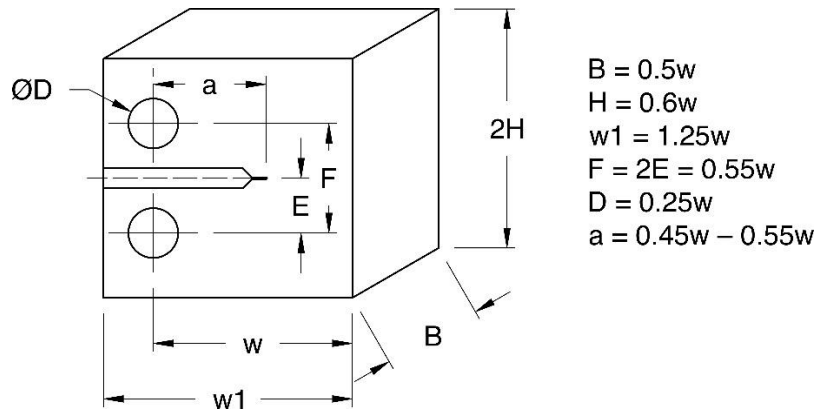


FIGURE 9 Compact Tension Specimen (ASTM E399)

8.3 SUMMARY OF ENVIRONMENTAL CRACK GROWTH TEST RESULTS

Crack growth rate experiments were conducted on pre-cracked specimens machined from the five alloys as shown in the previous section. These tests were conducted in a servo-hydraulic loading test frame that allowed for several loading variations to be performed. These crack growth experiments (FFP-type tests were based on ASTM Standard Test Method for Measurement of Fatigue Crack Growth Rates; and for exposure of specimens in an environment and ASTM E1681—Standard Test Method for Determining Threshold Stress Intensity Factor for Environmentally Assisted Crack Growth of Metallic Materials). Tests were conducted in a simulated sour production environment at elevated temperature (350°F) and in a simulated seawater environment (with and without applied cathodic potentials) at low temperatures. During the course of these tests, various test parameters (e.g., maximum loads, applied loading frequencies, static load hold times) were changed to observe their effect on the crack growth response. Major items of note from these tests were as follows.

8.4 SOUR PRODUCTION ENVIRONMENT

When an environmental effect contributes to a growing crack, the growth rate will change as the loading frequency changes. No loading frequency dependence was observed for the alloys 725, 945X, 955, or C22HS when tested in the sour environment. This means that no environmental effect contributed to the growing cracks in these tests which included a range of cyclic applied stresses. In addition, for static crack growth FFP tests these same four alloys showed no environmental effects for large applied stress intensities up to 90 ksi $\sqrt{\text{in}}$. Alloy 825 was susceptible to an environmental effect at a K_{max} value of 50 ksi $\sqrt{\text{in}}$ but displayed no effect when K_{max} was at a value of 25 ksi $\sqrt{\text{in}}$.

8.5 SEAWATER WITH CATHODIC PROTECTION ENVIRONMENT

All three of the precipitation hardening alloys in this study (i.e., 725, 945X, and 955) showed crack growth rates that were dependent on the loading frequency. In contrast, the two cold worked alloys (C22HS and 825) were loading frequency independent. This was demonstrated for two loading R ratios of 0.2 and 0.6 (where R = minimum load/maximum load during a loading cycle); Figure 10 illustrates this for the R ratio of 0.6.

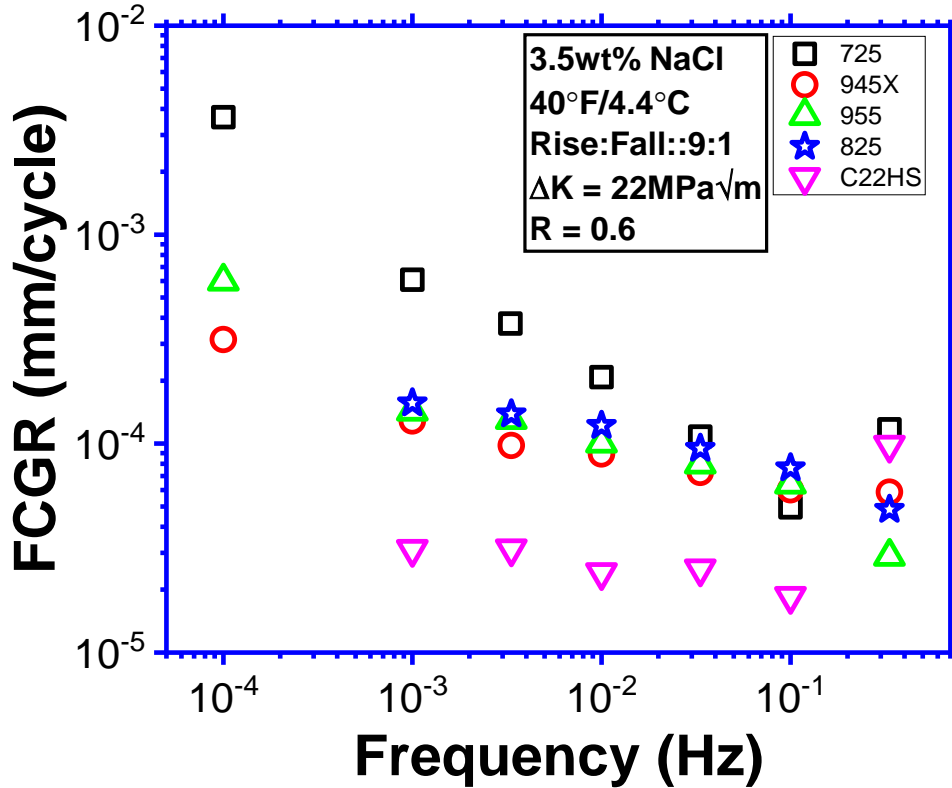


FIGURE 10 Fatigue Crack Growth Rate vs. Loading Frequency in Simulated Seawater with Cathodic Protection

During the course of these tests, hold times to impose steady applied loads were utilized. These steady loads imparted constant stress intensities upon the existing crack. This allowed for investigation into a static crack growth rate. For these alloys under applied cathodic protection, a crack growth rate of approximately 10^{-6} mm/sec was obtained for Alloy 725 at 50 ksi $\sqrt{\text{in}}$. stress intensity. This same static crack growth rate was noted for Alloys 945X and 955 when stressed to 80 ksi $\sqrt{\text{in}}$. Neither of the cold worked alloys (C22HS and 825) showed evidence of a static crack growth.

An effect of applied potential was noted for Alloys 945X and 955; the greater the applied potential, the greater the static crack growth rate. An example of this effect between -900 and -1,200 mV is shown as Figure 11 for Alloy 955.

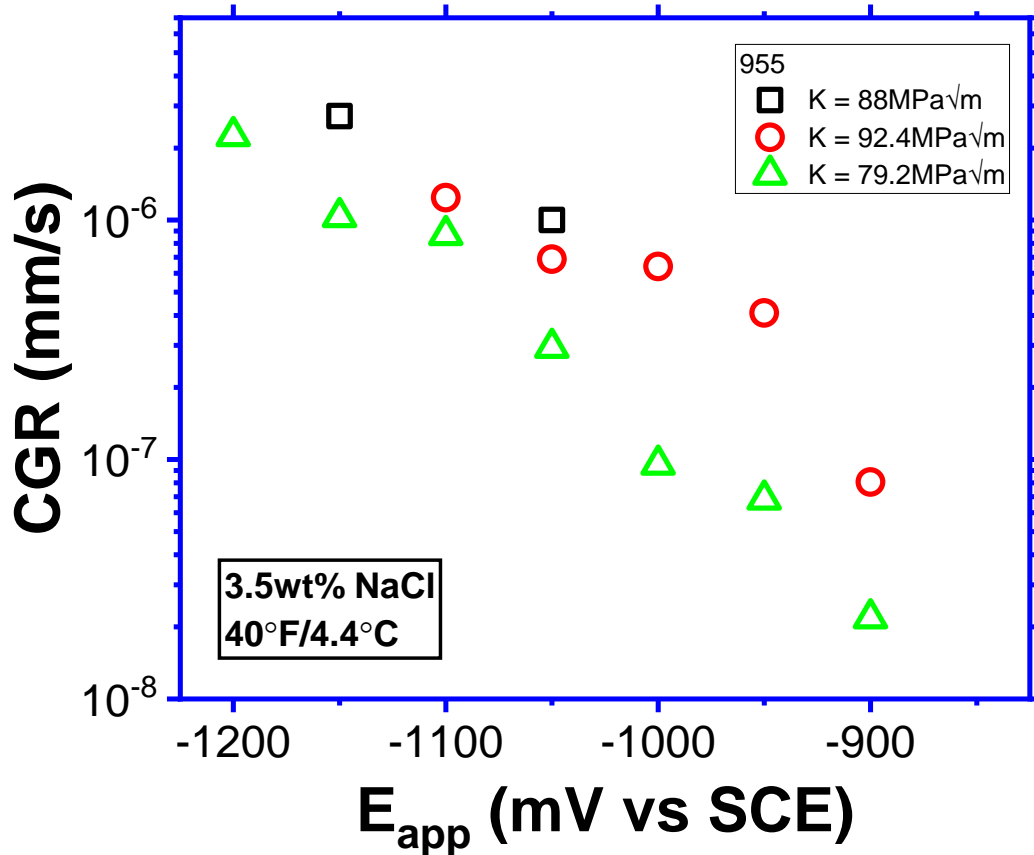


FIGURE 11 Static Crack Growth Rate of 955 in Simulated Seawater vs. Applied Potentials

8.6 SEAWATER ENVIRONMENT

Crevice corrosion in simulated seawater environment was evaluated based on ASTM G150-Standard Test Method for Electrochemical Critical Pitting Temperature Testing of Stainless Steels and Related Alloys. Creviced samples were used since these give lower and more conservative values. This evaluation method applies a potential of +700 mV (SCE) to the test specimen and measures the current density. The temperature at which the current density reaches $100 \mu\text{A}/\text{cm}^2$ is determined to be the CCT. This value can be used to determine the maximum temperature a component can expect to be free from localized corrosion. This test is considered to be conservative to also evaluate pitting, since pitting is a creviced free attack. Results are shown in Table 11.

TABLE 11 Critical Crevice Corrosion Temperature of Materials Tested in 3.5 wt% NaCl with +700 mV SCE

Alloy	Critical Crevice Temp (°C)			Crevice Corrosion
	Sample 1	Sample 2	Average	
725	67.5	65.6	66.6	Yes
945X	25.5	21.7	23.6	Yes
955	45.5	44.2	44.9	Yes
C22HS	77.1	75.6	76.4	No
825	24.8	23.5	24.2	Yes

A measure of an alloy’s resistance to pitting can be semi-quantitatively determined by its pitting resistance equivalent number (PREN). This number is determined by the chemical composition of the material and has two common formulations. These are shown below as Equations 1 and 2; plots of the critical crevice corrosion temperature data of Table 9 are then plotted versus PREN values and shown in Figure 12.

$$\text{PREN 1} = \%Cr + 1.5 (\%Mo + Nb + W) \tag{Eq. 1}$$

$$\text{PREN 2} = \%Cr + 3.3 (\%Mo) + 16(\%N) \tag{Eq. 2}$$

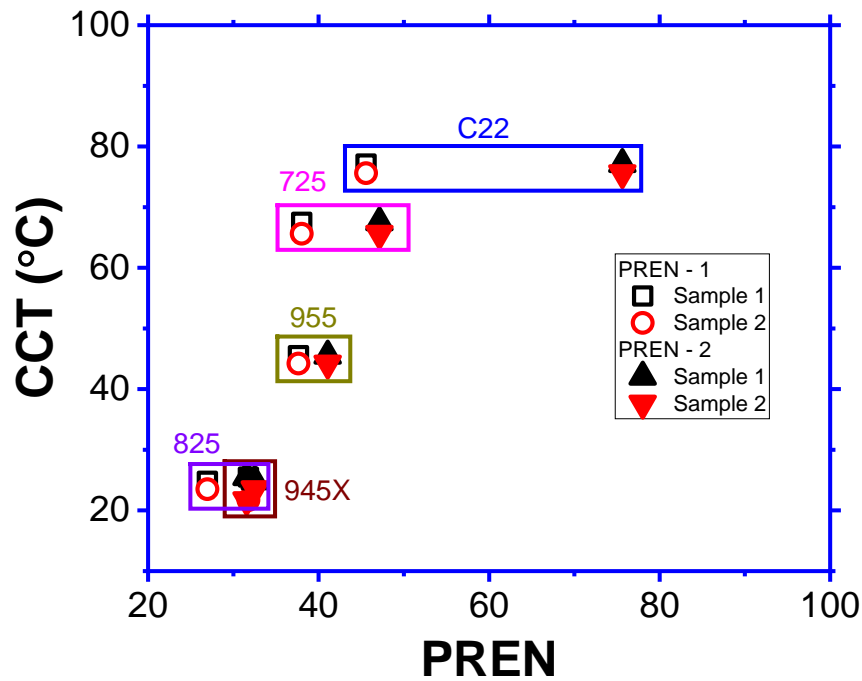


FIGURE 12 CCT vs. PREN Values for Five Alloys

Similar to the test results in the sour production environment, cyclic crack growth rate experiments conducted at 60°F showed no effect of loading frequency. This is true for all five of the alloys tested and suggests that materials under specified test conditions displayed no environmental effects. Figure 13 illustrates this point.

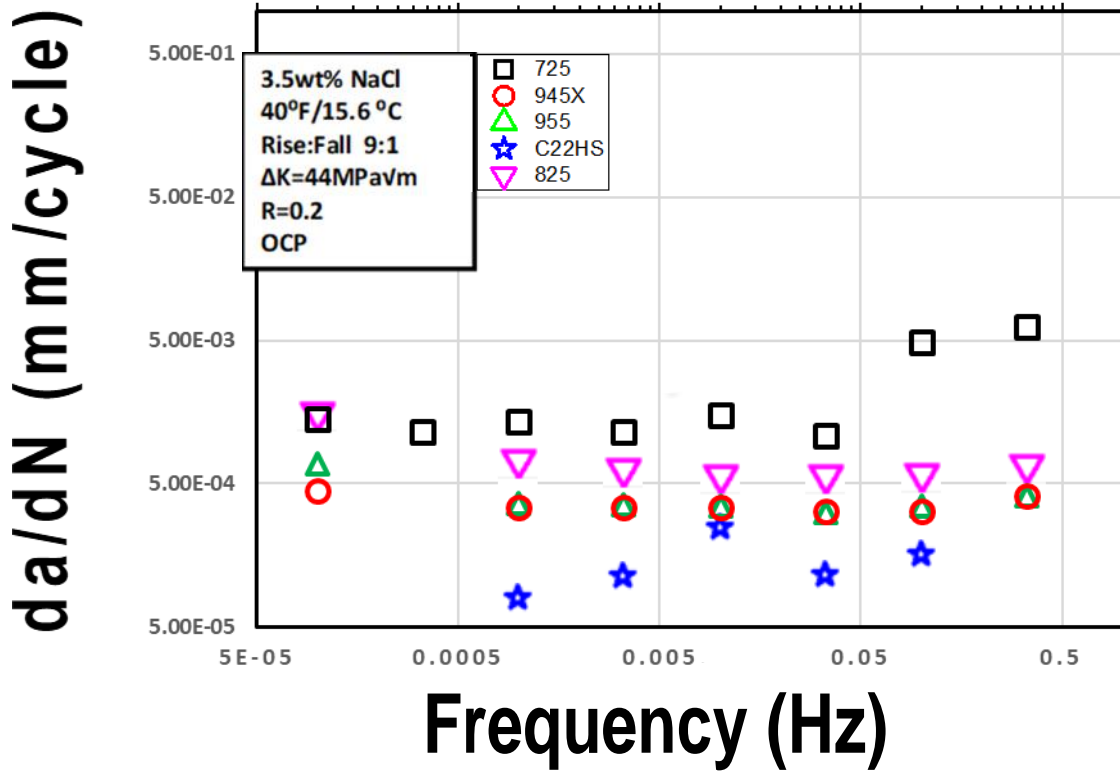


FIGURE 13 Cyclic Crack Growth Rate Versus Loading Frequency in Simulated Seawater for Five Alloys

8.7 POST-TEST MICROSCOPY ON DNV SAMPLES (ARGONNE)

This section describes microscopy work performed by Argonne.

8.7.1 Specimen Preparation

- After testing at DNV-GL, alloy specimens were cut and mounted to make cross-section samples for analysis of microstructure and cracking behavior by scanning electron microscopy (SEM) and optical microscopy. Disk specimens 3 mm in diameter were made from the section of the tested specimen far away from the crack for microstructural examination by transmission electron microscopy (TEM). SEM was performed using a Hitachi S-4700-II SEM, and TEM by a FEI Tecnai F20ST (S) TEM. Optical microscopy was performed by using a Moticam 580 microscope. To obtain detailed information, examination of the cross-section specimen was conducted before and after etching. The five alloys examined in this study demonstrated excellent resistance to corrosion. Each alloy has a best etching condition. Three etching conditions were used to achieve the best etching results.
- Etching condition 1: Waterless kalling’s reagent (5 g CuCl₂ + 100 cc HCl +100 cc ethyl alcohol),
- Etching condition 2: 30 mL HCl + 10 mL HNO₃ + 30 mL H₂O, and
- Etching condition 3: 30 mL HCl + 10 mL HNO₃ + 30 mL H₂O + 6 V electrochemical etching.

Times and condition of the etching processes is further defined in Table 12.

TABLE 12 Etching Condition for Each Alloy

Etching Condition	Alloy 725	Alloy 945X	Alloy 955	Alloy 825	Alloy C22HS
1			20 minutes		
2		10 minutes		2 minutes	
3	1 minute				3 minutes

Alloy materials were separated into two groups for post-test microscopy analysis, namely, precipitation hardening alloys (725, 945X, and 955) and work hardening alloys (825 and C22HS). As explained in the following sections, analysis for the two groups differs slightly.

8.7.2 Precipitation Hardening Alloys (725, 945X, and 955)

8.7.2.1 Optical and SEM Microscopy of PH Materials

The cracking behavior of tested compact tension specimens of precipitation hardened alloys, 725, 945X and 955 was investigated by optical and scanning electron microscopy. These specimens were tested in a 3.5 wt% NaCl electrolyte with a potential of -1050 mV/Saturated Calomel Electrode (SCE). Figure 14 shows an overview of the SCC crack of the polished specimen of Alloy 725. To obtain the detailed information on grain, the specimen was electrochemically etched by the etching condition 3. Optical microscopy of the etched specimen revealed that Alloy 725 had equiaxed grains with the grain size of 50–100 μm (Figure 15). Both SEM and optical microscopy show that the SCC cracks in Alloy 725 are predominantly intergranular. A high density of voids formed at grain boundaries, as shown in Figure 16 where the crack end was imaged. No evident slip traces were observed within grains of Alloy 725. It was suggested that that grain boundary cavitation was the primary failure mechanism in Alloy 725.

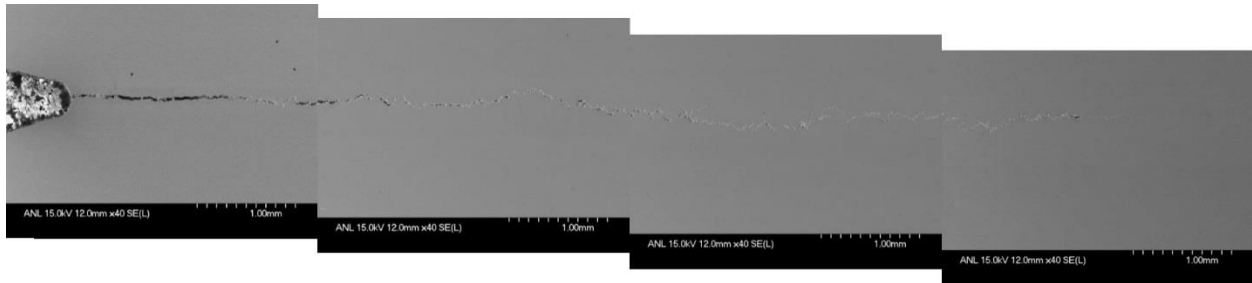


FIGURE 14 Overview of the Crack Observed in the Tested Alloy 725 specimen before Etching

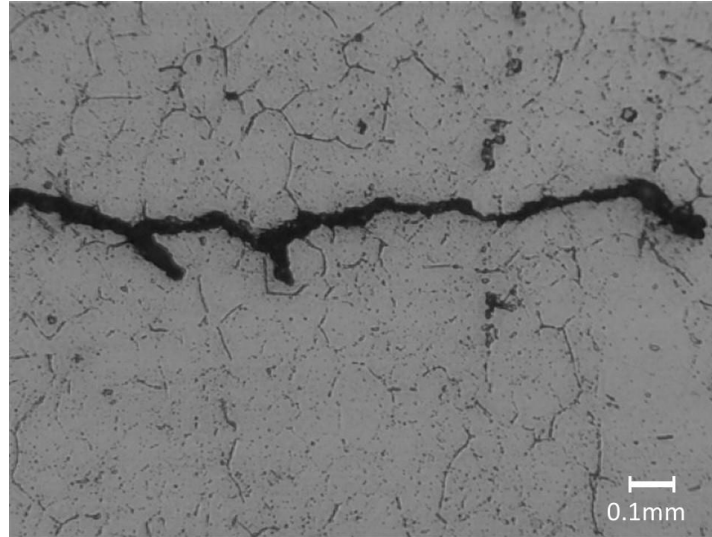


FIGURE 15 Optical Image of the Cracked Alloy 725 Specimen

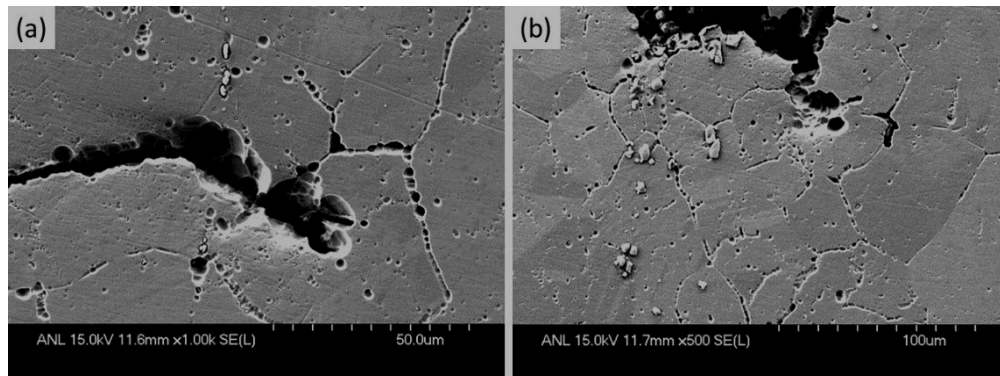


FIGURE 16 SEM Image Showing Grain Boundary Void Formation in Alloy 725

Figure 17 shows the grain structure and the cracking behavior in Alloy 945X. Annealing twins are prevalent in the alloy. The SCC crack path in Alloy 945X is primarily intergranular. In contrast to Alloy 725, no significant grain boundary voids were observed in Alloy 945X, and slip bands were clearly revealed within grains along the crack path in Alloy 945X, as shown in Figure 18. In some grains slip bands are oriented in one direction, and propagate into the neighboring grain (Figure 18b and c), while in some other grains, slip bands developed in two shear directions (Figure 18d). Slip bands observed in Alloy 945X are straight and continuous inside a grain, and have fine spacing between them.

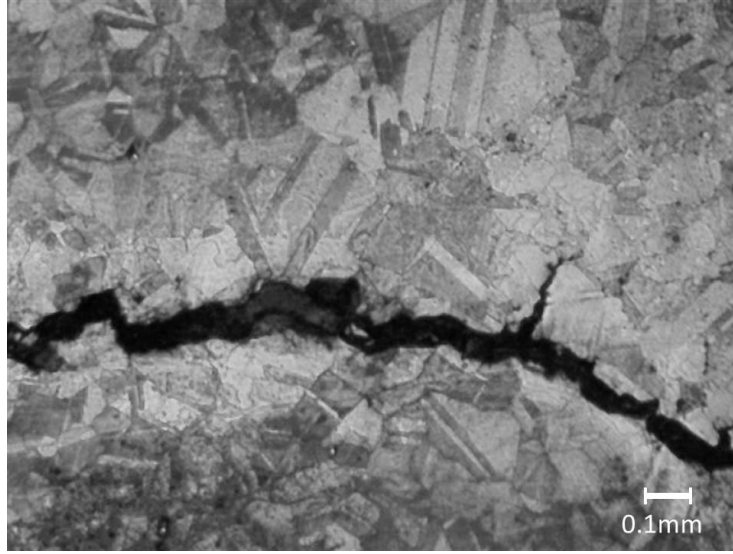


FIGURE 17 Optical Image of Alloy 945X Showing the Grain Structure and Cracking Behavior

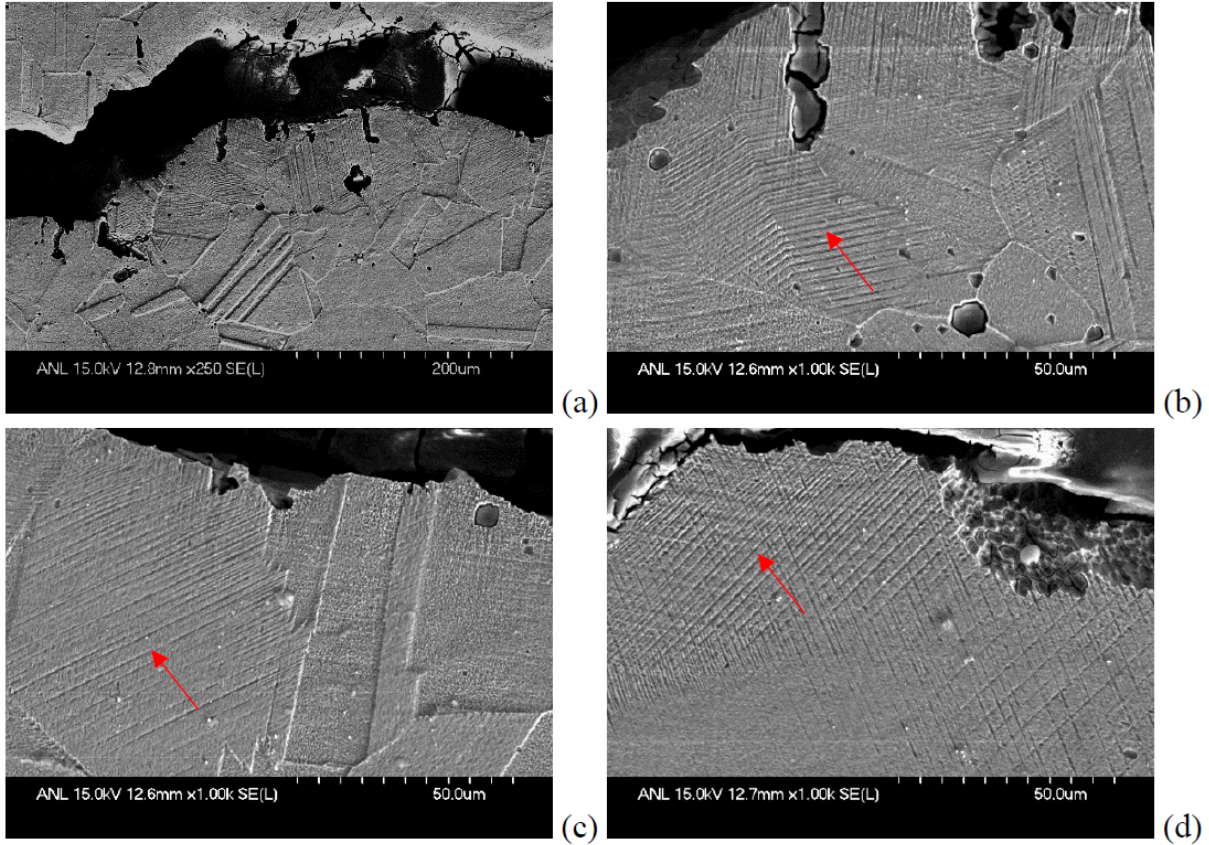


FIGURE 18 SEM Images Revealing Slip Bands (indicated by arrows) Formed within Grains along the Crack in Alloy 945X

Figure 19 shows the grain structure and the cracking behavior in Alloy 955. Similar to Alloy 945X, annealing twins are observed in Alloy 955. Like the other two PH Alloys of 725 and 945X, the SCC cracks in Alloy 955 are also intergranular. Similar to Alloy 945X, no grain boundary dimpled fracture was observed in Alloy 955. However, unlike Alloy 945X, slip bands were not clearly revealed in Alloy 955, as shown in Figure 20. Apparently grain boundary brittle fracture is dominant in Alloy 955.

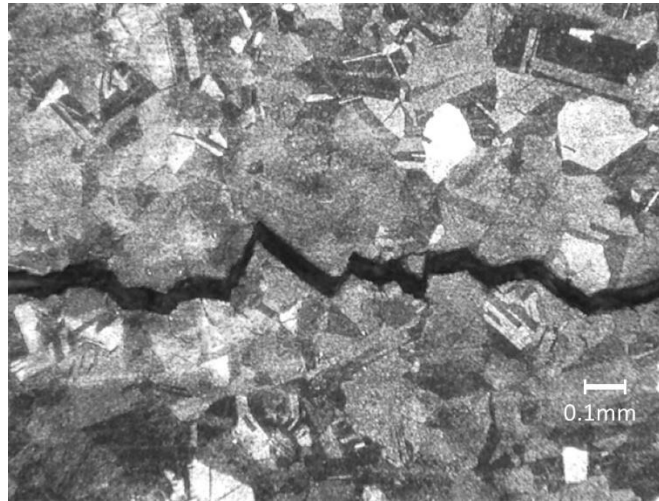


FIGURE 19 Optical Image Showing the Grain Structure and Cracking Behavior in Alloy 955

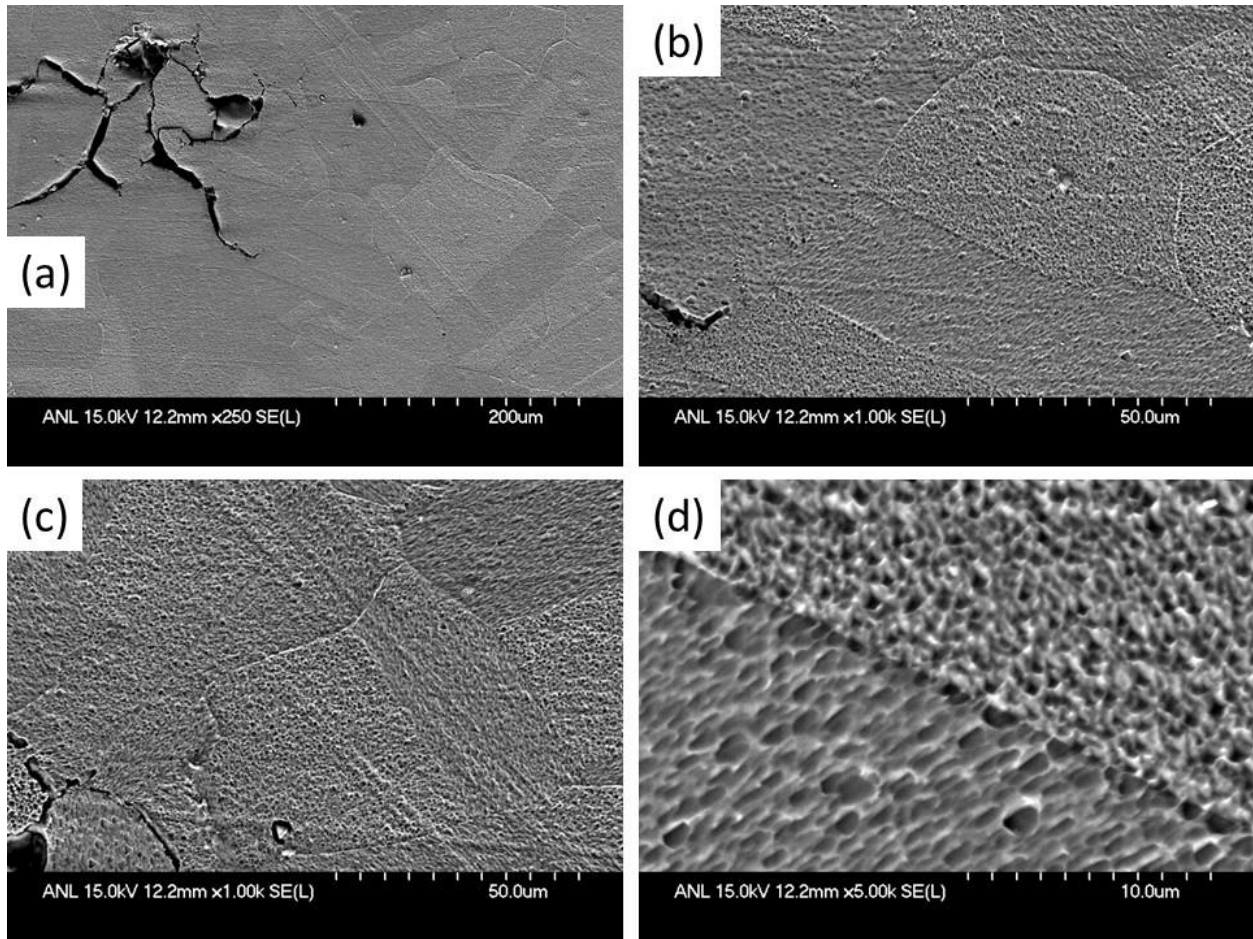


FIGURE 20 SEM Images of Alloy 955 after Etching

8.7.2.2 TEM Microscopy of PH Alloys

TEM was carried out to examine the microstructure of the alloys. Figure 21a shows the high-angle annular dark field (HAADF) image at the low-magnification. A high density of precipitates was observed at grain boundaries. The EDS elemental mapping of the same area indicates that these grain boundary precipitates are a mixture of $M(Cr,Mo)_{23}C_6$ carbides, $M(Nb,Ti)X(C,N)$ carbon-nitrides, and MoS sulphides. These precipitate particles were also observed inside grains with a lower number density (Figure 22). A high density of nano-size (~ 10 nm) precipitates of γ'' and γ' were observed within the grains in Alloy 725, as shown in Figure 23. The chemistry and crystal structure of the precipitates were verified by both EDS mapping and electron diffraction.

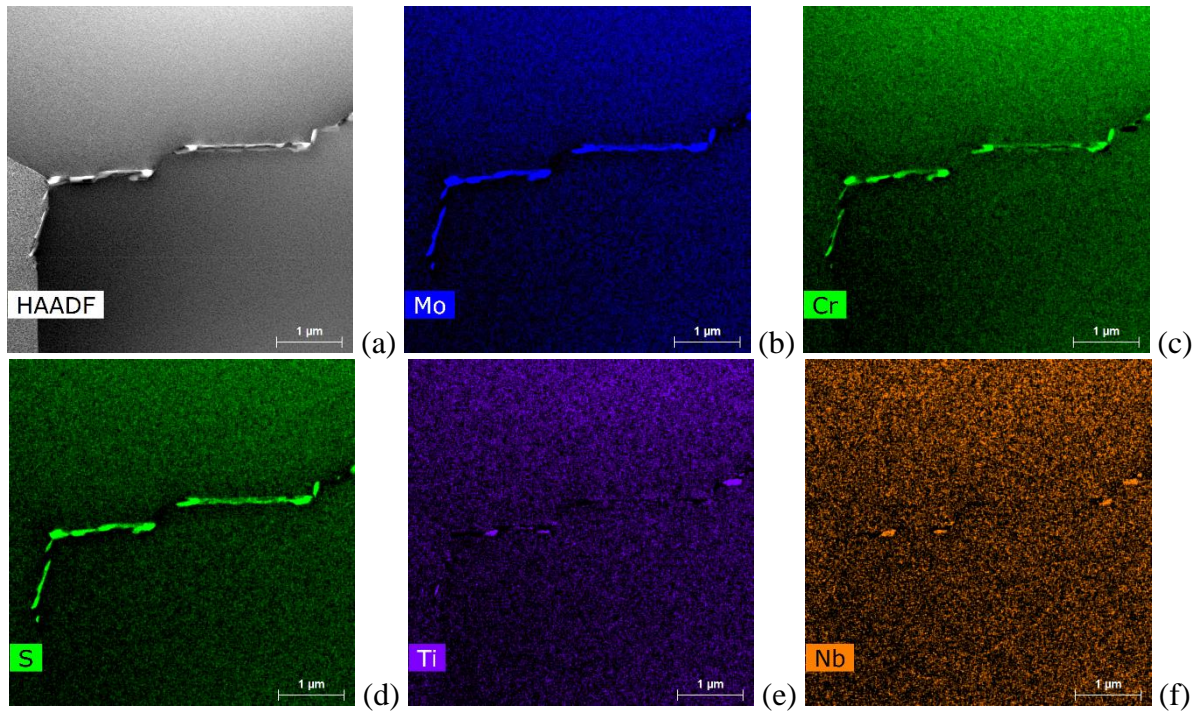


FIGURE 21 (a) TEM HAADF Image Showing Grain Boundary Precipitates; (b)–(f) EDS Elemental Mapping of Mo, Cr, S, Ti, and Nb in the Same Area in Alloy 725

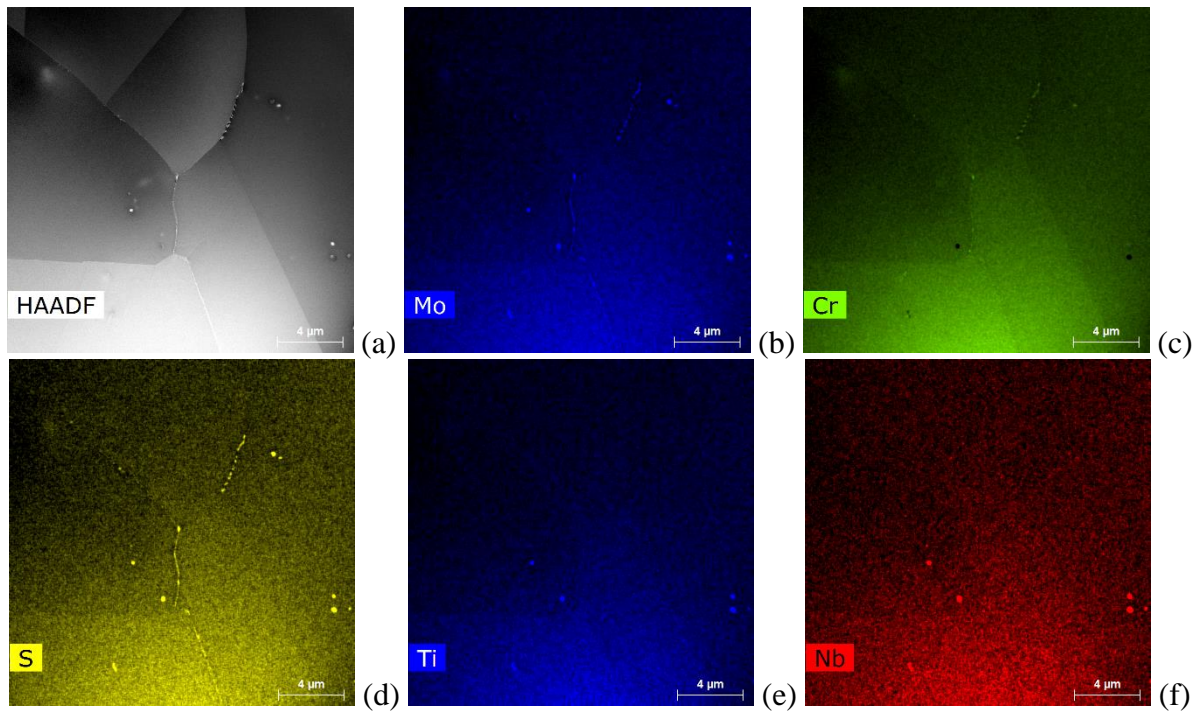


FIGURE 22 (a) TEM HAADF Image Showing Precipitates at Grain Boundaries and within Grains; (b)–(f) EDS Elemental Mapping of Mo, Cr, S, Ti, and Nb in the Same Area of (a) in Alloy 725

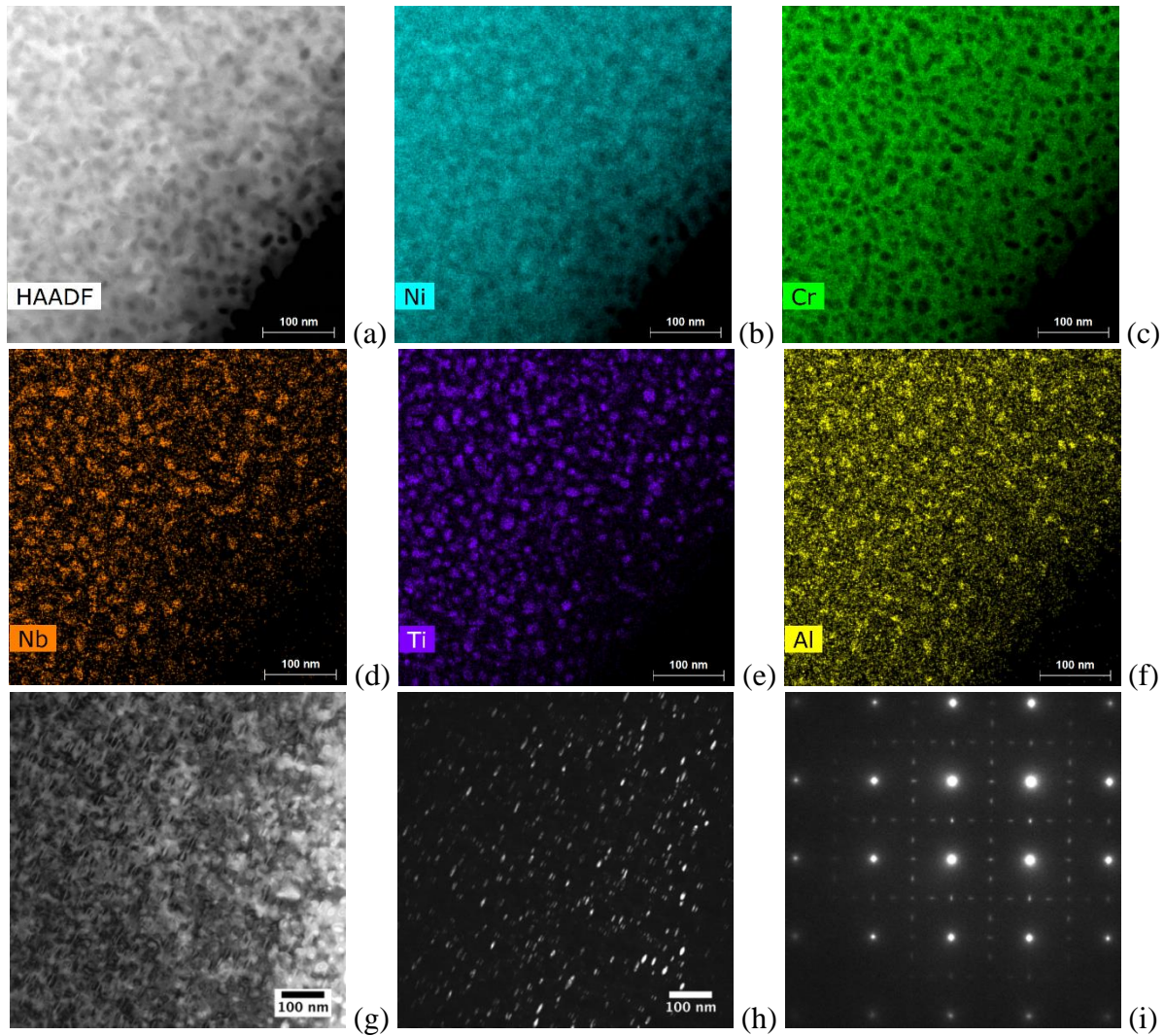


FIGURE 23 (a) TEM HAADF Image Showing Nano-Sized Precipitates in the Matrix; (b)–(f) EDS Elemental Mapping of Ni, Cr, Ti, Nb, and Al in the Same Area of (a); (g) Bright-Field Image; (h) Dark-Field Image; and (i) Electron Diffraction Pattern Showing the Precipitates in the Matrix in Alloy 725

Alloy 955 and Alloy 945X show similar precipitation of γ' and γ'' within the grains. The grain boundary precipitation in Alloy 945X and Alloy 955 is significantly less than in Alloy 725. Figure 24 shows the nano-sized precipitates in the matrix in Alloy 945X. Figures 25 and 26 show the nano-sized precipitates observed in the matrix and grain boundary precipitates in Alloy 955. The grain boundary precipitation in Alloy 945X and Alloy 955 is significantly less than in Alloy 725.

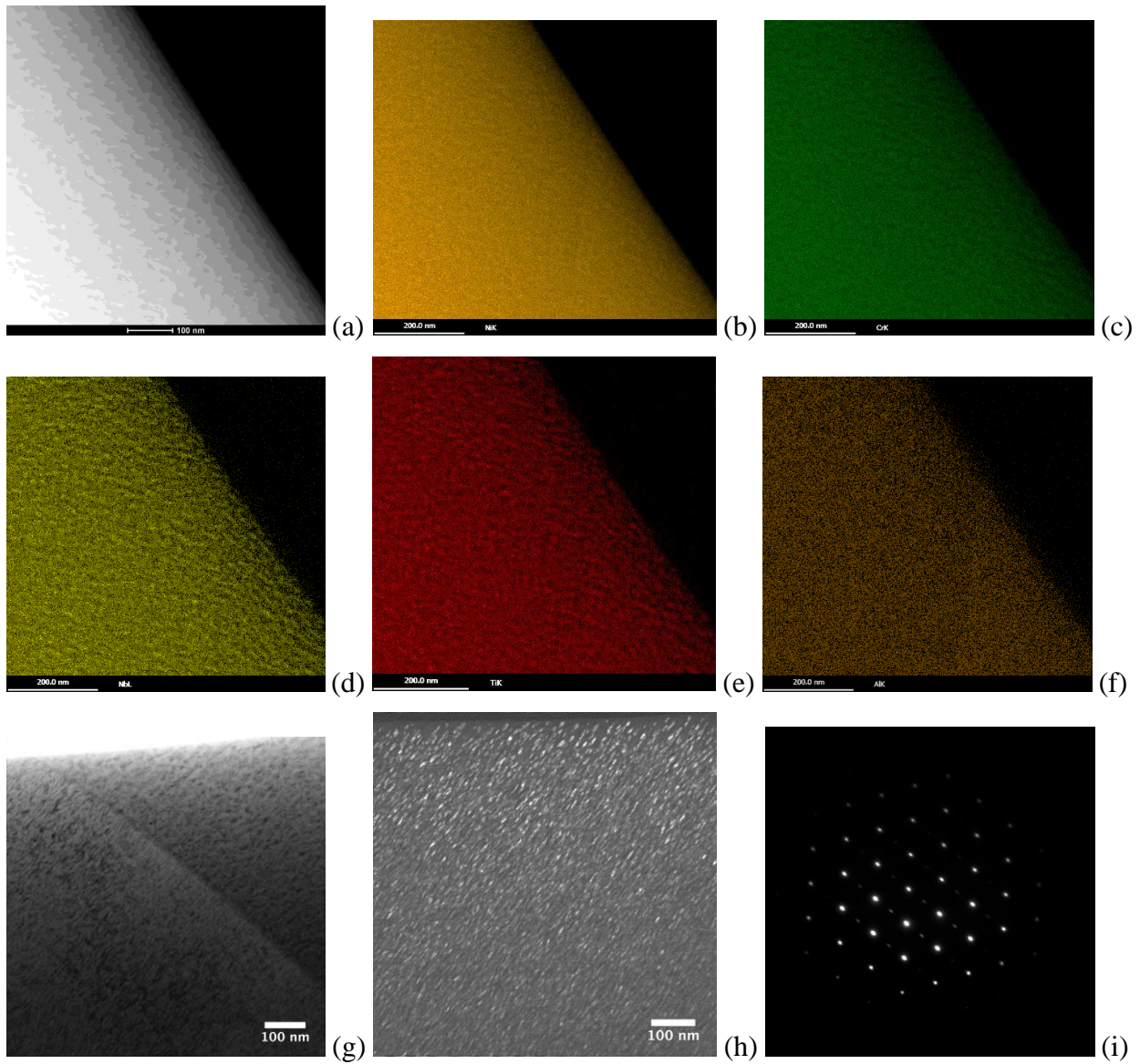


FIGURE 24 (a) TEM HAADF Image Showing Nano-Sized Precipitates in the Matrix; (b)–(f) EDS Elemental Mapping of Ni, Cr, Ti, Nb, and Al in the Same Area of (a); (g) Bright-Field Image; (h) Dark-Field Image; and (i) Electron Diffraction Pattern Showing the Precipitates in the Matrix in Alloy 945X

945X

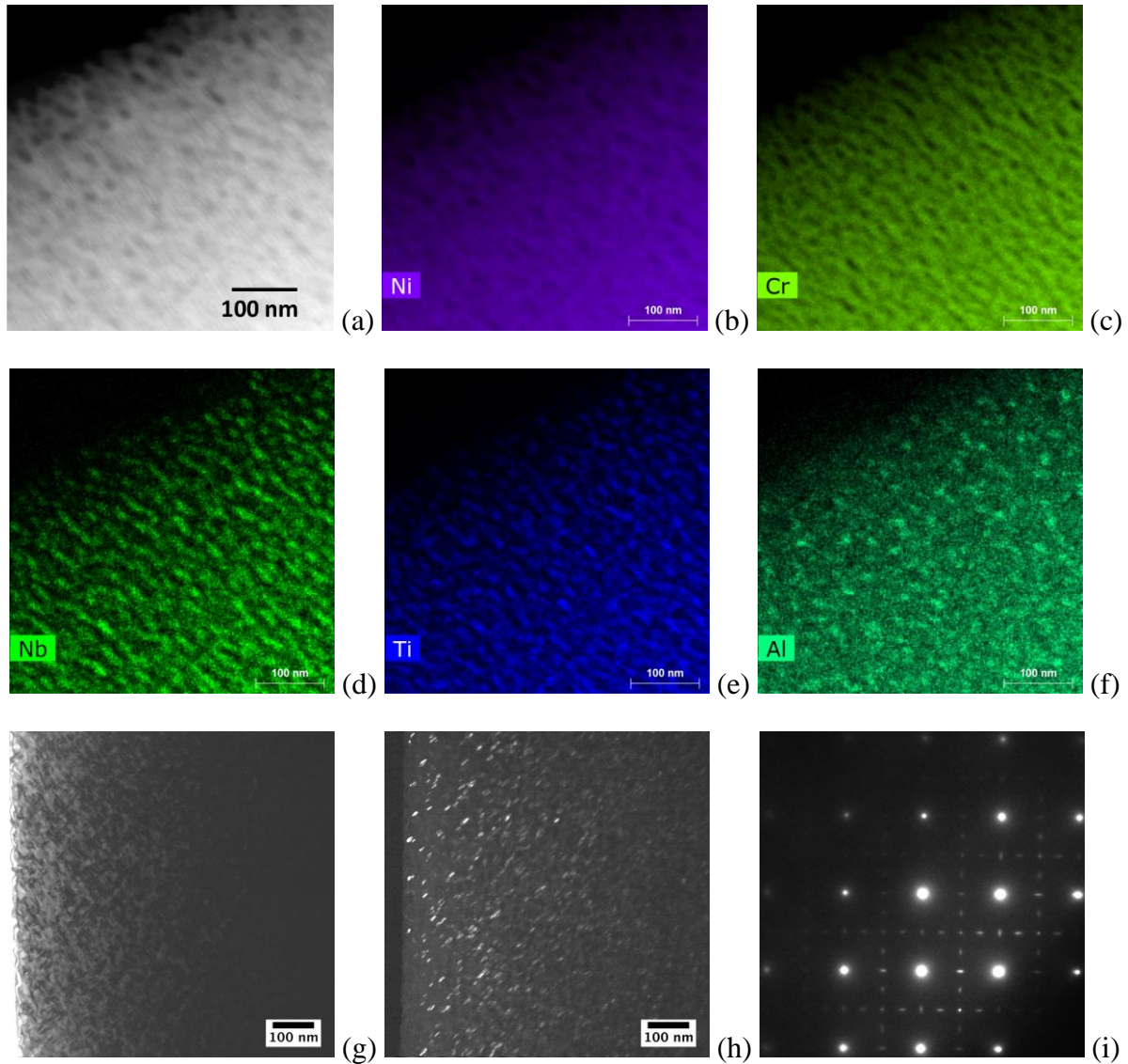


FIGURE 25 (a) TEM HAADF Image Showing Nano-Sized Precipitates within Grains; (b)–(f) EDS Elemental Mapping of Ni, Cr, Ti, Nb, and Al in the Same Area of (a); (g) Bright-Field Image; (h) Dark-Field Image; and (i) Electron Diffraction Pattern Showing the Precipitates within Grains in Alloy 955

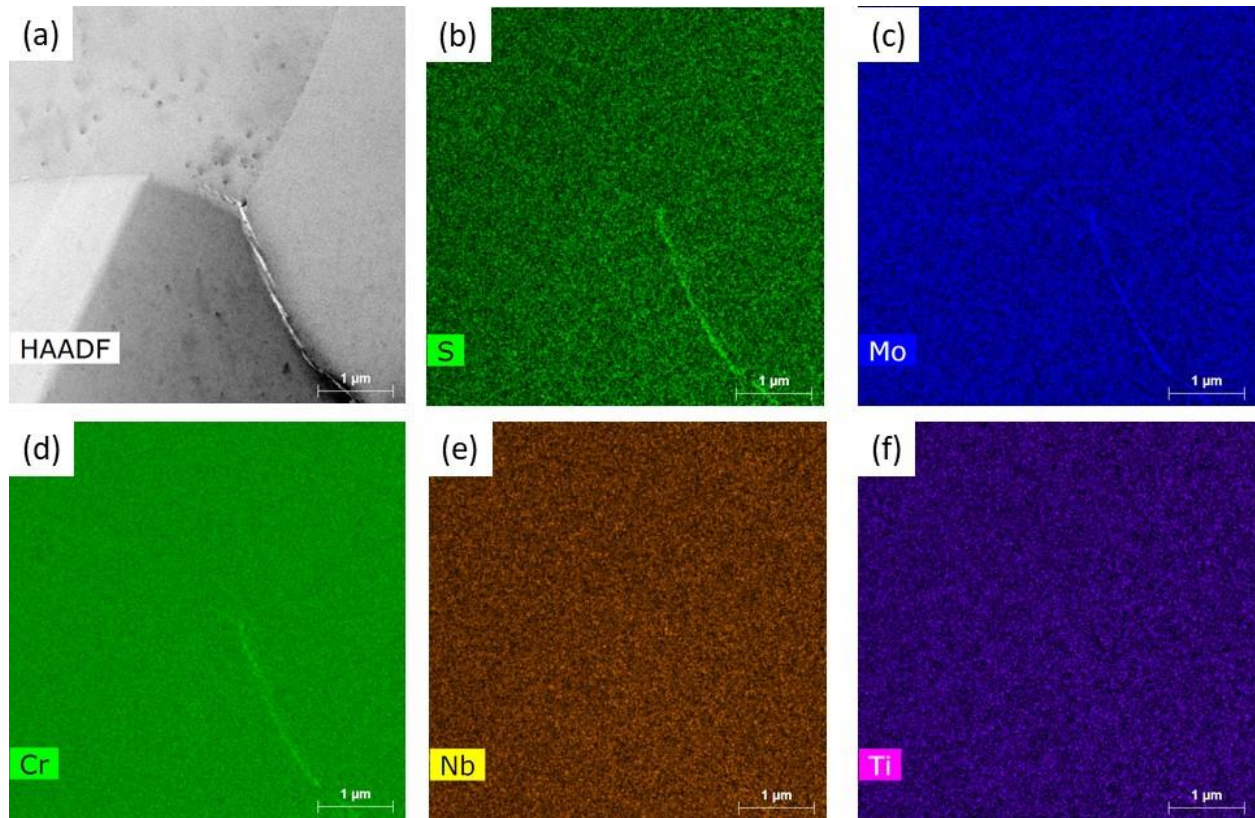


FIGURE 26 (a) TEM HAADF Image Showing Grain Boundary Precipitates and (b)-(f) EDS Elemental Mapping of Mo, Cr, S, Ti, and Nb in the Same Area of (a) in Alloy 955

8.7.3 Work Hardening Alloys (825 and C22HS)

8.7.3.1 SEM of Work Hardening Alloys

Figure 27 shows the cracks developed in Alloy 825, which are predominantly transgranular, in contrast to grain boundary cracking observed in precipitation-hardened alloys. Figure 28 shows the slip bands formed in Alloy 825 during the SCC test. Compared with Alloy 945X, the slip bands developed from plastic deformation in Alloy 825 are wavy, suggesting multiple slips in Alloy 825.

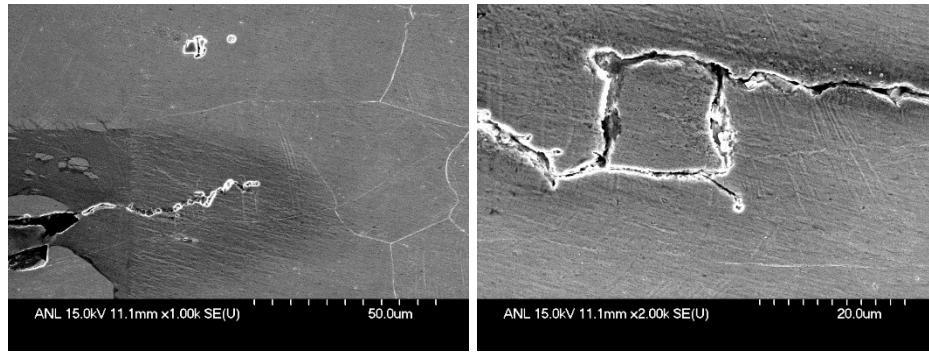


FIGURE 27 Cracks Developed in Alloy 825 During the SCC Test

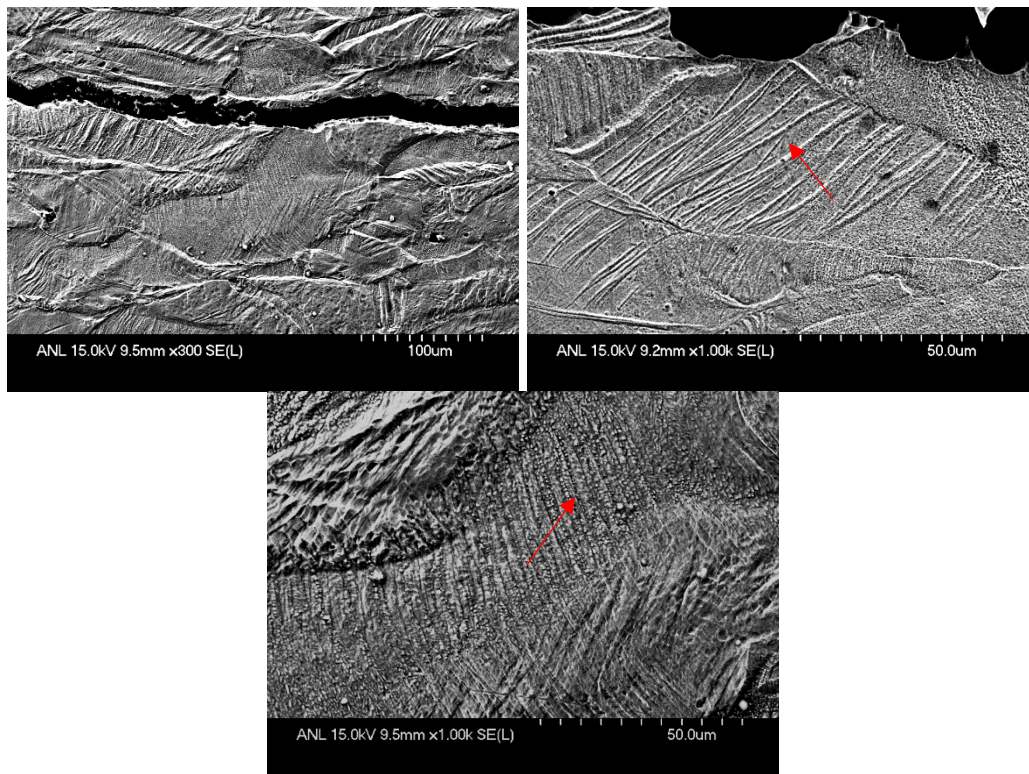


FIGURE 28 SEM Images Showing the Slip Activities (indicated by arrows) along the Crack in Alloy 825

8.7.3.2 TEM of Work Hardening Alloys

TEM of the microstructure of Alloy 825 revealed a mixture of large grains and columnar grains formed in Alloy 825 (Figure 29). A high number density of dislocations was observed in large grains. No precipitates were observed at grain or subgrain boundaries.

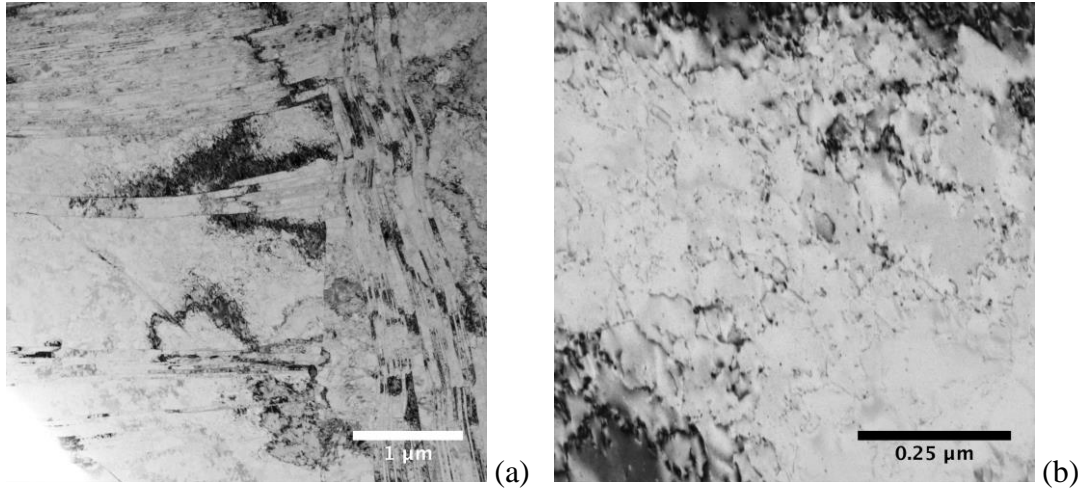


FIGURE 29 TEM Bright-Field Images Showing (a) the Grain Structure and (b) the Dislocation Density within the Grain in Alloy 825.

An overview of the SCC crack developed in Alloy C22HS is given in Figure 30. While the crack propagated in a normal direction to the tensile stress for the majority of the test, it grew in opposite directions along the stress direction at the later stage of the test. Alloy C22HS shows highly elongated grain structure, as shown in Figure 30. Slip bands were also observed in Alloy C22HS after test (Figure 31), but less pronounced compared to Alloy 825.

Figure 31 shows the microstructure of Alloy C22HS observed under TEM. The microstructure consists of a high density of dislocations and deformation bands. No precipitates at grain boundaries were easily observed in C22HS.

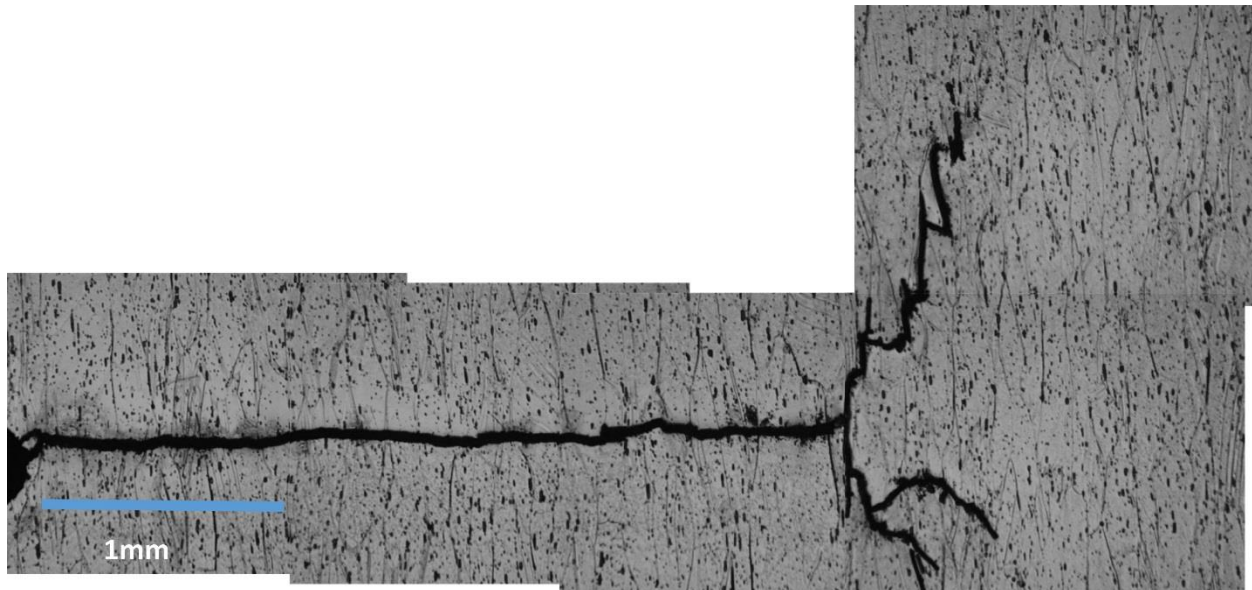


FIGURE 30 Overview of the Crack Developed During the SCC Test in Alloy C22HS

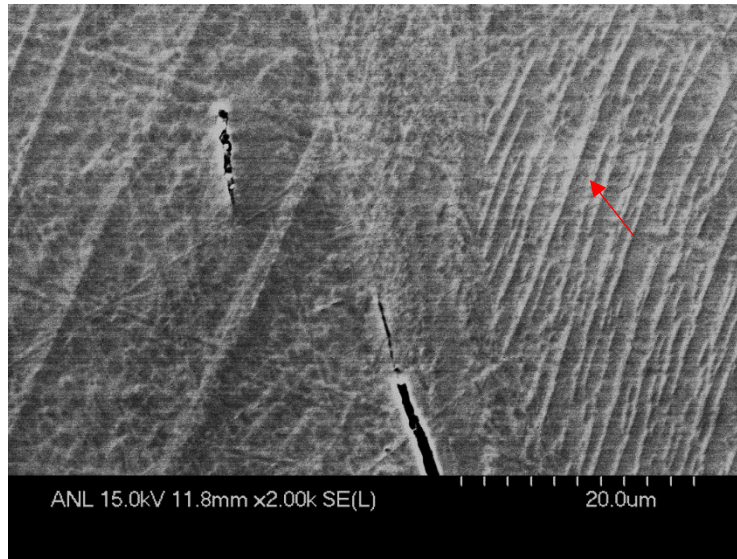


FIGURE 31 SEM Image Showing the Slip Activities (indicated by arrow) along the Crack in Alloy C22HS

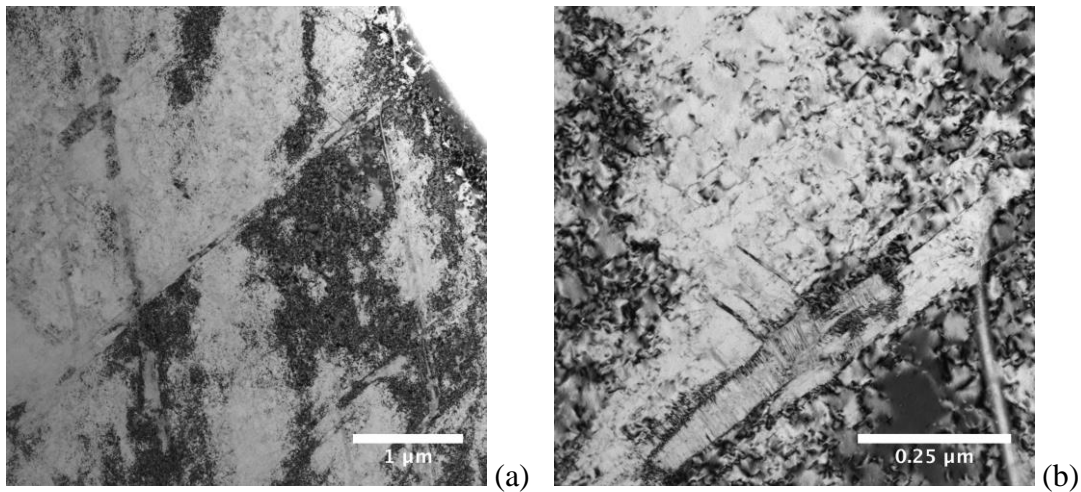


FIGURE 32 TEM Bright-Field Images Showing the Microstructure of Alloy C22HS (a) Low-Magnification Image and (b) High-magnification Image

8.7.4 Microscopy Summary

In summary, the three precipitation hardening alloys (725, 945X, and 955) showed predominantly intergranular cracking, while the two work hardening alloys (825 and C22HS) showed primarily transgranular cracking. Among the three precipitation hardening alloys, Alloy 725 shows dimpled grain boundary fracture, and Alloy 945X and Alloy 955 showed grain boundary brittle fracture. High-density, straight, and fine-spaced slip bands were developed by

plastic deformation within grains along the crack in Alloy 945X, while no significant slip bands were observed inside grains in Alloy 955.

Intergranular fracture is the decohesion of the weakened grain boundary. It appears that different grain boundary weakening mechanisms caused intergranular fracture in the three precipitation hardening alloys. TEM revealed a high density of particles precipitated at grain boundaries in Alloy 725, particularly MnS particles. Void nucleation at precipitates at the grain boundary and coalescence can result in grain boundary cracking observed in Alloy 725. The lack of slip activity within grains implies that the cohesive strength of the particle-boundary interface in the local region of the grain boundary is below the yield strength of the grain interior, and cracks tend to develop first with the grain boundary zone by microvoid coalescence. Accumulation of hydrogen at the particle interface in the grain boundary region can significantly reduce the particle cohesive strength, resulting in the hydrogen-enhanced decohesion of grain boundary particles.

In contrast to Alloy 725, a much lower density of grain boundary precipitates was observed in Alloy 945X and Alloy 955. It is noted that the molybdenum and niobium contents in Alloy 945X are less than that in Alloy 725, which may reduce the grain boundary precipitation in Alloy 945X. The planar slip activity observed in Alloy 945X implies that hydrogen-enhanced localized plasticity is the primary embrittlement mechanism in Alloy 945X. Accumulation of hydrogen at the intersection of planar slip bands results in high hydrogen susceptibility, and therefore brittle grain boundary fracture.

The lack of grain boundary voids and slip activity within grains in Alloy 955 suggests that the major cause of the intergranular fracture in Alloy 955 is the presence of grain boundary embrittling elements, e.g., sulfur. These elements in combination with hydrogen can lower the cohesive strength of the grain boundary, causing the brittle fracture at the grain boundaries. It also implies that the yield strength of the grain interior due to the formation of a high density of γ'' and γ' nanoparticles in the matrix is significantly higher than the cohesive strength of the grain boundary in Alloy 955, reducing the slip activity in Alloy 955 in the matrix at the crack tip. More detailed analysis of γ'' and γ' nano-precipitates in the matrix in Alloy 945X and Alloy 955 is needed to verify this hypothesis.

The heavily deformed microstructure in single-phased Alloy 825 and C22HS is associated with the transgranular (or a combination of transgranular and intergranular) cracking. The slip bands observed in these two work-hardening alloys may be associated with the formation of persistent slip bands developed under cyclic loading.

9 C-RING AND CORROSION RATE RESULTS SUMMARY (HCS)

C-Ring and corrosion rate laboratory work was performed at HCS as described and summarized in Table 13. Their entire report is included as Appendix C of this report. Some of the more relevant results are summarized and repeated in this section. HCS choose to identify pitting on the basis of visual inspection at 45 and 100X and no pitting was identified. To confirm this, Argonne obtained images at higher magnifications for comparison as given in Section 9.4 below. The 945X results are not consistent since both samples broke after 6 weeks of exposure but did not break at the longer exposure. Section 9.5 describes Argonne's microscopy work to compare the 945X material compositions.

9.1 TEST AND DATA MATRIX

Table 13 lists the HCS C-ring and corrosion coupon tests. All tests were performed in high pressure autoclaves. As described previously these are FFP tests that were chosen to answer "what-if" scenarios. The tests are longer duration (6, 12, 18, and 48 weeks) than specified as minimums in ANSI/NACE TM0177 (720 hours). In addition, tests were at pressure and temperature rather than ambient conditions.

TABLE 13 Test Matrix—Numbers of Tests by Alloy and Summaries of Test Conditions for C-Ring and Corrosion Testing (HCS)^a

Duration	Alloy (UNS)				
	725 (N07725)	945x (N09946)	955 (N09955)	825 (N08825)	C22HS (N07022)
Corrosion Coupons (for corrosion rate and pitting)					
6 weeks ^b (HCS Table 12)	2	2	2	2	2
12 weeks (HCS Table 14)	2	2	2	2	2
18 weeks (HCS Table 16)	2	2	2	2	2
48 weeks (HCS Table 18)	2	2	2	2	2
C-Ring (stress corrosion cracking-SCC rings stressed to 100% average yield strength at 350°F) ^c					
6 weeks (HCS Table 13)	1	1	1	None ^d	1
12 weeks ^e (HCS Table 15)	1	1	1	None	1
18 weeks ^f (HCS Table 17)	1	1	1	None	1
48 weeks (HCS Table 19) ^g	1	1	1	None	1
C-Ring (galvanic hydrogen stress cracking-GHSC rings stressed to 100% average yield strength at 350°F)					
6 weeks (HCS Table 13)	1	1	1	None	1
12 weeks (HCS Table 15)	1	1	1	None	1

^a Corrosion (coupon), Stress Corrosion Cracking (C-ring) and Galvanic Stress Corrosion Cracking (C-ring) Testing in autoclave at 15,000 psig and 350°F. Corrosion Testing (gases 3.3 ppmv H₂S, 8.325 ppm CO₂ balance Methane at 15,000 psig and 350°F and partial pressures of CO₂ and H₂S respectively of 0.05 psia and 125 psia, Brine-20 wt% NaCl with pH 4.0 at atmospheric pressure and room temperature). (Note: See Table 7 of HCS report in Appendix C for complete brine composition. Environment replenished at 6-week intervals.)

^b No brine replenishments.

^c C-Ring tests conducted at critical strain for 350°F.

^d No 825 C-Rings produced. Product was not available in tubular form.

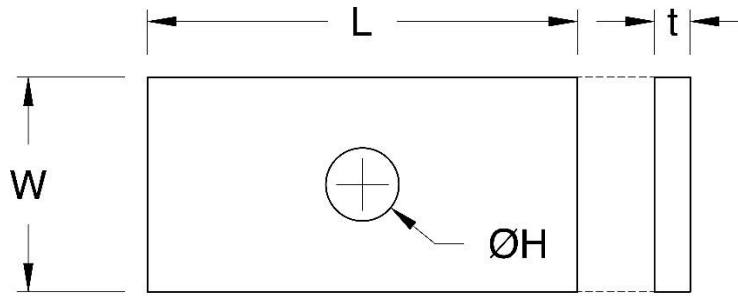
^e One brine replenishment.

^f Two brine replenishments.

^g Seven brine replenishments.

9.2 CORROSION AND C-RING TEST SPECIMENS

The exposure specimen used for corrosion rate determinations and for detecting presence of pitting from high-pressure autoclave testing is shown in Figure 33. Figures 34 and 35 show details of the C-ring tests, no galvanic contact and galvanic contact respectively.



Length (L) = 1.5 ± 0.01 inches
 Width (W) = 0.75 ± 0.01 inches
 Thickness (t) = 0.125 inches nominal
 Mounting Hole Dia (H) = 0.255 inches

FIGURE 33 Exposure Coupon For Corrosion Rate Determinations

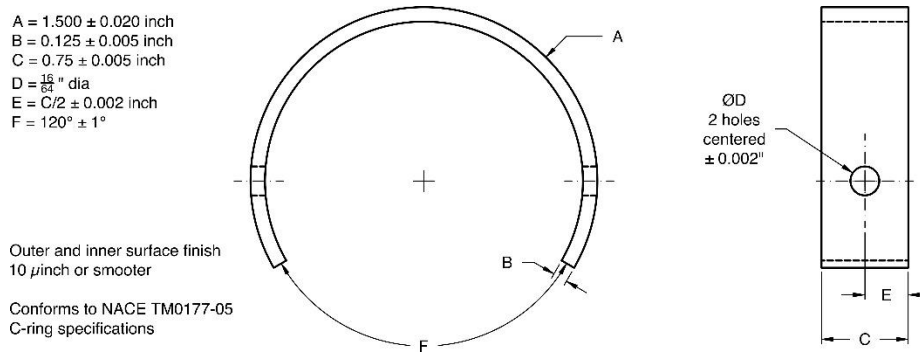


FIGURE 34 C-Ring Test Specimen Details

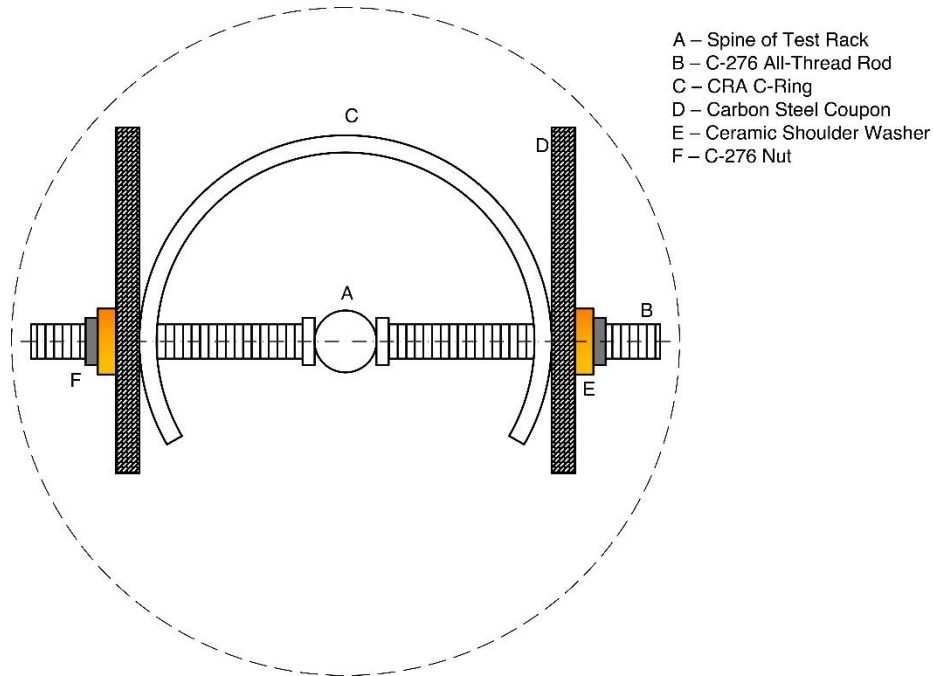


FIGURE 35 Galvanic C-Ring Test Specimen and Steel Contact Details

9.3 SUMMARY OF HCS RESULTS

The detailed final report from HCS is included as Appendix C. In terms of cracking of stressed specimens, there were two unanticipated failures (i.e., cracked specimens). These two specimens were both from the 6-wk exposure test and were both fabricated from the same 945X material. The HCS report concluded that these two failures were “anomalous” since the other specimens of this alloy survived intact after the 12, 18, and 24-week exposures. This will be discussed further in Section 9.5 of this report.

The HCS effort provides statistics on the corrosion rates of the materials from the four exposure times. These results are shown in Tables 20 and 21 of their report. In terms of corrosion rates, the range spanned from 0.035 to 1.177 $\mu\text{m}/\text{yr}$. A simpler way to see how these materials compared in terms of corrosion rate over time is included here as a plot of average corrosion rates for the four HPHT exposure times. This is shown as Figure 36. Also included in Figure 36 is an approximate fit of the data to illustrate the noted trend in the data over time. In particular, high corrosion rates were observed initially and remain relatively constant for longer exposures, then tapering off and remaining fairly steady over time as they seem to approach an asymptote.

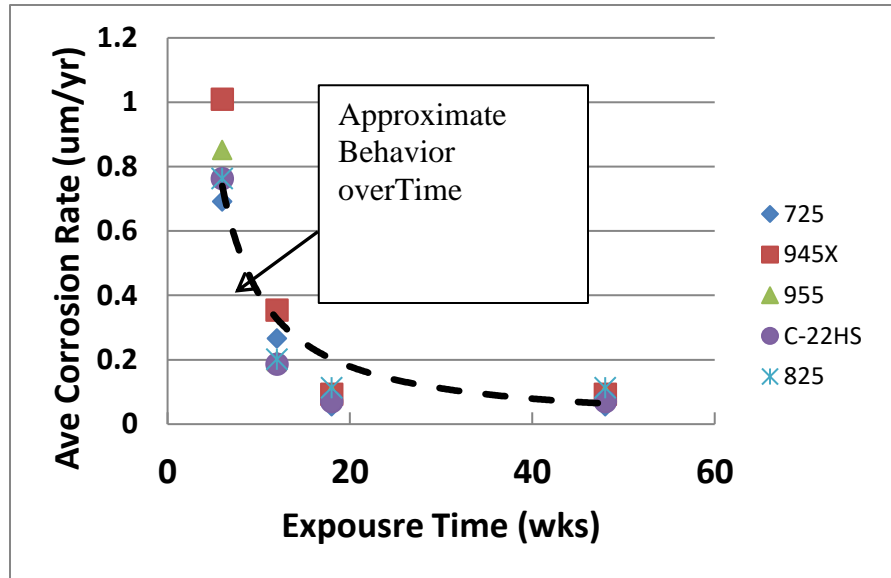


FIGURE 36 Plot of Average Corrosion Rate Under HPHT Conditions Versus Exposure Time

9.4 CORROSION COUPON SURFACE IMAGES (ARGONNE)

The pitting standard HCS used was based on visual examination of the exposed surface under 45X and 100X. Since no corrosion was observed at these levels, Argonne obtained images at higher magnification, Figures 37 through 41, to better characterize the surface after cleaning and to provide more information about the surface anomalies not visible at the lower magnifications.

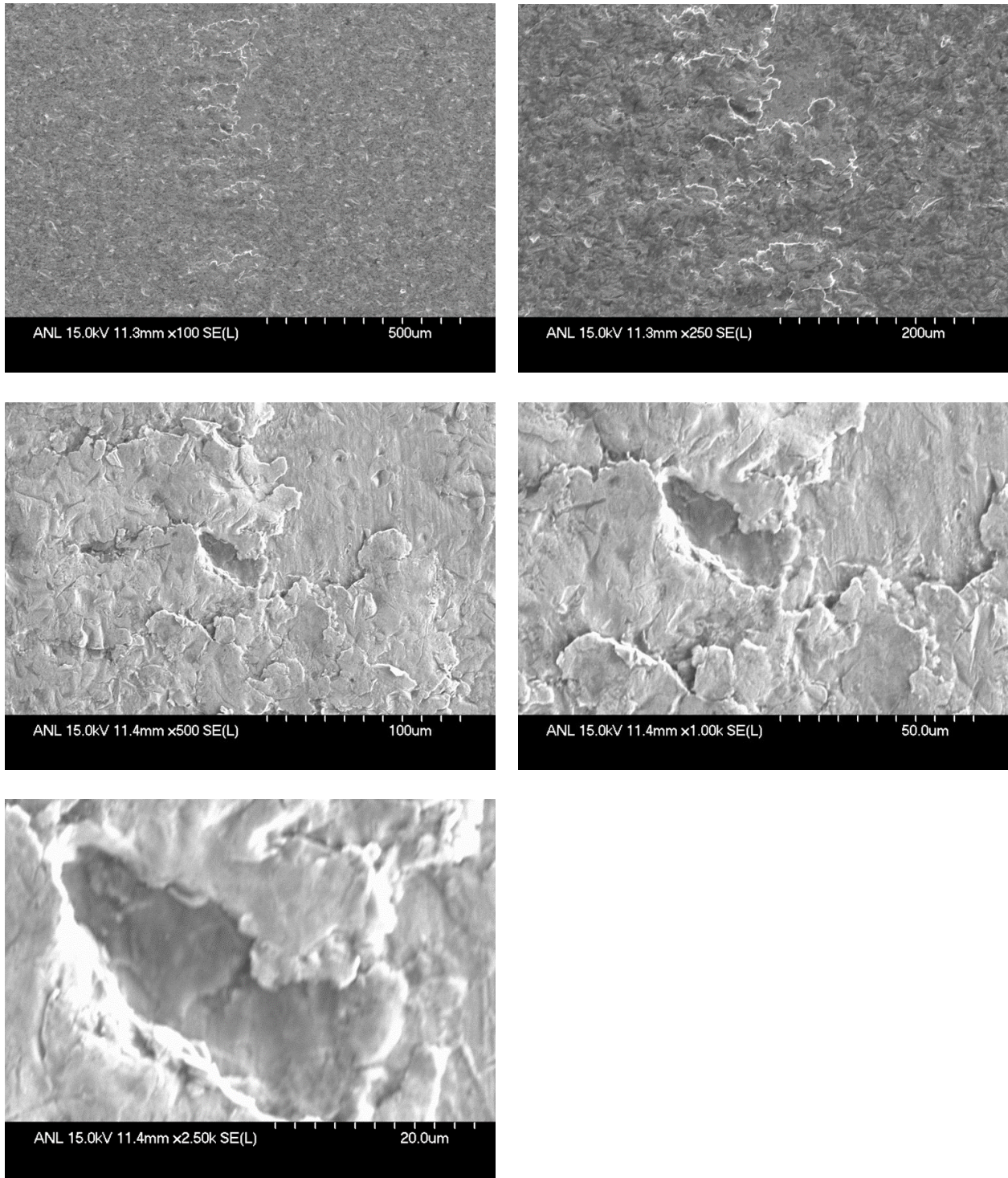


FIGURE 37 Alloy 725 Surface Images at Various Magnifications (Sample 8C)

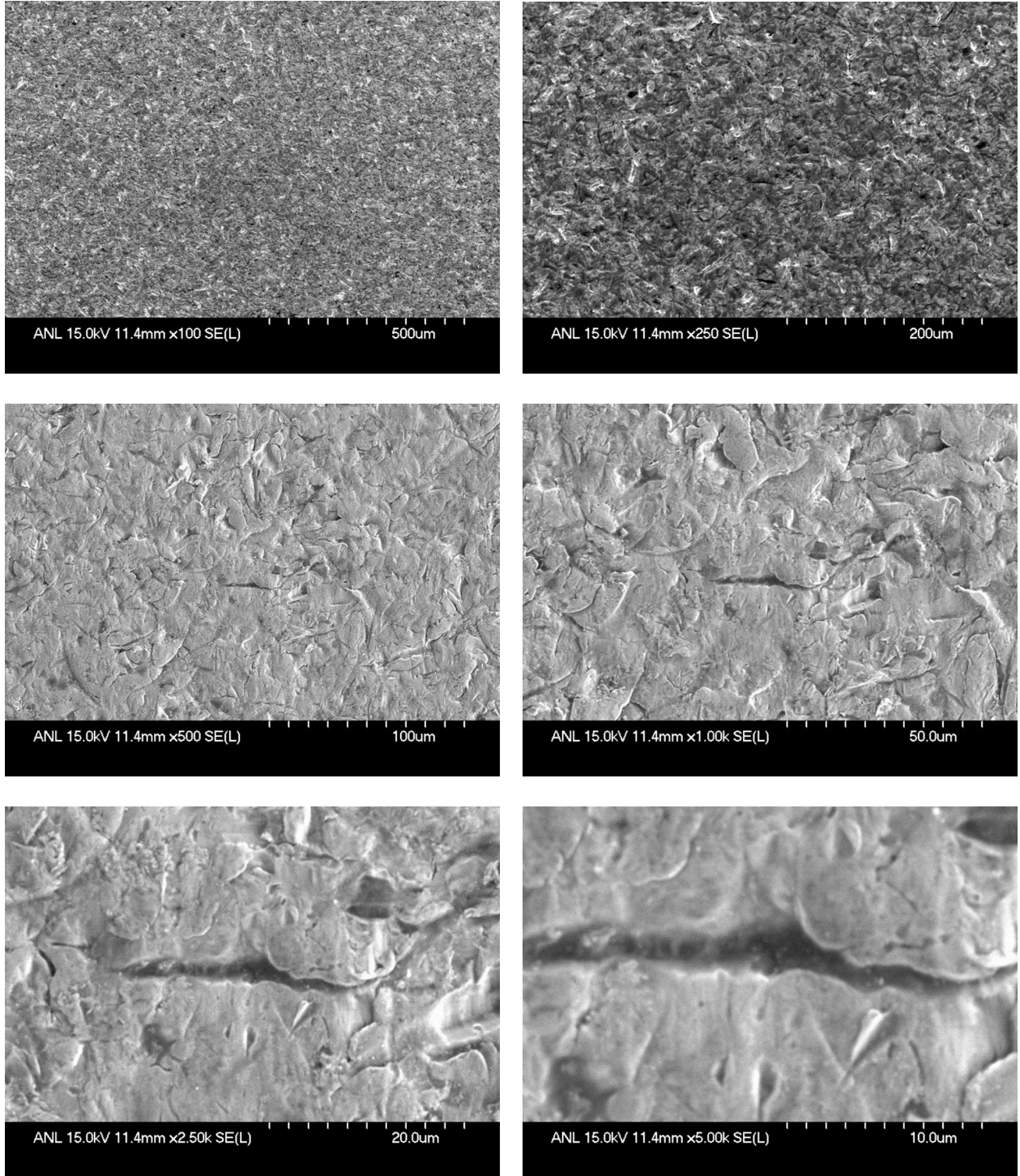


FIGURE 37 (Cont.)

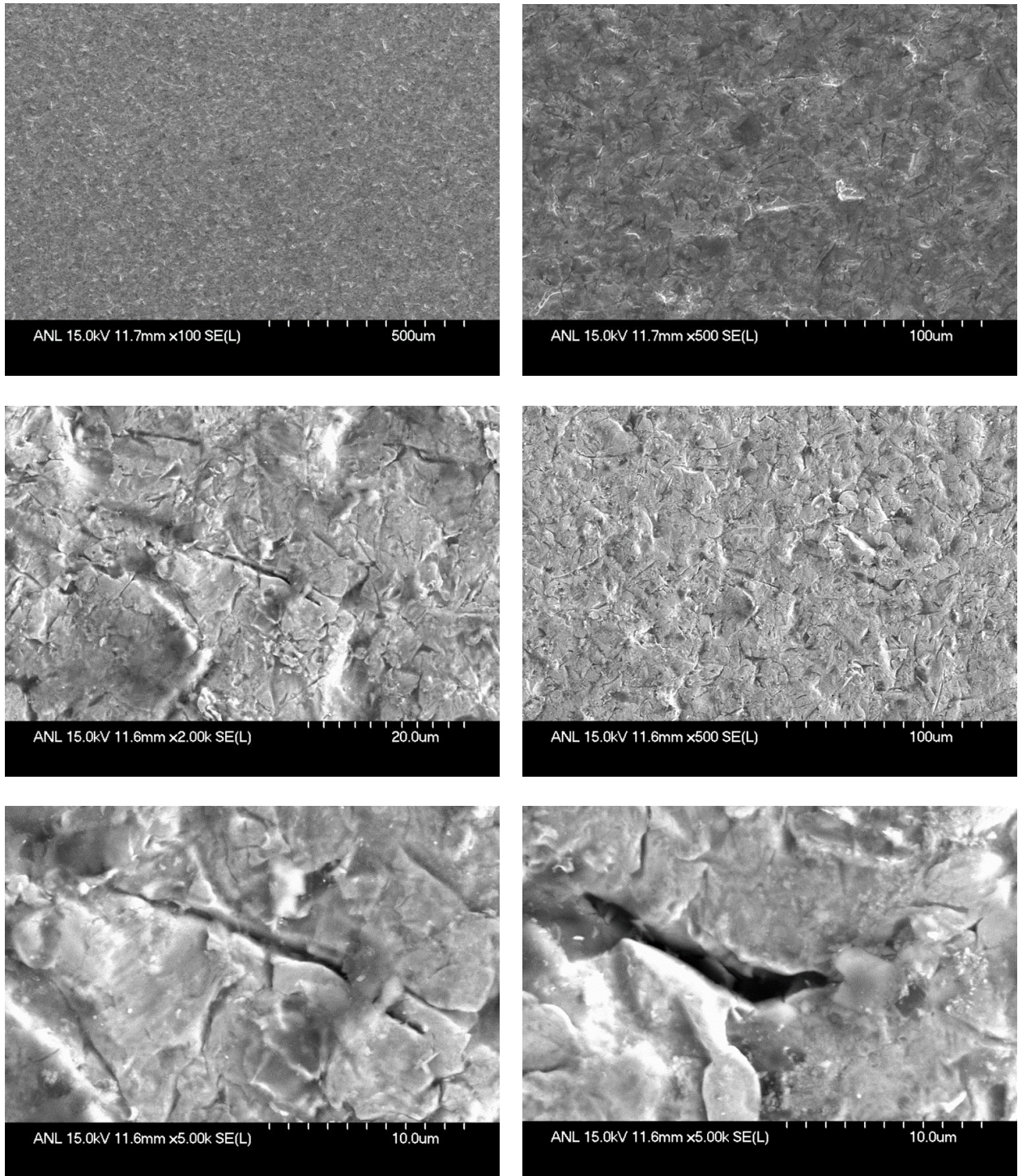


FIGURE 38 Alloy 945X Surface Images at Various Magnifications (Sample 8C)

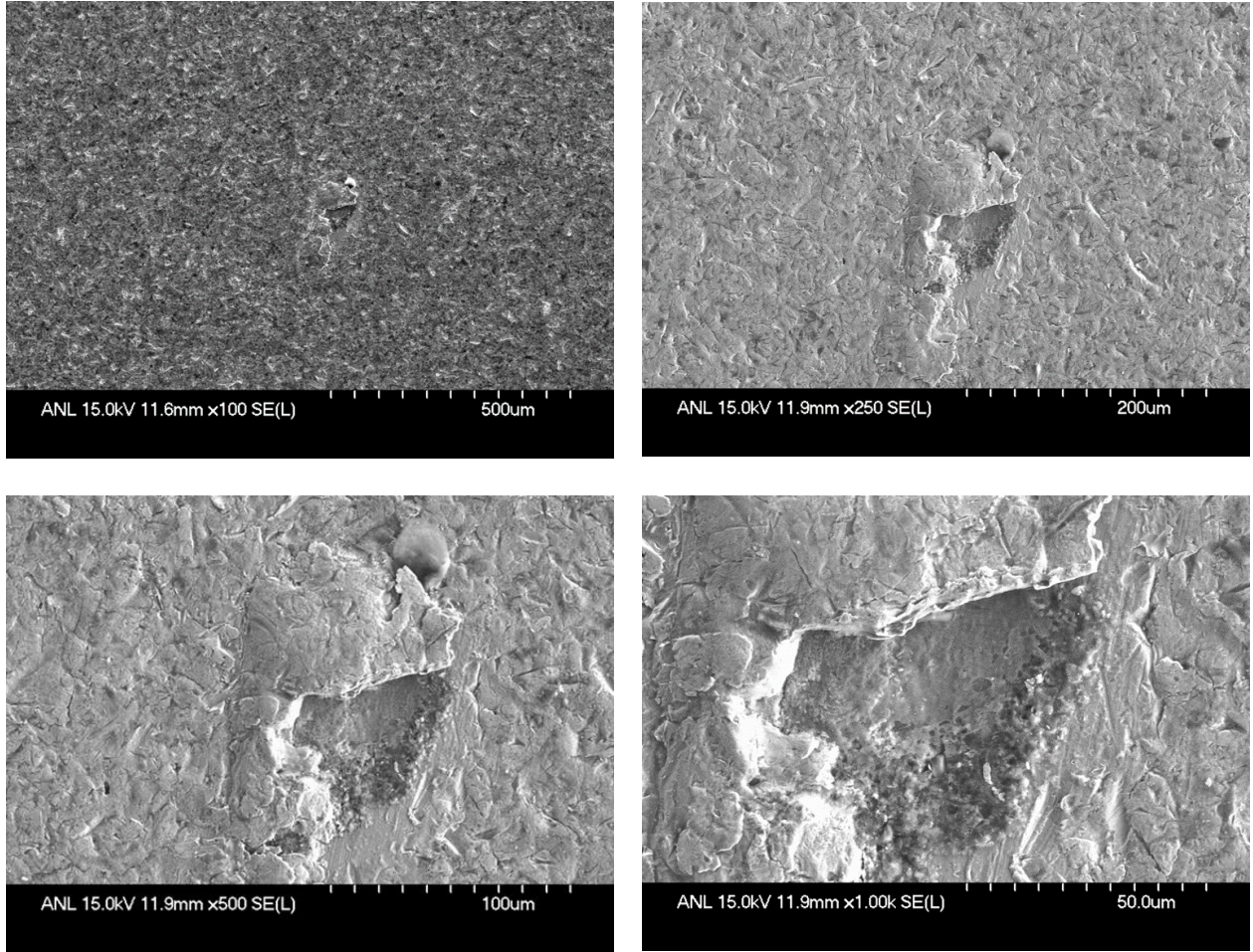


FIGURE 38 (Cont.)

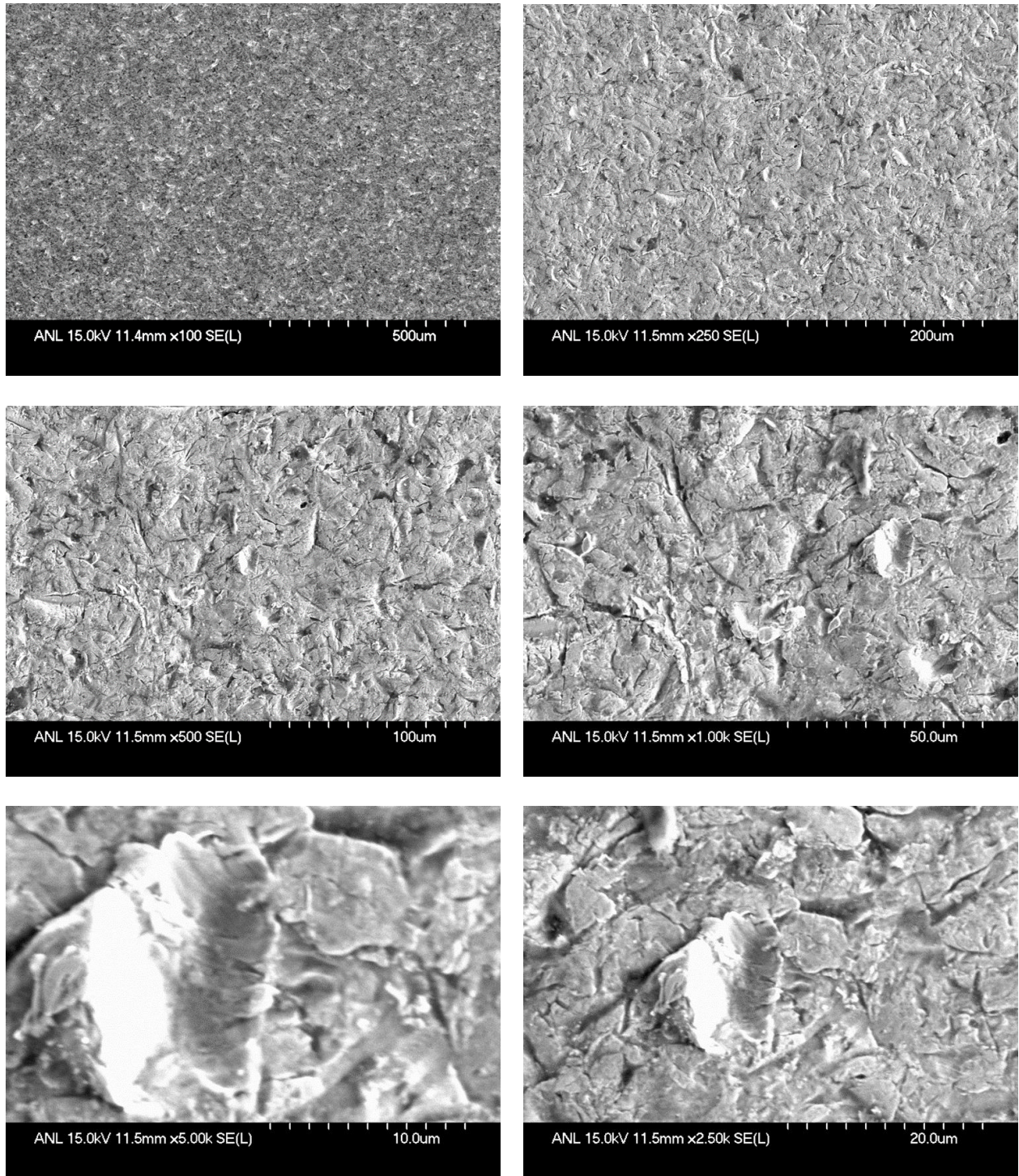


FIGURE 39 Alloy 955 Surface Images at Various Magnifications (Sample 8c)

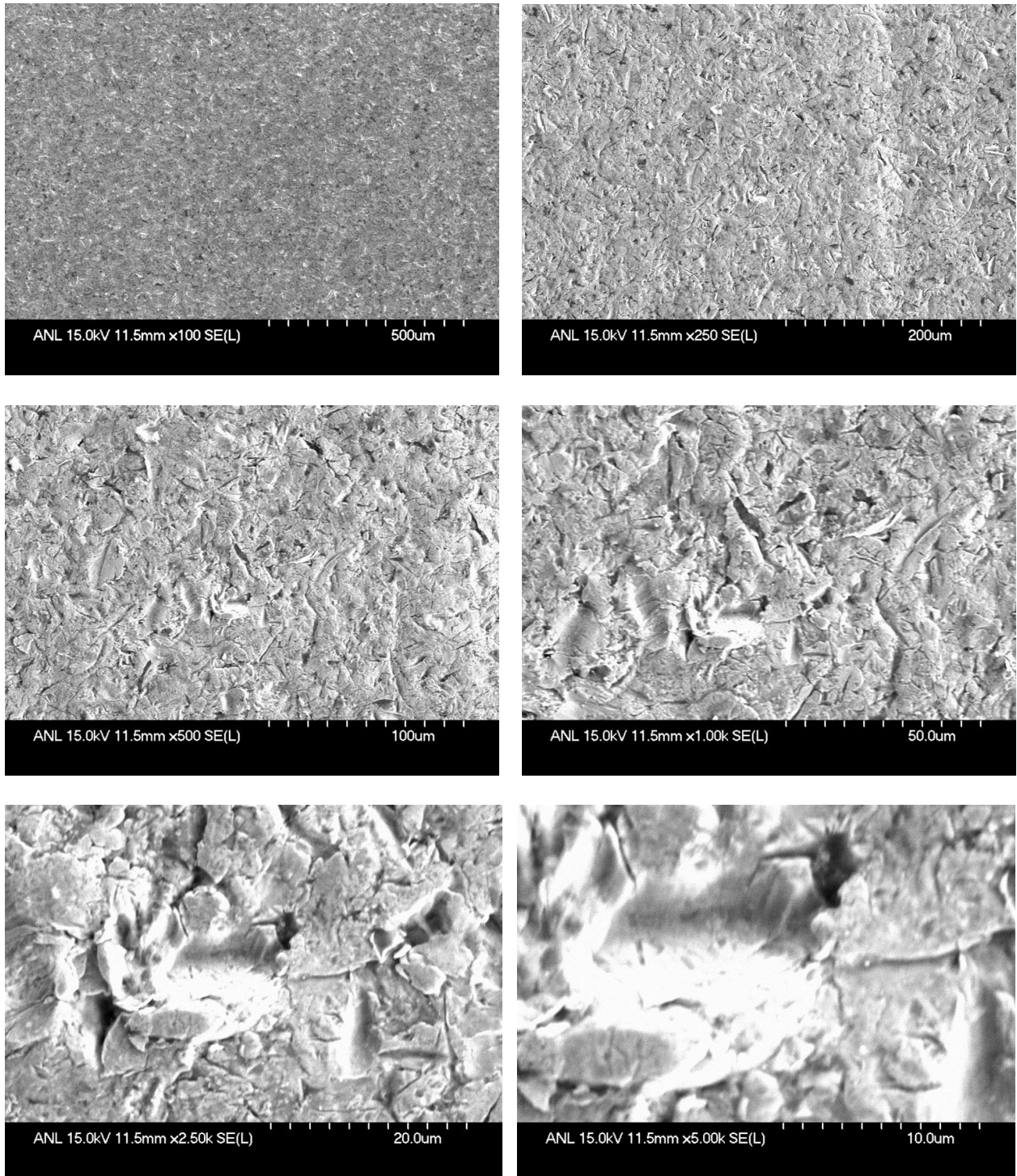


FIGURE 39 (Cont.)

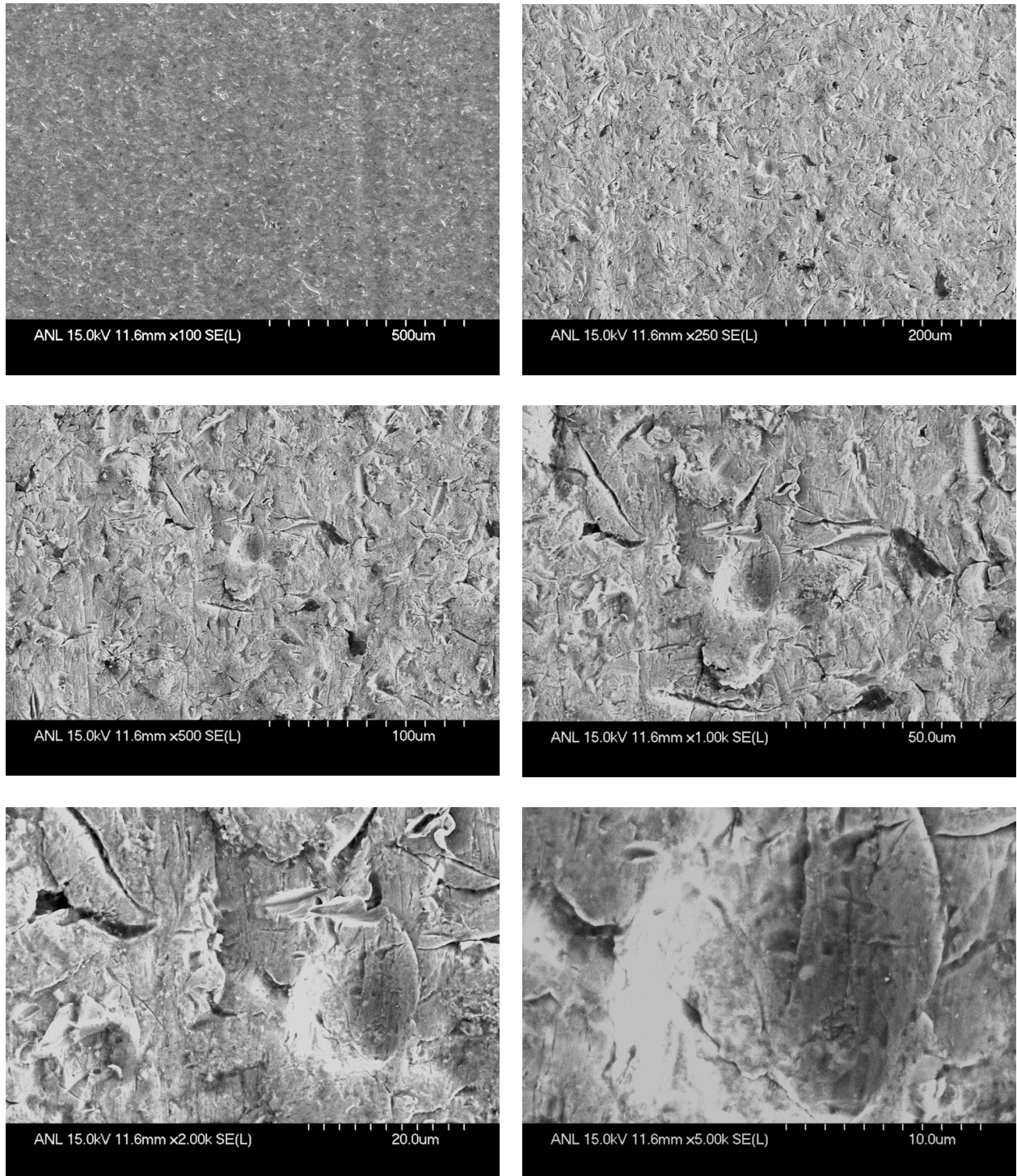


FIGURE 40 Alloy 825 Surface Images at Various Magnifications (Sample 8C)

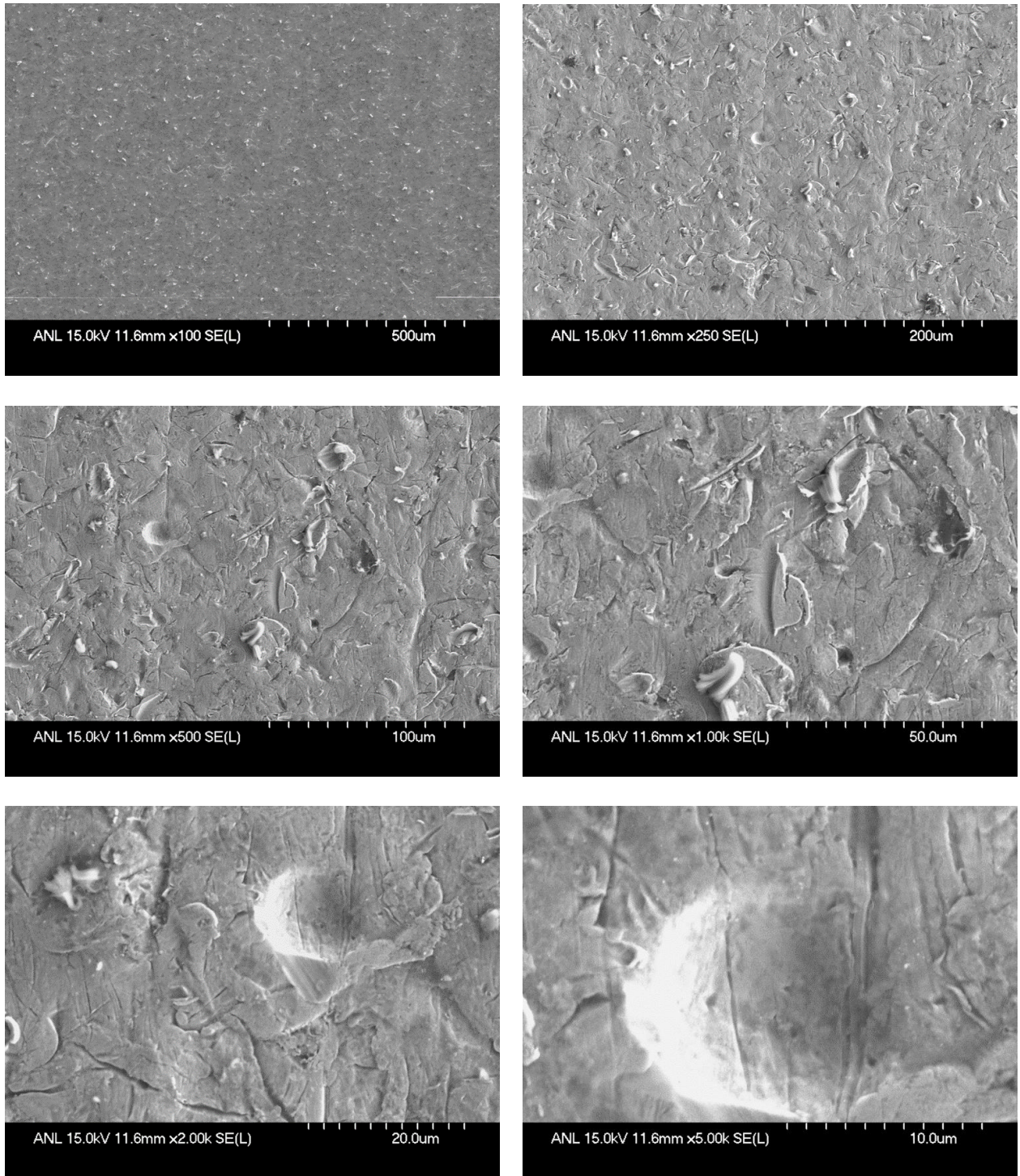


FIGURE 40 (Cont.)

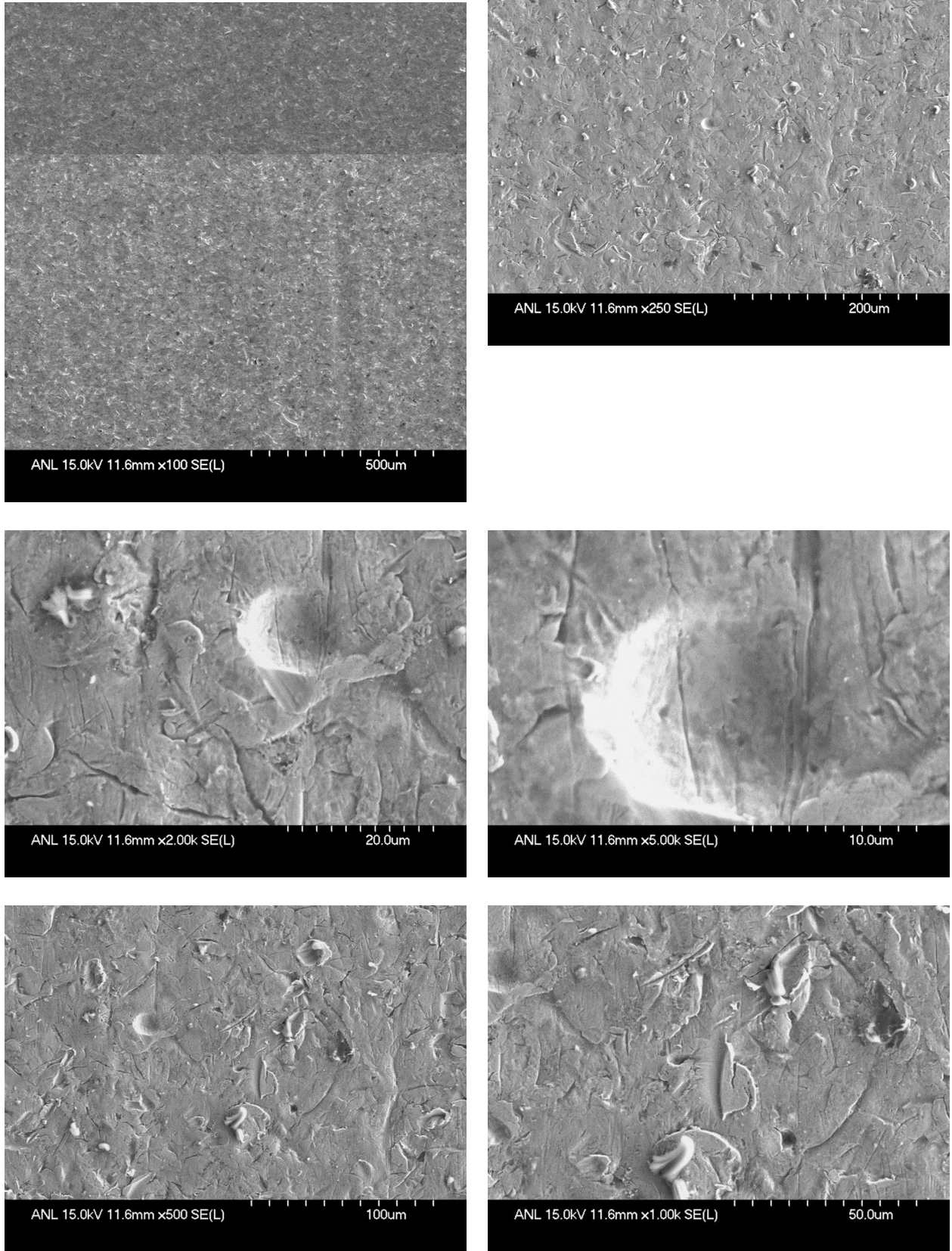


FIGURE 41 Alloy C22HS Surface Images at Various Magnifications (Sample 8C)

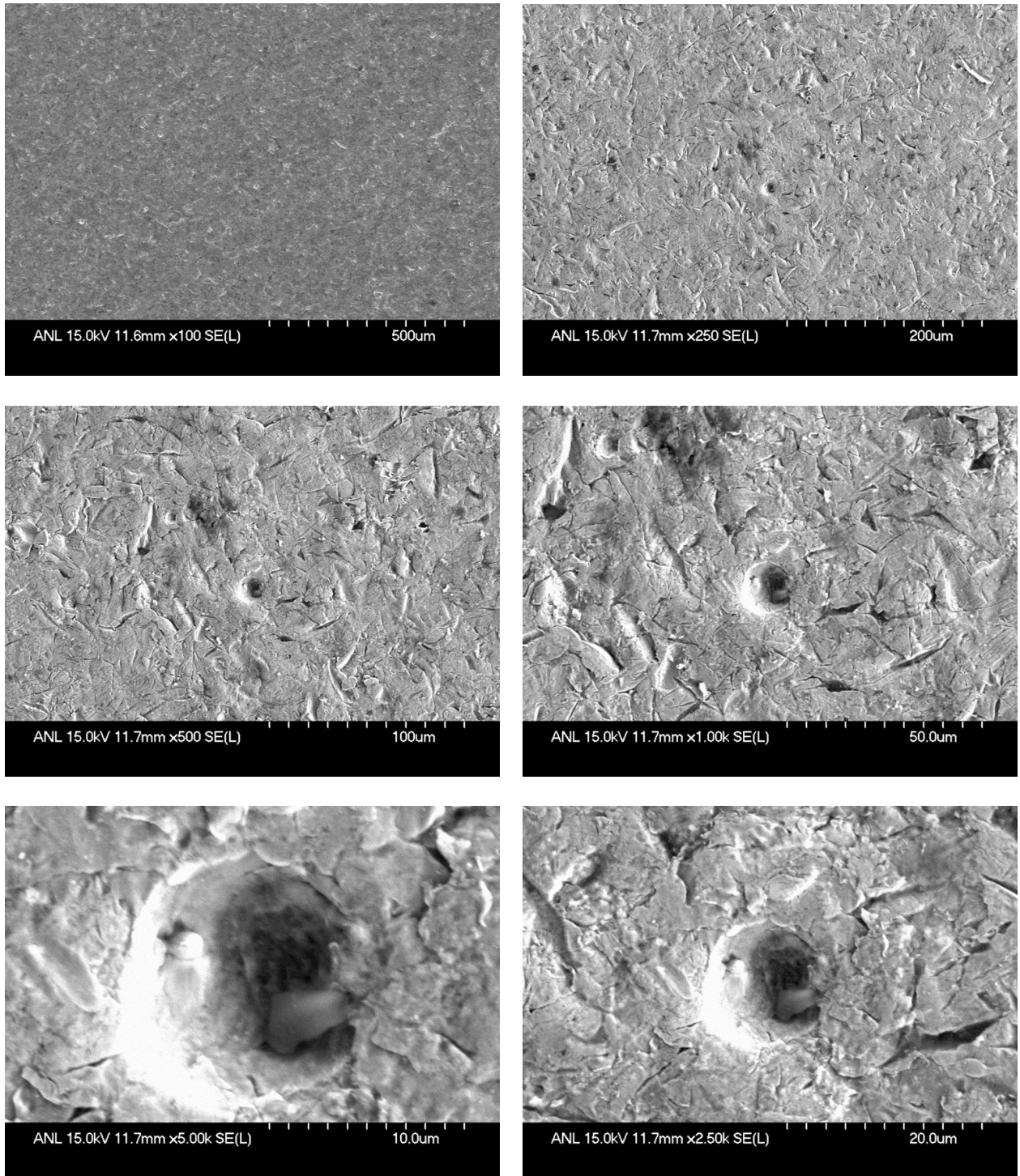


FIGURE 41 (Cont.)

9.5 MICROSCOPY EXAMINATIONS OF 945X C-RINGS

9.5.1 Reason for Alloys Specific Examinations

The tests series on crack growth and corrosion rate consisted of four test periods in high pressure autoclaves at HCS. These were 6-, 12-, 18-, and 48-week durations. Each period included all materials as explained and shown elsewhere in this report. Because there were only two autoclaves available, the shortest and longest periods were performed first with the intermediate periods being completed just before the conclusion of the HCS work. An unexpected result was that both 945X C-rings cracked sometime during the 6-week exposure,³ yet neither cracked during the 48-week exposure. This is counterintuitive thus Argonne initiated metallurgical examinations seeking to understand the reason for the early failure. Subsequently those examination were extended to the 12- and 18-week exposures as those test materials became available. The following sections pertain to this work beginning with the 6- and 48-week results followed by the 12- and 18-week microscopy examination results.

9.5.2 Six- and 48-week Chemistry Comparison

As shown in **Error! Reference source not found.**Table 14, the chemistry is not significantly different. The largest percentage variations are for elements constituting less than 1 weight percent. These differences alone would not be expected to be the cause for the different in cracking behavior observed.

TABLE 14 Chemistry Comparison for 6- and 48-Week C-Ring Sample 14149

Element	14149 (6 weeks) [wt%]	14149 (48 weeks) [wt%]
Titanium	1.97	1.58
Chromium	20.56	20.69
Iron	14.62	14.78
Cobalt	0.06	0.39
Nickel	52.92	52.91
Copper	2.19	2.25
Aluminum	0.2	0.18
Silicon	0.24	0.18
Niobium	3.57	3.33
Molybdenum	3.68	3.71
Total	100	100

³ Do not know exact time since autoclave was not opened during the entire 6-week test period.

9.5.3 SEM Images and Observations for 6- and 48-Week Exposures

From comparisons of Figures 42 through 45, microscopy images the difference is the presence of an established oxide layer in the range of 5 microns at 48 weeks and no observable oxide layer on the both the ring and coupons samples from 6-week exposures.

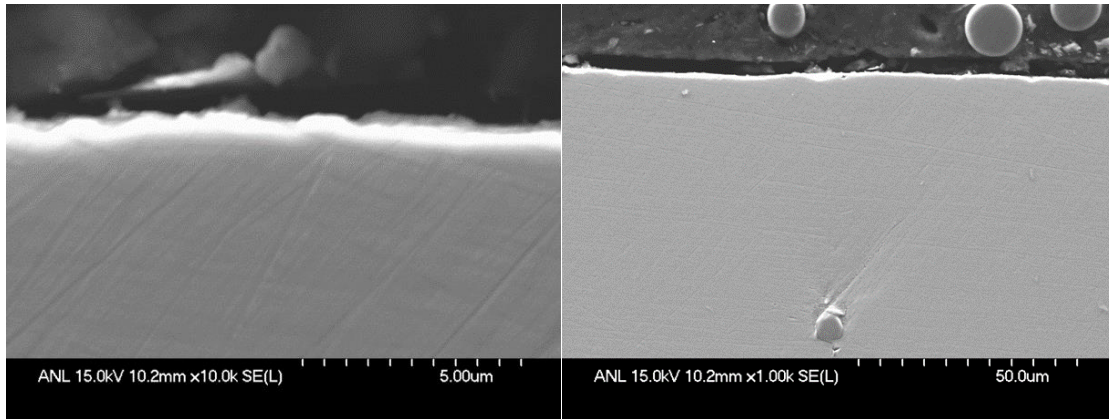


FIGURE 42 SEM Images of 14149.1X (Coupon) from 6-Week Exposure

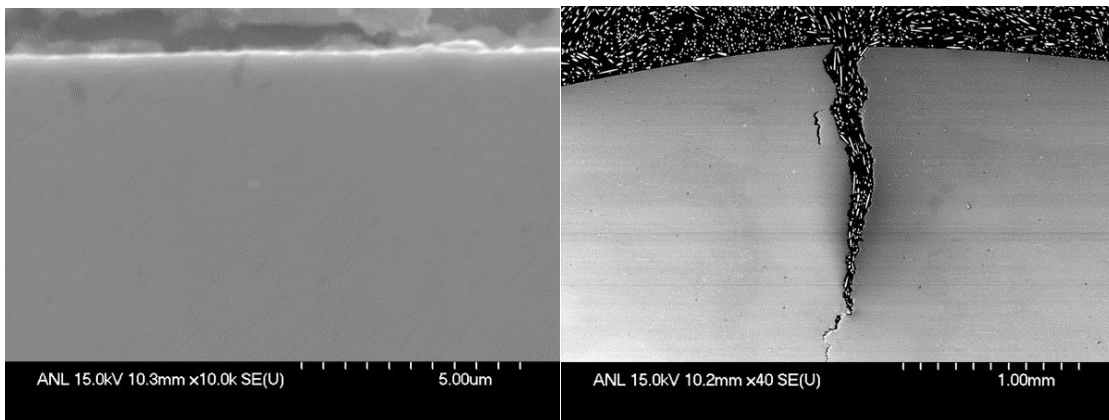


FIGURE 43 SEM Images of 14149.1R (C-Ring) from 6-Week Exposure

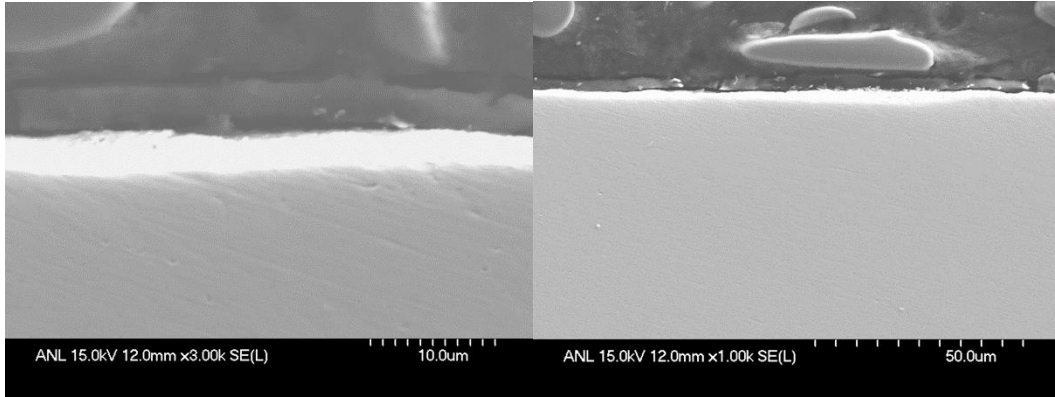


FIGURE 44 SEM Images of 14149.7C (Coupon) from 48-Week Exposure

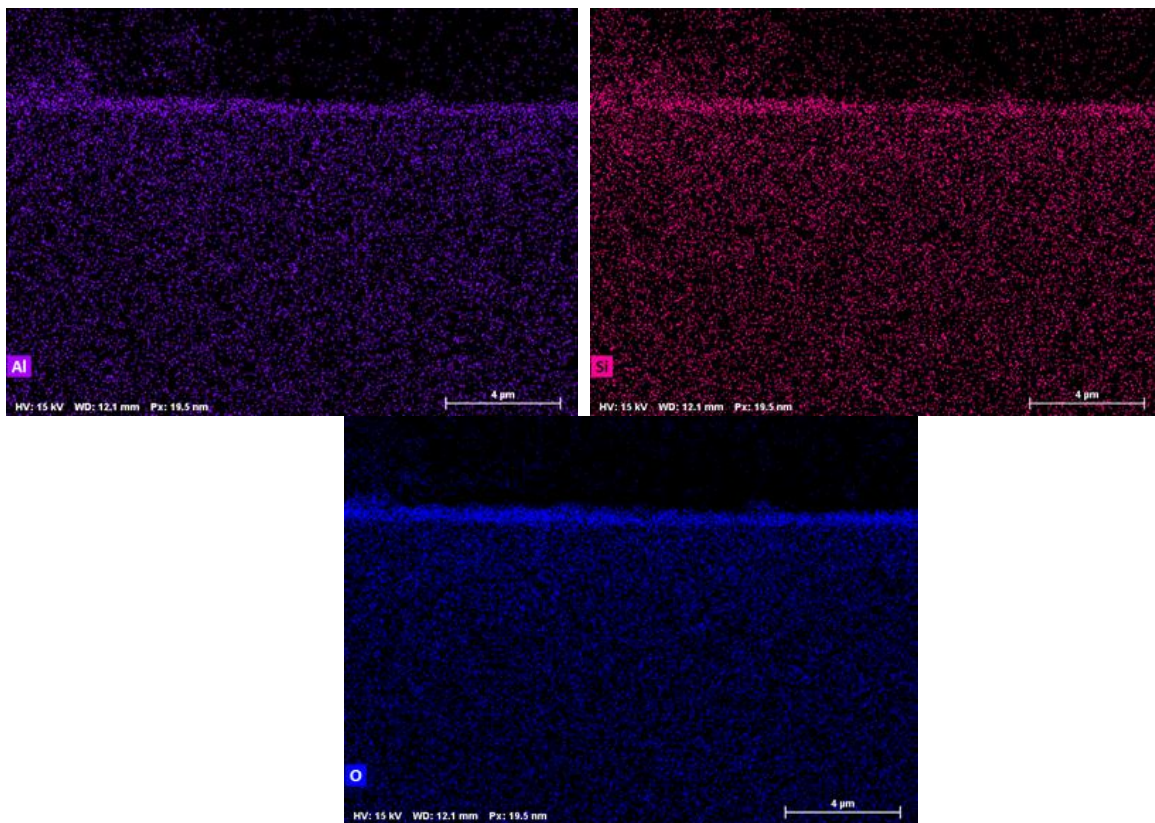
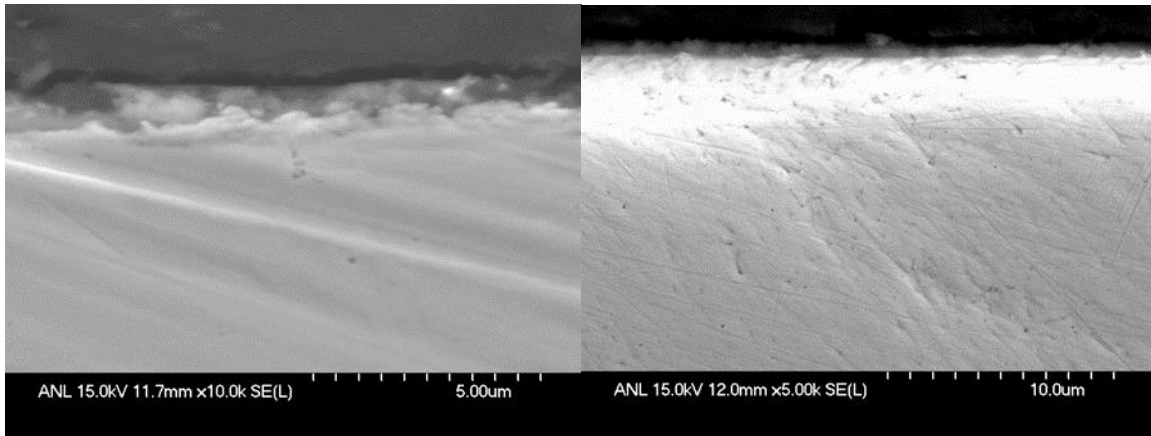


FIGURE 45 SEM Images with EDS of 14149-7R (Ring) from 48-Week Exposure

9.5.4 SEM Results from 12-Week Exposure

No oxide scale was observed on any of the samples from 12 week exposure. There is the possibility there may be some scale at 12 weeks because of the random nature of scale formations in such alloys.

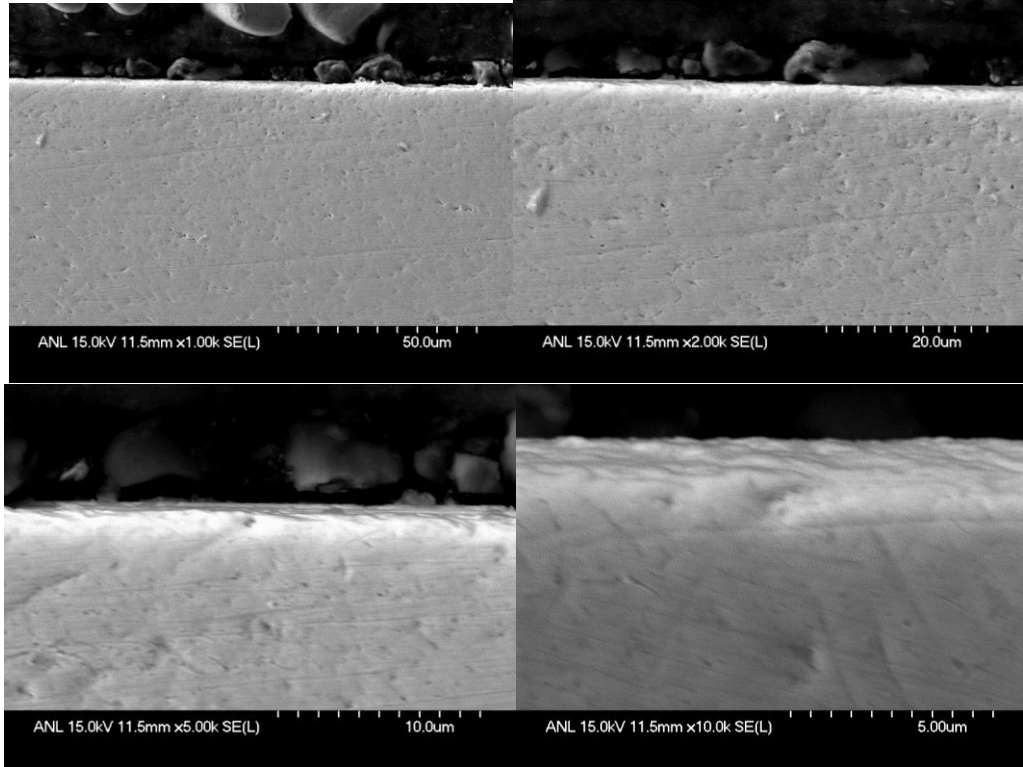


FIGURE 46 SEM Images of the SCC C-Ring 14149.3R from 12-Week Exposure

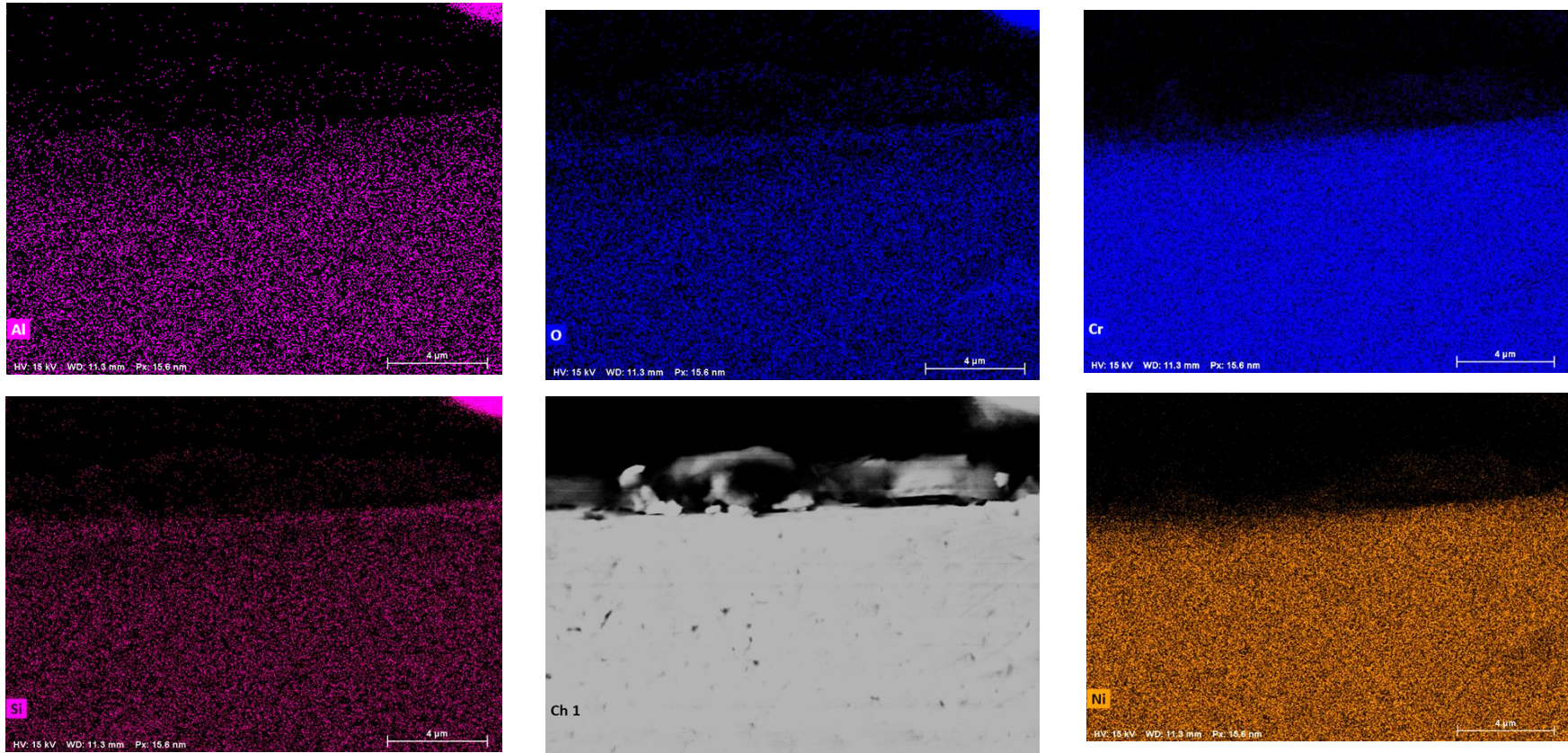


FIGURE 47 SEM with EDS of the SCC C-Ring 14149.3R from 12-Week Exposure

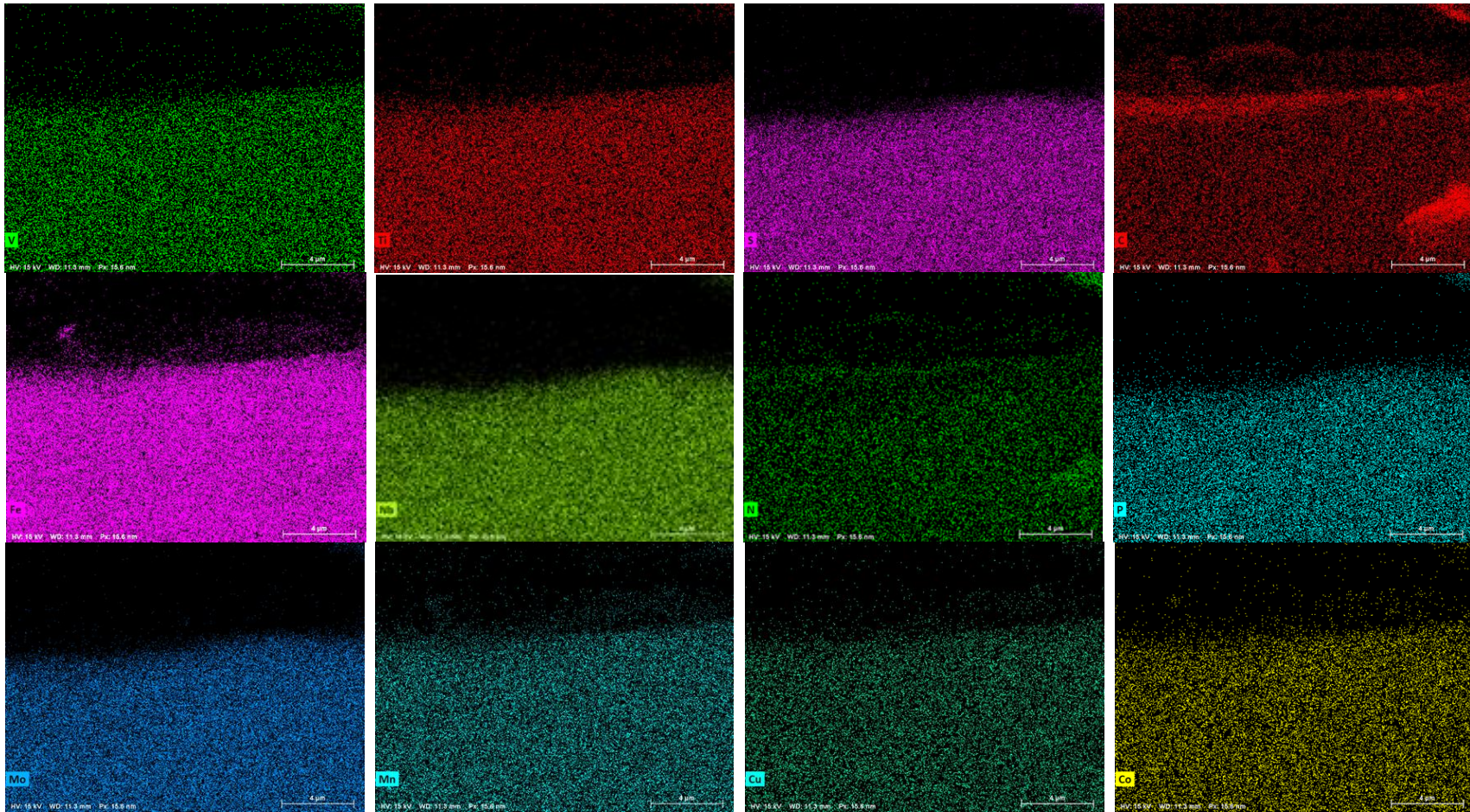


FIGURE 48 Further EDS of the SCC C-Ring 14149.3R from 12-Week Exposure

9.5.5 SEM Results from 18-Week Exposure

Figures 49 through 53 are SEM and EDS mappings for SCC C-Ring 14149.5R from 18-week environmental exposure. Oxide scale appears in some areas but not others. Figures 49 and 50 show details for an area where there was no oxide scale. The remaining figures show areas with oxide scale in the range or 5 micron which is about the same as was observed for 48 weeks. A thinner scale might be anticipated but this may be related to the fact that the 18-week samples were not introduced to the test environments immediately after machining as there was a nearly 1-year interim period without testing. In contrast, the 6- and 48-week samples were introduced to the autoclave environment within just a few weeks of machining. From Argonne's experience with similar alloys, full characterization of scale formation requires evaluation of more samples than were done here because pitting corrosion and SCC cracks generally occur randomly.

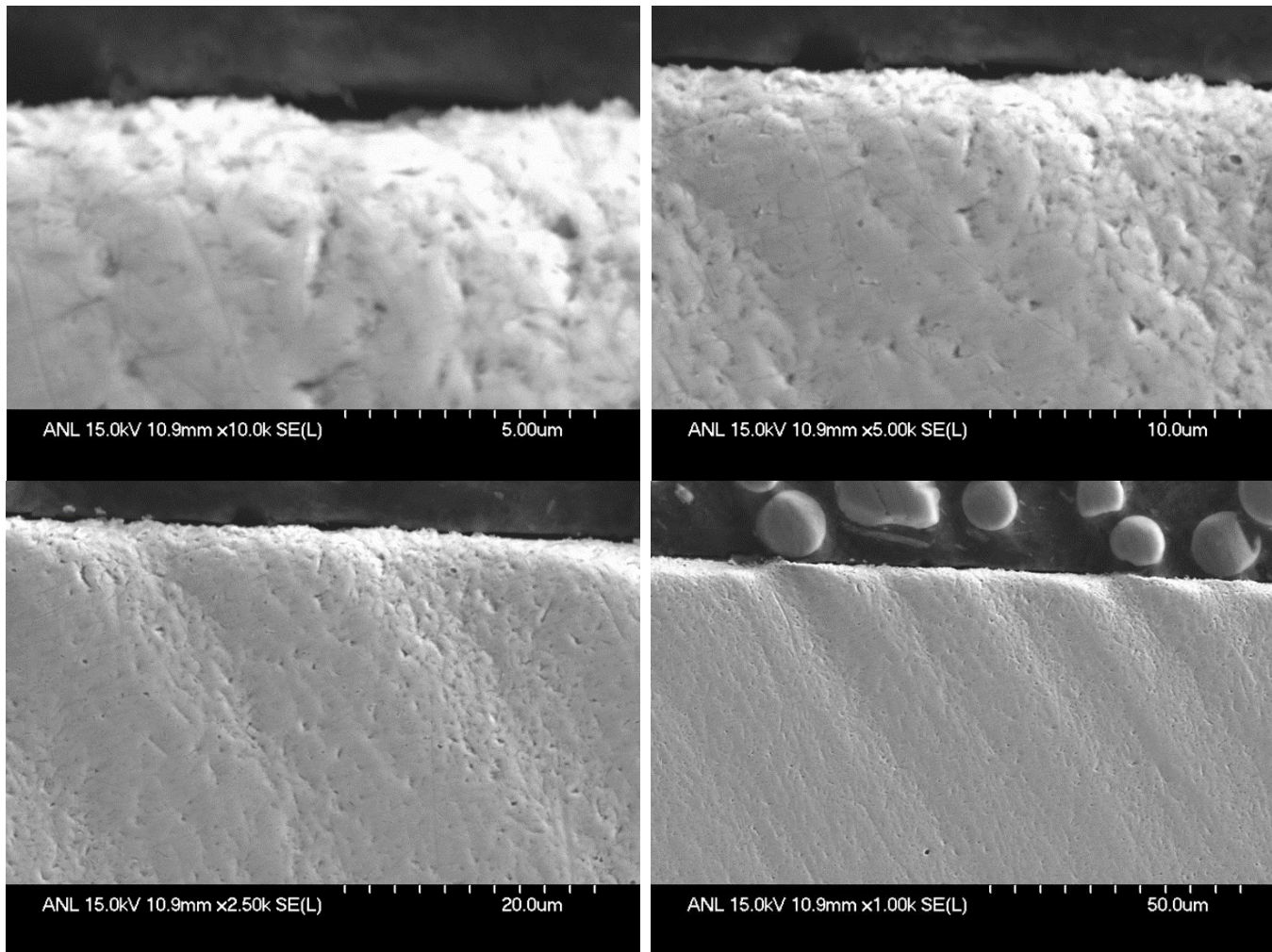


FIGURE 49 SEM Images in Areas without Oxide Scale for 18-Week Exposure SCC C-Ring 14149.5R

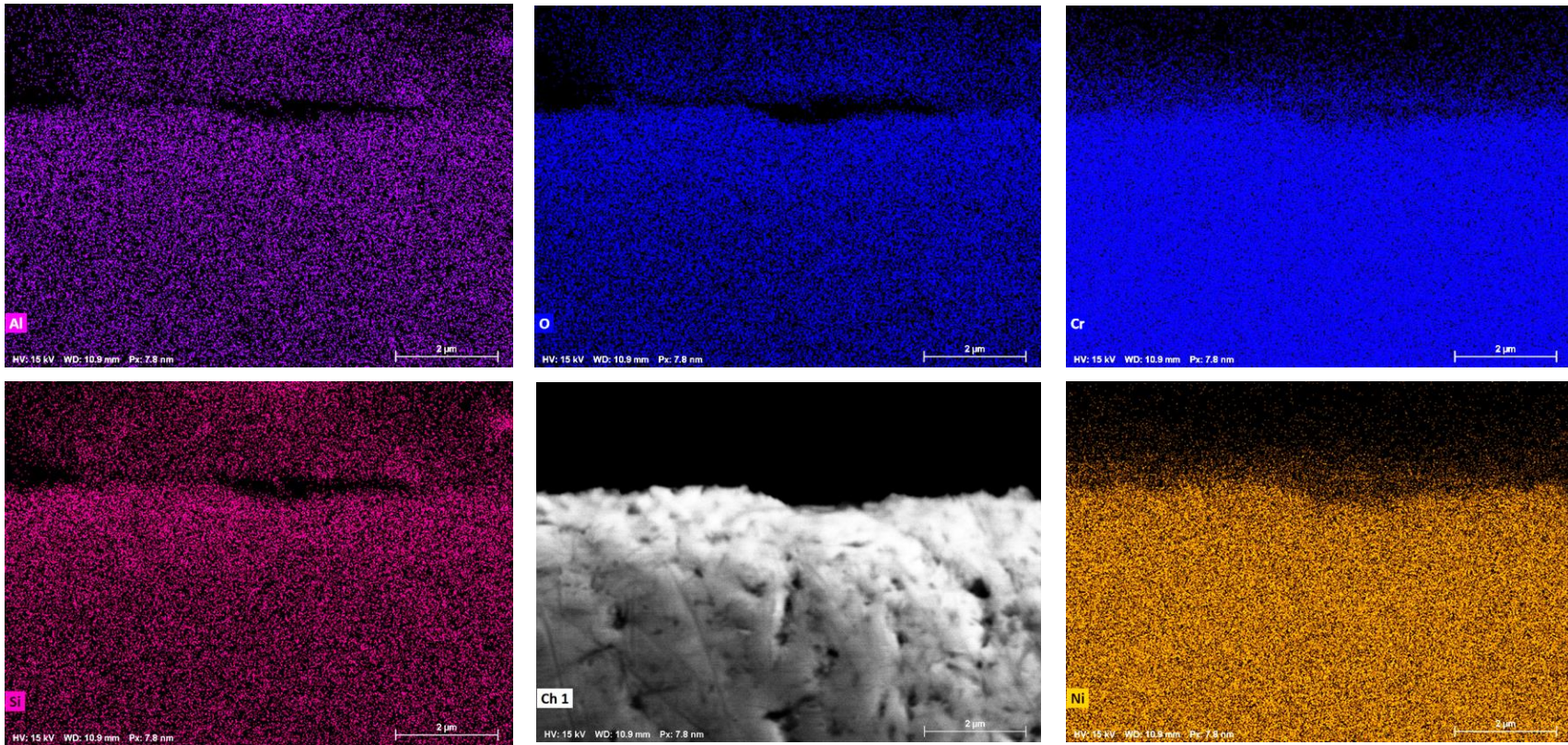


FIGURE 50 EDS Mappings for Areas without Oxide Scale for 18-Week Exposure SCC C-Ring 14149.5R

74

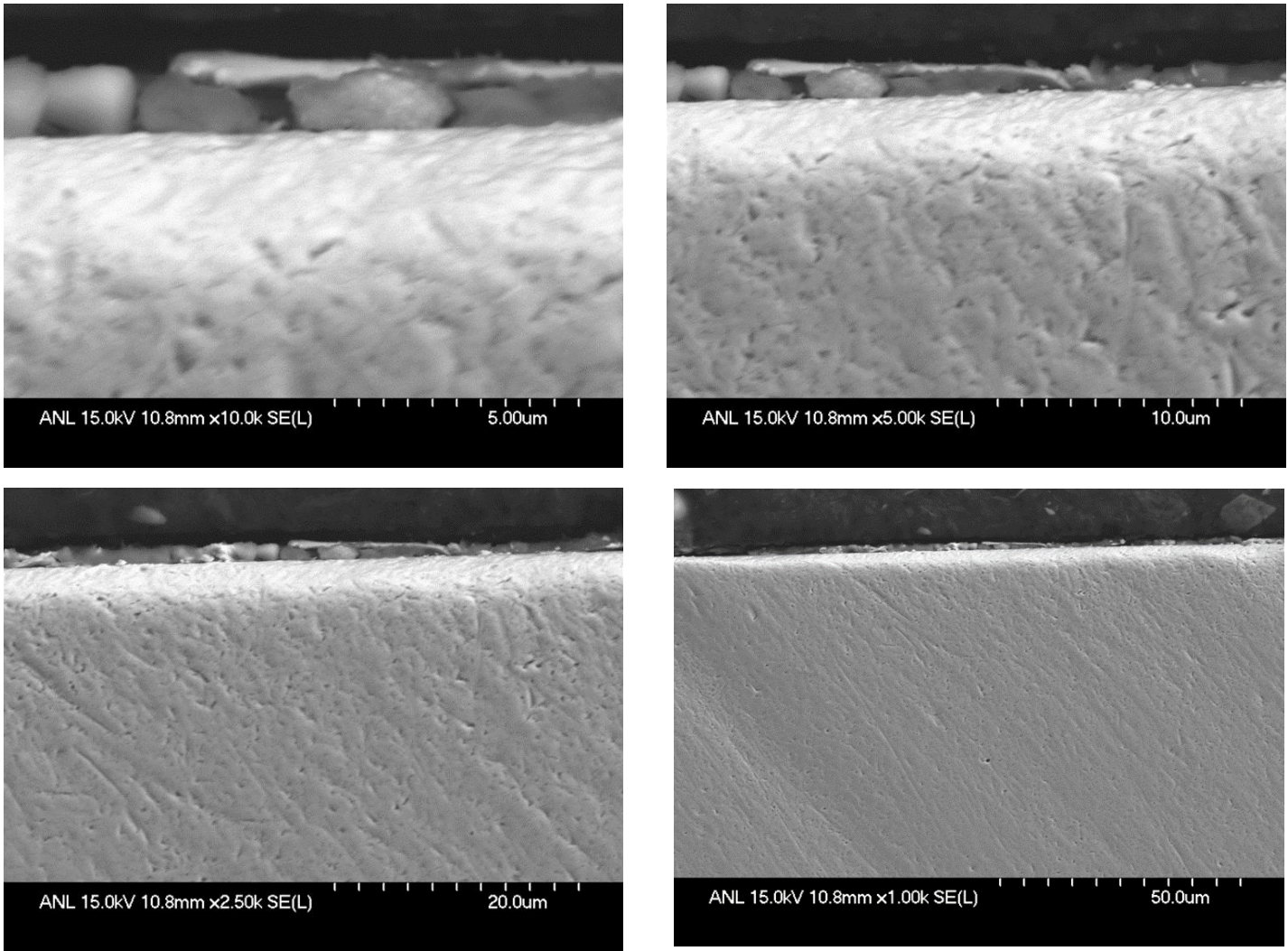
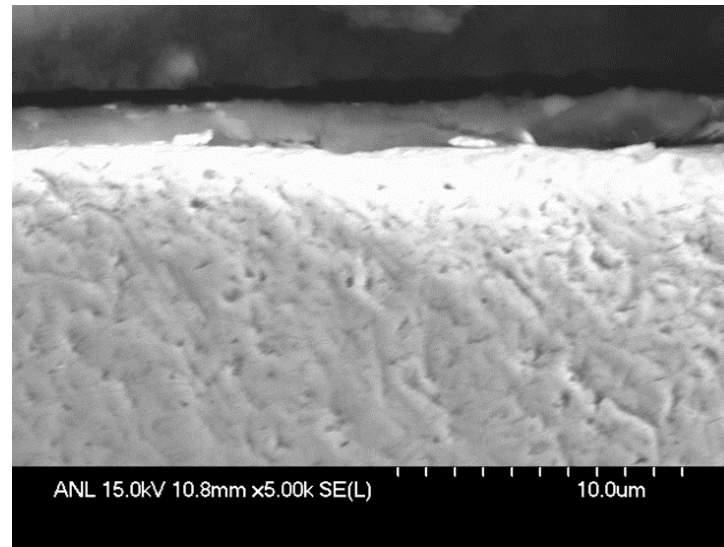
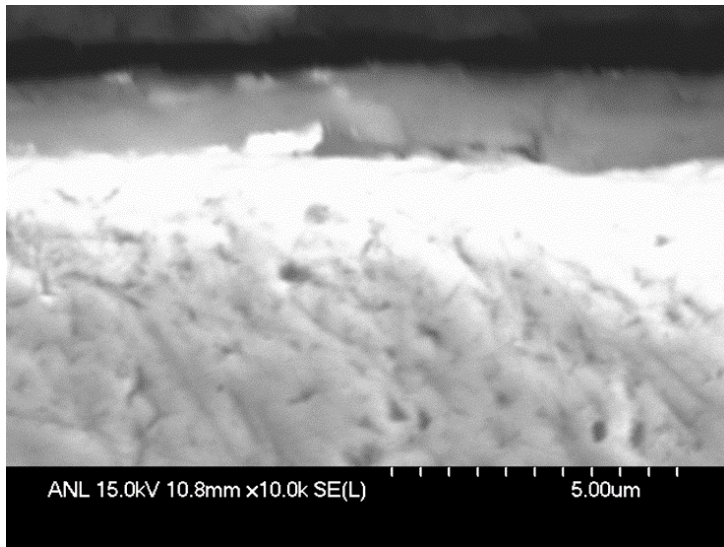


FIGURE 51 SEM Images for Areas with Oxide Scale for 18-Week Exposure SCC C-Ring 14149.5R



75

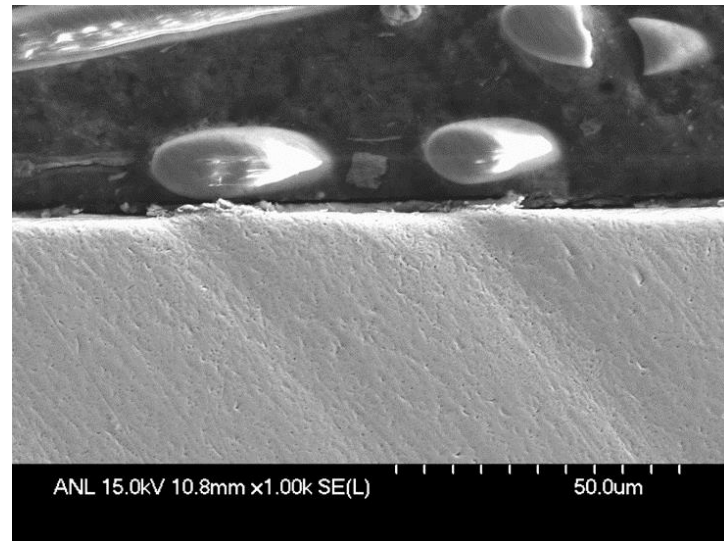
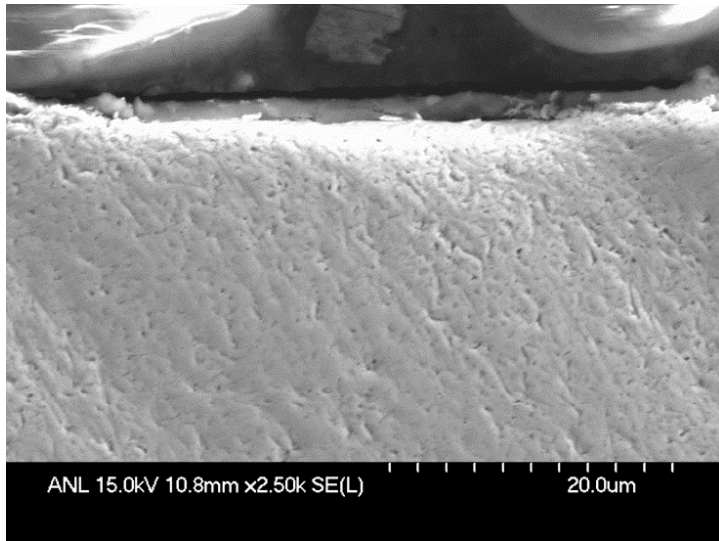


FIGURE 51 (Cont.)

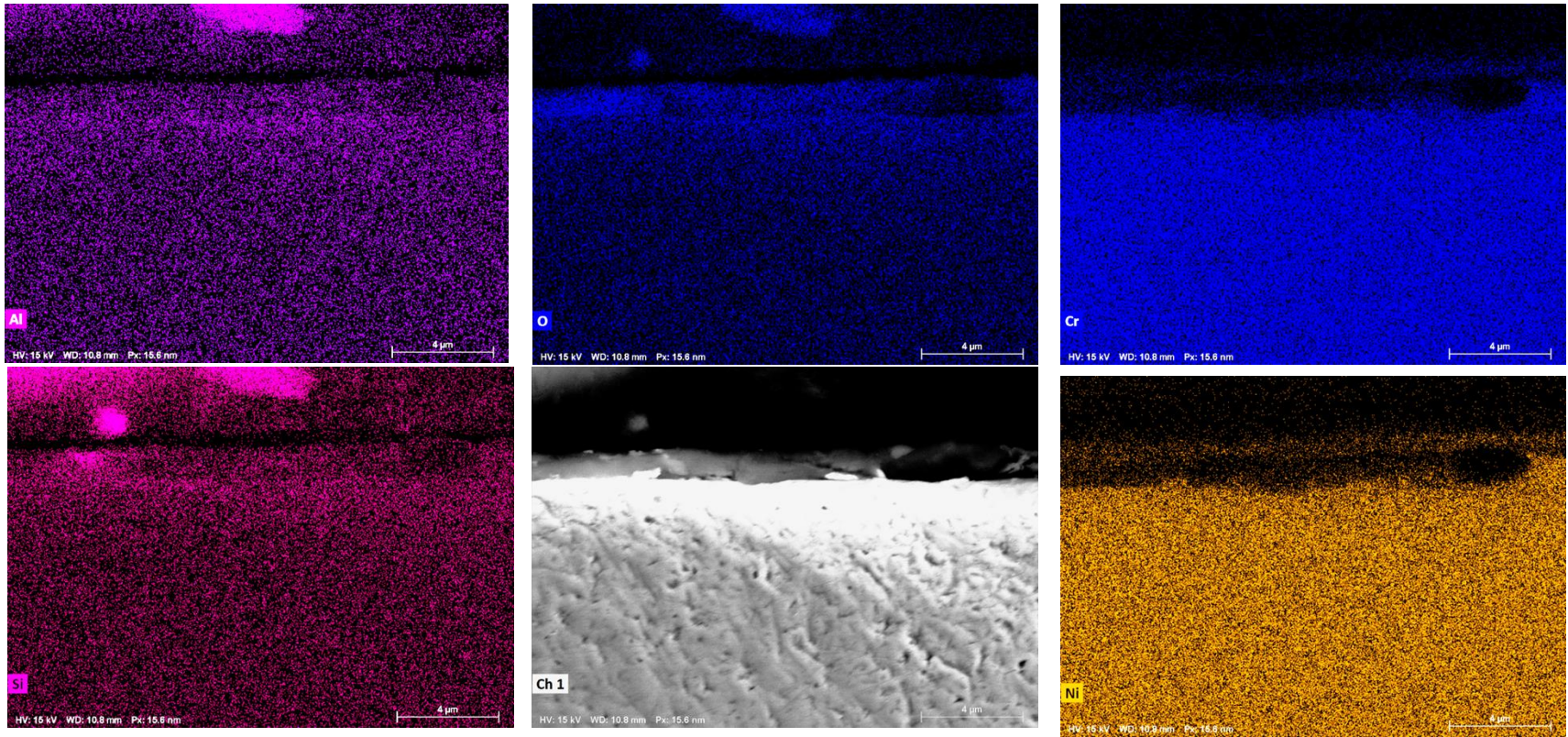


FIGURE 52 EDS Mapping for Areas with Oxide Scale For 18-Week Exposure SCC C-Ring 14149.5R

9.5.6 Observations from 945X Electron Microscopy

Based on the microscopy work performed, oxide scale appears to be a possible factor contributing to the failure of the 945X C-rings are 6 weeks but not 12, 18 or 48 weeks. The samples seemed to have full scale at 48 but only partial scale coverage at 18 weeks and none at 12 weeks. Without further study with a statistically significant number of samples, positive attribution to oxide scales is not possible as the full explanation for the early failure. Such additional examinations might look at a range of surface conditions including polished, scratched, etched, et al.

10 GENERAL DISCUSSION AND INTERPRETATION OF RESULTS

Five CRAs were investigated in this study. As has been noted several times throughout this report, these five alloys were either precipitation hardening types (725, 945X, and 955) or were work hardening types (C22HS and 825). Since there two types of alloys behaved somewhat differently, they will be discussed in the context of these two groups

10.1 PRECIPITATION HARDENING ALLOYS (725, 945X AND 955)

Precipitation hardening occurs when fine particles are formed during the heat treatment of a material. The formation of these particles depends on the composition of the material and the temperatures. These fine particles impede the movement of dislocations and thus raise the yield and ultimate strength of the material. Because thermal processing is a well understood process, it is fairly easy to get uniformity of mechanical properties in thick cross sections of materials with proper processing

Several comparisons of these three materials are possible from the results obtained in this program. The ranking of the CCT was determined to be:

Worst 945X < 955 < 725 Best

This ranking corresponds to the PREN (pitting resistance equivalent number) and also the general corrosion rates of these materials after 6-weeks and 48 weeks of HPHT exposure (PREN comparison appears in DNV-GL report). These observations all indicate that the corrosion of these materials is directly related to alloy content with higher percentages of alloy content providing more resistance.

In the HCS HPHT autoclave exposures, only the two, 945X C-ring specimens failed within the 6-week test, but not in the 12, 18, or 48-week tests. None of the other specimens failed. HCS concluded that that this was "anomalous". It is perhaps better to deem this as "inconsistent"; test specimens failing in the shortest duration test but not in longer duration tests are truly inconsistent. However, the fact that the material with the lowest critical crevice resistance and highest corrosion rate cracked does not necessarily seem "anomalous." When these bolt-loaded C-rings test results in sour HPHT conditions are compared to the environmental fatigue crack growth tests in sour conditions, there is good agreement. More specifically, the dynamically loaded pre-cracked specimens displayed no effect of loading frequency meaning no environmentally enhanced contribution.

When these alloys were tested under dynamically loaded conditions in simulated seawater, no loading frequency (hence no environmental) effect was observed. However, cathodically applied potentials did show an environmental effect for these three precipitation hardening alloys. In that case, the rank ordering becomes:

Slowest crack growth rate 945X < 955 ≤ 725 Fastest growth rate

In addition, with applied potentials to both materials, it was noted that the 725 produced significantly faster growing crack than either the 945X or the 955 when the environmental fatigue crack was transitioned to a static growing crack.

The microscopy results for these three materials following the environmentally assisted cracking tests showed predominantly intergranular cracking; but the 725 displayed dimpled grain boundary fracture while the 945X and the 955 showed brittle grain boundary fracture. The 725 alloy had a high density of precipitates, particularly MnS. These particles can act as sites for hydrogen accumulation resulting in enhanced cracking during the cathodic protection charging. It was also noted that the 945X and the 955 had much lower densities of grain boundary precipitates than the 725 suggesting that these two materials were more resistant to hydrogen embrittlement than 725.

10.2 WORK HARDENING ALLOYS (825 AND C22HS)

The compositions of these alloys are such that precipitates do not occur during thermal processing. These materials get their enhanced strength through mechanical working processes (e.g., forging). As reported in the microscopy section 12.0, these two alloys displayed a single-phase microstructure that was heavily deformed. The mode of crack propagation in these two alloys was transgranular.

As was the case with the precipitation hardening alloys, the CCT also tracked well with the PREN values. Where for these two alloys:

Worst 825 < C22HS Best

The cyclic loading tests in simulated seawater, sour production environment, and simulated seawater with applied potential did not show any frequency effect indicating no environmental contribution to crack growth under the conditions investigated. Also, not being able to get a static crack to grow during constant loading hold times further supports the case that these alloys were resistant to the test conditions imposed.

The one unexpected result with these materials was the failure of the 825 specimens at 46.5 hours at 950°F in the creep program at Westmoreland. Review of this particular sample revealed that the reported tensile test results at 950°F were about 20% higher than those at 350°F (i.e., YS was 103.6 ksi at 350°F versus 127.1 ksi at 950°F). Thus, it is probable that this particular specimen was overloaded since the requested load of 83% of YS for a material with a YS of 127.1 ksi is 105.5 ksi. Time constraints on this project did not allow a repeat of the 950°F creep test nor of the 950°F tensile test. One can, however, use an extrapolation/interpolation technique to investigate the consequences of this unexpected failure at 46.5 hours being real (i.e., repeatable).

Creep testing typically involves very long durations at very high temperatures. Creep research work on turbine blade materials have used a Larson-Miller approach to extrapolate test

results. The Larson-Miller Parameter (LMP) approach assumes that creep processes are linear with absolute exposure temperature and logarithmic with exposure time. This is represented by:

$$LMP = T[C + \log(t)]$$

where

T = absolute temperature in °R

C = a constant most often given as a value of 20

t = the exposure time in hours.

Using the test conditions that led to failure of the 825 specimen at 46.5 hours at 950°F, one can calculate an LMP value. Knowing this LMP, one can then calculate different temperatures and/or times that would produce this same LMP. For this case, the LMP is 30,529 for a failure at 46.5 hours at 950°F. Using this LMP, that failure should occur at 1.78×10^5 hours at 750°F. In other words, operation of an 825 component loaded to 83% of YS at 750°F would fail after 20 years. A similar calculation projects a life of 3,850 years if the operational temperature were 650°F. Thus, these results indicate that creep is not an issue for these materials exposed to oil and gas production temperatures including extreme HPHT.

11 CONCLUDING REMARKS

This laboratory test program was intended to determine how well five CRA materials perform in offshore oil and gas production scenarios. These scenarios included cold seawater exposure with and without imposed cathodic protection and HPHT exposure to a sour environment for various and extended time periods. The testing used both self-loaded and dynamically loaded specimens in the environments chosen. The five alloys selected for testing varied metallurgically in the sense that they gain their strength from either precipitation of particles in the matrix or from mechanical working (e.g., forging) of the material. In terms of alloy content, a fairly wide spectrum was investigated as noted by the PREN range of low 20s to high 70s. From an economic perspective, this wide range in PREN also results in a cost differential factor of about four or five. In short, these five alloys offer a large range of possibilities.

This program illustrates that there are many material choices to solve material/environment compatibility issues in a robust fashion. In the sour HPHT testing, all of the materials were acceptable for exposures up to 48 weeks. The failures of the duplicate 945X specimens after the 6-week exposure should be explored further in an attempt to understand the noted inconsistency. The precipitation hardening alloys should be used with some caution if and when seawater cathodic protection systems impose electrical currents on these materials. Although not a part of this work, a successful application includes verifying that through-thickness mechanical properties are achieved when one orders work hardening alloys. This is especially important for large thickness components.

Lastly, there is most likely no single "right" materials choice for an offshore oil and gas production application. The prime selection criterion needs be that the potential materials candidates will be suitable for the foreseeable environments and loading conditions over the intended life of the component. In addition, the materials need to be available and delivered when they are needed and that they have the specified properties. Further, the delivered materials costs need to meet the financial constraints imposed on the project. This particular program has demonstrated that several potential candidate materials can meet a range of technical needs. Their specific applications depend on the particular offshore project.

12 REFERENCES

- [1] Special Metals, “Special Metals Flyer (725),” [Online]. Available: www.specialmetals.com.
- [2] ASTM Web Site, [Online]. Available: https://compass.astm.org/EDIT/html_annot.cgi?B983+16e1.
- [3] Special Metals, “Speical Metals Flyer (945X),” [Online]. Available: <http://www.specialmetals.com/assets/smc/documents/incoloy-alloy-945x%20v3.pdf>.
- [4] L. Foroni, C. Malara, R. Montani and S. Gregory, “UNS N09955: A New Ni-Base Alloy For H2S and Hydrogen Charging Enviornments,” in *NACE Corrosion 2015*, Dallas, TX, March 15-19, 2015.
- [5] L. Foroni, C. Malara, R. Montani and S. Gregory, “UNS N09955 Corrosion Cracking Resistance,” in *NACE Corrosion 2016*, Vancouver, Canada.
- [6] Special Metals, “Special Metals Flyer (825),” [Online]. Available: www.specialmetals.com.
- [7] Haynes International, “Haynes International Technical Library,” June 2018. [Online]. Available: www.haynesintl.com/alloys/technical-literature-list.
- [8] ASM International, “ASM Specialty Handbook,” 2000. [Online]. Available: https://books.google.com/books?hl=en&lr=&id=IePhmnbmRWkC&oi=fnd&pg=PA3&dq=N08825+melting+temperature&ots=kpf7MGFdQC&sig=RMb7V8rXSl_gZKlcAf_7GoyqhUE#v=onepage&q&f=true. [Accessed 28 June 2018].
- [9] ASTM International, “Standard Specification for Welded Precipitation Hardenable or Cold Worked, Nickel Alloy Tube,” 2017. [Online]. Available: https://compass.astm.org/EDIT/html_annot.cgi?B1007+17. [Accessed 10 July 2018].
- [10] ASTM International, “Standard Specification for Precipitation Hardened or Cold Worked, Seamless Nickel Alloy Pipe and Tube1Standard Specification for Precipitation Hardened or Cold Worked, Seamless Nickel Alloy Pipe and Tube,” 2016. [Online]. Available: https://compass.astm.org/EDIT/html_annot.cgi?B983+16e1. [Accessed 7 June 2018].
- [11] ASTM International, “Standard Specification for Precipitation-Hardening and Cold Worked Nickel Alloy Bars, Forgings, and Forging Stock for Moderate or High Temperature Service,” 2016. [Online]. Available: https://compass.astm.org/EDIT/html_annot.cgi?B637+16. [Accessed 22 June 2018].
- [12] E. J. Czyryca, “Fatigue and Corrosion Fatigue Properties of Alloys 625 Plus, 718, 725 and K-500,” The Minerals Metals & Materials Society, 1997.
- [13] ASTM International, “Standard Specification for Precipitation-Hardening Nickel Alloys Plate, Sheet, and Strip,” 2016. [Online]. Available: [https://compass.astm.org/EDIT/html_annot.cgi?B872+06\(2016\)](https://compass.astm.org/EDIT/html_annot.cgi?B872+06(2016)). [Accessed 22 June 2018].

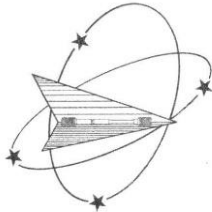
- [14] ASTM International, "Standard Specification for Precipitation Hardening Nickel Alloys Bar and Wire," 2017. [Online]. Available: [https://compass.astm.org/EDIT/html_annot.cgi?B805+06\(2017\)e1](https://compass.astm.org/EDIT/html_annot.cgi?B805+06(2017)e1). [Accessed 22 June 2018].
- [15] ASTM International, "Standard Specification for Nickel Alloy Forgings," 2017. [Online]. Available: https://compass.astm.org/EDIT/html_annot.cgi?B564+17a. [Accessed 29 June 2018].
- [16] ASTM International, "Standard Specification for Ni-Fe-Cr-Mo-Cu Alloy (UNS N08825, UNS N08221, and UNS N06845) Plate, Sheet, and Strip," 2016. [Online]. Available: [https://compass.astm.org/EDIT/html_annot.cgi?B424+11\(2016\)](https://compass.astm.org/EDIT/html_annot.cgi?B424+11(2016)). [Accessed 22 June 2018].
- [17] Special Metals, "Special Metals Flyer (718)," [Online]. Available: <http://www.specialmetals.com/assets/smc/documents/alloys/inconel/inconel-alloy-718.pdf>. [Accessed 4 6 2019].
- [18] S. A. P. B. C. a. H. E. L. McCoy, "High-Performance age hardenable nickel alloys solve problems in sour oil & gas service," *Stainless Steel World*, October 2013.
- [19] K. Sadananda and P. Shahinian, "Creep Crack Growth in Alloy 718," *Metallurgical Transactions A*, vol. 8A, pp. 439-449, 1977.
- [20] T. Chen, J. Nutter, J. Hawk and X. Liu, "Corrosion Fatigue Crack Growth Behavior of Oil-Grade Nickel-Based Alloy 718. Part 1: Effect of Corrosive Environment," *Corrosion Science*, vol. 89, pp. 146-153, 2014.
- [21] G. Stenerud, R. Johnsen and J. S. Olsen, "Hydrogen Stress Cracking and Crack Initiation in Precipitation Hardened Ni-Alloys," *Engineering Failure Analysis*, vol. 89, pp. 74-87, 2018.
- [22] L. Bartosiewicz, A. R. Krause, A. Spis, J. Raghavan and S. K. Putatunda, "Fatigue Crack Growth Behavior of a Solid Solution-Strengthened Nickel-Base Superalloy (Incoloy 825)," *JMEPEG*, vol. 1, pp. 67-74, 1992.
- [23] ASTM International, "Standard Specification for Ni-Fe-Cr-Mo-Cu Alloy (UNS N08825, UNS N08221, and UNS N06845) Rod and Bar," 2017. [Online]. Available: [https://compass.astm.org/EDIT/html_annot.cgi?B425+11\(2017\)](https://compass.astm.org/EDIT/html_annot.cgi?B425+11(2017)). [Accessed 21 June 2018].
- [24] L. L. Machuca, S. I. Bailey, R. Gubner, E. L. Watkin, M. P. Ginige, A. H. Kaksonen and K. Heidersbach, "Effect of Oxygen and Biofilms on Crevice Corrosion of UNS S31803 and UNS N08825 in Natural Seawater," *Corrosion Science*, vol. 67, pp. 242-255, 2013.
- [25] D. Agarwal, "Nickel and Nickel Alloys," John Wiley & Sons, Inc., New Jersey, 2004.
- [26] J. Kangazian and M. Shamanian, "Mechanical and Microstructural Evaluation of SAF 2507 and Incoloy 825 Dissimilar Welds," *Journal of Manufacturing Processes*, vol. 26, pp. 407-418, 2017.

- [27] V. Demetriou, J. D. Robson, M. Preuss and R. Morana, "Effect of Hydrogen on the Mechanical Properties of Alloy 945X (UNS N09945) and Influence of Microstructural Features," *Materials Science and Engineering: A*, vol. 684, pp. 423-434, 2017.
- [28] L. Foroni, C. Malara and R. Montani, "UNS N09955: A New Ni-Base Alloy For H₂S and Hydrogen Charging Environments," Foroni - Stainless Steels and Superalloys, Gorla Minore.
- [29] N. S. Zadorozne, C. M. Giordano, M. A. Rodriguez, R. M. Carranza and R. B. Rebak, "Crevice Corrosion Kinetics of Nickel Alloys Bearing Chromium and Molybdenum," *Electrochimica Acta*, vol. 76, pp. 94-101, 2012.
- [30] K. Kadirgama, K. A. Abou-El-Hossein, M. M. Noor, K. V. Sharma and B. Mohammad, "Tool Life and Wear Mechanism When Machining Hastelloy C-22HS," *Wear*, vol. 270, pp. 258-268, 2011.
- [31] ASTM International, "Standard Specification for Forged or Rolled UNS N06030, UNS N06022, UNS N06035, UNS N06200, UNS N06059, UNS N10362, UNS N06686, UNS N08020, UNS N08367, UNS N10276, UNS N10665, UNS N10675, UNS N10629, UNS N08031, UNS N06045, UNS N06025, UNS R20033 Alloy Pi," 2015. [Online]. Available: https://compass.astm.org/EDIT/html_annot.cgi?B462+15. [Accessed 26 June 2018].
- [32] J. I. Akhter, M. A. Shaikh, M. Ahmad, M. Iqbal, K. A. Shoaib and W. Ahmad, "Effect of aging on the hardness and impact properties of Hastelloy C-27," *Journal of Materials Science Letters*, vol. 20, pp. 333-335, 2001.
- [33] G. E. Gdowski, "Survey of Degradation Modes of Four Nickel-Chromium-Molybdenum Alloys," Lawrence Livermore National Laboratory, Livermore, 1991.

APPENDIX A:

MECHANICAL PROPERTY TEST REPORTS

A.1 MECHANICAL TEST REPORTS FOR ALLOY 725



Westmoreland Mechanical Testing & Research, Inc.
 P.O.Box 388; 221 Westmoreland Drive
 Youngstown, PA 15696-0388 U.S.A.
 Telephone: 724-537-3131 Fax: 724-537-3151
 Website: www.wmtr.com E-Mail: admin@wmtr.com
WMT&R is a technical leader in the material testing industry.



October 12, 2017
 Honeywell Corrosion Solutions
 11201 Greens Crossing
 Suite 700
 Houston, TEXAS 77067

WMT&R Report No. 7-74525
 P.O. No. 4410873689
 WMT&R Quote No. QN173308 Rev.2
 Project No. USP-012888

CERTIFICATION

Attention: Jie He
 Subject: All processes, performed upon the material as received, were conducted at WMT&R, Inc. in accordance with the WMT&R Quality Assurance Manual, Rev. 11, dated 12/03/2008.
 The following tests were performed on this order: IMPACT and TENSILE

IMPACT RESULTS: ASTM E23-16b

No Requirements

MATERIAL: 725

SAMPLE TYPE: Charpy V-Notch

DISPOSITION: Report

DNV	Sample	TestLog Number	Sample Size	Temp. °F	Energy ft-lbs	Mils Lat Exp	% Shear Fracture	AUAR
2810	Charpy-4	3836JH	Standard	32	74	34	25	Report
2810	Charpy-5	3837JH	Standard	32	68	32	20	Report
2810	Charpy-6	3838JH	Standard	32	68	27	20	Report

IMPACT RESULTS: ASTM E23-16b

No Requirements

MATERIAL: 725

SAMPLE TYPE: Charpy V-Notch

DISPOSITION: Report

DNV	Sample	TestLog Number	Sample Size	Temp. °F	Energy ft-lbs	Mils Lat Exp	% Shear Fracture	AUAR
2810	Charpy-1	3833JH	Standard	73	66	32	20	Report
2810	Charpy-2	3834JH	Standard	73	72	36	20	Report
2810	Charpy-3	3835JH	Standard	73	65	31	20	Report

E23 8mm Striker used for testing.

"NOTE: THE RECORDING OF FALSE, FICTITIOUS OR FRAUDULENT STATEMENTS OR ENTRIES ON THIS DOCUMENT MAY BE PUNISHABLE AS A FELONY UNDER FEDERAL STATUTE."
 THIS CERTIFICATE OR REPORT SHALL NOT BE REPRODUCED EXCEPT IN FULL, WITHOUT THE WRITTEN APPROVAL OF WMTR, INC.

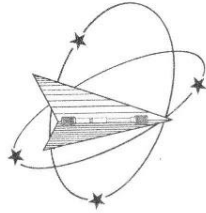
Matthew Wojton
 Matt Wojton
 Tensile Supervisor

October 12, 2017



Testing Specialists for Aerospace, Automotive, and Material Testing Fields
 Locations in Youngstown, PA U.S.A. ~ Tel. (724) 537-3131 and
 Banbury, Oxon U.K. ~ Tel. +44 (0) 1295 261211

A-2



Westmoreland Mechanical Testing & Research, Inc.
 P.O. Box 388; 221 Westmoreland Drive
 Youngstown, PA 15696-0388 U.S.A.
 Telephone: 724-537-3131 Fax: 724-537-3151
 Website: www.wmtr.com E-Mail: admin@wmtr.com
WMT&R is a technical leader in the material testing industry.



CERTIFICATION

October 12, 2017
 Honeywell Corrosion Solutions
 11201 Greens Crossing
 Suite 700
 Houston, TEXAS 77067

WMT&R Report No. 7-74525
 P.O. No. 4410873689
 WMT&R Quote No. QN173308 Rev.2
 Project No. USP-012688

Attention: Jie He

Subject: All processes, performed upon the material as received, were conducted at WMT&R, Inc. in accordance with the WMT&R Quality Assurance Manual, Rev. 11, dated 12/03/2008.
 The following tests were performed on this order: IMPACT and TENSILE

TENSILE RESULTS: ASTM E8-16a

SPEED OF TESTING: 0.005 in./in./min., Extensometer travel exceeded - Test continued at last stroke rate

DISPOSITION: Report

MATERIAL: 725

DNV	Sample	TestLog Number	Temp.	UTS ksi	0.2% YS ksi	YS (0.2% EUL) ksi	Elong %	RA %	Modulus Msi	Ult. Load lbf	0.2% YLD. lbf	Load (0.2% EUL) lbf
2810	Ten-1	3827JH	Room	190.7	129.5	66.8	38	50	33.9	9562	6497	3351
2810	Ten-2	3828JH	Room	189.6	129.8	58.4	37	48	29.3	9519	6516	2930
2810	Ten-3	3829JH	Room	193.1	133.5	56.6	35	49	28.5	9670	6687	2835

AIUR: A=ACCEPTABLE, U=UNACCEPTABLE, R=REPORT

DISPOSITION: Report

DNV	Sample	TestLog Number	Orig. Dia. (in.)	Final Dia. (in.)	4D Orig GL (in.)	4D Final GL (in.)	Orig. Area (sq. in.)	Machine Number	AIUR
2810	Ten-1	3827JH	0.2527	0.1792	1.00	1.38	0.05015340	M26	R
2810	Ten-2	3828JH	0.2528	0.1816	1.00	1.37	0.05019310	M26	R
2810	Ten-3	3829JH	0.2525	0.1796	1.00	1.35	0.05007404	M26	R

AIUR: A=ACCEPTABLE, U=UNACCEPTABLE, R=REPORT

A-3

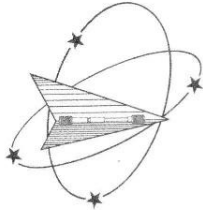
*NOTE: THE RECORDING OF FALSE, FICTITIOUS OR FRAUDULENT STATEMENTS OR ENTRIES ON THIS DOCUMENT MAY BE PUNISHABLE AS A FELONY UNDER FEDERAL STATUTES * THIS CERTIFICATE OR REPORT SHALL NOT BE REPRODUCED EXCEPT IN FULL, WITHOUT THE WRITTEN APPROVAL OF WMTR, INC.

Matt Wojton
 Tensile Supervisor

October 12, 2017



Testing Specialists for Aerospace, Automotive, and Material Testing Fields
 Locations in Youngstown, PA U.S.A. ~ Tel. (724) 537-3131 and
 Banbury, Oxon U.K. ~ Tel. +44 (0) 1295 261211



Westmoreland Mechanical Testing & Research, Inc.
 P.O. Box 388, 221 Westmoreland Drive
 Youngstown, PA 15696-0388 U.S.A.
 Telephone: 724-537-3131 Fax: 724-537-3151
 Website: www.wmtr.com E-Mail: admin@wmtr.com
 WMT&R is a technical leader in the material testing industry.



October 12, 2017
 Honeywell Corrosion Solutions

CERTIFICATION

WMT&R Report No. 7-74525
 P.O. No. 4410873689

TENSILE RESULTS: ASTM E21-09

SOAK TIME: 30 Minutes

SPEED OF TESTING: 0.005 in./in./min., Extensometer travel exceeded - Test continued at last stroke rate

MATERIAL: 725

DISPOSITION: Report

DNV	Sample	TestLog Number	Temp. °F	UTS ksi	0.2% YS ksi	YS (0.2% EUL) ksi	Elong %	RA %	Modulus Msi	Ult. Load lbf	0.2% YLD. lbf	Load (0.2% EUL) lbf
2810	Ten-4	3830JH	350	179.4	122.4	61.6	36.0	51.0	30.7	9012	6149	3094
2810	Ten-5	3831JH	350	179.6	123.2	59.1	33.0	51.0	29.7	9029	6196	2969
2810	Ten-6	3832JH	350	181.3	124.8	63.8	34.0	53.5	31.3	9094	6258	3202

A/U/R: A=ACCEPTABLE, U=UNACCEPTABLE, R=REPORT

DISPOSITION: Report

DNV	Sample	TestLog Number	Orig. Dia. (in.)	Final Dia. (in.)	4D Orig GL (in.)	4D Final GL (in.)	Orig. Area (sq. in.)	Machine Number	A/U/R
2810	Ten-4	3830JH	0.2529	0.1768	1.00	1.36	0.05023282	M20	R
2810	Ten-5	3831JH	0.2530	0.1769	1.00	1.33	0.05027255	M20	R
2810	Ten-6	3832JH	0.2527	0.1726	1.00	1.34	0.05015340	M20	R

A/U/R: A=ACCEPTABLE, U=UNACCEPTABLE, R=REPORT

A-4

Matthew Wojton
 Matt Wojton
 Tensile Supervisor

October 12, 2017



NOTE: THE RECORDING OF FALSE, FICTITIOUS OR FRAUDULENT STATEMENTS OR ENTRIES ON THIS DOCUMENT MAY BE PUNISHABLE AS A FELONY UNDER FEDERAL STATUTE. THIS CERTIFICATE OR REPORT SHALL NOT BE REPRODUCED EXCEPT IN FULL, WITHOUT THE WRITTEN APPROVAL OF WMTR, INC.

Testing Specialists for Aerospace, Automotive, and Material Testing Fields
 Locations in Youngstown, PA U.S.A. ~ Tel. (724) 537-3131 and
 Banbury, Oxon U.K. ~ Tel. +44 (0) 1295 261211

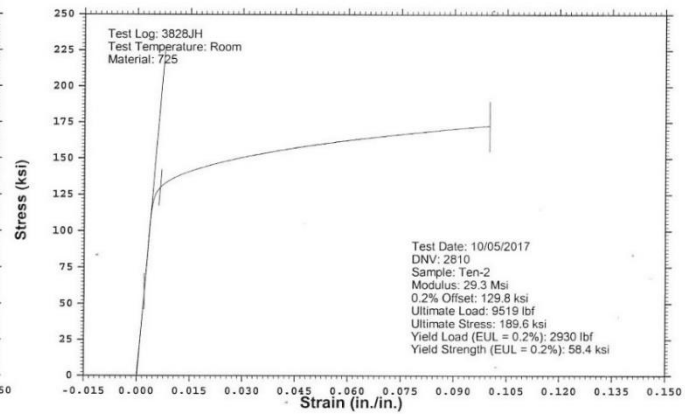
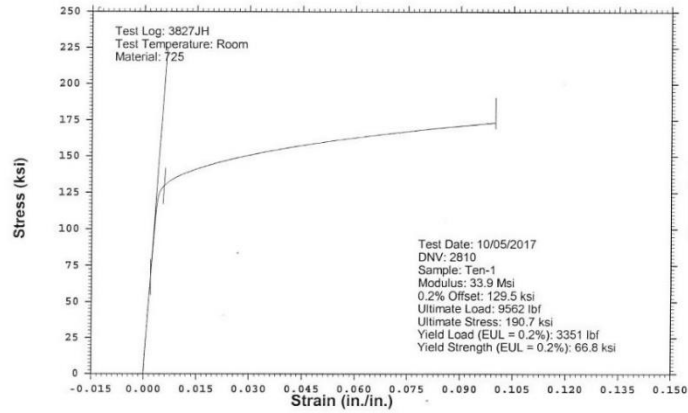
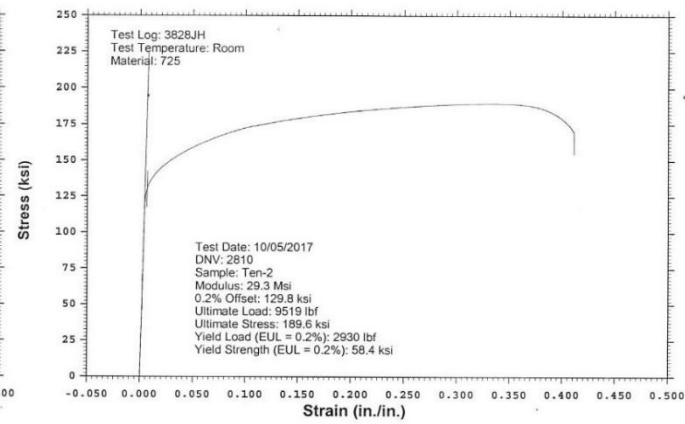
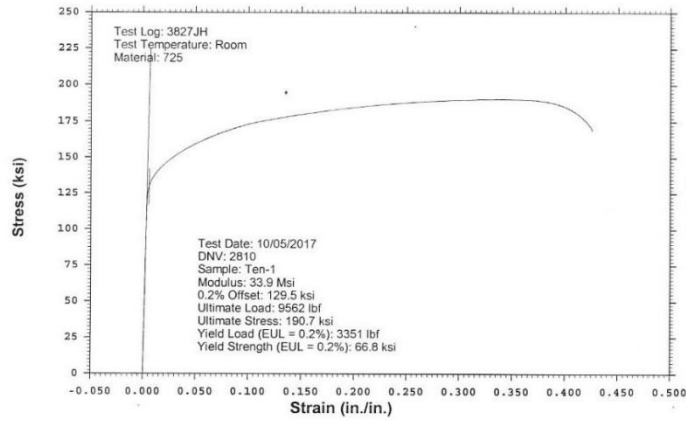
WESTMORELAND MECHANICAL TESTING & RESEARCH, Inc

Stress vs. Strain

Phone: (724)537-3131

Customer: Honeywell Corrosion Solutions
WMT&R Report: 7-74525

P.O. No.: 4410873689
WMT&R Quote No.: QN173308 Rev.2
Project No.: USP-012888



*NOTE: THE RECORDING OF FALSE, FICTITIOUS OR FRAUDULENT STATEMENTS OR ENTRIES ON THIS DOCUMENT
MAY BE PUNISHABLE AS A FELONY UNDER FEDERAL STATUTE.*

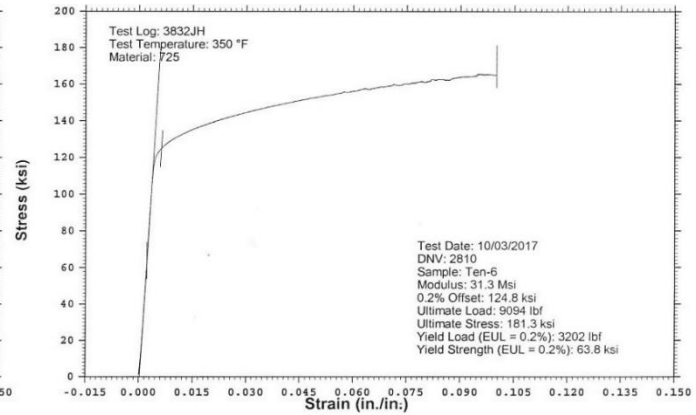
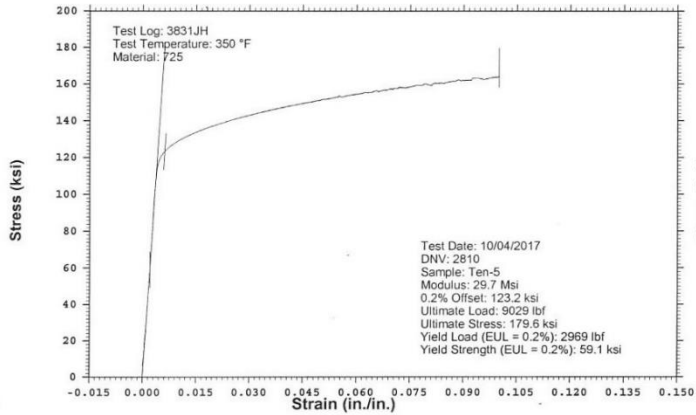
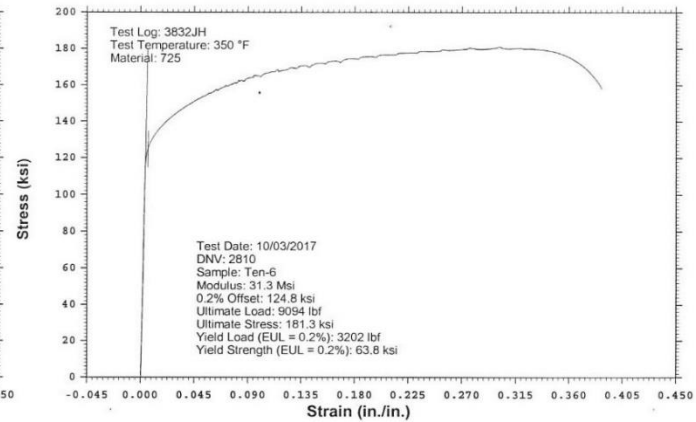
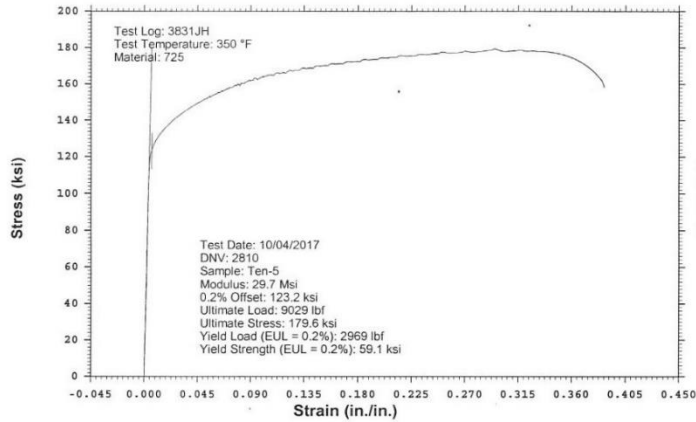
WESTMORELAND MECHANICAL TESTING & RESEARCH, Inc

Stress vs. Strain

Phone: (724)537-3131

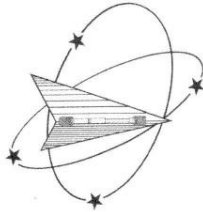
Customer: Honeywell Corrosion Solutions
WMT&R Report: 7-74525

P.O. No.: 4410873689
WMT&R Quote No.: QN173308 Rev.2
Project No.: USP-012888



"NOTE: THE RECORDING OF FALSE, FICTITIOUS OR FRAUDULENT STATEMENTS OR ENTRIES ON THIS DOCUMENT MAY BE PUNISHABLE AS A FELONY UNDER FEDERAL STATUTE."

A.2 MECHANICAL TEST REPORTS FOR ALLOY 945X



Westmoreland Mechanical Testing & Research, Inc.
 P.O. Box 388; 221 Westmoreland Drive
 Youngstown, PA 15696-0388 U.S.A.
 Telephone: 724-537-3131 Fax: 724-537-3151
 Website: www.wmtr.com E-Mail: admin@wmtr.com
WMT&R is a technical leader in the material testing industry.



CERTIFICATION

October 18, 2017
 Honeywell Corrosion Solutions
 11201 Greens Crossing
 Suite 700
 Houston, TEXAS 77067

WMT&R Report No. 7-74526
 P.O. No. 4410873689
 WMT&R Quote No. QN173308 Rev.2
 Project No. USP-012888

Attention: Jie He

Subject: All processes, performed upon the material as received, were conducted at WMT&R, Inc. in accordance with the WMT&R Quality Assurance Manual, Rev. 11, dated 12/03/2008.
 The following tests were performed on this order: IMPACT and TENSILE

IMPACT RESULTS: ASTM E23-16b

No Requirements

MATERIAL: 945X

SAMPLE TYPE: Charpy V-Notch

DISPOSITION: Report

DNV	Sample	TestLog Number	Sample Size	Temp. °F	Energy ft-lbs	Mils Lat Exp	% Shear Fracture	AIUR
2805	Charpy-4	3848JH	Standard	32	112	47	30	Report
2805	Charpy-5	3849JH	Standard	32	106	44	25	Report
2805	Charpy-6	3850JH	Standard	32	99	53	25	Report

IMPACT RESULTS: ASTM E23-16b

No Requirements

MATERIAL: 945X

SAMPLE TYPE: Charpy V-Notch

DISPOSITION: Report

DNV	Sample	TestLog Number	Sample Size	Temp. °F	Energy ft-lbs	Mils Lat Exp	% Shear Fracture	AIUR
2805	Charpy-1	3845JH	Standard	73	101	42	25	Report
2805	Charpy-2	3846JH	Standard	73	105	48	25	Report
2805	Charpy-3	3847JH	Standard	73	96	47	25	Report

E23 8mm Striker used for testing.

"NOTE: THE RECORDING OF FALSE, FICTITIOUS OR FRAUDULENT STATEMENTS OR ENTRIES ON THIS DOCUMENT MAY BE PUNISHABLE AS A FELONY UNDER FEDERAL STATUTE." THIS CERTIFICATE OR REPORT SHALL NOT BE REPRODUCED EXCEPT IN FULL, WITHOUT THE WRITTEN APPROVAL OF WMT&R, INC.

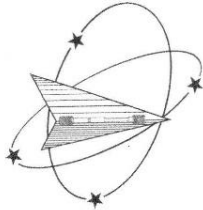
Matthew Wojton
 Matt Wojton
 Tensile Supervisor

October 18, 2017



Testing Specialists for Aerospace, Automotive, and Material Testing Fields
 Locations in Youngstown, PA U.S.A. ~ Tel. (724) 537-3131 and
 Banbury, Oxon U.K. ~ Tel. +44 (0) 1295 261211

A-8



Westmoreland Mechanical Testing & Research, Inc.
 P.O. Box 388; 221 Westmoreland Drive
 Youngstown, PA 15696-0388 U.S.A.
 Telephone: 724-537-3131 Fax: 724-537-3151
 Website: www.wmtr.com E-Mail: admin@wmtr.com
 WMT&R is a technical leader in the material testing industry.



CERTIFICATION

October 18, 2017
 Honeywell Corrosion Solutions
 11201 Greens Crossing
 Suite 700
 Houston, TEXAS 77067

WMT&R Report No. 7-74526
 P.O. No. 4410873689
 WMT&R Quote No. QN173308 Rev.2
 Project No. USP-012888

Attention: Jie He

Subject: All processes, performed upon the material as received, were conducted at WMT&R, Inc. in accordance with the WMT&R Quality Assurance Manual, Rev. 11, dated 12/03/2008.
 The following tests were performed on this order: IMPACT and TENSILE

TENSILE RESULTS: ASTM E8-16a

SPEED OF TESTING: 0.005 in./in./min., Extensometer travel exceeded - Test continued at last stroke rate

DISPOSITION: Report

MATERIAL: Alloy 945X

DNV	Sample	TestLog Number	Temp.	UTS ksi	0.2% YS ksi	YS (0.2% EUL) ksi	Elong %	RA %	Modulus Msi	Ult. Load lbf	0.2% YLD. lbf	Load (0.2% EUL) lbf
2805	Ten-1	3839JH	Room	181.0	149.5	60.6	24	35	30.5	9030	7456	3025
2805	Ten-2	3840JH	Room	189.2	148.2	63.3	31	49	31.6	9438	7391	3157
2805	Ten-3	3841JH	Room	184.3	147.9	60.8	32	50	30.4	9198	7384	3033

A/U/R: A=ACCEPTABLE, U=UNACCEPTABLE, R=REPORT

DISPOSITION: Report

DNV	Sample	TestLog Number	Orig. Dia. (in.)	Final Dia. (in.)	4D Orig GL (in.)	4D Final GL (in.)	Orig. Area (sq. in.)	Machine Number	A/U/R
2805	Ten-1	3839JH	0.2520	0.2030	1.00	1.24	0.04987592	M13	R
2805	Ten-2	3840JH	0.2520	0.1796	1.00	1.31	0.04987592	M13	R
2805	Ten-3	3841JH	0.2521	0.1781	1.00	1.32	0.04991552	M13	R

A/U/R: A=ACCEPTABLE, U=UNACCEPTABLE, R=REPORT

A-9

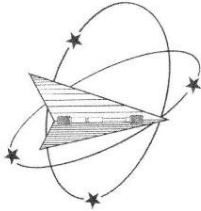
*NOTE: THE RECORDING OF FALSE, FICTITIOUS OR FRAUDULENT STATEMENTS OR ENTRIES ON THIS DOCUMENT MAY BE PUNISHABLE AS A FELONY UNDER FEDERAL STATUTE. THIS CERTIFICATE OR REPORT SHALL NOT BE REPRODUCED EXCEPT IN FULL, WITHOUT THE WRITTEN APPROVAL OF WMT&R, INC.

Matt Wojton
 Tensile Supervisor

October 18, 2017



Testing Specialists for Aerospace, Automotive, and Material Testing Fields
 Locations in Youngstown, PA U.S.A. ~ Tel. (724) 537-3131 and
 Banbury, Oxon U.K. ~ Tel. +44 (0) 1295 261211



Westmoreland Mechanical Testing & Research, Inc.
 P.O. Box 388; 221 Westmoreland Drive
 Youngstown, PA 15696-0388 U.S.A.
 Telephone: 724-537-3131 Fax: 724-537-3151
 Website: www.wmtr.com E-Mail: admin@wmtr.com
WMT&R is a technical leader in the material testing industry.



CERTIFICATION

October 18, 2017
 Honeywell Corrosion Solutions

WMT&R Report No. 7-74526
 P.O. No. 4410873689

TENSILE RESULTS: ASTM E21-09

SOAK TIME: 30 Minutes

SPEED OF TESTING: 0.005 in./in./min., Extensometer travel exceeded - Test continued at last stroke rate

MATERIAL: Alloy 945X

DISPOSITION: Report

DNV	Sample	TestLog Number	Temp. °F	UTS ksi	0.2% YS ksi	YS (0.2% EUL) ksi	Elong %	RA %	Modulus Msi	Ult. Load lbf	0.2% YLD. lbf	Load (0.2% EUL) lbf
2805	Ten-4	3842JH	350	175.5	140.5	57.0	29.0	52.0	28.5	8745	7004	2843
2805	Ten-5	3843JH	350	176.7	140.9	64.6	30.0	54.5	32.3	8815	7026	3223
2805	Ten-6	3844JH	350	175.5	140.0	61.8	29.0	54.0	30.8	8752	6982	3083

A/U/R: A=ACCEPTABLE, U=UNACCEPTABLE, R=REPORT

DISPOSITION: Report

DNV	Sample	TestLog Number	Orig. Dia. (in.)	Final Dia. (in.)	4D Orig GL (in.)	4D Final GL (in.)	Orig. Area (sq. in.)	Machine Number	A/U/R
2805	Ten-4	3842JH	0.2519	0.1741	1.00	1.29	0.04983635	M20	R
2805	Ten-5	3843JH	0.2520	0.1698	1.00	1.30	0.04987592	M20	R
2805	Ten-6	3844JH	0.2520	0.1709	1.00	1.29	0.04987592	M20	R

A/U/R: A=ACCEPTABLE, U=UNACCEPTABLE, R=REPORT

A-10

"NOTE: THE RECORDING OF FALSE, FICTITIOUS OR FRAUDULENT STATEMENTS OR ENTRIES ON THIS DOCUMENT MAY BE PUNISHABLE AS A FELONY UNDER FEDERAL STATUTE."
 THIS CERTIFICATE OR REPORT SHALL NOT BE REPRODUCED EXCEPT IN FULL, WITHOUT THE WRITTEN APPROVAL OF WMT&R, INC.

Matthew Wojton
 Matt Wojton
 Tensile Supervisor

October 18, 2017



Testing Specialists for Aerospace, Automotive, and Material Testing Fields
 Locations in Youngstown, PA U.S.A. ~ Tel. (724) 537-3131 and
 Banbury, Oxon U.K. ~ Tel. +44 (0) 1295 261211

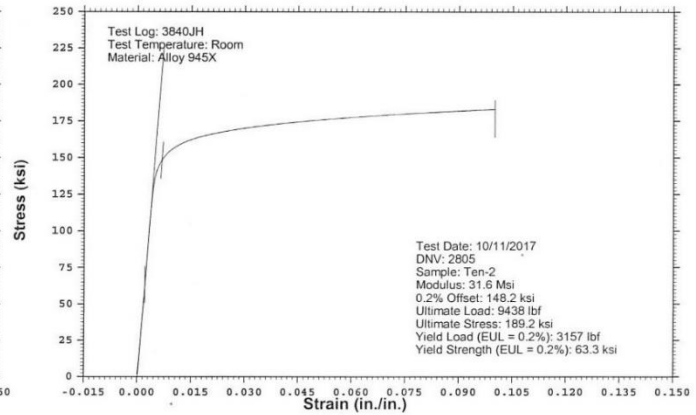
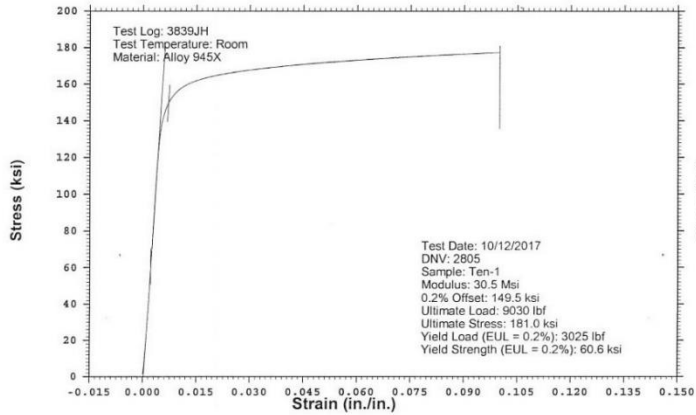
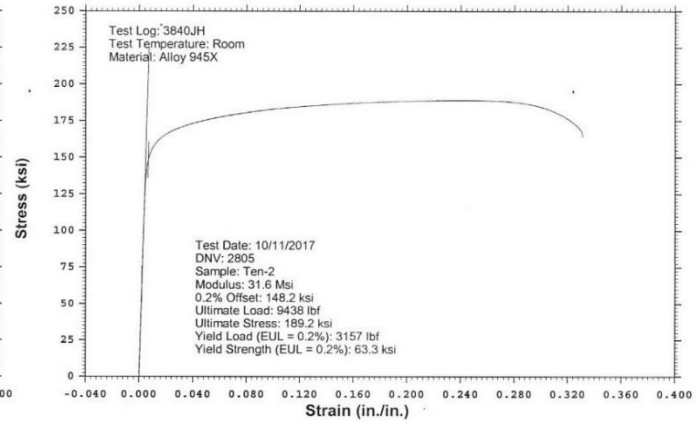
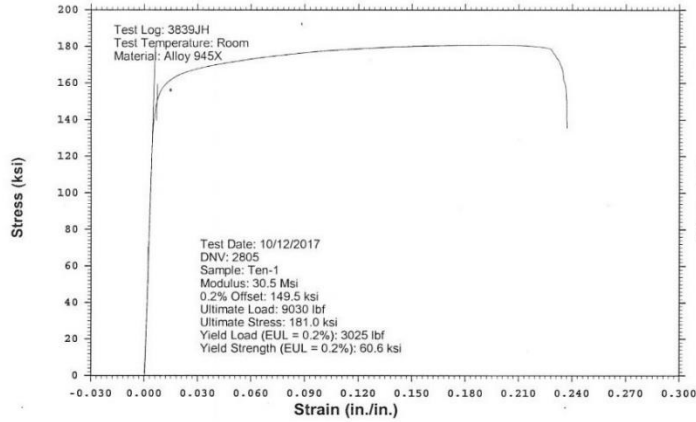
WESTMORELAND MECHANICAL TESTING & RESEARCH, Inc

Stress vs. Strain

Phone: (724)537-3131

Customer: Honeywell Corrosion Solutions
WMT&R Report: 7-74526

P.O. No.: 4410873689
WMT&R Quote No.: QN173308 Rev.2
Project No.: USP-012888



"NOTE: THE RECORDING OF FALSE, FICTITIOUS OR FRAUDULENT STATEMENTS OR ENTRIES ON THIS DOCUMENT MAY BE PUNISHABLE AS A FELONY UNDER FEDERAL STATUTE."

11-V

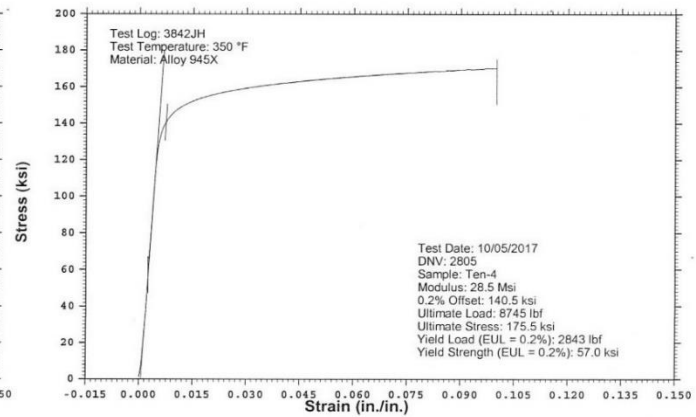
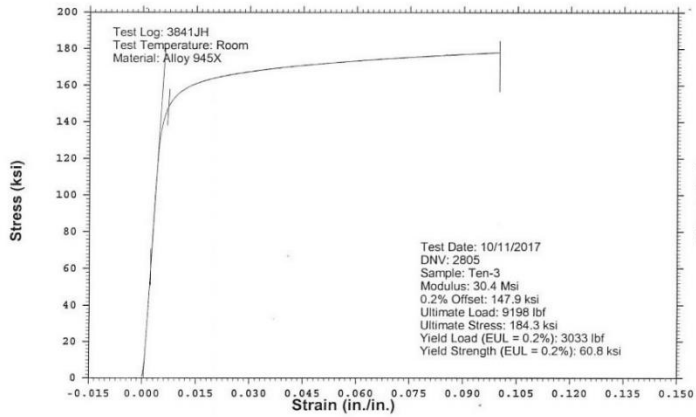
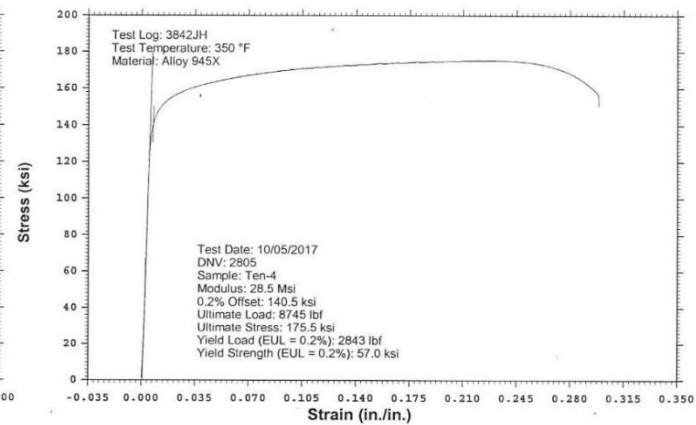
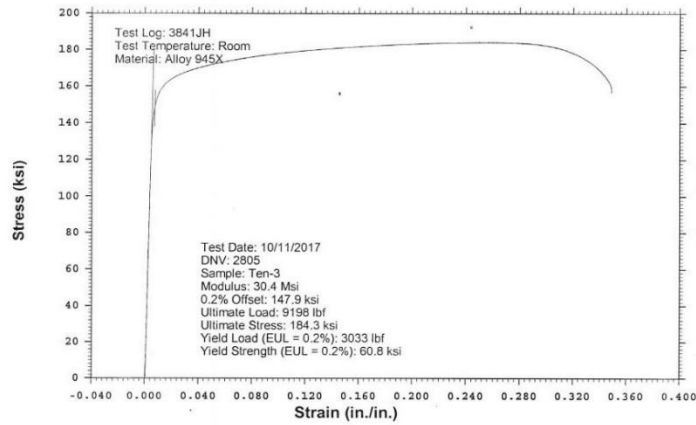
WESTMORELAND MECHANICAL TESTING & RESEARCH, Inc

Stress vs. Strain

Phone: (724)537-3131

Customer: Honeywell Corrosion Solutions
WMT&R Report: 7-74526

P.O. No.: 4410873689
WMT&R Quote No.: QN173308 Rev.2
Project No.: USP-012888



"NOTE: THE RECORDING OF FALSE, FICTITIOUS OR FRAUDULENT STATEMENTS OR ENTRIES ON THIS DOCUMENT MAY BE PUNISHABLE AS A FELONY UNDER FEDERAL STATUTE."

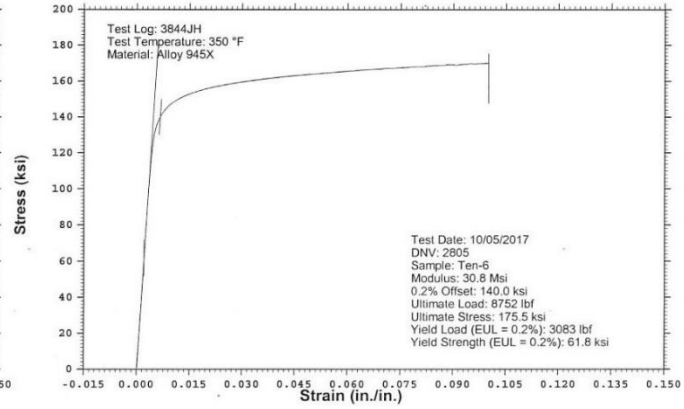
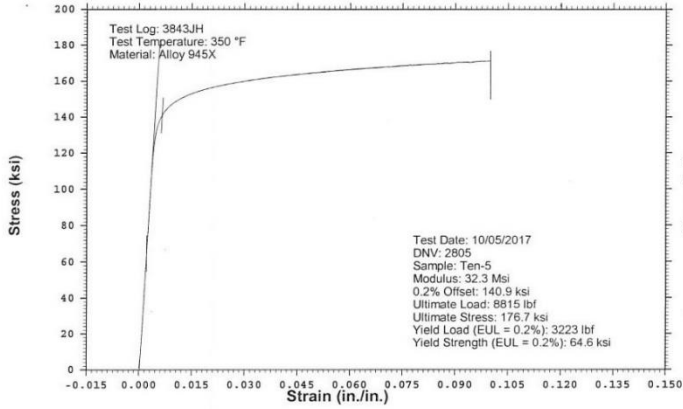
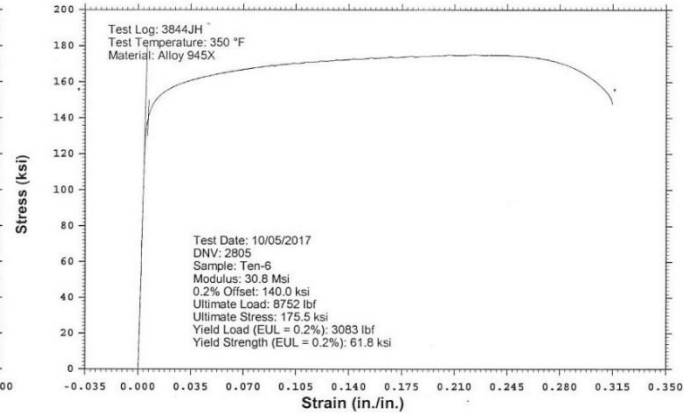
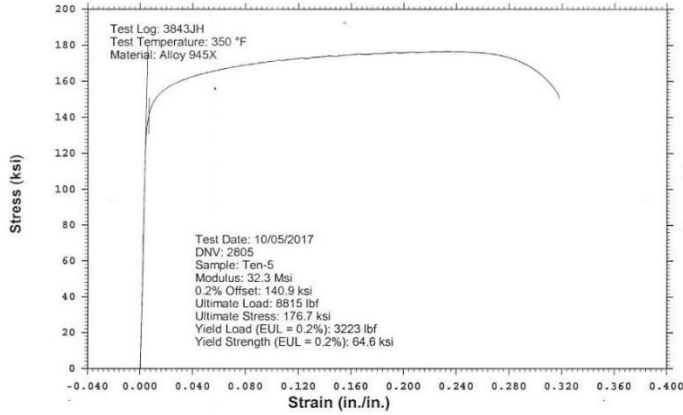
WESTMORELAND MECHANICAL TESTING & RESEARCH, Inc

Stress vs. Strain

Phone: (724)537-3131

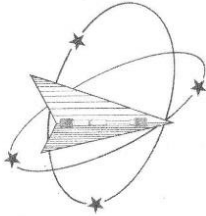
Customer: Honeywell Corrosion Solutions
WMT&R Report: 7-74526

P.O. No.: 4410873689
WMT&R Quote No.: QN173308 Rev.2
Project No.: USP-012888



"NOTE: THE RECORDING OF FALSE, FICTITIOUS OR FRAUDULENT STATEMENTS OR ENTRIES ON THIS DOCUMENT
MAY BE PUNISHABLE AS A FELONY UNDER FEDERAL STATUTE."

A.3 MECHANICAL TEST REPORTS FOR ALLOY 955



Westmoreland Mechanical Testing & Research, Inc.
 P.O. Box 388; 221 Westmoreland Drive
 Youngstown, PA 15696-0388 U.S.A.
 Telephone: 724-537-3131 Fax: 724-537-3151
 Website: www.wmtr.com E-Mail: admin@wmtr.com
 WMT&R is a technical leader in the material testing industry.



CERTIFICATION

October 7, 2017
 Honeywell Corrosion Solutions
 11201 Greens Crossing
 Suite 700
 Houston, TEXAS 77067

WMT&R Report No. 7-74520
 P.O. No. 4410873689
 WMT&R Quote No. QN173308 Rev.2
 Project No. USP-012888

Attention: Jie He
 Subject: All processes, performed upon the material as received, were conducted at WMT&R, Inc. in accordance with the WMT&R Quality Assurance Manual, Rev. 11, dated 12/03/2008.
 The following tests were performed on this order: IMPACT and TENSILE

IMPACT RESULTS: ASTM E23-16b

No Requirements

MATERIAL: 955

SAMPLE TYPE: Charpy V-Notch

DISPOSITION: Report

DNV	Sample	TestLog Number	Sample Size	Temp. °F	Energy ft-lbs	Mils Lat Exp	% Shear Fracture	AUR
2808	Charpy-4	3792JH	Standard	32	96	43	20	Report
2808	Charpy-5	3793JH	Standard	32	95	41	20	Report
2808	Charpy-6	3794JH	Standard	32	98	46	25	Report

IMPACT RESULTS: ASTM E23-16b

No Requirements

MATERIAL: 955

SAMPLE TYPE: Charpy V-Notch

DISPOSITION: Report

DNV	Sample	TestLog Number	Sample Size	Temp. °F	Energy ft-lbs	Mils Lat Exp	% Shear Fracture	AUR
2808	Charpy-1	3789JH	Standard	73	91	41	20	Report
2808	Charpy-2	3790JH	Standard	73	92	43	20	Report
2808	Charpy-3	3791JH	Standard	73	85	41	20	Report

E23 8mm Striker used for testing.

NOTE: THE RECORDING OF FALSE, FICTITIOUS OR FRAUDULENT STATEMENTS OR ENTRIES ON THIS DOCUMENT MAY BE PUNISHABLE AS A FELONY UNDER FEDERAL STATUTE.
 THIS CERTIFICATE OR REPORT SHALL NOT BE REPRODUCED EXCEPT IN FULL, WITHOUT THE WRITTEN APPROVAL OF WMTR, INC.

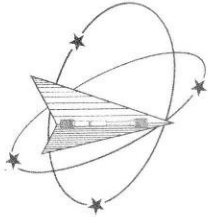
Matthew Wojton
 Matt Wojton
 Tensile Supervisor

October 7, 2017



Testing Specialists for Aerospace, Automotive, and Material Testing Fields
 Locations in Youngstown, PA U.S.A. ~ Tel. (724) 537-3131 and
 Banbury, Oxon U.K. ~ Tel. +44 (0) 1295 261211

A-15



Westmoreland Mechanical Testing & Research, Inc.
 P.O. Box 388; 221 Westmoreland Drive
 Youngstown, PA 15696-0388 U.S.A.
 Telephone: 724-537-3131 Fax: 724-537-3151
 Website: www.wmtr.com E-Mail: admin@wmtr.com
 WMT&R is a technical leader in the material testing industry.



CERTIFICATION

October 7, 2017
 Honeywell Corrosion Solutions
 11201 Greens Crossing
 Suite 700
 Houston, TEXAS 77067

WMT&R Report No. 7-74520
 P.O. No. 4410873689
 WMT&R Quote No. QN173308 Rev.2
 Project No. USP-012888

Attention: Jie He

Subject: All processes, performed upon the material as received, were conducted at WMT&R, Inc. in accordance with the WMT&R Quality Assurance Manual, Rev. 11, dated 12/03/2008.
 The following tests were performed on this order: IMPACT and TENSILE

TENSILE RESULTS: ASTM E8-16a

SPEED OF TESTING: 0.005 in./in./min., Extensometer travel exceeded - Test continued at last stroke rate

MATERIAL: ALLOY 955

DISPOSITION: Report

DNV	Sample	TestLog Number	Temp.	UTS ksi	0.2% YS ksi	Elong %	RA %	Modulus Msi	Ult. Load lbf	0.2% YLD. lbf	Orig. Dia. (in.)	Final Dia. (in.)	4D Orig GL (in.)	4D Final GL (in.)	Orig. Area (sq. in.)	Machine Number	AUIR
2808	Ten-1	3783JH	Room	186.3	148.0	34	52	26.4	9297	7386	0.2521	0.1749	1.00	1.34	0.04991552	M13	R
2808	Ten-2	3784JH	Room	185.3	146.6	34	50	29.5	9256	7322	0.2522	0.1775	1.00	1.34	0.04995512	M13	R
2808	Ten-3	3785JH	Room	182.9	147.2	34	55	30.1	9139	7351	0.2522	0.1699	1.00	1.34	0.04995512	M13	R

AUIR: A=ACCEPTABLE, U=UNACCEPTABLE, R=REPORT

TENSILE RESULTS: ASTM E21-09

SOAK TIME: 30 Minutes

SPEED OF TESTING: 0.005 in./in./min., Extensometer travel exceeded - Test continued at last stroke rate

MATERIAL: ALLOY 955

DISPOSITION: Report

DNV	Sample	TestLog Number	Temp. °F	UTS ksi	0.2% YS ksi	Elong %	RA %	Modulus Msi	Ult. Load lbf	0.2% YLD. lbf	Orig. Dia. (in.)	Final Dia. (in.)	4D Orig GL (in.)	4D Final GL (in.)	Orig. Area (sq. in.)	Machine Number	AUIR
2808	Ten-4	3786JH	350	171.4	138.0	33.0	51.5	31.4	8557	6891	0.2521	0.1757	1.00	1.33	0.04991552	M20	R
2808	Ten-5	3787JH	350	168.3	137.5	35.0	57.5	30.7	8385	6854	0.2519	0.1645	1.00	1.35	0.04983635	M20	R
2808	Ten-6	3788JH	350	168.9	137.6	34.0	53.5	30.9	8424	6865	0.2520	0.1718	1.00	1.34	0.04987592	M20	R

AUIR: A=ACCEPTABLE, U=UNACCEPTABLE, R=REPORT

Matthew Wojton
 Matt Wojton
 Tensile Supervisor

October 7, 2017



*NOTE: THE RECORDING OF FALSE, FICTITIOUS OR FRAUDULENT STATEMENTS OR ENTRIES ON THIS DOCUMENT MAY BE PUNISHABLE AS A FELONY UNDER FEDERAL STATUTE. THIS CERTIFICATE OR REPORT SHALL NOT BE REPRODUCED EXCEPT IN FULL, WITHOUT THE WRITTEN APPROVAL OF WMTR, INC.

Testing Specialists for Aerospace, Automotive, and Material Testing Fields
 Locations in Youngstown, PA U.S.A. ~ Tel. (724) 537-3131 and
 Banbury, Oxon U.K. ~ Tel. +44 (0) 1295 261211

A-16

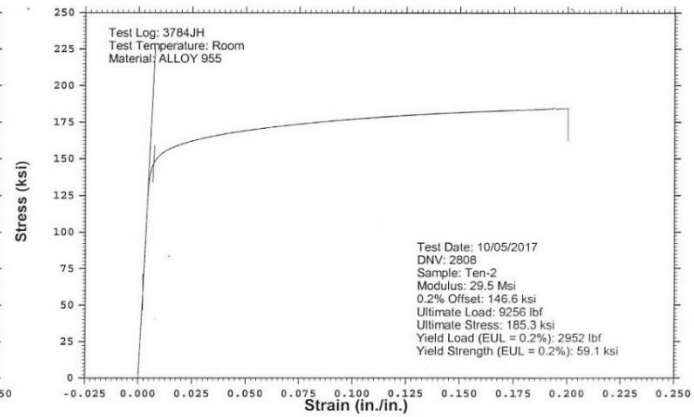
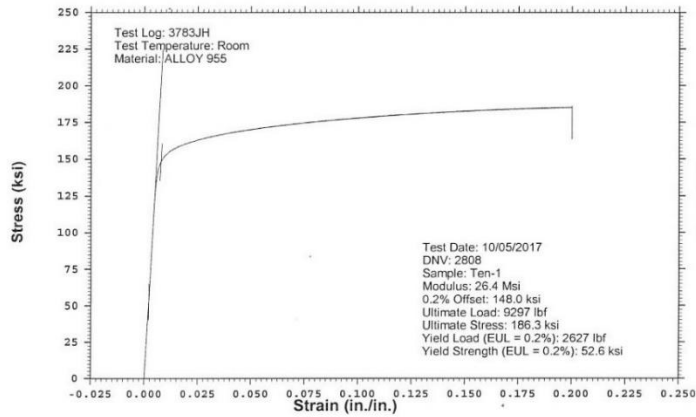
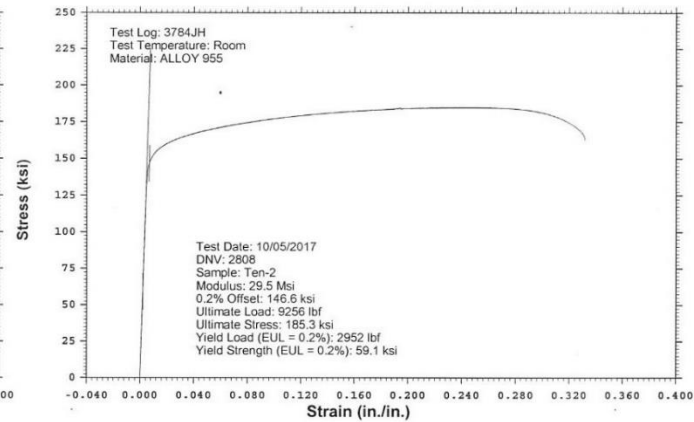
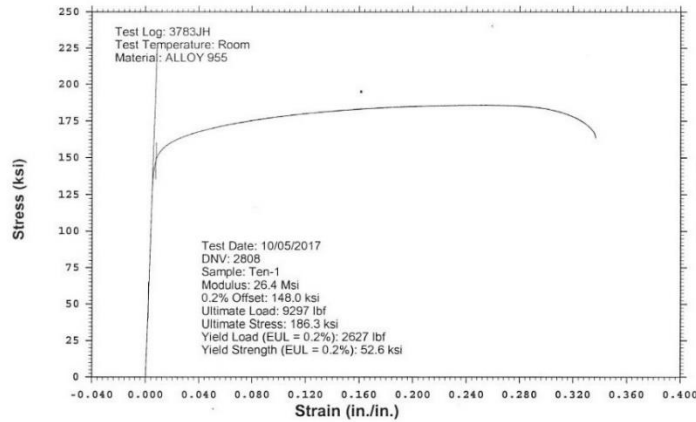
WESTMORELAND MECHANICAL TESTING & RESEARCH, Inc

Stress vs. Strain

Phone: (724)537-3131

Customer: Honeywell Corrosion Solutions
WMT&R Report: 7-74520

P.O. No.: 4410873689
WMT&R Quote No.: QN173308 Rev.2
Project No.: USP-012888



"NOTE: THE RECORDING OF FALSE, FICTITIOUS OR FRAUDULENT STATEMENTS OR ENTRIES ON THIS DOCUMENT MAY BE PUNISHABLE AS A FELONY UNDER FEDERAL STATUTE."

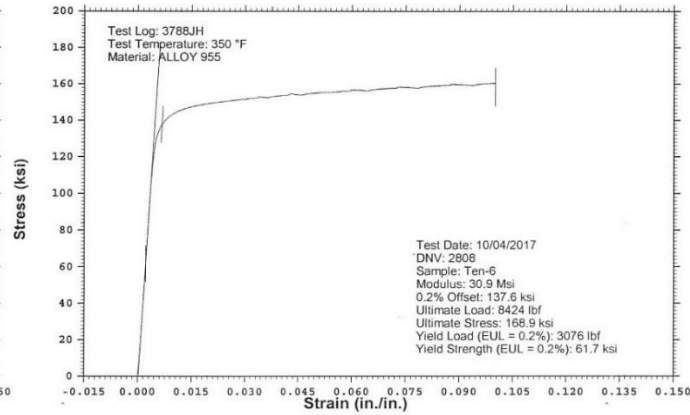
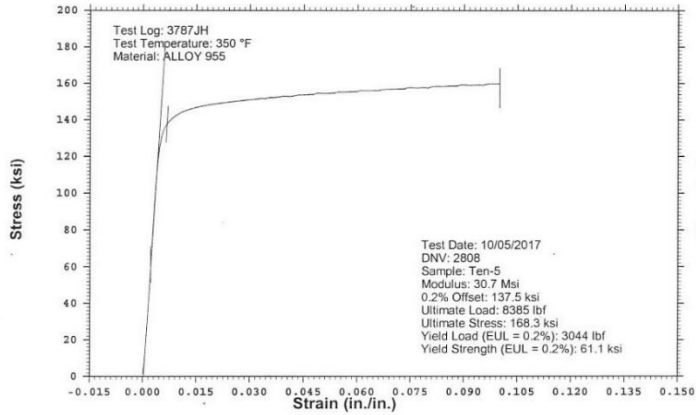
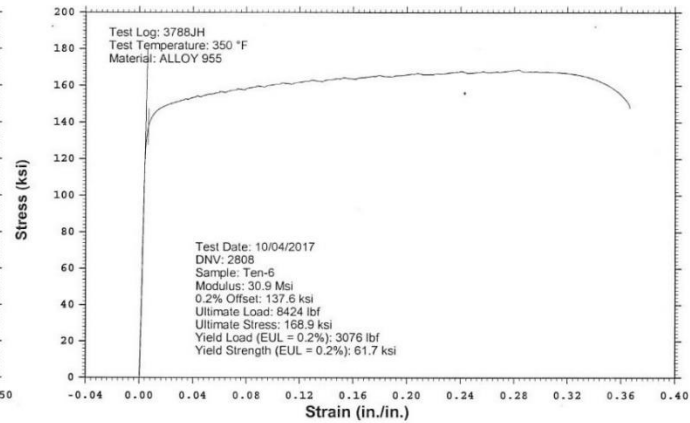
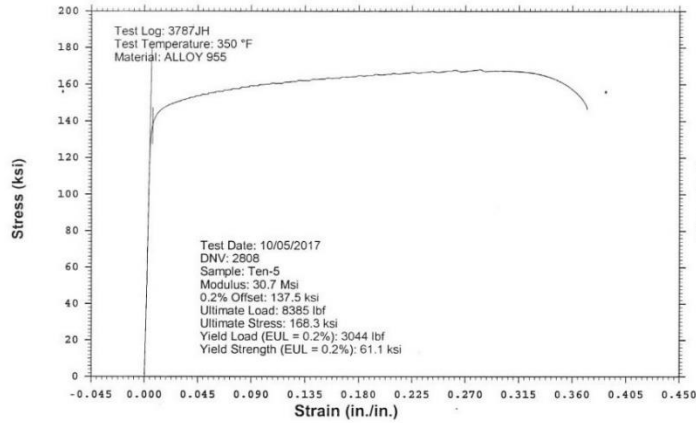
WESTMORELAND MECHANICAL TESTING & RESEARCH, Inc

Stress vs. Strain

Phone: (724)537-3131

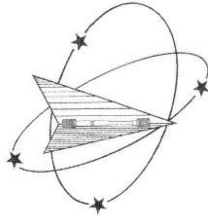
Customer: Honeywell Corrosion Solutions
WMT&R Report: 7-74520

P.O. No.: 4410873689
WMT&R Quote No.: QN173308 Rev.2,
Project No.: USP-012888



"NOTE: THE RECORDING OF FALSE, FICTITIOUS OR FRAUDULENT STATEMENTS OR ENTRIES ON THIS DOCUMENT MAY BE PUNISHABLE AS A FELONY UNDER FEDERAL STATUTE."

A.4 MECHANICAL TEST REPORTS FOR ALLOY 825



Westmoreland Mechanical Testing & Research, Inc.
 P.O. Box 388; 221 Westmoreland Drive
 Youngstown, PA 15696-0388 U.S.A.
 Telephone: 724-537-3131 Fax: 724-537-3151
 Website: www.wmtr.com E-Mail: admin@wmtr.com
WMT&R is a technical leader in the material testing industry.



CERTIFICATION

October 18, 2017
 Honeywell Corrosion Solutions
 11201 Greens Crossing
 Suite 700
 Houston, TEXAS 77067

WMT&R Report No. 7-74523
 P.O. No. 4410873689
 WMT&R Quote No. QN173308 Rev.2
 Project No. USP-012888

Attention: Jie He

Subject: All processes, performed upon the material as received, were conducted at WMT&R, Inc. in accordance with the WMT&R Quality Assurance Manual, Rev. 11, dated 12/03/2008.
 The following tests were performed on this order: IMPACT and TENSILE

IMPACT RESULTS: ASTM E23-16b

No Requirements

MATERIAL: 825

SAMPLE TYPE: Charpy V-Notch

DISPOSITION: Report

DNV	Sample	TestLog Number	Sample Size	Temp. °F	Energy ft-lbs	Mils Lat Exp	% Shear Fracture	AU/R
2833	Charpy-4	3820JH	Standard	32	192	70	100	Report
2833	Charpy-5	3821JH	Standard	32	171	65	100	Report
2833	Charpy-6	3822JH	Standard	32	179	68	100	Report

IMPACT RESULTS: ASTM E23-16b

No Requirements

MATERIAL: 825

SAMPLE TYPE: Charpy V-Notch

DISPOSITION: Report

DNV	Sample	TestLog Number	Sample Size	Temp. °F	Energy ft-lbs	Mils Lat Exp	% Shear Fracture	AU/R
2833	Charpy-1	3817JH	Standard	73	182	66	100	Report
2833	Charpy-2	3818JH	Standard	73	176	63	100	Report
2833	Charpy-3	3819JH	Standard	73	179	66	100	Report

E23 8mm Striker used for testing.

NOTE: THE RECORDING OF FALSE, FICTITIOUS OR FRAUDULENT STATEMENTS OR ENTRIES ON THIS DOCUMENT MAY BE PUNISHABLE AS A FELONY UNDER FEDERAL STATUTES. THIS CERTIFICATE OR REPORT SHALL NOT BE REPRODUCED EXCEPT IN FULL, WITHOUT THE WRITTEN APPROVAL OF WMT&R, INC.

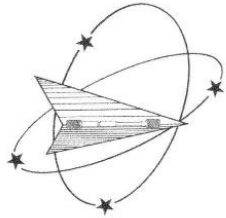
Matthew Wojton
 Matt Wojton
 Tensile Supervisor

October 18, 2017



Testing Specialists for Aerospace, Automotive, and Material Testing Fields
 Locations in Youngstown, PA U.S.A. ~ Tel. (724) 537-3131 and
 Banbury, Oxon U.K. ~ Tel. +44 (0) 1295 261211

A-20



Westmoreland Mechanical Testing & Research, Inc.
 P.O. Box 388; 221 Westmoreland Drive
 Youngstown, PA 15696-0388 U.S.A.
 Telephone: 724-537-3131 Fax: 724-537-3151
 Website: www.wmtr.com E-Mail: admin@wmtr.com
WMT&R is a technical leader in the material testing industry.



CERTIFICATION

October 18, 2017
 Honeywell Corrosion Solutions
 11201 Greens Crossing
 Suite 700
 Houston, TEXAS 77067

WMT&R Report No. 7-74523
 P.O. No. 4410873689
 WMT&R Quote No. QN173308 Rev.2
 Project No. USP-012888

Attention: Jie He

Subject: All processes, performed upon the material as received, were conducted at WMT&R, Inc. in accordance with the WMT&R Quality Assurance Manual, Rev. 11, dated 12/03/2008.
 The following tests were performed on this order: IMPACT and TENSILE

TENSILE RESULTS: ASTM E8-16a

SPEED OF TESTING: 0.005 in./in./min., Extensometer travel exceeded - Test continued at last stroke rate

MATERIAL: Alloy 825

DISPOSITION: Report

DNV	Sample	TestLog Number	Temp.	UTS ksi	0.2% YS ksi	YS (0.2% EUL) ksi	Elong %	RA %	Modulus Msi	Ult. Load lbf	0.2% YLD. lbf	Load (0.2% EUL) lbf
2833	Ten-1	3811JH	Room	116.4	103.6	51.4	23	78	26.3	5812	5171	2568
2833	Ten-2	3812JH	Room	116.1	101.5	55.1	23	76	29.4	5796	5065	2750
2833	Ten-3	3813JH	Room	116.6	104.6	49.5	23	80	25.9	5822	5224	2473

A\U\R: A=ACCEPTABLE, U=UNACCEPTABLE, R=REPORT

DISPOSITION: Report

DNV	Sample	TestLog Number	Orig. Dia. (in.)	Final Dia. (in.)	4D Orig GL (in.)	4D Final GL (in.)	Orig. Area (sq. in.)	Machine Number	A\U\R
2833	Ten-1	3811JH	0.2521	0.1194	1.00	1.23	0.04991552	M13	R
2833	Ten-2	3812JH	0.2521	0.1235	1.00	1.23	0.04991552	M13	R
2833	Ten-3	3813JH	0.2522	0.1134	1.00	1.23	0.04995512	M13	R

A\U\R: A=ACCEPTABLE, U=UNACCEPTABLE, R=REPORT

A-21

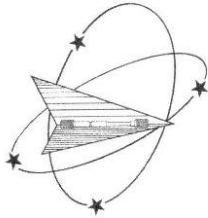
*NOTE: THE RECORDING OF FALSE, FICTITIOUS OR FRAUDULENT STATEMENTS OR ENTRIES ON THIS DOCUMENT MAY BE PUNISHABLE AS A FELONY UNDER FEDERAL STATUTE.
THIS CERTIFICATE OR REPORT SHALL NOT BE REPRODUCED EXCEPT IN FULL, WITHOUT THE WRITTEN APPROVAL OF WMTR, INC.

Testing Specialists for Aerospace, Automotive, and Material Testing Fields
 Locations in Youngstown, PA U.S.A. ~ Tel. (724) 537-3131 and
 Banbury, Oxon U.K. ~ Tel. +44 (0) 1295 261211

Matt Wojton
 Tensile Supervisor

October 18, 2017





Westmoreland Mechanical Testing & Research, Inc.
 P.O.Box 388; 221 Westmoreland Drive
 Youngstown, PA 15696-0388 U.S.A.
 Telephone: 724-537-3131 Fax: 724-537-3151
 Website: www.wmtr.com E-Mail: admin@wmtr.com
 WMT&R is a technical leader in the material testing industry.



CERTIFICATION

October 18, 2017
 Honeywell Corrosion Solutions

WMT&R Report No. 7-74523
 P.O. No. 4410873689

TENSILE RESULTS: ASTM E21-09

SOAK TIME: 30 Minutes

SPEED OF TESTING: 0.005 in./in./min., Extensometer travel exceeded - Test continued at last stroke rate

MATERIAL: Alloy 825

DISPOSITION: Report

DNV	Sample	TestLog Number	Temp. °F	UTS ksi	0.2% YS ksi	YS (0.2% EUL) ksi	Elong %	RA %	Modulus Msi	Ult. Load lbf	0.2% YLD. lbf	Load (0.2% EUL) lbf
2833	Ten-4	3814JH	350	109.7	102.9	57.8	15.0	59.0	29.6	5465	5127	2880
2833	Ten-5	3815JH	350	109.5	103.5	54.7	16.0	65.0	27.3	5504	5204	2751
2833	Ten-6	3816JH	350	110.2	104.4	55.8	15.0	65.0	28.4	5504	5213	2787

A/U/R: A=ACCEPTABLE, U=UNACCEPTABLE, R=REPORT

DISPOSITION: Report

DNV	Sample	TestLog Number	Orig. Dia. (in.)	Final Dia. (in.)	4D Orig GL (in.)	4D Final GL (in.)	Orig. Area (sq. in.)	Machine Number	A/U/R
2833	Ten-4	3814JH	0.2519	0.1617	1.00	1.15	0.04983635	M20	R
2833	Ten-5	3815JH	0.2530	0.1502	1.00	1.16	0.05027255	M20	R
2833	Ten-6	3816JH	0.2522	0.1491	1.00	1.15	0.04995512	M20	R

A/U/R: A=ACCEPTABLE, U=UNACCEPTABLE, R=REPORT

A-22

"NOTE: THE RECORDING OF FALSE, FICTITIOUS OR FRAUDULENT STATEMENTS OR ENTRIES ON THIS DOCUMENT MAY BE PUNISHABLE AS A FELONY UNDER FEDERAL STATUTE." THIS CERTIFICATE OR REPORT SHALL NOT BE REPRODUCED EXCEPT IN FULL, WITHOUT THE WRITTEN APPROVAL OF WMT&R, INC.

Matthew Wojton
 Matt Wojton
 Tensile Supervisor

October 18, 2017



Testing Specialists for Aerospace, Automotive, and Material Testing Fields
 Locations in Youngstown, PA U.S.A. ~ Tel. (724) 537-3131 and
 Banbury, Oxon U.K. ~ Tel. +44 (0) 1295 261211

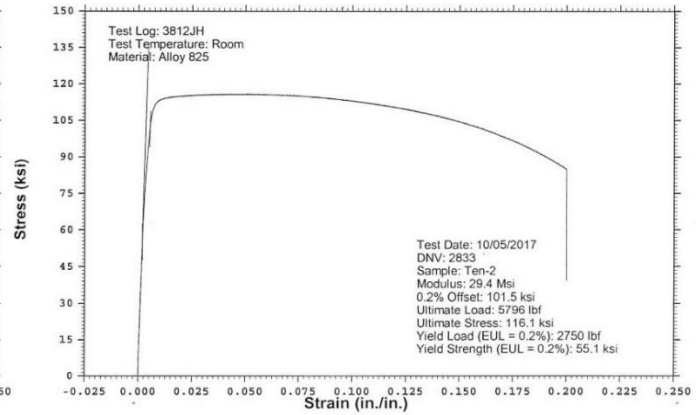
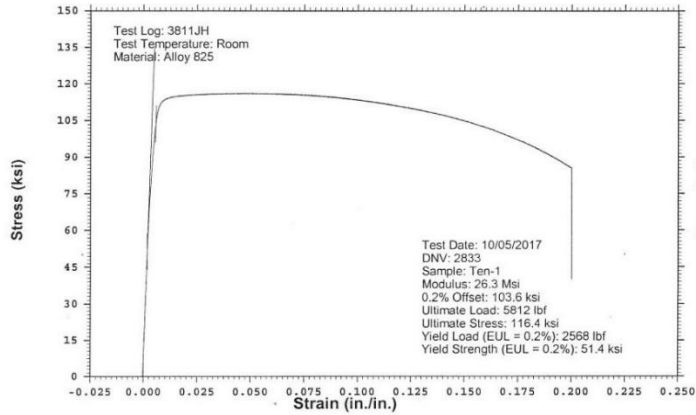
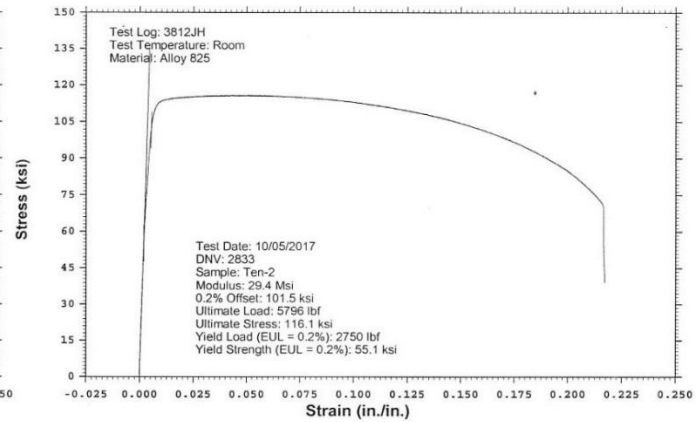
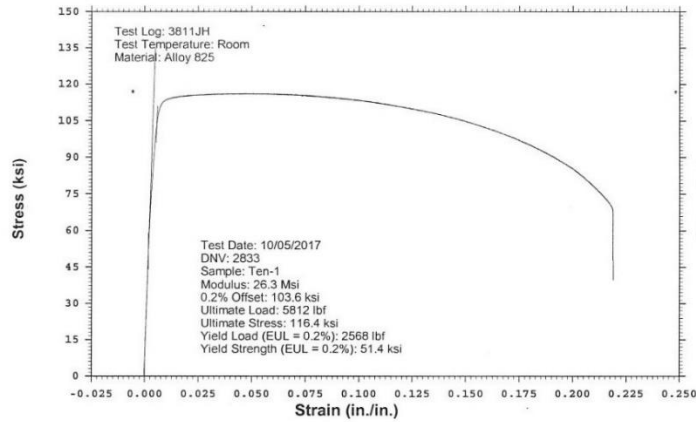
WESTMORELAND MECHANICAL TESTING & RESEARCH, Inc

Stress vs. Strain

Phone: (724)537-3131

Customer: Honeywell Corrosion Solutions
WMT&R Report: 7-74523

P.O. No.: 4410873689
WMT&R Quote No.: QN173308 Rev.2
Project No.: USP-012888



"NOTE: THE RECORDING OF FALSE, FICTITIOUS OR FRAUDULENT STATEMENTS OR ENTRIES ON THIS DOCUMENT MAY BE PUNISHABLE AS A FELONY UNDER FEDERAL STATUTE."

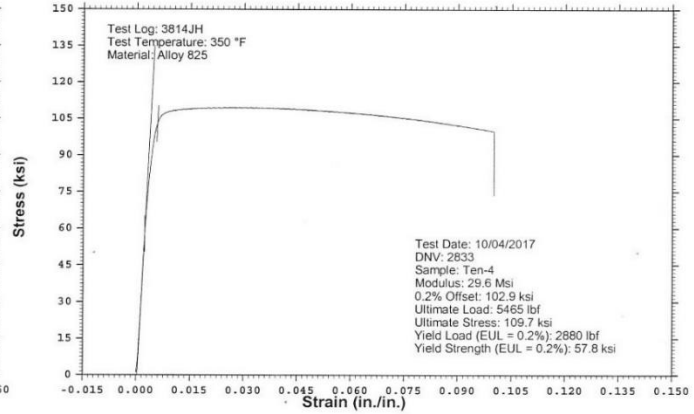
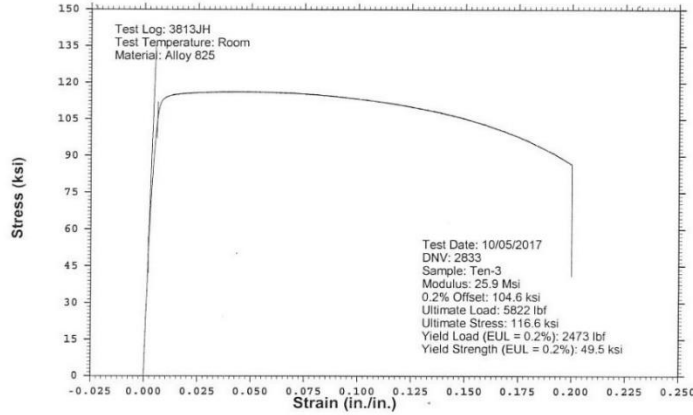
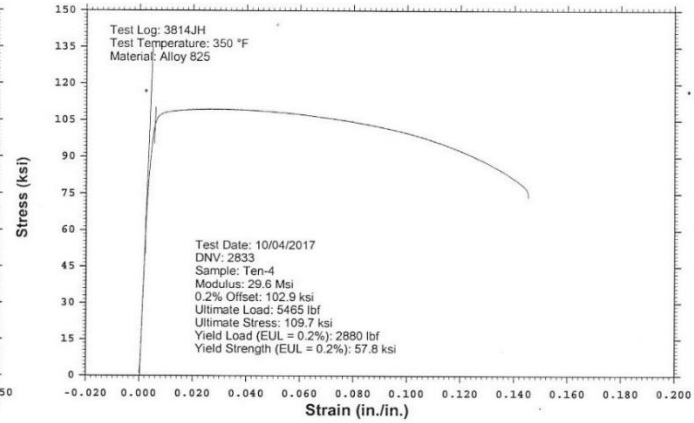
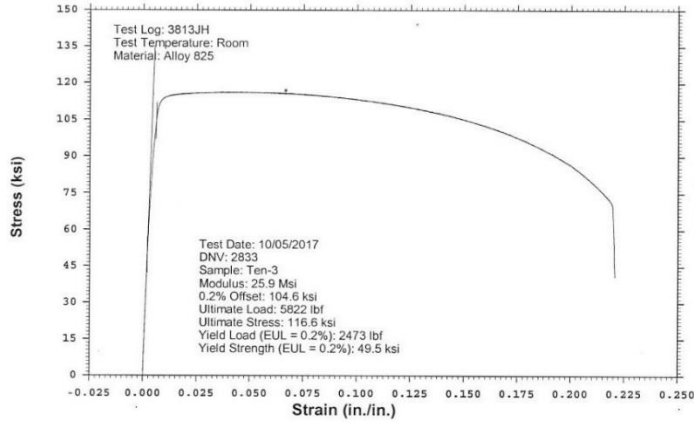
WESTMORELAND MECHANICAL TESTING & RESEARCH, Inc

Stress vs. Strain

Phone: (724)537-3131

Customer: Honeywell Corrosion Solutions
WMT&R Report: 7-74523

P.O. No.: 4410873689
WMT&R Quote No.: QN173308 Rev.2
Project No.: USP-012888



"NOTE: THE RECORDING OF FALSE, FICTITIOUS OR FRAUDULENT STATEMENTS OR ENTRIES ON THIS DOCUMENT
MAY BE PUNISHABLE AS A FELONY UNDER FEDERAL STATUTE."

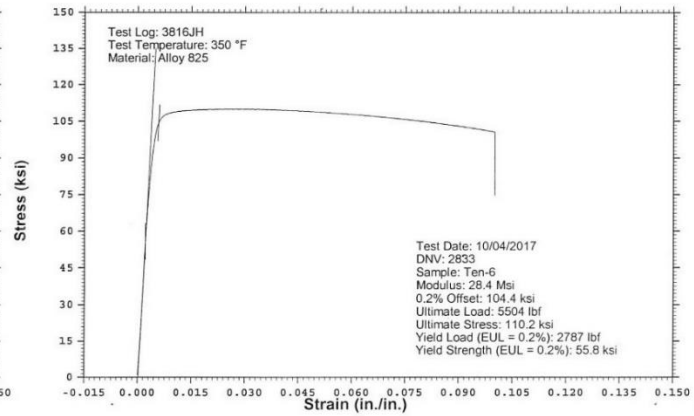
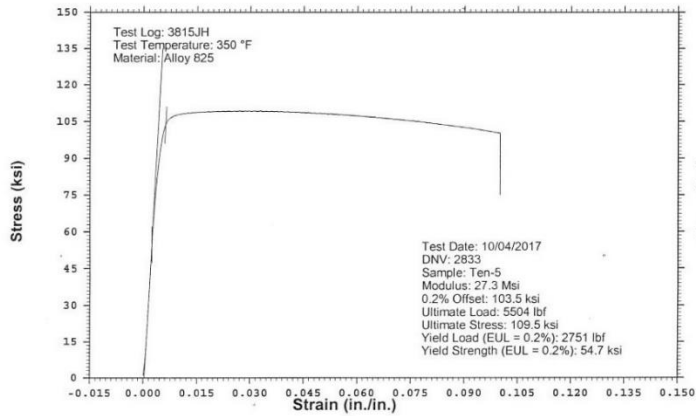
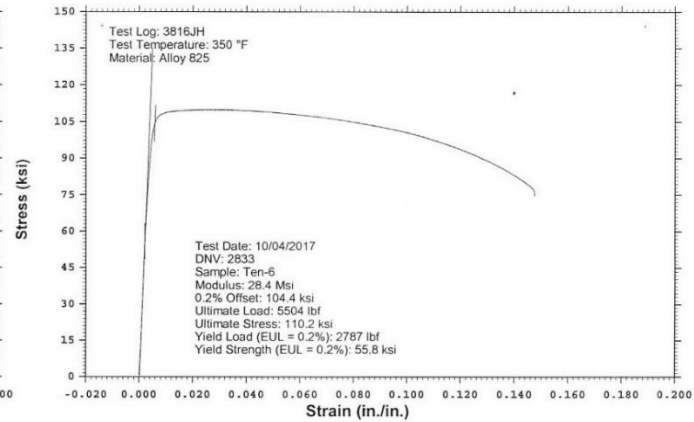
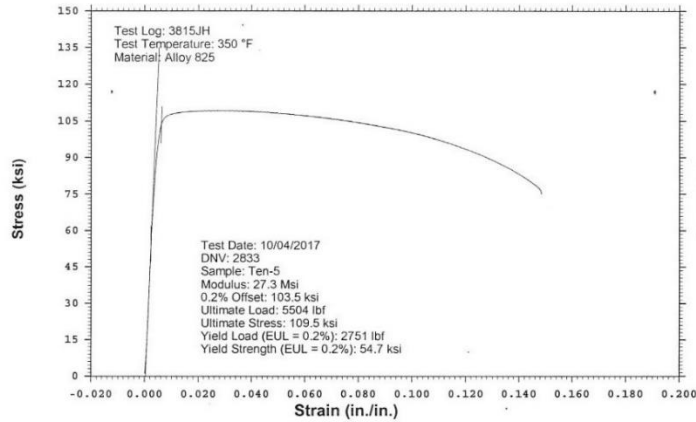
WESTMORELAND MECHANICAL TESTING & RESEARCH, Inc

Stress vs. Strain

Phone: (724)537-3131

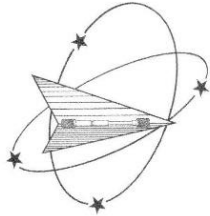
Customer: Honeywell Corrosion Solutions
WMT&R Report: 7-74523

P.O. No.: 4410873689
WMT&R Quote No.: QN173308 Rev.2
Project No.: USP-012888



"NOTE: THE RECORDING OF FALSE, FICTITIOUS OR FRAUDULENT STATEMENTS OR ENTRIES ON THIS DOCUMENT
MAY BE PUNISHABLE AS A FELONY UNDER FEDERAL STATUTE."

A.5 MECHANICAL TEST REPORTS FOR ALLOY C22HS



Westmoreland Mechanical Testing & Research, Inc.
 P.O. Box 388; 221 Westmoreland Drive
 Youngstown, PA 15696-0388 U.S.A.
 Telephone: 724-537-3131 Fax: 724-537-3151
 Website: www.wmtr.com E-Mail: admin@wmtr.com
 WMT&R is a technical leader in the material testing industry.



CERTIFICATION

October 13, 2017
 Honeywell Corrosion Solutions
 11201 Greens Crossing
 Suite 700
 Houston, TEXAS 77067

WMT&R Report No. 7-74521
 P.O. No. 4410873689
 WMT&R Quote No. QN173308 Rev.2
 Project No. USP-012888

Attention: Jie He

Subject: All processes, performed upon the material as received, were conducted at WMT&R, Inc. in accordance with the WMT&R Quality Assurance Manual, Rev. 11, dated 12/03/2008.
 The following tests were performed on this order: IMPACT and TENSILE

IMPACT RESULTS: ASTM E23-16b

No Requirements

MATERIAL: C22-HS

SAMPLE TYPE: Charpy V-Notch

DISPOSITION: Report

DNV	Sample	TestLog Number	Sample Size	Temp. °F	Energy ft-lbs	Mils Lat Exp	% Shear Fracture	AUUR
2785	Charpy-4	3804JH	Standard	32	105	38	65	Report
2785	Charpy-5	3805JH	Standard	32	107	45	65	Report
2785	Charpy-6	3806JH	Standard	32	105	44	65	Report

IMPACT RESULTS: ASTM E23-16b

No Requirements

MATERIAL: C22-HS

SAMPLE TYPE: Charpy V-Notch

DISPOSITION: Report

DNV	Sample	TestLog Number	Sample Size	Temp. °F	Energy ft-lbs	Mils Lat Exp	% Shear Fracture	AUUR
2785	Charpy-1	3801JH	Standard	73	140	59	100	Report
2785	Charpy-2	3802JH	Standard	73	131	56	100	Report
2785	Charpy-3	3803JH	Standard	73	120	52	100	Report

E23 8mm Striker used for testing.

"NOTE: THE RECORDING OF FALSE, FICTITIOUS OR FRAUDULENT STATEMENTS OR ENTRIES ON THIS DOCUMENT MAY BE PUNISHABLE AS A FELONY UNDER FEDERAL STATUTE."
 THIS CERTIFICATE OR REPORT SHALL NOT BE REPRODUCED EXCEPT IN FULL, WITHOUT THE WRITTEN APPROVAL OF WMT&R, INC.

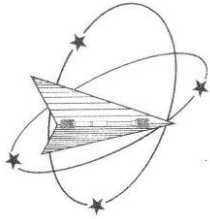
Matthew Wojton
 Matt Wojton
 Tensile Supervisor

October 13, 2017



Testing Specialists for Aerospace, Automotive, and Material Testing Fields
 Locations in Youngstown, PA U.S.A. ~ Tel. (724) 537-3131 and
 Banbury, Oxon U.K. ~ Tel. +44 (0) 1295 261211

A-27



Westmoreland Mechanical Testing & Research, Inc.
 P.O. Box 388; 221 Westmoreland Drive
 Youngstown, PA 15696-0388 U.S.A.
 Telephone: 724-537-3131 Fax: 724-537-3151
 Website: www.wmtr.com E-Mail: admin@wmtr.com
WMT&R is a technical leader in the material testing industry.



CERTIFICATION

October 13, 2017
 Honeywell Corrosion Solutions
 11201 Greens Crossing
 Suite 700
 Houston, TEXAS 77067

WMT&R Report No. 7-74521
 P.O. No. 4410873689
 WMT&R Quote No. QN173308 Rev.2
 Project No. USP-012888

Attention: Jie He

Subject: All processes, performed upon the material as received, were conducted at WMT&R, Inc. in accordance with the WMT&R Quality Assurance Manual, Rev. 11, dated 12/03/2008.
 The following tests were performed on this order: IMPACT and TENSILE

TENSILE RESULTS: ASTM E8-16a

SPEED OF TESTING: 0.005 in./in./min.

MATERIAL: C22-HS

DISPOSITION: Report

DNV	Sample	TestLog Number	Temp.	UTS ksi	0.2% YS ksi	YS (0.2% EUL) ksi	Elong %	RA %	Modulus Msi	Ult. Load lbf	0.2% YLD. lbf	Load (0.2% EUL) lbf
2785	Ten-1	3795JH	Room	182.8	176.2	49.5	21	71	24.8	9125	8795	2473
2785	Ten-2	3796JH	Room	183.4	178.4	48.2	20	70	24.1	9141	8892	2402
2785	Ten-3	3797JH	Room	205.4	199.9	47.8	16	61	28.7	10227	9955	2382

AIUR: A=ACCEPTABLE, U=UNACCEPTABLE, R=REPORT

DISPOSITION: Report

DNV	Sample	TestLog Number	Orig. Dia. (in.)	Final Dia. (in.)	4D Orig GL (in.)	4D Final GL (in.)	Orig. Area (sq. in.)	Machine Number	AIUR
2785	Ten-1	3795JH	0.2521	0.1360	1.00	1.21	0.04991552	M13	R
2785	Ten-2	3796JH	0.2519	0.1391	1.00	1.20	0.04983635	M13	R
2785	Ten-3	3797JH	0.2518	0.1576	1.00	1.16	0.04979679	M13	R

AIUR: A=ACCEPTABLE, U=UNACCEPTABLE, R=REPORT

A-28

"NOTE: THE RECORDING OF FALSE, FICTITIOUS OR FRAUDULENT STATEMENTS OR ENTRIES ON THIS DOCUMENT MAY BE PUNISHABLE AS A FELONY UNDER FEDERAL STATUTE." THIS CERTIFICATE OR REPORT SHALL NOT BE REPRODUCED EXCEPT IN FULL, WITHOUT THE WRITTEN APPROVAL OF WMTR, INC.

Matt Wojton
 Tensile Supervisor

October 13, 2017



Testing Specialists for Aerospace, Automotive, and Material Testing Fields
 Locations in Youngstown, PA U.S.A. ~ Tel. (724) 537-3131 and
 Banbury, Oxon U.K. ~ Tel. +44 (0) 1295 261211

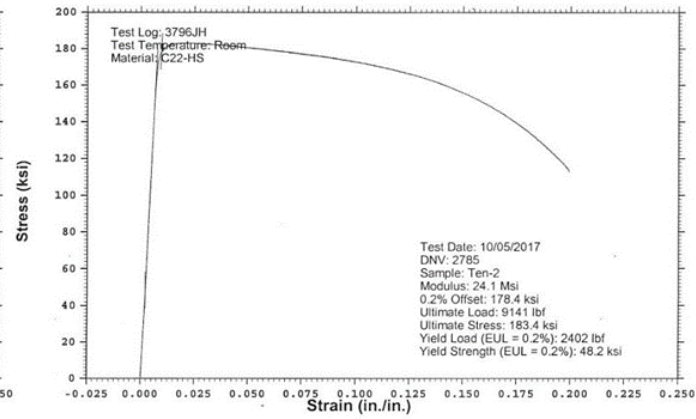
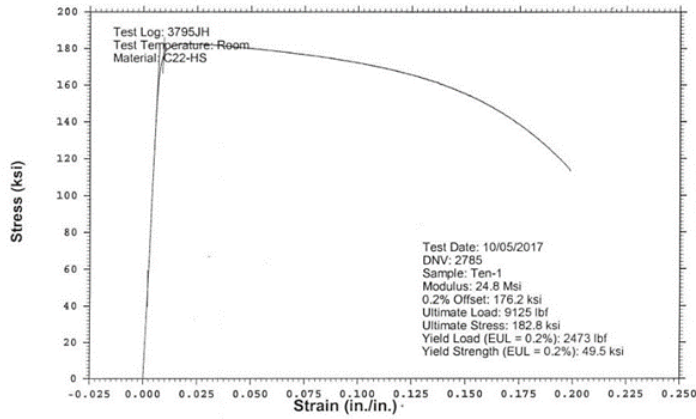
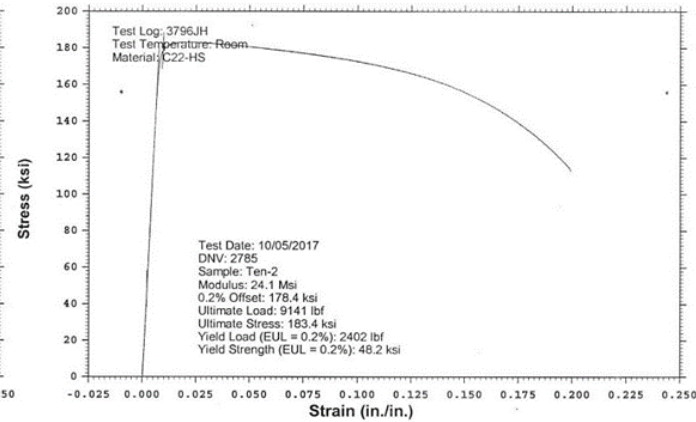
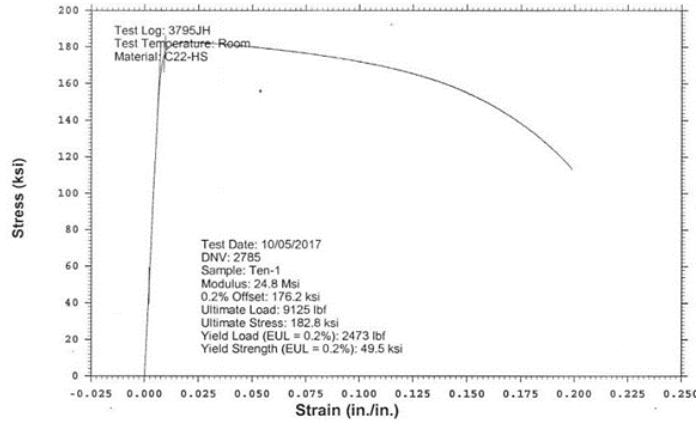
WESTMORELAND MECHANICAL TESTING & RESEARCH, Inc

Stress vs. Strain

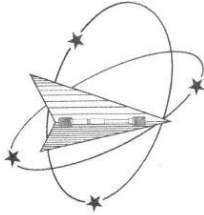
Phone: (724)537-3131

Customer: Honeywell Corrosion Solutions
WMT&R Report: 7-74521

P.O. No.: 4410873689
WMT&R Quote No.: QN173308 Rev.2
Project No.: USP-012888



"NOTE: THE RECORDING OF FALSE, FICTITIOUS OR FRAUDULENT STATEMENTS OR ENTRIES ON THIS DOCUMENT MAY BE PUNISHABLE AS A FELONY UNDER FEDERAL STATUTE."



Westmoreland Mechanical Testing & Research, Inc.
 P.O.Box 388; 221 Westmoreland Drive
 Youngstown, PA 15696-0388 U.S.A.
 Telephone: 724-537-3131 Fax: 724-537-3151
 Website: www.wmtr.com E-Mail: admin@wmtr.com
 WMT&R is a technical leader in the material testing industry.



CERTIFICATION

October 13, 2017
 Honeywell Corrosion Solutions

WMT&R Report No. 7-74521
 P.O. No. 4410873689

TENSILE RESULTS: ASTM E21-09

SOAK TIME: 30 Minutes

SPEED OF TESTING: 0.005 in./in./min., Extensometer travel exceeded - Test continued at last stroke rate

MATERIAL: C22-HS

DISPOSITION: Report

DNV	Sample	TestLog Number	Temp. °F	UTS ksi	0.2% YS ksi	YS (0.2% EUL) ksi	Elong %	RA %	Modulus Msi	Ult. Load lbf	0.2% YLD. lbf	Load (0.2% EUL) lbf
2785	Ten-4	3798JH	350	186.1	180.9	57.0	15.0	57.0	28.4	9270	9007	2839
2785	Ten-5	3799JH	350	174.4	168.8	47.9	17.0	67.0	23.9	8713	8433	2391
2785	Ten-6	3800JH	350	171.7	166.3	52.8	16.0	66.5	26.3	8550	8280	2630

A/U/R: A=ACCEPTABLE, U=UNACCEPTABLE, R=REPORT

DISPOSITION: Report

DNV	Sample	TestLog Number	Orig. Dia. (in.)	Final Dia. (in.)	4D Orig GL (in.)	4D Final GL (in.)	Orig. Area (sq. in.)	Machine Number	A/U/R
2785	Ten-4	3798JH	0.2518	0.1652	1.00	1.15	0.04979679	M17	R
2785	Ten-5	3799JH	0.2522	0.1451	1.00	1.17	0.04995512	M17	R
2785	Ten-6	3800JH	0.2518	0.1452	1.00	1.16	0.04979679	M17	R

A/U/R: A=ACCEPTABLE, U=UNACCEPTABLE, R=REPORT

A-30

"NOTE: THE RECORDING OF FALSE, FICTITIOUS OR FRAUDULENT STATEMENTS OR ENTRIES ON THIS DOCUMENT MAY BE PUNISHABLE AS A FELONY UNDER FEDERAL STATUTE."
 THIS CERTIFICATE OR REPORT SHALL NOT BE REPRODUCED EXCEPT IN FULL, WITHOUT THE WRITTEN APPROVAL OF WMTR, INC.

Matthew Wojton
 Matt Wojton
 Tensile Supervisor

October 13, 2017



Testing Specialists for Aerospace, Automotive, and Material Testing Fields
 Locations in Youngstown, PA U.S.A. ~ Tel. (724) 537-3131 and
 Banbury, Oxon U.K. ~ Tel. +44 (0) 1295 261211

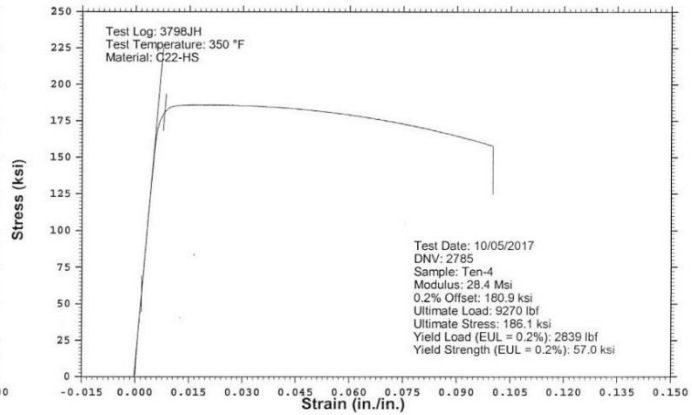
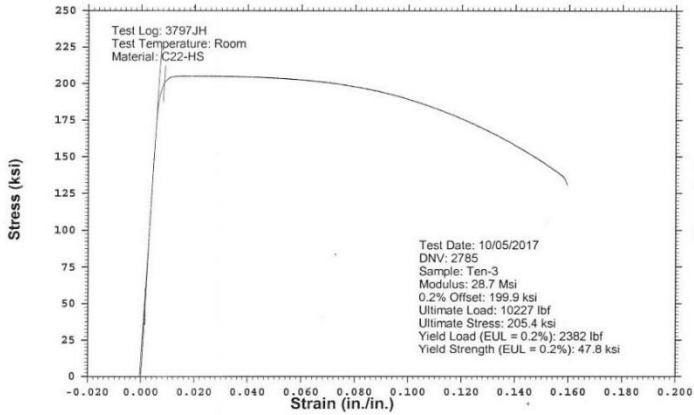
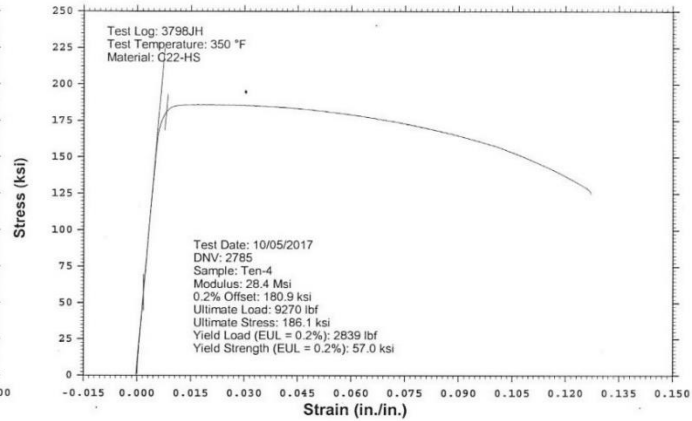
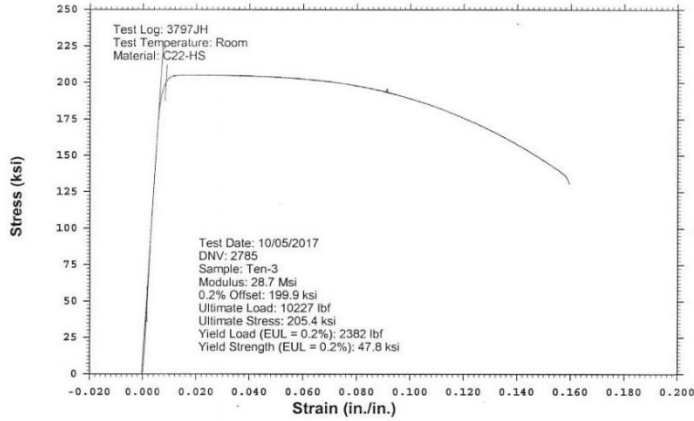
WESTMORELAND MECHANICAL TESTING & RESEARCH, Inc

Stress vs. Strain

Phone: (724)537-3131

Customer: Honeywell Corrosion Solutions
WMT&R Report: 7-74521

P.O. No.: 4410873689
WMT&R Quote No.: QN173308 Rev.2
Project No.: USP-012888



"NOTE: THE RECORDING OF FALSE, FICTITIOUS OR FRAUDULENT STATEMENTS OR ENTRIES ON THIS DOCUMENT MAY BE PUNISHABLE AS A FELONY UNDER FEDERAL STATUTE."

A-31

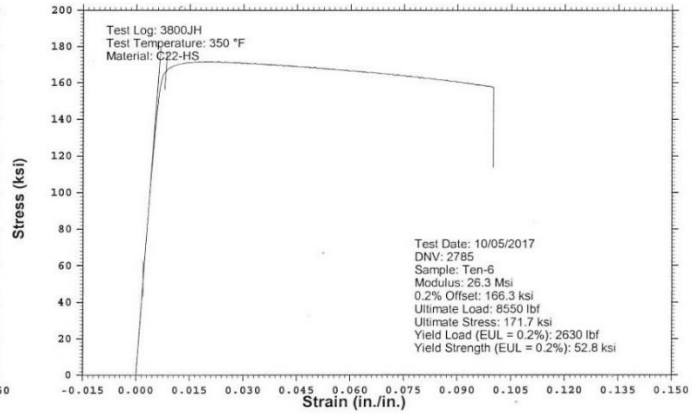
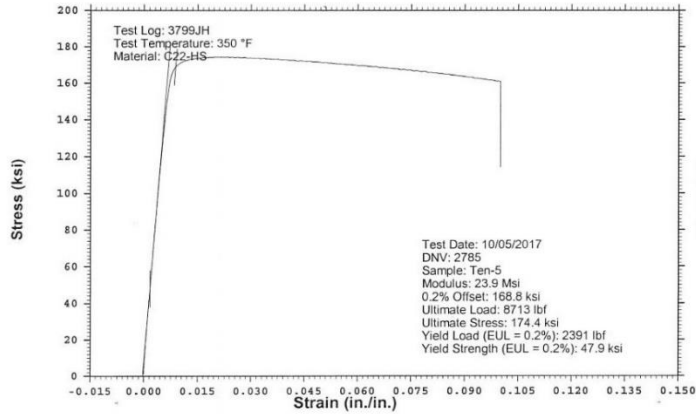
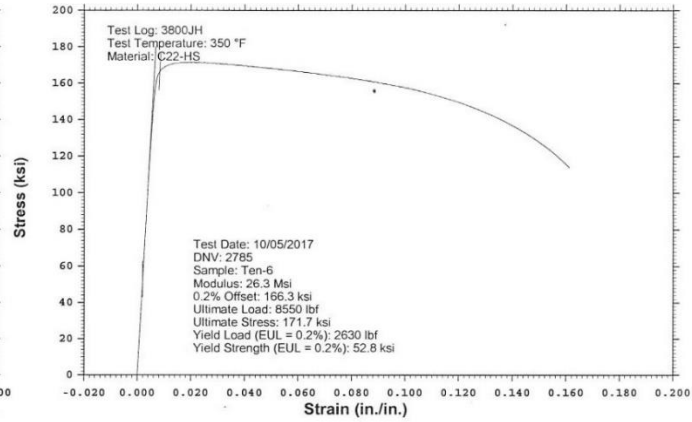
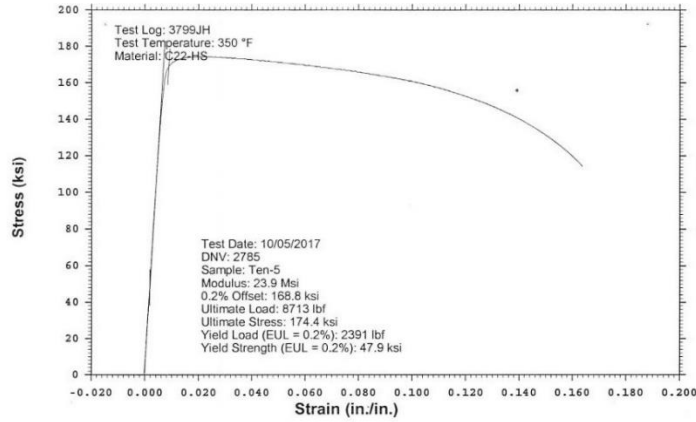
WESTMORELAND MECHANICAL TESTING & RESEARCH, Inc

Stress vs. Strain

Phone: (724)537-3131

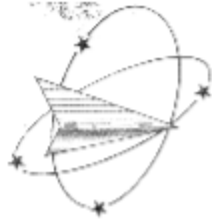
Customer: Honeywell Corrosion Solutions
WMT&R Report: 7-74521

P.O. No.: 4410873689
WMT&R Quote No.: QN173308 Rev.2
Project No.: USP-012888



"NOTE: THE RECORDING OF FALSE, FICTITIOUS OR FRAUDULENT STATEMENTS OR ENTRIES ON THIS DOCUMENT
MAY BE PUNISHABLE AS A FELONY UNDER FEDERAL STATUTE."

A.6 TENSILE TEST REPORTS FOR ALL ALLOYS AT 950°F



Westmoreland Mechanical Testing & Research, Inc.
 P.O. Box 388; 221 Westmoreland Drive
 Youngstown, PA 15696-0388 U.S.A.
 Telephone: 724-537-3131 Fax: 724-537-3151
 Website: www.wmtr.com E-Mail: admin@wmtr.com
 WMT&R is a technical leader in the material testing industry.



CERTIFICATION

July 16, 2019
 Argonne National Laboratory
 9700 S. Cass Avenue
 Argonne, IL 60439

WMT&R Report No. 9-60149
 P.O. No. 0F-00137
 WMT&R Quote No. QN151524

Attention: Jackie Ariaga

Subject: All processes, performed upon the material as received, were conducted at WMT&R, Inc. in accordance with the WMT&R Quality Assurance Manual, Rev. 11, dated 12/03/2008.
 The following tests were performed on this order: STRESS and TENSILE

TENSILE RESULTS: ASTM E21-17

SOAK TIME: 30 Minutes

SPEED OF TESTING: 0.005 in./in./min., 6.05 in./min./in.

MATERIAL: 725

DISPOSITION: Report

SID	TestLog Number	Temp. °F	UTS ksi	0.2% YS ksi	Elong %	RA %	Modulus Msi	Ult. Load lbf	0.2% YLD. lbf	Orig. Dia. (in.)	Final Dia. (in.)	4D Orig GL (in.)	4D Final GL (in.)	Orig. Area (sq. in.)	Machine Number	AU/R
725	573JJH	950	163.3	116.0	31.0	49.5	23.7	8191	5919	0.2527	0.1793	1.00	1.31	0.05015340	MS	R

AU/R: A=ACCEPTABLE, U=UNACCEPTABLE, R=REPORT

TENSILE RESULTS: ASTM E21-17

SOAK TIME: 30 Minutes

SPEED OF TESTING: 0.005 in./in./min., 0.05 in./min./in.

MATERIAL: 825

DISPOSITION: Report

SID	TestLog Number	Temp. °F	UTS ksi	0.2% YS ksi	Elong %	RA %	Modulus Msi	Ult. Load lbf	0.2% YLD. lbf	Orig. Dia. (in.)	Final Dia. (in.)	4D Orig GL (in.)	4D Final GL (in.)	Orig. Area (sq. in.)	Machine Number	AU/R
825	574JJH	950	158.6	127.1	15.0	38.5	26.0	7000	6328	0.2518	0.1975	1.00	1.15	0.04979572	MS	R

AU/R: A=ACCEPTABLE, U=UNACCEPTABLE, R=REPORT

A-34

NOTE: THE PROCEEDINGS OF ALL PEER REVIEW DETERMINATIONS
 REMAIN THE PROPERTY OF THE OCCASION AND ARE
 FURNISHED TO YOU UNDER NON-REPRODUCTION RIGHTS.
 THIS DOCUMENT IS UNCLASSIFIED EXCEPT WHERE SHOWN OTHERWISE.
 EXEMPT FROM AUTOMATIC DOWNGRADING AND DECLASSIFICATION.

Ryan Hout
 Quality Representative

July 16, 2019

Testing Specialists for Aerospace, Automotive, and Material Testing Fields
 Locations in Youngstown, PA U.S.A. - Tel. (724) 537-3131 and
 Saabury, Oregon U.K. - Tel. +44 (0) 1295 261211





Westmoreland Mechanical Testing & Research, Inc.
 P.O. Box 388, 221 Westmoreland Drive
 Youngstown, PA 15696 0388 U.S.A.
 Telephone: 724 537 3131 Fax 724 537 3151
 Website: www.wmtr.com E-Mail: admin@wmtr.com
WMTR is a technical leader in the material testing industry.



TESTING CERT 621-01 & 621-02

CERTIFICATION

July 18, 2019
 Argonne National Laboratory

WMTR Report No. 9-60149
 P.O. No. 9F-66137

TENSILE RESULTS: ASTM E21-17
SOAK TIME: 30 Minutes
SPEED OF TESTING: 0.005 in./in./min., 0.05 in./min./in.
MATERIAL: 925

DISPOSITION: Report

SID	Test Log Number	Temp. °F	UTS ksi	0.2% YS ksi	Elong %	RA %	Modulus Msi	Ult Load lbf	0.2% YLD lbf	Orig. Dia. (in.)	Final Dia. (in.)	4D Orig GL (in.)	4D Final GL (in.)	Orig. Area (sq. in.)	Machine Number	AIUR
925	575JJH	950	109.5	102.1	31.0	40.5	21.7	5504	5135	0.2530	0.1800	1.00	1.31	0.05027255	M9	R

AIUR: A=ACCEPTABLE, U=UNACCEPTABLE, R=REPORT

TENSILE RESULTS: ASTM E21-17
SOAK TIME: 30 Minutes
SPEED OF TESTING: 0.005 in./in./min., 0.05 in./min./in.
MATERIAL: 945X

DISPOSITION: Report

SID	Test Log Number	Temp. °F	UTS ksi	0.2% YS ksi	Elong %	RA %	Modulus Msi	Ult Load lbf	0.2% YLD lbf	Orig. Dia. (in.)	Final Dia. (in.)	4D Orig GL (in.)	4D Final GL (in.)	Orig. Area (sq. in.)	Machine Number	AIUR
945x	576JJH	950	155.0	128.4	26.0	51.5	21.0	7776	6439	0.2527	0.1762	1.00	1.26	0.05015340	M9	R

AIUR: A=ACCEPTABLE, U=UNACCEPTABLE, R=REPORT

TENSILE RESULTS: ASTM E21-17
SOAK TIME: 30 Minutes
SPEED OF TESTING: 0.005 in./in./min., 0.05 in./min./in.
MATERIAL: C22HS

DISPOSITION: Report

SID	Test Log Number	Temp. °F	UTS ksi	0.2% YS ksi	Elong %	RA %	Modulus Msi	Ult Load lbf	0.2% YLD lbf	Orig. Dia. (in.)	Final Dia. (in.)	4D Orig GL (in.)	4D Final GL (in.)	Orig. Area (sq. in.)	Machine Number	AIUR
C22HS	577JJH	950	156.6	146.2	16.0	53.0	25.0	7823	7402	0.2592	0.1732	1.00	1.16	0.04995512	M9	R

AIUR: A=ACCEPTABLE, U=UNACCEPTABLE, R=REPORT

WMTR HAS RECEIVED ISO 9001:2015 CERTIFICATION
 ACCREDITATION FOR TESTING OF METALS AND ALLOYS
 FOR MECHANICAL PROPERTY TESTING AND TENSILE
 TESTING OF METALS AND ALLOYS. WMTR IS A MEMBER OF
 QUALITY ASSOCIATION FOR MECHANICAL TESTING.

Ryan Hallett
 Quality Representative

Testing Specialists for Aerospace, Automotive, and Material Testing Fields
 Locations in Youngstown, PA U.S.A. - Tel: (724) 537 3131 and
 Danbury, Conn U.S.A. - Tel: (440) 1295 261211

July 18, 2019



A.7 CREEP TEST REPORT MECHANICAL TEST REPORTS FOR ALLOY C22HS



Westmoreland Mechanical Testing & Research, Inc.
 P.O. Box 388, 221 Westmoreland Drive
 Youngstown, PA 15696-0388 U.S.A.
 Telephone: 724-537-3131 Fax: 724-537-3131
 Website: www.wmtr.com E-Mail: admin@wmtr.com
 WMT&R is a technical leader in the material testing industry.



Section 1 of 3

WMT&R Report No. 14-19002846
 PO Number Contract No. SF-60137
 Quote Number QN191524

July 15, 2019

CERTIFICATION

Argonne National Laboratory
 9700 S. Cass Ave
 Argonne, IL 60439
 United States

Attention: Jackie Arriaga

Subject: All processes performed upon the material as received, were conducted at WMT&R, Inc. in accordance with the WMT&R Quality Assurance Manual, Rev. 11, dated 12/03/2008.
 The following tests were performed on this order: Creep Rupture

CREEP RESULTS: ASTM E139-11
 NO REQUIREMENTS
 SOAK TIME: 90 Mins.
 MATERIAL: 725

DISPOSITION: Report

Sample ID	Test Log Number	Temp °F	Rupture Time Hrs	Total Creep %	Pen Ld. LBS.	Stress KSI	Orig Dia (in.)	Eff GL (in.)	Orig GL (in.)	Machine Number	AUIR
725(1)	8644FB	350	1000.0**	0.0651	314.7	102.48	0.2501	1.3636	1.00	338	R
725(2)	8645FB	350	1000.0**	0.0481	301.2	97.94	0.2503	1.3700	1.00	572	R

AUIR: A=ACCEPTABLE, U=UNACCEPTABLE, R=REPORT

CREEP RESULTS: ASTM E139-11
 NO REQUIREMENTS
 SOAK TIME: 90 Mins.
 MATERIAL: 825

DISPOSITION: Report

Sample ID	Test Log Number	Temp °F	Rupture Time Hrs	Total Creep %	Pen Ld. LBS.	Stress KSI	Orig Dia (in.)	Eff GL (in.)	Orig GL (in.)	Machine Number	AUIR
825(1)	8646FB	350	1000.0**	0.0570	263.2	80	0.2497	1.3700	1.00	331	R

AUIR: A=ACCEPTABLE, U=UNACCEPTABLE, R=REPORT

A-37

Sheet 14 of 14
 THIS IS A PRELIMINARY COPY OF THE REPORT. IT IS NOT TO BE USED FOR ANY PURPOSES WITHOUT THE WRITTEN PERMISSION OF WMT&R. IT IS THE PROPERTY OF WMT&R AND IS TO BE RETURNED TO WMT&R UPON REQUEST. IT IS NOT TO BE REPRODUCED OR TRANSMITTED IN ANY FORM OR BY ANY MEANS, ELECTRONIC OR MECHANICAL, INCLUDING PHOTOCOPYING, RECORDING, OR BY ANY INFORMATION STORAGE AND RETRIEVAL SYSTEM.

Testing Specialists for Aerospace, Automotive, and Material Testing Needs
 Locations in Youngstown, PA U.S.A. - Tel. (724) 537-3131 and
 Danbury, Conn. U.S.A. - Tel. (978) 1295-261211

July 15, 2019



Page 3 of 5



Westmoreland Mechanical Testing & Research, Inc.
 P.O. Box 388, 221 Westmoreland Drive
 Youngstown, PA 15696-0388 U.S.A.
 Telephone: 724-537-3131 Fax: 724-537-3151
 Website: www.wmt.com E-Mail: admin@wmt.com
WMT&R is a technical leader in the material testing industry.



Section 2 of 3

WMT&R Report No. 14-19002846
 PO Number Contract No. 9F 60137

July 15, 2019

CERTIFICATION

Argonne National Laboratory

CREEP RESULTS: ASTM E139-11
NO REQUIREMENTS
SOAK TIME: 90 Mins.
MATERIAL: 925

DISPOSITION: Report

Sample ID	Test Log Number	Temp °F	Rupture Time Hrs.	Total Creep %	Elong %	RA %	Pan Ld LBS	Stress KSI	Orig Dia (in.)	Final Dia (in.)	El GL (in.)	Org GL (in.)	Final GL (in.)	Machine Number	A/U/R
925(2)	8647FB	950	46.4	17.8832	23.0	25.3	323.9	106.5	0.2501	0.2162	1.3595	1.30	1.230	102	R

A/U/R: A=ACCEPTABLE, U=UNACCEPTABLE, R = REPORT

CREEP RESULTS: ASTM E139-11
NO REQUIREMENTS
SOAK TIME: 90 Mins.
MATERIAL: 955

DISPOSITION: Report

Sample ID	Test Log Number	Temp °F	Rupture Time Hrs.	Total Creep %	Pan Ld LBS	Stress KSI	Orig Dia (in.)	El GL (in.)	Org GL (in.)	Machine Number	A/U/R
955(1)	8648FB	350	1000.0**	0.0149	351.2	114.29	0.2502	1.3678	1.00	180	R
955(2)	8649FB	950	1000.0**	0.0613	4139.7	84.74	0.2500	1.3665	1.00	60	R

A/U/R: A=ACCEPTABLE, U=UNACCEPTABLE, R = REPORT

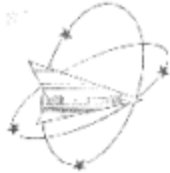
A-38

Std. 14 Step 8 Draw
 WMT&R is a technical leader in the material testing industry.
 WMT&R is a technical leader in the material testing industry.
 WMT&R is a technical leader in the material testing industry.
 WMT&R is a technical leader in the material testing industry.
 WMT&R is a technical leader in the material testing industry.

Testing Specialists for Aerospace, Automotive, and Material Testing Fields
 Locations in Youngstown, PA U.S.A. - Tel: (724) 537-3131 and
 Cranbury, New Jersey - Tel: (908) 261-2111

July 15, 2019





Westmoreland Mechanical Testing & Research, Inc.
 211 Box 388, 221 Westmoreland Drive
 Youngstown, PA 15696-0388 U.S.A.
 Telephone: 724 537 3131 Fax: 724 537 3131
 Website: www.wmtr.com E-Mail: admin@wmtr.com
WMTR is a technical leader in the material testing industry.



Section 3 of 3

WMTR Report No. 14-15092646
 PO Number Contract No. 5F-60137

July 15, 2019

CERTIFICATION

Argonne National Laboratory

CREEP RESULTS: ASTM E139-11
 NO REQUIREMENTS
 SOAK TIME: 90 Mins.
 MATERIAL: 945X

DISPOSITION: Report

Sample ID	Test Log Number	Temp °F	Rupture Time Hrs	Total Creep %	Pen Lt. LBS.	Stress KSI	Orig Dia (in.)	EF GL (in.)	Orig GL (in.)	Machine Number	AUR
945X(1)	9502FR	350	1000.0**	0.0612	0.7368	119.59	0.2503	1.3613	1.00	67	R

AUR: A=ACCEPTABLE, U=UNACCEPTABLE, R=REPORT

CREEP RESULTS: ASTM E139-11
 NO REQUIREMENTS
 SOAK TIME: 90 Mins.
 MATERIAL: C22H5

DISPOSITION: Report

Sample ID	Test Log Number	Temp °F	Rupture Time Hrs	Total Creep %	Pen Lt. LBS.	Stress KSI	Orig Dia (in.)	EF GL (in.)	Orig GL (in.)	Machine Number	AUR
C22H5(1)	9502FR	350	1000.0**	0.0364	7055.8	142.76	0.2505	1.3708	1.00	90	R
C22H5(2)	9502FR	350	363.0	0.0245	377.7	122	0.2501	1.2634	1.00	155	R

AUR: A=ACCEPTABLE, U=UNACCEPTABLE, R=REPORT

**Electron read

Reference WMTR Report Number 9-60745

SPT-14 Test Data
 WMTR REPORTING: 10/15/2019
 PREPARED BY: JEFF HANDEL
 REVIEWED BY: JEFF HANDEL
 APPROVED BY: JEFF HANDEL
 DATE: 07/15/2019

Jeff Handel
 Chief Engineer

Testing Specialists for Aerospace, Automotive, and Material Testing Fields
 Locations in Youngstown, PA U.S.A. - Tel: 724 537 3131 and
 Youngstown, Ohio U.S.A. - Tel: 44 00 1 295 361211



SPT-14 Test Data

This page intentionally left blank.

APPENDIX B:

ENVIRONMENTALLY ASSISTED CRACKING DATA REPORT (DNV-GL)

The following is DNV-GL’s technical report on material testing. The report has been reformatted slightly and tables have been added to give numerical values for figures. The narrative is unaltered.

(301) BSEE: MATERIALS EVALUATION IN HPHT ENVIRONMENTS

Environmentally Assisted Cracking Behavior of High Strength Nickel Based Alloys in HPHT Applications

Aiken Engineering

Report No.: Rev. 1 (with DNV provided data values (tables and revised figures added by ANL)

Document No.: OAPUS301RAMGO ()-1

Date: 2019-06-23



Project name: (301) BSEE: Materials Evaluation in HPHT Environments Det Norske Veritas (U.S.A.), Inc. Oil & Gas

Report title: Environmentally Assisted Cracking Behavior of High Strength Nickel Based Alloys in HPHT Applications O&G Fatigue and Fracture

Customer: Aiken Engineering, 9720 Cypresswood Drive, Suite 340 Houston, TX 77070 USA 5777 Frantz Road 43017-1386 Dublin OH United States Tel: +1 614 761 1214

Customer contact: Maurice Peltier

Date of issue: 2019-06-23

Project No.: 10064186

Organization unit: Material Technology Development

Report No.: , Rev. 1

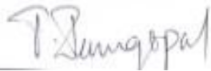
Document No.: OAPUS301RAMGO (-)1

Applicable contract(s) governing the provision of this Report:

Objective:

Please see executive summary

Prepared by:



Dr. Ramgopal Thodla
Senior Principal Engineer
Head of Section, Materials Technology Development

Verified by:



Ashwini Chandra
Senior Engineer
Oil&Gas Fracture and Fatigue Materials Technology Development

Approved by:



Dr. Feng Gui
Principal Engineer
Group Leader, Oil&Gas Fracture and Fatigue Materials Technology Development

DNV GL undertakes no duty of care toward any third party. Reference to part of this publication which may lead to misinterpretation is prohibited. DNV GL and the Horizon Graphic are trademarks of DNV GL AS.

DNV GL Distribution:

- Unrestricted distribution (internal and external)
- Unrestricted distribution within DNV GL Group
- Unrestricted distribution within DNV GL contracting party
- No distribution (confidential)

Keywords:

Nickel Based Alloys, Fatigue Crack Growth Rate, Sour Service, Seawater + Cathodic Polarization.

Rev. No.	Date	Reason for Issue	Prepared by	Verified by	Approved by
0	2018-06-10	Draft	RAMGO	ACHAN	FGUI

Note: Argonne modified this report. Modifications were to add information about data collected and appearing in figures and tables. These additions are numerical values achieved through revised figures with labels and additional tables corresponding to the figures. Apart from minor typographic level items, the narrative is as provided by DNV-GL

TABLE OF CONTENTS

1	EXECUTIVE SUMMARY	1
2	INTRODUCTION	2
3	BACKGROUND	3
4	EXPERIMENTAL	4
4.1	Critical Crevice Temperature	4
4.2	Environmental Conditions	4
4.3	Materials and Specimens	5
4.4	Crack Length Measurements	8
4.5	Test Method	8
5	RESULTS	12
5.1	Critical Crevice Temperature	12
5.2	Sour Service	19
5.2.1	725 (Specimen ID 2810 CL-3)	19
5.2.2	945X (Specimen ID 2805-CL1)	21
5.2.3	955 (Specimen ID 2808-CL4)	25
5.2.4	C22HS (Specimen ID – 2785-CL3)	27
5.2.5	825 (Specimen ID 2833 - CL4)	30
5.3	Seawater + CP	32
5.3.1	725 (Specimen ID 2810-LR1)	32
5.3.2	945X (Specimen ID 2805-LR1)	36
5.3.3	955 (Specimen ID 2808-LR3/LR5)	44
5.3.4	C22HS (Specimen ID 2785-LR4)	50
5.3.5	825 (Specimen ID 2833-CL3)	53
5.4	Seawater Under OCP	58
6	DISCUSSION	66
6.1	Fatigue Crack Growth of PH Nickel Alloys	66
6.2	Static Crack Growth Rate of PH Nickel Alloys	68
6.2.1	Effect of Applied Potential	71
6.3	Implications for Oil and Gas Industry	72
6.3.1	Sour Service	73
6.3.2	Seawater + CP	73
6.3.3	Seawater at OCP	73
7	SUMMARY	76
8	REFERENCES	78
9	LIST OF VARIABLES AND ACRONYMS	79

1

LIST OF TABLES

Table 1: Chemistry of the sour service test solution used	4
Table 2: Chemistry of the materials tested.	5
Table 3: Heat treatment of the materials tested.....	5
Table 4: Mechanical properties of the materials tested.	5
Table 5: Numerical values for Figure 3.....	9
Table 6: Critical crevice temperature of the various materials tested in 3.5 wt% NaCl at +700 mV SCE.	17
Table 7: Numerical values for Figure 6.....	18
Table 8: Color coded numerical values for Figure 7.....	20
Table 9: Color coded numerical date for Figure 9.....	22
Table 10: Color coded numerical values for Figure 13.....	26
Table 11: Color coded numerical values for Figure 14.....	28
Table: 12: Numerical values for Figure 16.....	31
Table 13: Color coded numerical values for Figure 17.....	33
Table 14: Color coded numerical values for Figure 19.....	35
Table 15: Color coded numerical values for Figure 20.....	36
Table 16: Color coded numerical values for Figure 23.....	41
Table 17: Numerical values for Figure 25.....	44
Table 18: Color coded numerical values for Figure 26.....	45
Table 19: Color coded numerical values for Figure 30 (two tables).....	49
Table 20: Numerical values for Figure 31.....	50
Table 21: Color coded numerical values for Figure 32.....	51
Table 22: Numerical values for Figure 34.....	54
Table 23: Color coded numerical values for Figure 36a.....	56
Table 24: Color coded numerical values for Figure 36b.....	57
Table 25: Numerical values for Figure 37a.....	61
Table 26: Numerical values for Figure 37b.....	61
Table 27: Numerical values for Figure 37c.....	61
Table 28: Numerical values for Figure 38a.....	63
Table 29: Numerical values for Figure 38b.....	63
Table 30: Color coded numerical values for Figure 39.....	64
Table 31: Color coded numerical values for Figure 40.....	66
Table 32: Numerical values for Figure 42.....	69
Table 33: Numerical values for Figure 43.....	72
Table 34: Comparison of the K_{th} in seawater at -1050 mV SCE, and critical crevice temperature of various alloys tested in this program with 718-120K and 150K in seawater.....	74

LIST OF FIGURES

Figure 1: Schematic of the compact tension (CT) sample used in this test program.....	6
Figure 2: Schematic illustrations of the cells used for sour service and seawater + CP testing.	7
Figure 3: Effect of stress level, and crack length on the resulting K value assuming a YS of 120ksi (828MPa).....	9
Figure 4: Critical crevice temperatures of the various alloys evaluated in 3.5 wt% NaCl at +700 mV SCE.	14
Figure 5: Post test photographs of critical crevice temperature samples.	16
Figure 6: Relationship between the critical crevice temperature and the PREN number formulations.	18
Figure 7: FCGR frequency scans on 725 (2810-CL3) in sour environment over a range of ΔK values at 350°F and 400°F.	19
Figure 8: Crack length vs time as a function frequency and hold time of 725 (2810-CL3) in sour environment at 400°F (204°C) and K_{max} of 60 ksi \sqrt{in} (66 MPa \sqrt{m}).	21
Figure 9: FCGR frequency scans on 945X (2805-CL1) in sour environment at 350°F (177°C) over a range of ΔK values.....	22
Figure 10: Crack length as a function of time for 945X (2805-CL1) at 350°F (177°C) under 9000 s holds at 50 ksi \sqrt{in} (55 MPa \sqrt{m}) and transitioning to 72 ksi \sqrt{in} (79.2 MPa \sqrt{m}).	23
Figure 11: Crack length as a function of time for 945X (2805-CL1) at 350°F (177°C) under 9000 s holds and constant K at 72 ksi \sqrt{in} (79.2 MPa \sqrt{m}).	24
Figure 12: Crack length as a function of time for 945X (2805-CL1) at 350°F (177°C) under 9000 s and 1 day holds at 100 ksi \sqrt{in} (110 MPa \sqrt{m}).	25
Figure 13: FCGR frequency scans on 955 (2808-CL4) in sour environment at 350°F (177°C) over a range of ΔK values.....	26
Figure 14: FCGR frequency scans on C22HS (2785-CL3) in sour environment at 350°F (177°C) over a range of ΔK values.....	28
Figure 15: Crack length vs time for C22HS (2785-CL3) in sour environment at 350°F (177°C) 72 ksi \sqrt{in} (79.2 MPa \sqrt{m}), R = 0.6 and 9000 s holds.....	30
Figure 16: FCGR frequency scans on 825 (2835-CL4) in sour environment at 350°F (177°C) at 20 ksi \sqrt{in} (22 MPa \sqrt{m}).....	31
Figure 17: FCGR as a function of ΔK and frequency for 725 (2810-LR1) in seawater + CP at -1050 mV SCE.	33
Figure 18: Crack length vs time under constant K and varying K for 725 (2810-LR1) in seawater + CP at -1050 mV SCE.....	34
Figure 19: Crack growth rate as function of K and loading mode for 725 (2810-LR1) in seawater at -1050 mV SCE.....	35
Figure 20: FCGR as a function of ΔK and frequency for 945X (2805-LR1) in seawater + CP at -1050 mV SCE.....	36
Figure 21: Crack length vs time under constant K and varying K for 945X (2805-LR1) in seawater + CP at -1050 mV SCE.....	39
Figure 22: Crack length vs time under constant K and varying K for 945X (2805-LR1) in seawater + CP at -1050 mV SCE.....	40
Figure 23: K vs CGR for 945X under constant K as well as decreasing K.	41
Figure 24: Crack length as a function of time for 945X (2805-LR1) at a K value of 71.2 ksi \sqrt{in} (78.3 MPa \sqrt{m}) over a range of applied potential.	43
Figure 25: CGR of 945X (2805-LR1) as a function of applied potential at 71.2 ksi \sqrt{in} (78.3 MPa \sqrt{m}).	43
Figure 26: FCGR as a function of frequency and ΔK of 955 (2808-LR3) in seawater under cathodic polarization of -1050 mV SCE.	45

Figure 27: Crack length vs time for 955 (2808-LR3) at constant K and under decreasing K conditions.....	46
Figure 28: Crack length vs time for 955 (2808-LR3) as a function of applied potential at K = 84 ksi√in (92.4 MPa√m).....	47
Figure 29: Crack length vs time for 955 (2808-LR5) as a function of applied potential at 72 ksi√in (79.2 MPa√m).....	48
Figure 30: Effect of applied potential on crack growth rate for 955 over a range of K values.....	48
Figure 31: CGR as a function of K for 955 at -1050 mV SCE.....	50
Figure 32: FCGR as a function of frequency for C22HS (2785-LR4) over a range of ΔK values, and potentials.....	51
Figure 33: Crack growth rate at constant K of 90 ksi√in (99 MPa√m) and -1200 mV SCE for C22HS (2785-LR1).....	53
Figure 34: FCGR as a function of frequency for 825 (2833-CL3) over a range of ΔK values.....	54
Figure 35: Crack length vs time for 825 (2833-CL3) at 60 ksi√in (66 MPa√m) to determine behavior under constant K conditions.....	55
Figure 36: Comparison of the FCGR as a function of frequency at two different ΔK values for all the alloys evaluated under cathodic polarization.....	56
Figure 37: FCGR as a function of frequency for the precipitation hardened alloys (725, 945X, and 955) at OCP.....	60
Figure 38: FCGR as a function of frequency for the precipitation hardened alloys (C22HS, and 825) at OCP.....	62
Figure 39: FCGR as a function of frequency for all the alloys in seawater under OCP conditions.....	64
Figure 40: FCGR as a function of ΔK for 725, 955, and 945X at 1 mHz and 0.1 mHz.....	66
Figure 41: FCGR as a function of ΔK for 725, 955, and 945X at 1 mHz and 0.1 mHz in seawater under cathodic polarization at -1050 mV SCE.....	68
Figure 42: Crack growth rate as a function of K at constant K and under decreasing K for 725, 955, 945X, 718, and 625+ in 3.5 wt% NaCl at -1050 mV SCE.....	69
Figure 43: Effect of applied potential on crack growth rate for 955 and 945X.....	71

1 EXECUTIVE SUMMARY

Environmentally assisted cracking of high strength precipitation hardened (PH) nickel-based alloys 725, 945X, 955, as well as cold worked C22HS, and 825 were evaluated in environments relevant to subsea high pressure and high temperature (HPHT) applications. The primary environments of interest in this effort were 3.5 wt% NaCl, at pH 8.2 with and without cathodic polarization (CP) at low temperatures, and sour production environments at elevated temperature and pressure. Materials were evaluated in the sour production environment at 350°F/400°F (177°C/204°C), with 125 psia CO₂ and 0.08 psia H₂S. Fatigue crack growth rate (FCGR) and static crack growth rate measurements were performed in both the environments. The results of the program are summarized below:

Sour Service

In sour environments, the alloys exhibited excellent resistance to environmentally assisted fatigue and stress corrosion cracking. FCGR in four of the five tested alloys at (725, 945X, 955, C22HS) did not exhibit a frequency dependence, when tested over a range of ΔK values. These alloys also did not exhibit any evidence of static crack growth rate up to a stress intensity factor (90 ksi $\sqrt{\text{in}}$ (99 MPa $\sqrt{\text{m}}$). However, 825 did exhibit susceptibility when tested at a K_{max} of 50 ksi $\sqrt{\text{in}}$ (55 MPa $\sqrt{\text{m}}$). At a lower K_{max} value of 25 ksi $\sqrt{\text{in}}$ (27.5 MPa $\sqrt{\text{m}}$) there was no evidence of environmental effect as evident from the FCGR being frequency independent over a range of frequencies.

Seawater + Cathodic Polarization

FCGR of all the PH nickel-based alloys under CP exhibits a strong dependence on frequency in the range of 0.3 Hz to 0.1 mHz, at two different values of $^{\circ}K$ (40 ksi $\sqrt{\text{in}}$ /44M Pa $\sqrt{\text{m}}$ and 20 ksi $\sqrt{\text{in}}$ /22 MPa $\sqrt{\text{m}}$). A comparison of the FCGR behavior suggests that 725 exhibited the highest susceptibility, while the FCGR of 955 and 945X were lower similar to each other but lower than 725. In all the PH nickel-based alloys, stable static crack growth rate (CGR) was observed. Static crack growth rate of 10⁻⁶ mm/s (under constant K conditions) was obtained on 725 at 50 ksi $\sqrt{\text{in}}$ (55 MPa m). However, for 945X and 955, a static crack growth rate of 10⁻⁶ mm/s was observed at a higher K value of 80 ksi in (88 MPa $\sqrt{\text{m}}$) for 945X and 955. Applied potential in the range of -1050 mV to -850 mV SCE had a significant effect on the crack growth rate, with crack growth rate of 945X and 955 decreasing sharply with decreasing cathodic potential. The measured crack growth rate at -850mV SCE for 945X and 955 was very low on the order of 10⁻⁸ mm/s. In considering the use of high strength PH nickel-based alloys, it is recommended that methods to control the cathodic protection potential to values below - 1050 mV SCE be considered. FCGR of the cold worked nickel-based alloys C22HS, and 825 did not exhibit a frequency dependence. For both these alloys (C22HS and 825), there was no evidence of static crack growth. This suggests that under these conditions, C22HS and 825 were resistant to environmentally assisted fatigue and static crack growth.

Seawater at Open Circuit Potential (OCP)

The resistance to seawater exposure in the absence of cathodic protection, was evaluated, by performing critical crevice temperature tests in 3.5 wt% NaCl. The critical crevice temperature increased with increasing alloy content of Chromium (Cr), Molybdenum (Mo), and Tungsten (W). Alloy 825, and 945X exhibited the lowest critical crevice temperature, at ~24°C. Increasing Cr, Mo, and W content resulted in increasing critical crevice temperature. C22HS did not exhibit any evidence of crevice attack even at temperatures as high as 95°C. The resistance to environmentally assisted fatigue behavior was also evaluated at OCP for all the alloys at 15.6°C (60°F). The FCGR did not vary with frequency in any of the materials, consistent with excellent resistance to environmentally assisted fatigue at OCP.

2 INTRODUCTION

Increasing energy demand has led to expanding production from offshore High-Pressure, High Temperature fields (HPHT). The fields being developed typically are at temperatures greater than 350 F, and at pressures greater than 15ksi. In addition to higher temperatures, and higher pressures subsea equipment used in Oil and Gas (O&G) production for these fields is being subjected to increasing fatigue loads over a range of frequencies. Specifically, start up and shutdown sequences involve large strains associated with pressure and thermal cycles. Typically, these loading events occur over the course of hours to days. In addition to cyclic loading, subsea equipment is also subject to high mean stresses. This has necessitated the use of high strength material.

The HPHT fields that are being developed in the Gulf of Mexico are also likely to have low pH, high chloride concentration, coupled with the presence of H₂S (sour service). The combination of these extreme conditions of loads, temperature, and environment places significant demands on the materials both in terms of strength as well as corrosion resistance. These factors have led to the use, and evaluation of high strength nickel-based alloys for HPHT applications.

The intent of this program is to understand the performance of new high strength nickel-based alloys that are likely to be used in O&G equipment for HPHT applications. The materials were evaluated for various possible damage modes (environmentally assisted fatigue, static crack growth, and localized corrosion in seawater) in a range of applicable environments. The test program was designed to not only develop comparative data between the alloys, but also develop an understanding of the damage accumulation mechanisms.

3 BACKGROUND

High strength nickel-based alloys are being increasingly used in O&G applications in HPHT applications. PH nickel-based alloys provide high strength and ductility along with excellent resistance to localized corrosion and stress corrosion cracking in sour service conditions in HPHT conditions. This is evident by the successful use of PH nickel alloys like 718 in a wide range of subsea applications. The resistance to localized corrosion and stress corrosion cracking at elevated temperatures is primarily dependent on chloride concentration, pH, H₂S level, and temperature. While 718 has proved to be effective, for the industry over a wide range of conditions, higher temperatures and pressures have necessitated the need to consider the use of alloys like 725, 945X, and 955. These alloys are more highly alloyed than 718, with higher concentrations of Cr, and Mo, which typically help with localized corrosion resistance. The increased Nickel (Ni) content, helps with stress corrosion cracking resistance[1]. However, there is a need to characterize some of the newer materials in the context of the higher temperatures and pressures that are likely to be experienced in service. There is also a need to understand the behavior of high strength nickel-based alloys that are strengthened by cold worked as opposed to precipitation hardening mechanisms.

In addition to improved sour service performance for HPHT applications, there is a need to characterize the behavior of these alloys in seawater under cathodic polarization for subsea applications. There have been reported failures of high strength nickel-based alloys, 718 and 725 in subsea applications due to low temperature hydrogen embrittlement (HE) [2-5]. In the case of 718 it was found that extensive precipitation of phase along grain boundaries was responsible for the failure[2]. In the case of 725 there were two failures[3, 5], one in which grain boundary carbide precipitation was thought to be responsible[3], while in the other failure decoration of sigma phase along the boundaries was believed to be responsible[5]. These failures highlight the need to characterize the resistance to cracking of PH nickel alloys at lower temperatures. There is currently little or no information on the behavior of high strength nickel-based alloys that are strengthened by cold work.

For low temperature conditions, it is also important to characterize the resistance to localized corrosion of these materials in seawater environments, since a number of components made from these materials are likely to be exposed to seawater environments in the absence of cathodic protection. Characterizing their resistance to localized corrosion is important for understanding the use of these materials in O&G applications.

Apart from the increasingly aggressive conditions that are expected in HPHT applications, there is a desire to apply a fracture mechanics-based design for HPHT applications. This has led to the development of API17TR8 guideline for HPHT applications. This guideline emphasizes the need to characterize the fatigue and fracture behavior of materials in service conditions i.e. both sour service and in seawater under cathodic polarization.

The current program is an effort to characterize the fatigue and fracture behavior of newer grades of high strength nickel-based alloys specifically in both sour service and seawater under cathodic polarization.

4 EXPERIMENTAL

4.1 Critical Crevice Temperature

Electrochemical tests were performed on creviced samples to determine resistance to localized corrosion. The choice of crevice samples was based on the fact that the deposits that form on metal surfaces, seals, and interfaces could act as crevices where localized corrosion may initiate. It was also decided to perform critical crevice temperature tests at +700 mV SCE to mimic the presence of bio films in seawater environments, which serve to anodically polarize materials.

All electrochemical tests were performed in 3.5 wt% NaCl. Crevices were formed on samples, using a ceramic crevice former with a Teflon tape on the crevice former. The tests were started at 10°C and the temperature was increased at 0.2°C/min. The current was measured and the temperature at which the current was higher than 100 $\mu\text{A}/\text{cm}^2$ was identified as the critical crevice temperature. The samples were also evaluated visually after the test to confirm the occurrence of localized corrosion.

4.2 Environmental Conditions

Fatigue and fracture tests were performed in different sets of environments:

1. Sour Service — Tests in sour service was performed at pH = 4.0 with p_{CO_2} = 125 psia, $p_{\text{H}_2\text{S}}$ = 0.08 psia. The partial pressures indicated correspond to the values associated with the test temperature. The pH of the test solution was buffered with sodium acetate. The details of the chemistry of the test solution are shown below in Table 1. The test solution was de-aerated prior to introducing the solution into the autoclave. The test solution was transferred under a blanket of N_2 into the autoclave, saturated with the test gas at room temperature followed by addition of CO_2 to raise the pressure to 83.8 psia. N_2 pressure was then applied to raise the total pressure to 236 psia. The autoclave was then heated to 350°F (177°C) and the test temperature controlled to $\pm 2^\circ\text{F}$ in all the tests. In one case after the test at 350°F/177°C was completed, the autoclave was heated to 400°F/204°C. The details of the sour service environment were based on the conditions consistent with API17TR8, as well as DNVGL’s experience in HPHT testing environments. It is believed that the choice of sour service conditions in this test program are representative of HPHT fields in the GoM.

Table 1: Chemistry of the sour service test solution used.

Constituent	wt%
Acetic Acid	0.007
Sodium Acetate	0.008
NaCl	20
Water	80

2. Seawater + CP – Tests were performed in 3.5 wt% NaCl at 40 F. The tests were initiated at - 1050 mV SCE, which is the typical anode potential in subsea applications. When static crack growth rate was established, the potential was varied in the range of -1150 mV to -850 mV SCE. The pH of the test solution was adjusted to 8.2 using NaOH. All tests were performed in either a C-276 or acrylic cell. The temperature was controlled by running cooling coils into the cell, to achieve the desired temperature. The temperature in the test cell was typically within ± 2 F. A platinized Niobium (Nb) counter electrode was used and

a saturated calomel (SCE) reference electrode was used. The fracture mechanics samples were the working electrode and were isolated from the clevises and test cell using ceramic coated pins.

4.3 Materials and Specimens

Three different precipitation hardened high strength nickel-based alloys were studied in this program, along with two cold worked nickel-based alloys. The details of the chemistry, heat treatment, and mechanical properties at room temperature of the materials studied are shown in Table 2 through Table 4. The chemistry and heat treatment information are from the materials MTR's provided. The mechanical properties were from tensile tests performed.

Table 2: Chemistry of the materials tested.

Alloy	DNV-GL #	C	Si	Mn	P	S	Cr	Mo	Ni	Al	B	Co	Cu	Nb	Pb	Ti	Bi	Ca	Mg	Se	Ta	Fe	Nb+Ta
C22-HS	2785	0.003	0.015	0.25	<.01	<.0001	20.5	16.6		0.23	0.006	0.05		0.08		<.01		0.034			<.1	1.1	0.18
725	2810	0.015	0.04	0.03	0.003	0.0006	20.7	8.01	57.5	0.32	0.0035	0.05	0.01	3.54	0.00001	1.56	0.0003	0.0003	<.00005	<.00005	0.004	Bal	3.544
945X (140ksi)	2805	0.011	0.07	0.08	0.01	0.001	20.8	3.26	53.3	0.11		0.3	1.99	4.06		1.52		0.003	0.0004		0.01	14.4	4.06
955	2808	0.015	0.09	0.08	0.009	0.0002	21.6	5.9	57.4	0.43	0.0043	0.01	0.037	4.8		0.86						8.7	4.8
825	2833	0.01	0.4	0.75	0.017	0.0002	22.35	3.08	38.37	0.12			1.86			0.83						32	

Table 3: Heat treatment of the materials tested.

Alloy	DNV-GL #	HT #	Description	Procured From	Solutionizing	Heat Treatment
C22-HS	2785	2321-2-2505	2.25" DIA x 60" Length	Howco Metals Management LLC		
725	2810	Z0403-1	4.50" DIA x 24" Length	Special Quality Alloys, INC	1038C/2.06h	738C/8.1h FC to 621C- Hold for 8h followed by AC
945X (140ksi)	2805	XX5778RY11	4.00" DIA x 24" Length	Howco Metals Management LLC	1038C/2h	704C/8h FC to 621C - Hold for 8.5h followed by AC
955	2808	VAR41519/Heat 06930	8.00" DIA x 7" Length	Foroni S.p.A		
825	2833	F06919	7.625"OD x 5" Length	Special Quality Alloys, INC		

Table 4: Mechanical properties of the materials tested.

Alloy	DNV-GL #	HRC	RR	YS (ksi)	TS (ksi)	%Elon	%RA
C22-HS	2785	40		190	198	17	57
725	2810	38		131	191	36.7	49
945X (140ksi)	2805	40.7	36	149	185	29	45
955	2808	43	16	147	185	34	52
825	2833			127	130	19.6	

Tests were performed on compact tension specimens with the following nominal dimensions:

$$W = 1" (25.4 \text{ mm})$$

$$B = 0.5" (12.7 \text{ mm})$$

$$a/W_{int} = 0.35$$

Samples were side grooved 5%. Samples tested in sour service were tested in the L-C orientation, while samples tested in seawater + CP were tested in the L-R orientation with the crack running from the OD to the ID. Representative specimen drawings for the CT specimens are shown in Figure 1.

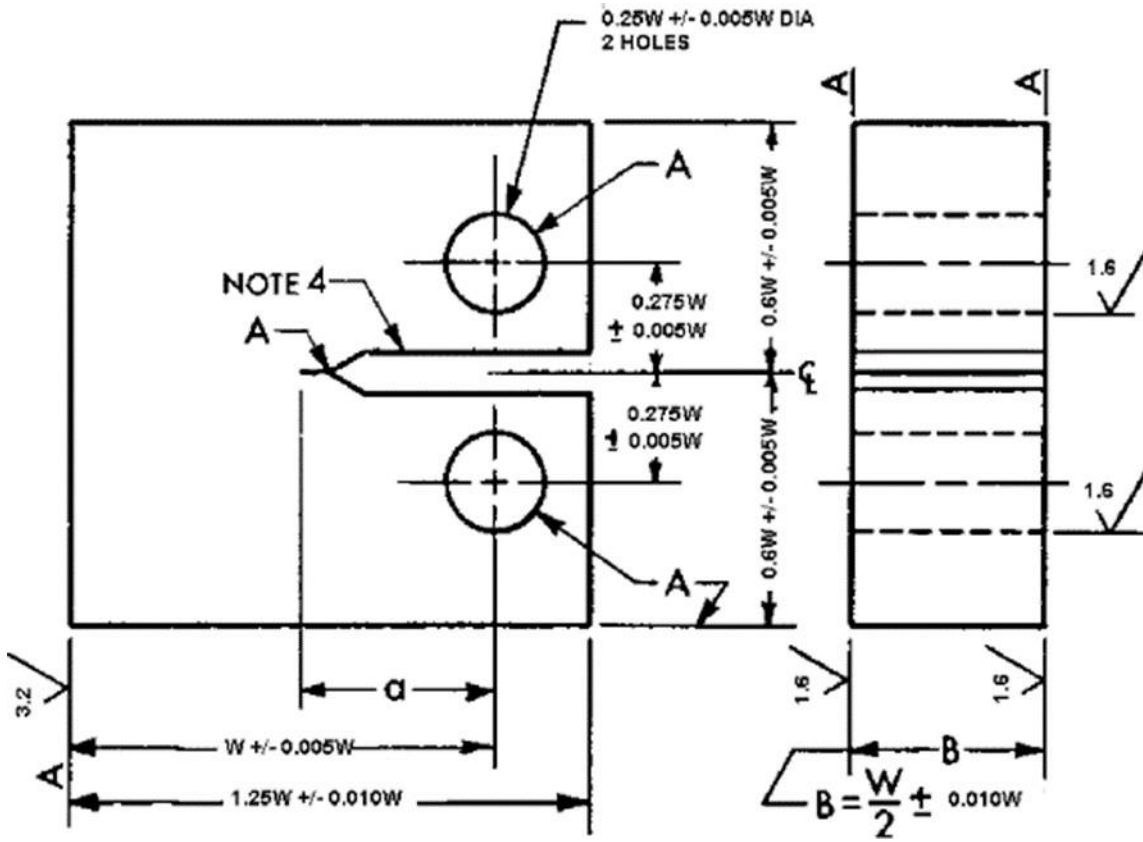
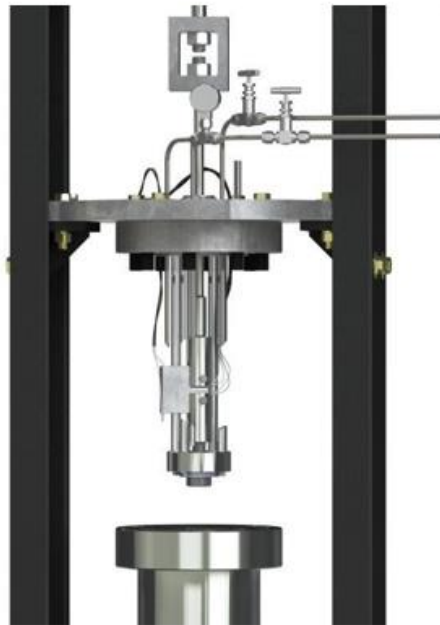
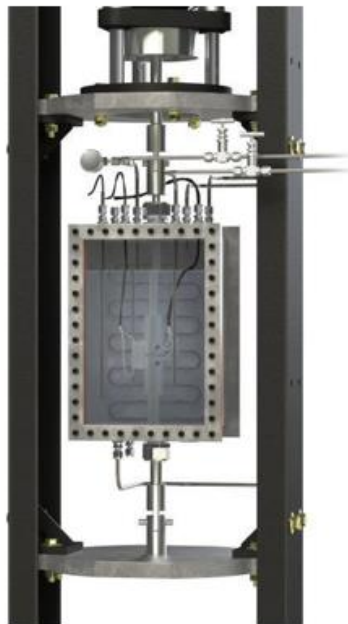


Figure 1: Schematic of the compact tension (CT) sample used in this test program.

The cell assembly for the sour service autoclave tests and the seawater + CP tests are shown in Figure 2



a) Sour Service autoclave setup with CT sample



b) Seawater + CP cell setup with CT sample

Figure 2: Schematic illustrations of the cells used for sour service and seawater + CP testing.

4.4 Crack Length Measurements

Crack length measurements were performed using reversing Direct Current Potential Drop (DCPD) method. A constant current of 4 Amperes (A) was applied to the actively loaded sample as well as reference sample which was not loaded, and the voltage from both the sample and reference were measured. Polytetrafluoroethylene (PTFE) heat shrunk Platinum wires of 1 mm were used for current and voltage probes. The voltage of the sample was normalized with the voltage of the reference sample to correct for drifts in temperature and noise from electronics. The changes in the reference also compensated for any changes in the voltage due to dissolution of the oxide under cathodic protection. The polarity was reversed about every 1 second to offset thermal junction effects. Voltage measurements were performed on both \pm polarity and the absolute value averaged to generate a single datum. Typically, anywhere from 100 to 1000 data were averaged to generate a single point. The choice of averaging was based on the estimated crack growth, typically for slow portions of test segments, 1000 data were averaged.

4.5 Test Method

The objective of the various loading forms was to determine the response of the material-environment system to various possible loading scenarios that may be experienced in service. Low cycle fatigue loading is a common occurrence during start-up and shut down conditions. However, extended continuous operation closely approximates a constant load or constant K situation. It is also likely that components like bolts, which operate under fixed displacement conditions are likely to experience decreasing K conditions as the crack propagates. In certain scenarios based on the profile of the residual stresses in the material, the crack could experience a rapidly increasing K profile, which is associated with an increase in crack length coupled with the crack growing into a region of increasing stress. The performed tests attempted to understand the material response under these various loading scenarios to accurately quantify damage as well as determine the effect of critical variables associated with each of these loading modes.

A range of K and ΔK values were explored over the course of the test program. This was based on the fact, that pits/defects of various kinds may initiate in these materials, which may lead to cracks. In general, these defects have to be the range of about 1-2 mm to be able to detect them, and likely have to be in the 3 mm range to size them accurately. Components that are threaded, and/or have sharp stress concentrators could act as sites for crack initiation. The applied loads can vary anywhere from about 50% of yield strength (YS) to values as high as a 100% of YS depending on the geometry and the specific components of interest. The applied loads, and defect size influence the K value associated with a crack like feature. A relatively simplistic analysis, for evaluating K is shown below in equation [1].

$$K = 1.12\sigma\sqrt{\pi a} \quad [1]$$

Where K is the stress intensity factor ($\text{MPa}\sqrt{\text{m}}$), σ is the applied stress (MPa), and a is the crack/defect length (mm). The effect of crack size, and stress on the resulting K values is shown in Figure 3. The assumption made in this calculation is that the YS of the material is 120 ksi (828 MPa).

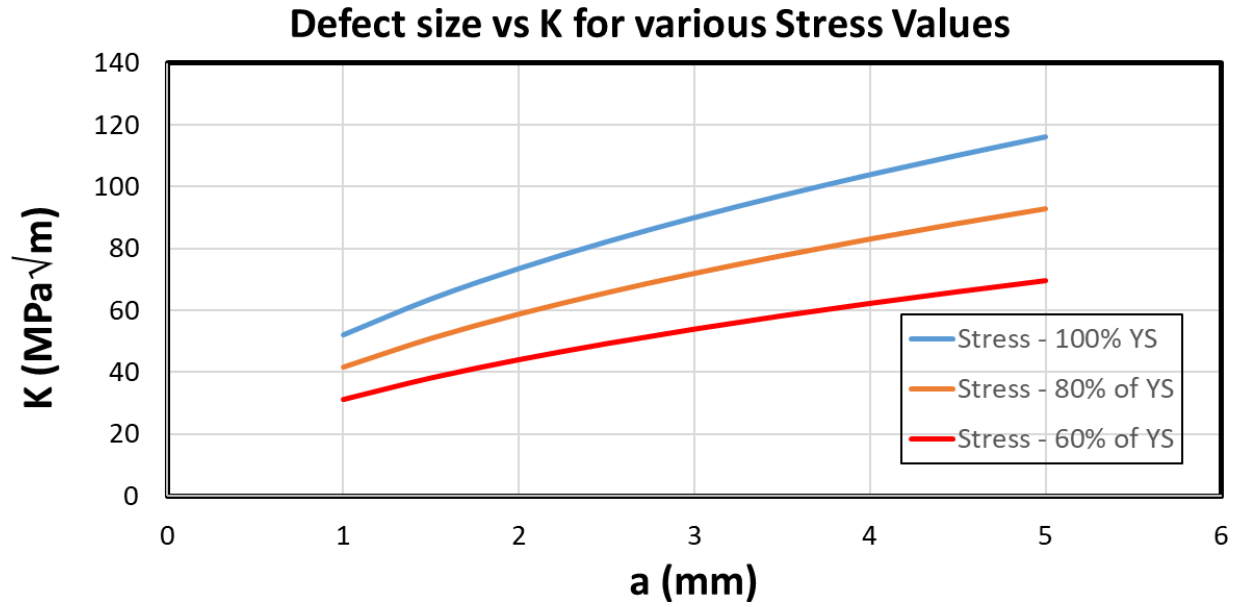


Figure 3: Effect of stress level, and crack length on the resulting K value assuming a YS of 120ksi (828MPa).

Table 5: Numerical values for Figure 3

Stress (ksi)	Crack Length (mm)	K (MPa√m)
120	1	51.99361714
	1.5	63.67891594
	2	73.53007852
	2.5	82.20912698
	3	90.05558656
	3.5	97.27115082
	4	103.9872343
	4.5	110.2951178
	5	116.2612623
96	1	41.59489371
	1.5	50.94313275
	2	58.82406282
	2.5	65.76730159
	3	72.04446925
	3.5	77.81692066
	4	83.18978743
	4.5	88.23609423
	5	93.00900986

Stress (ksi)	Crack Length (mm)	K (MPa√m)
72	1	31.19617029
	1.5	38.20734956
	2	44.11804711
	2.5	49.32547619
	3	54.03335194
	3.5	58.36269049
	4	62.39234057
	4.5	66.17707067
	5	69.7567574

NOTE: 120 KSI is 100%.

Based on the above analysis, the initial K values for a small defect would be in the range of about 25 to 50 ksi√in (27.5 to 55 MPa√m), while for a deep crack can be in the range of 65 to 105 ksi√in (71.5 to 115 MPa√m). In the context of the analysis, the tests were initially started in the low end of the K range i.e. with a K of about 50 ksi√in (55 MPa√m). Based on the material response, the K value was increased to the high end of the range, about 80-100 ksi√in (88 to 110 MPa√m). The details of the K values and the various loading modes applied in the tests is described below.

K controlled tests — Tests were performed under K-control for both FCGR as well as a static crack growth rate, the load was adjusted to maintain the desired constant K or varying K as needed. Load adjustments were made only when changes in crack length resulted in the K value changing by more than 0.1%. No load adjustments were made when the crack length appeared to decrease based on DCPD signals. In all cases where fatigue loading was applied, a triangular wave form was used, with a ratio of rise to fall time of 9:1. The wave frequency is the inverse of the total period of the wave. The test methodology for the tests are described below:

1. Sour Service: Tests were started at an initial K_{max} of 50 ksi√in (55 MPa√m), and an R-ratio (K_{min}/K_{max}) of 0.2. The frequency was scanned from 0.3 Hz to 0.1 mHz. After the frequency scan was completed, the R-ratio was increased to 0.6 and the frequency scan repeated from 0.3 Hz to 0.1 mHz. Upon completion of the frequency scan, an attempt was made to transition the crack to static conditions, this was achieved by cycling at 1 mHz and $R = 0.6$ followed by introduction of holds of increasing duration at K_{max} to facilitate a transition to stable crack growth at constant K. If stable crack growth was not achieved, the K value was increased, and the sequence repeated to obtain stable crack growth under constant K conditions.
2. Seawater + CP: Tests were started at an initial K_{max} of 50 ksi√in (55 MPa√m) and an R-ratio of 0.2. The frequency was scanned from 300 mHz to 0.1 mHz. After the frequency scan at $R = 0.2$ was completed, the R-ratio was increased to 0.6 and the frequency scan repeated from 0.3 Hz to 0.1 mHz. Upon completion of the frequency scan at R of 0.6, the cathodic polarization was turned off and the temperature increased to 60°F (15.6°C). Once the temperature and the open circuit potential (OCP) of the sample stabilized, a frequency scan was performed. The frequency scan was performed at a K_{max} of 50 ksi√in (55 MPa√m) and $R = 0.2$ from a frequency of 300 mHz to 1 mHz. Following the completion of the frequency scan test at OCP, the temperature was changed to 40°F (4.4°C) and a cathodic polarization of - 1050mV SCE was applied to the sample, which was the same potential at which the

frequency scan tests were performed. The test was then transitioned to measure static crack growth which was achieved by cycling at 1 mHz and $R = 0.6$ followed by introduction of holds of increasing duration at K_{max} to facilitate a transition to stable crack growth at constant K . If stable crack growth rate was obtained, the K value was decreased using a decreasing K profile under a constant K -gradient profile ($1/K (dK/da) = -30/in$) to a lower value of K . The change in K was applied at intervals of 0.2 mills ($5 \mu m$) of crack extension. The variation in K during the decreasing K profile was controlled as shown in equation [2]:

$$K = K_0 \exp(C\Delta a) \quad [2]$$

Where K_0 is the initial value of K ($MPa\sqrt{m}$)

C is $1/K(dK/da)$ ($1/mm$)

Δa is the crack extension (mm)

The sample was then transitioned to constant K by turning off the K -profile to measure stable crack growth rate. This was repeated to obtain crack growth rate over a range of K values.

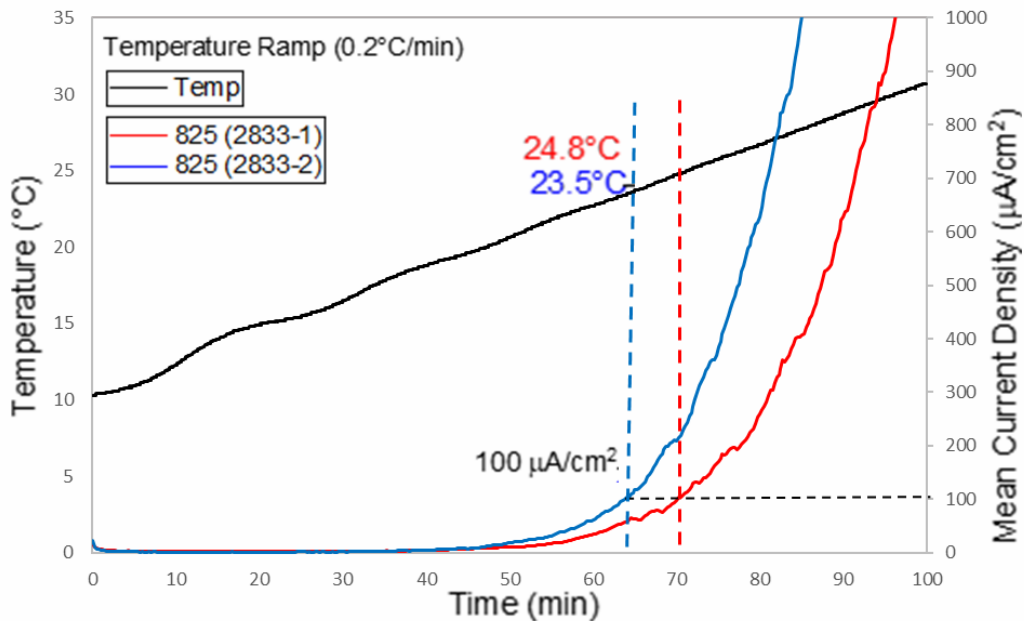
5 RESULTS

The results of the various tests performed below is reported in this section:

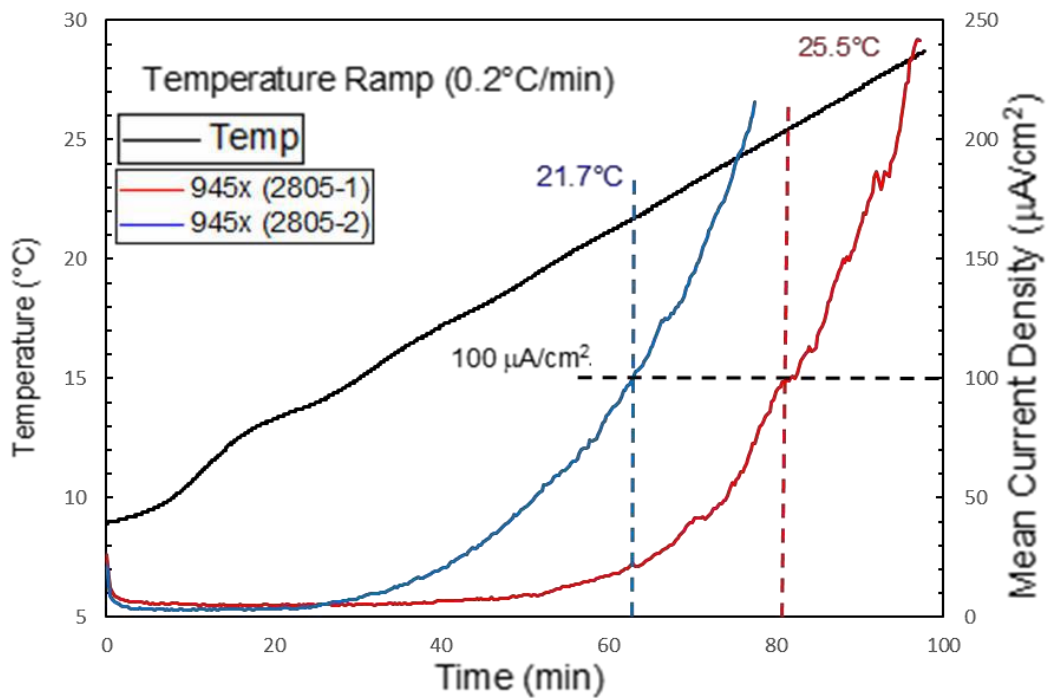
1. Critical Crevice Temperature in 3.5wt% NaCl
2. FCGR in Sour Service
3. FCGR and Static Crack Growth Rate in Seawater + CP
4. FCGR in Seawater at OCP

5.1 Critical Crevice Temperature

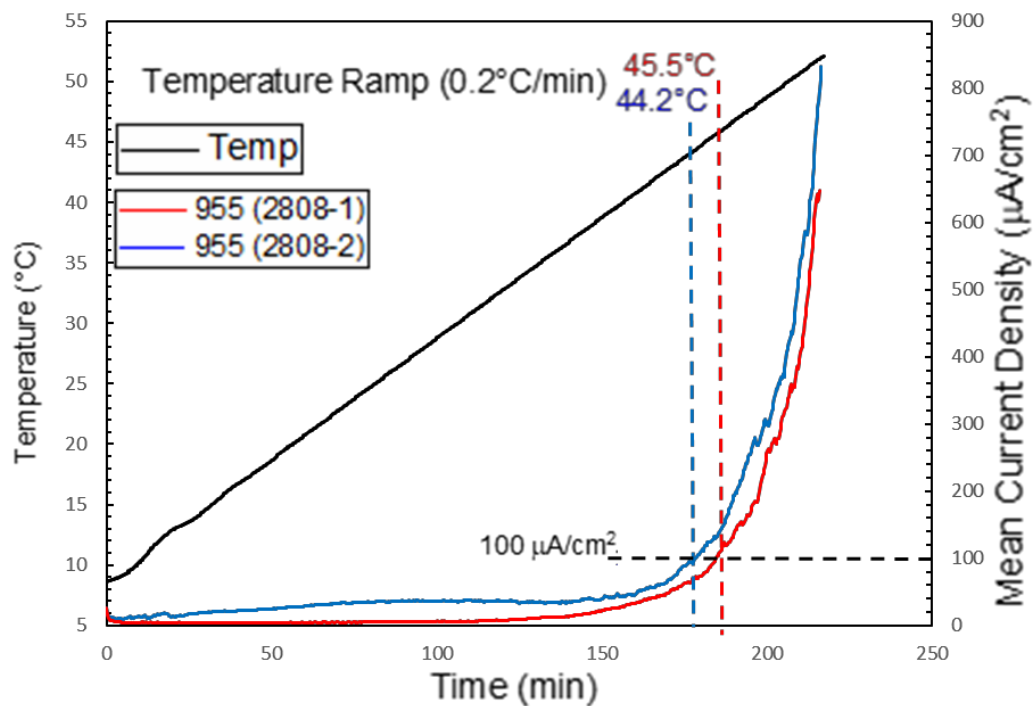
The results of the critical crevice temperature for the different materials studied is shown in Figure 4. The plots show the applied temperature profile on the left y axis and the resulting current density at +700 mV SCE on the right y axis. Increasing temperature leads to an increasing current density. The temperature at which the current density exceeds $100 \mu\text{A}/\text{cm}^2$ is identified as the temperature at which localized corrosion initiates. The temperature at which $100 \mu\text{A}/\text{cm}^2$ is indicated on each plot. It is clear from the data, the crevice corrosion resistance of 825 and 945X are similar at about 24°C . Alloy 955 exhibits a higher critical crevice temperature in the range of 45°C , and 725 has a significantly higher critical crevice temperature of 66°C . 725 exhibits higher critical crevice temperature than 955 and is consistent with the higher Mo content. C22HS exhibits $100 \mu\text{A}/\text{cm}^2$ current density at about 77°C , which is likely associated with the transpassive dissolution of chromium. The data in Figure 4 is arranged in order of increasing critical crevice temperature. As a note to the reader the scales on each of the plots are different to highlight the critical crevice temperature for each alloy. The wide range in the critical crevice temperature and current density make it impractical to have all plots on the same scale.



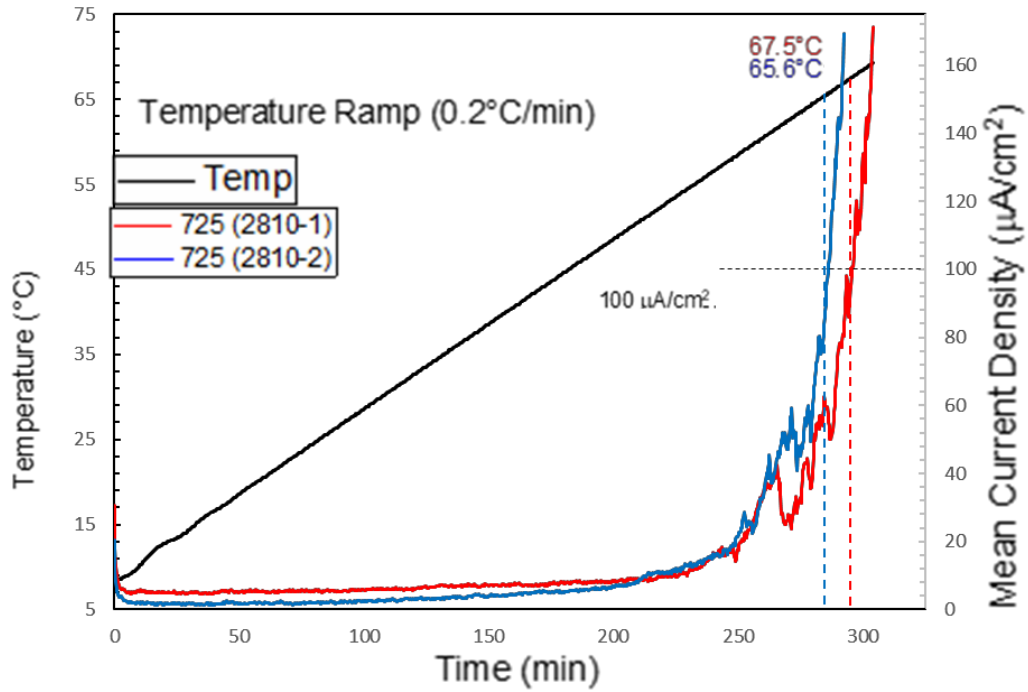
a) 825



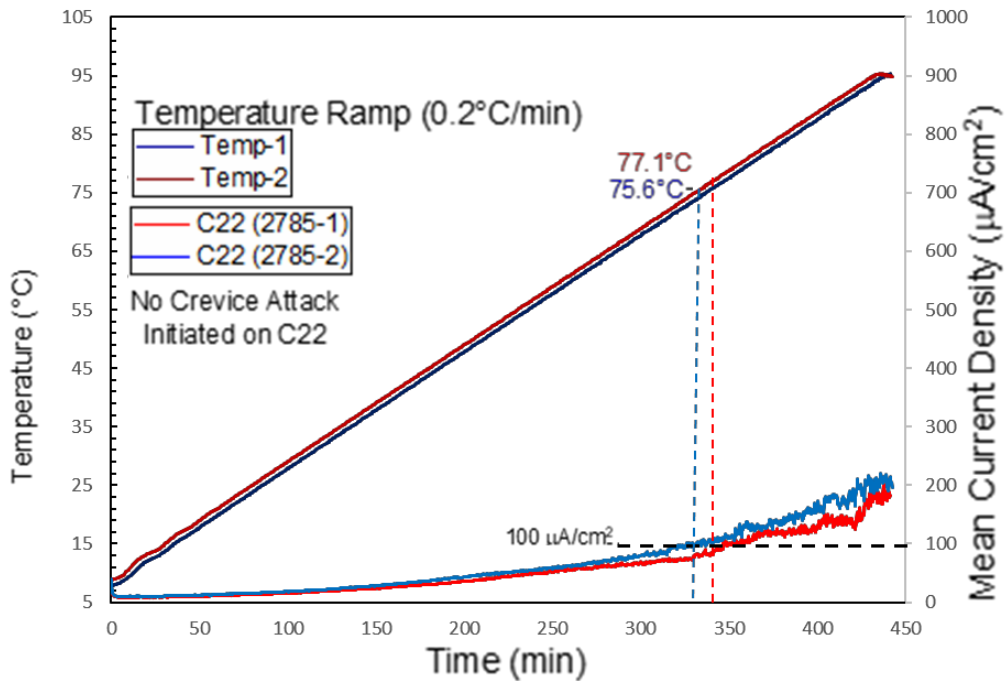
b) 945X



c) 955



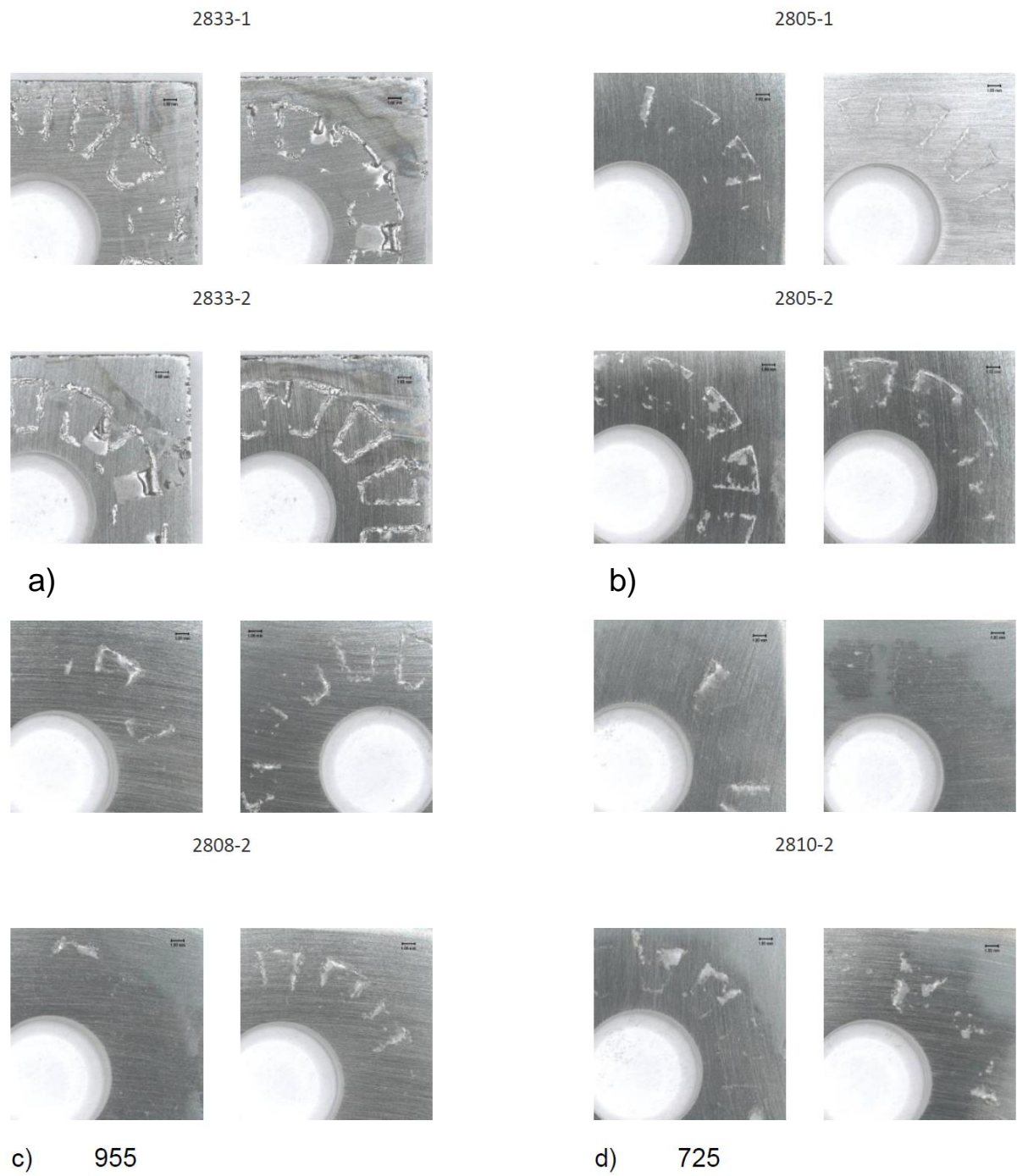
d) 725



e) C22HS

Figure 4: Critical crevice temperatures of the various alloys evaluated in 3.5 wt% NaCl at +700 mV SCE.

Post tests of the samples are shown in Figure 5 and there is clear evidence of crevice corrosion on all the samples, except C22HS. The extent of attack on 825 is significantly more than that observed on 955 and 725. It is also evident from the photographs, that there is no evidence of crevice corrosion on C22HS, consistent with the idea that the increase in current is associated with the transpassive dissolution of chromium. This is consistent with the measured critical crevice temperatures.



The results of the critical crevice temperature are summarized in Table 5. The temperature at which the current density is higher than 100 $\mu\text{A}/\text{cm}^2$ is shown and identified as the critical crevice temperature in all cases except for C22HS. In the case of C22HS there was no evidence of crevice corrosion, and the increase in current is likely associated with the transpassive dissolution of chromium.

Table 6: Critical crevice temperature of the various materials tested in 3.5 wt% NaCl at +700 mV SCE.

Alloy	Critical Crevice Temperature* (°C)			Crevice Corrosion (Y/N)
	Sample 1	Sample 2	Average	
725	67.5	65.6	66.6	Y
825	24.8	23.5	24.2	Y
945x	25.5	21.7	23.6	Y
955	45.5	44.2	44.9	Y
C22	77.1	75.6	76.4	N

*Determined where Mean Current Density was 100 $\mu\text{A}/\text{cm}^2$ while polarized to +700 mV(SCE)

The results obtained are consistent with the frame work that increasing alloying content increases the resistance to localized corrosion. The increase in alloying content is usually represented in the form of a PREN number, which weighted differing alloying elements for their contribution to the localized corrosion resistance. Two formulations of PREN numbers have been used, one which includes the effect of Nitrogen (N), and another which incorporates the effect of Tungsten (W), and Nb shown below in equations [3] and [4].

$$PRE-1 = \%Cr + 1.5(\%Mo + Nb + W) \quad [3]$$

$$PRE-2 = \%Cr + 3.3(\%Mo) + 16(\%N) \quad [4]$$

A summary plot of the critical crevice temperature as a function of the two PREN formulations for the alloys studied is shown in Figure 6. While the general trend in the critical crevice temperature follows the PREN number formulation, PREN-1 formulation likely fits the data better. This would be consistent with the fact that all the materials tested have similar concentration of Cr, and the key difference among them is the varying Mo, and Nb content.

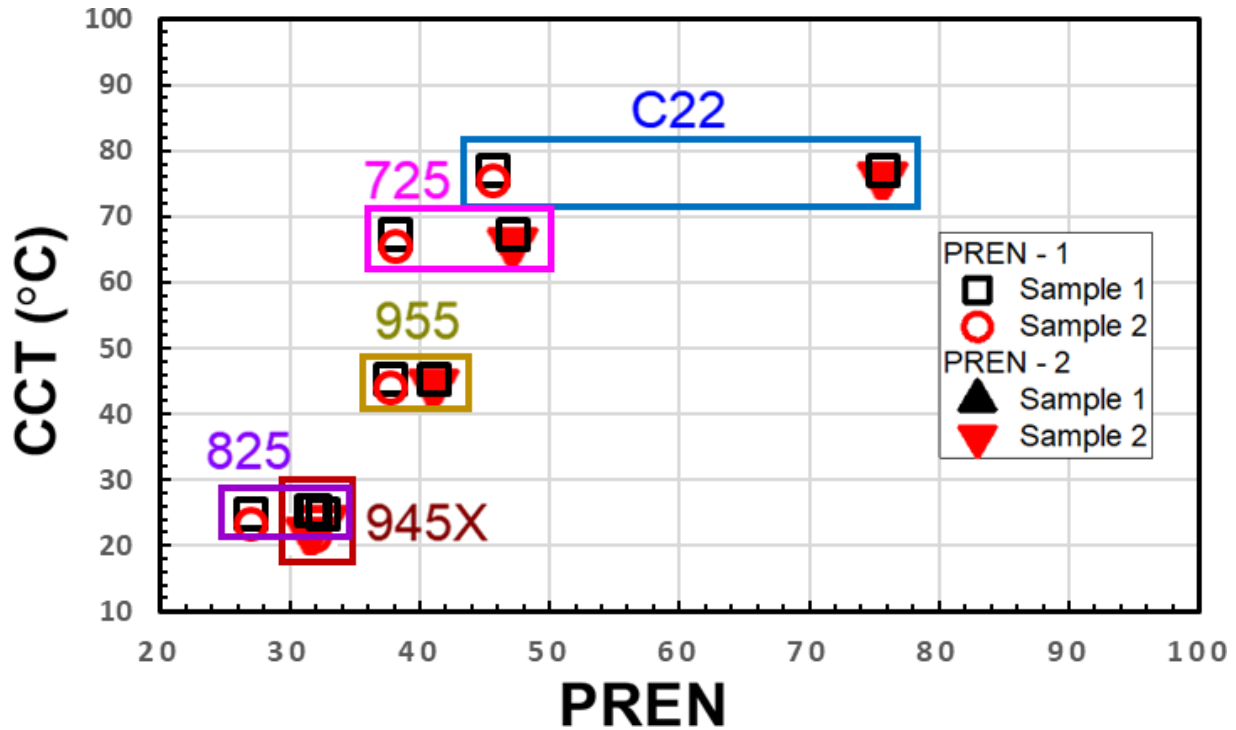


Figure 6: Relationship between the critical crevice temperature and the PREN number formulations.

Table 7: Numerical values for Figure 6

	Sample 1	Sample 2	PREN - 1	PREN - 2
725	67.5	65.6	38.025	47.133
825	24.8	23.5	26.97	32.514
945x	25.5	21.7	31.78	31.558
955	45.5	44.2	37.65	41.07
C22	77.1	75.6	45.565	75.632

The above discussion supports the notion that increasing alloy content promotes passivity and resistance to localized corrosion. In the context of using these materials in high strength applications, where they be exposed to salt water environments in the absence of cathodic protection, 825 and 945X are likely the most susceptible, though in service they are unlikely to experience the high anodic potentials applied here. All the other materials (955, 725, and C22HS) exhibit significantly higher critical crevice temperatures, and are unlikely to be susceptible to localized corrosion in seawater environments at near ambient temperatures. A note of caution is warranted in applying these results, the environments considered here are seawater type of conditions and not production chemistry environments. Typical production environments have lower pH, higher chloride concentrations, high temperatures, and high concentrations of acid gases like CO₂ and H₂S.

5.2 Sour Service

Environmental fatigue tests were performed in sour service at elevated temperature and pressure to mimic production environments that subsea components are exposed to. Characterizing the environmentally assisted FCGR is important in developing design data that can be applied for HPHT applications. It also provides a basis for quantitatively comparing the performance of material, as opposed to a simple pass/fail criterion. The section below presents the analysis for data generated on set of PH nickel-based alloys (725, 945X, and 955) as well as a set of nickel based alloys that are strengthened via cold working (C22HS, and 825).

5.2.1 725 (Specimen ID 2810 CL-3)

The results of the frequency scan on 725 at 350°F (177°C) and 400°F (204°C) are shown in Figure 7. There is no significant effect of frequency on the fatigue crack growth at either temperature. There also appears to be no significant effect of ΔK on the frequency dependence. These results suggest that in the studied sour service environments do not have significant impact on the FCGR under the ΔK conditions evaluated. These results are consistent with data in literature where FCGR and fracture toughness tests performed on 625+ in sour environments containing similar chloride levels but at much higher partial pressures of H₂S, did not show any susceptibility to environmentally assisted fatigue[1].

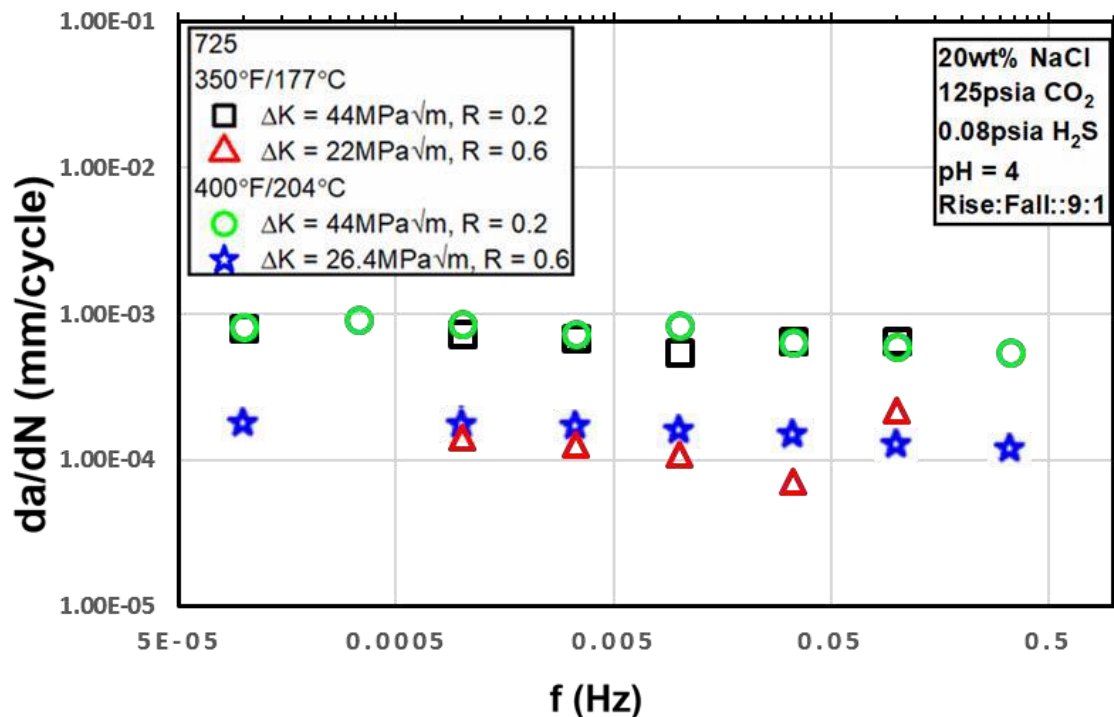


Figure 7: FCGR frequency scans on 725 (2810-CL3) in sour environment over a range of ΔK values at 350°F and 400°F.

Table 8: Color coded numerical values for Figure 7

Kmax	Kmin	f (Hz)	da/dt (mm/s)	Da (in)	Comments	Rise Time (s)	Fall Time (s)	Hold Time (s)	da/dN (mm/cycle)
50	10	0.1	6.56E-05	0.02812	'9/1'	9	1		6.56E-04
50	10	0.03333	2.19E-05	0.00334	'27/3'	27	3		6.58E-04
50	10	0.01	5.49E-06	0.00401	'90/10'	90	10		5.49E-04
50	10	0.00333	2.26E-06	0.00682	'270/30'	270	30		6.77E-04
50	10	0.001	7.25E-07	0.00192	'Change to 1mHz'	900	100		7.25E-04
50	10	1.00E-04	8.05E-08	0.00358	'Change to 900/100'	9000	1000		8.05E-04
50	30	0.1	2.19E-05	0.0042	'Change to R=0.6'	9	1		2.19E-04
50	30	0.03333	2.37E-06	0.02342	'27/3'	27	3		7.10E-05
50	30	0.01	1.10E-06	0.00901	'90/10'	90	10		1.10E-04
50	30	0.00333	4.29E-07	0.00316	'270/30'	270	30		1.29E-04
50	30	0.001	1.44E-07	9.88E-05	'Change to 1mHz'	900	100		1.44E-04
50	10	0.33333	1.82E-04	0.00809	'Beff=0.4743'''	2.7	0.3		5.45E-04
50	10	0.1	5.93E-05	0.0084	'9/1'	9	1		5.93E-04
50	10	0.03333	2.14E-05	0.00796	'27/3'	27	3		6.42E-04
50	10	0.01	8.40E-06	0.0035	'90/10'	90	10		8.40E-04
50	10	0.00333	2.44E-06	0.00534	'270/30'	270	30		7.33E-04
50	10	0.001	8.58E-07	0.00323	'900/100'	900	100		8.58E-04
50	10	3.33E-04	3.05E-07	0.002	'2700/300'	2700	300		9.14E-04
50	10	1.00E-04	8.18E-08	9.34E-04	'9000/1000'	9000	1000		8.18E-04
60	36	0.33333	3.94E-05	0.00746	'Restart at Kmax=60'	2.7	0.3		1.18E-04
60	36	0.1	1.26E-05	0.03586	'9/1'	9	1		1.26E-04
60	36	0.03333	4.89E-06	0.00432	'27/3'	27	3		1.47E-04
60	36	0.01	1.56E-06	0.00488	'90/10'	90	10		1.56E-04
60	36	0.00333	5.54E-07	0.0051	'270/30'	270	30		1.66E-04
60	36	0.001	1.81E-07	0.00318	'900/100'	900	100		1.81E-04
60	36	1.00E-04	-6.17E-09	3.24E-04	'9000s holds'	900	100		-6.17E-05
60	36	0.001	1.71E-07	0.00116	'900/100'	900	100		1.71E-04
60	36	1.00E-04	1.74E-08	6.12E-04	'9000s holds'	900	100	9000	1.74E-04

An attempt was made to transition the test to constant K at this point, by introducing 9000 s holds. The results of the crack growth rate at the transition to 9000s hold periods are shown below in Figure 8. The changes made in the test during this period are indicated in the plot with vertical comments. The comments along with the time stamp are located on the plot when the change was made. The

data clearly indicates that no stable crack growth was possible at 9000 s (2.5 h) holds suggesting that stable static crack growth was not possible under these conditions. The test was then terminated, with the conclusion that no stable crack growth was possible in 725 at 400°F (204°C) at a high K_{max} value of 60 ksi√in (66 MPa√m).

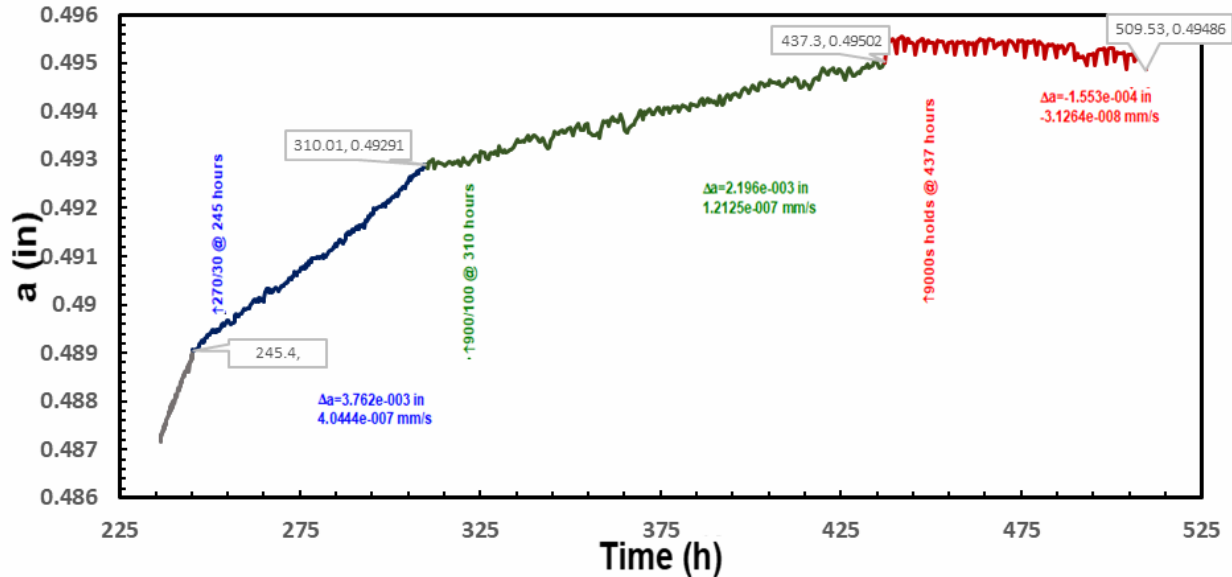


Figure 8: Crack length vs time as a function frequency and hold time of 725 (2810-CL3) in sour environment at 400°F (204°C) and K_{max} of 60 ksi√in (66 MPa√m).

5.2.2 945X (Specimen ID 2805-CL1)

The results of the FCGR frequency scan tests on 945X are shown below in Figure 9. The results suggest that over a range of ΔK conditions there is no effect of frequency on the FCGR behavior. This would suggest that there is little or no environmental effect in these conditions. 718 did not exhibit susceptibility to environmentally assisted fatigue and exhibited high values of K_{int} (120 MPa√m) measured in the rising displacement tests in similar environments[1]. These results are consistent with results on 718, which has lower Cr content compared to 945X.

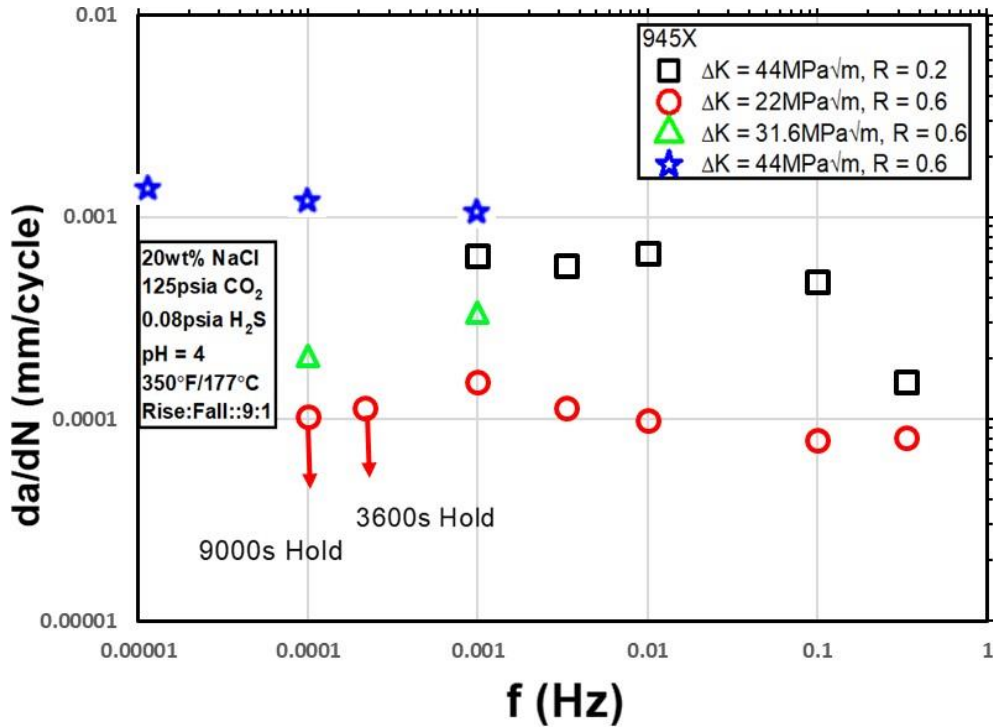


Figure 9: FCGR frequency scans on 945X (2805-CL1) in sour environment at 350°F (177°C) over a range of ΔK values.

Table 9: Color coded numerical data for Figure 9

Kmax	Kmin	f (Hz)	da/dt (mm/s)	Da (in)	Comments	da/dN (mm/cycle)
50	10	0.3333	5.10E-05	-0.0022	2.7/0.3	1.53E-04
50	10	0.1	4.78E-05	0.0214	1-Sep	4.78E-04
50	10	0.01	6.59E-06	0.02	27/3	6.59E-04
50	10	0.0033	1.90E-06	0.0126	270/30	5.76E-04
50	10	0.001	6.41E-07	0.0077	900/100	6.41E-04
50	30	0.3333	2.69E-05	-7.78E-04	R=0.6	8.09E-05
50	30	0.1	7.83E-06	0.0274	1-Sep	7.83E-05
50	30	0.01	9.92E-07	0.0041	change to 90 and 10	9.92E-05
50	30	0.0033	3.73E-07	0.0023	Change to 270/30	1.13E-04
50	30	0.001	1.54E-07	0.0024	Change to 900/100	1.54E-04
50	30	2.17E-04	2.48E-08	0.00132	'3600s holds'	1.14E-04
50	30	1.00E-04	1.03E-08	5.64E-04	'Change to 9000s hold'	1.03E-04

Kmax	Kmin	f (Hz)	da/dt (mm/s)	Da (in)	Comments	da/dN (mm/cycle)
72	43.2	0.001	3.38E-07	0.00711	restart from power outage'	3.38E-04
72	43.2	1.00E-04	2.06E-08	0.00213	'Introduce 9000s holds'	2.06E-04
100	60	1.00E-03	1.04E-06	0.00651	'begin cycling 900/100 @Kmax=100'	0.00104
100	60	1.00E-04	1.18E-07	6.82E-04	'begin 9000s holds'	0.00118
100	60	1.14E-05	1.56E-08	2.62E-04	'1 day holds'	0.00137

An attempt was made to transition to constant K at 50 ksi√in (55 MPa√m) by introducing hold periods of 9000 s (Figure 10). The changes made in the test during this period are indicated in the plot with vertical comments. The comments along with the time stamp are located on the plot when the change was made. The measured crack growth rate was 1×10^{-8} mm/s, a very low value. It was then decided to increase K under 9000 s hold from 50 ksi√in (55 MPa√m) to 72 ksi√in (79.2 MPa√m). The crack growth rate during the increasing K portion even under cycling with 9000 s hold periods was 2×10^{-8} mm/s, which is not significantly higher compared to these measured under constant K and 9000 s hold periods. This suggests that at these K-levels even in the presence of a positive K- gradient there is no significant increase in the crack growth rate.

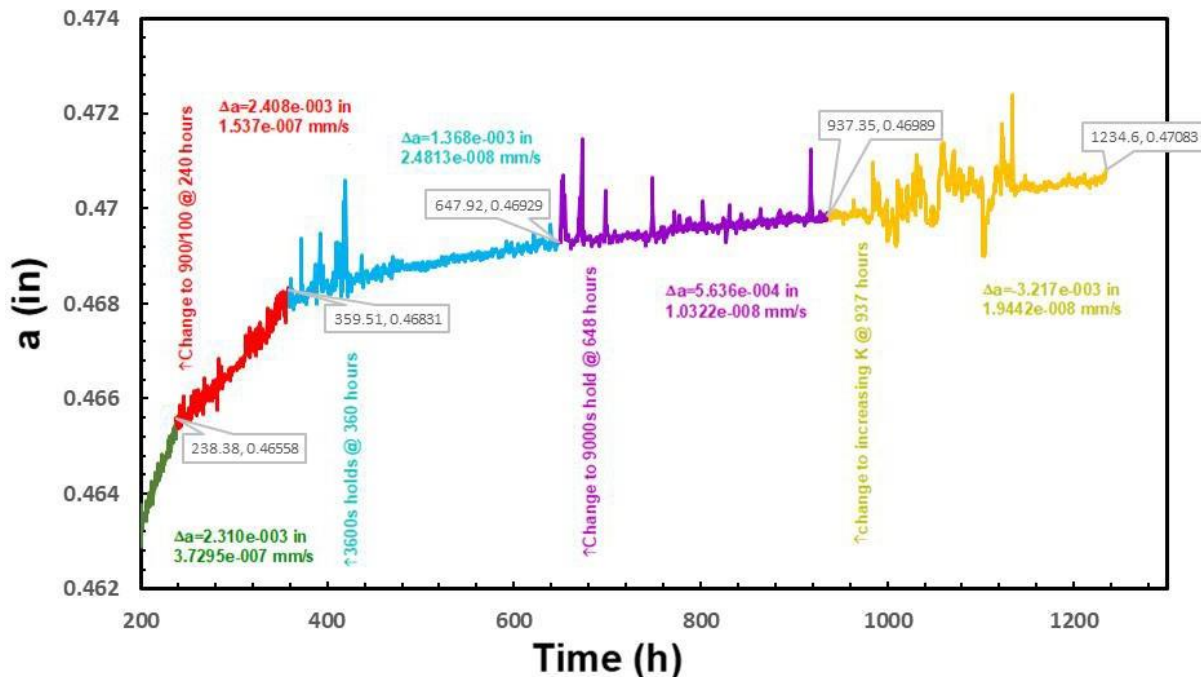


Figure 10: Crack length as a function of time for 945X (2805-CL1) at 350°F (177°C) under 9000 s holds at 50 ksi√in (55 MPa√m) and transitioning to 72 ksi√in (79.2 MPa√m).

The crack was then transitioned to a K_{max} of 72 ksi \sqrt{in} (79.2 MPa \sqrt{m}) and 9000 s holds, followed by a transition to constant K (Figure 11). The changes made in the test during this period are indicated in the plot with vertical comments. The comments along with the time stamp are located on the plot when the change was made. The crack growth rate under 9000 s hold periods was 2×10^{-8} mm/s, similar to the value obtained during the rising K portion from 50 ksi \sqrt{in} (55 MPa \sqrt{m}) to 72 ksi \sqrt{in} (79.2 MPa \sqrt{m}). There was no measurable crack growth rate under constant K conditions, suggesting that under the constant K conditions stable crack growth rate cannot be sustained.

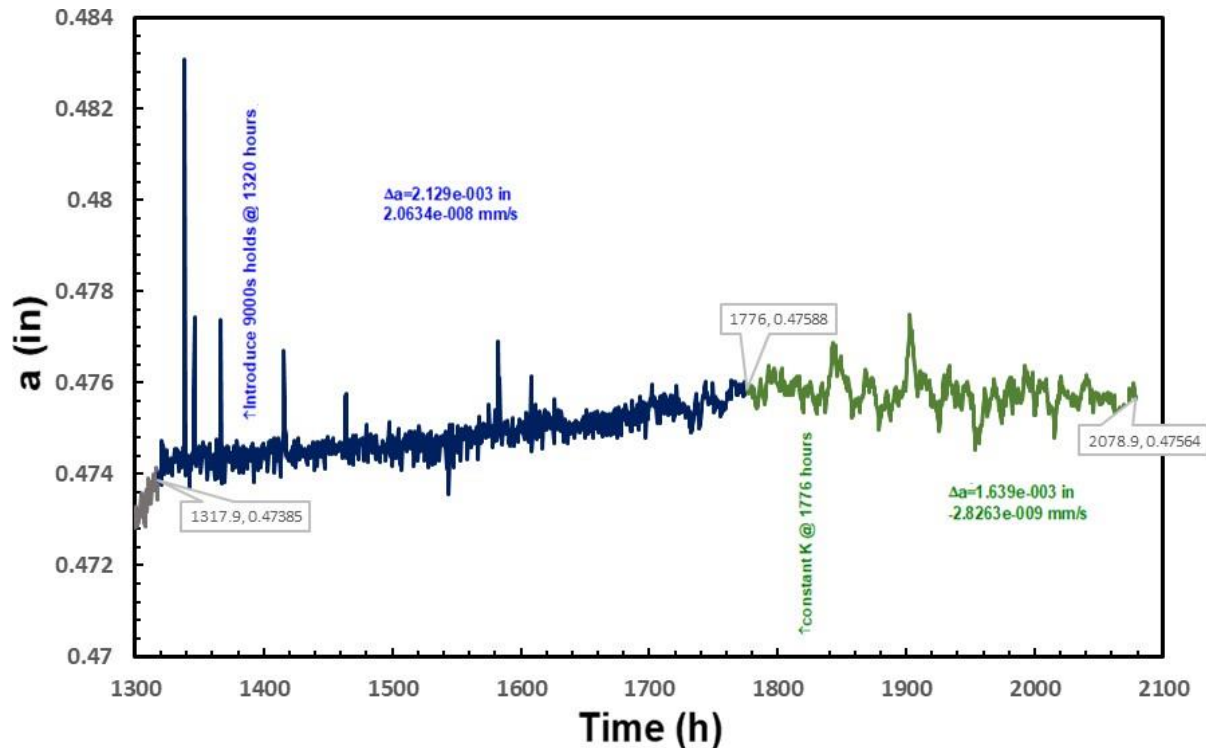


Figure 11: Crack length as a function of time for 945X (2805-CL1) at 350°F (177°C) under 9000 s holds and constant K at 72 ksi \sqrt{in} (79.2 MPa \sqrt{m}).

The sample was transitioned to a K_{max} of 100 ksi \sqrt{in} (110 MPa \sqrt{m}), which is above the ASTM E647 criteria for this sample geometry[6]. The resulting crack growth rate at 1 mHz, 1 mHz + 9000 s holds and 1 mHz + 1-day holds is shown in Figure 12. The changes made in the test during this period are indicated in the plot with vertical comments. The comments along with the time stamp are located on the plot when the change was made. The measured crack growth rate decreases by about 10x for each of these segments, suggesting that there is no significant environmental effect. At this point, the test was terminated and the conclusion from the test was that no stable static crack growth rate was possible up to K values of 100 ksi \sqrt{in} (110 MPa \sqrt{m}), under the tested conditions. This behavior is consistent with the observations on 718, in similar conditions where the K_{int} was observed at 120 MPa \sqrt{m} from rising displacement tests[1]. It is expected that 945X which has a higher Cr content would behave at least as well as 718 if not better.

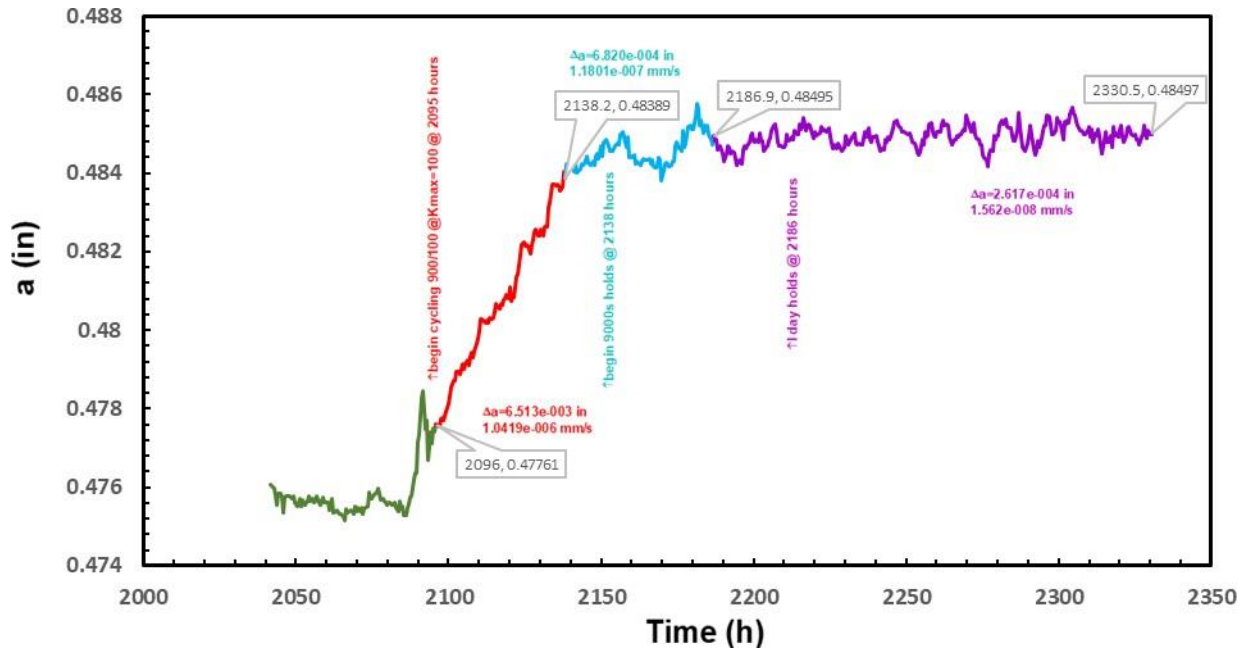


Figure 12: Crack length as a function of time for 945X (2805-CL1) at 350°F (177°C) under 9000 s and 1 day holds at 100 ksi√in (110 MPa√m).

5.2.3 955 (Specimen ID 2808-CL4)

FCGR frequency scans at various ΔK 's and R-ratios are summarized in Figure 13. There is no effect of frequency on the fatigue crack growth over the range of ΔK 's explored. The initial set of frequency scan at 40 ksi√in (44 MPa√m) and 20 ksi√in (22 MPa√m) were performed at a K_{max} of 50 ksi√in (55 MPa√m). The K_{max} was then increased from 50 ksi√in (55 MPa√m) to 72 ksi√in (79.2 MPa√m) and frequency scans were performed over a range of frequencies. The lack of frequency dependence over a wide range of frequencies clearly suggests that there is little or no environmental effect on the corrosion fatigue behavior in this environment. This is consistent with the behavior of 725 discussed earlier, which has a similar alloying additions and heat treatment. It is expected that the resistance to environmentally assisted cracking of 955 would be comparable if not better than that of 945X (which has lower Mo content and a higher Fe content).

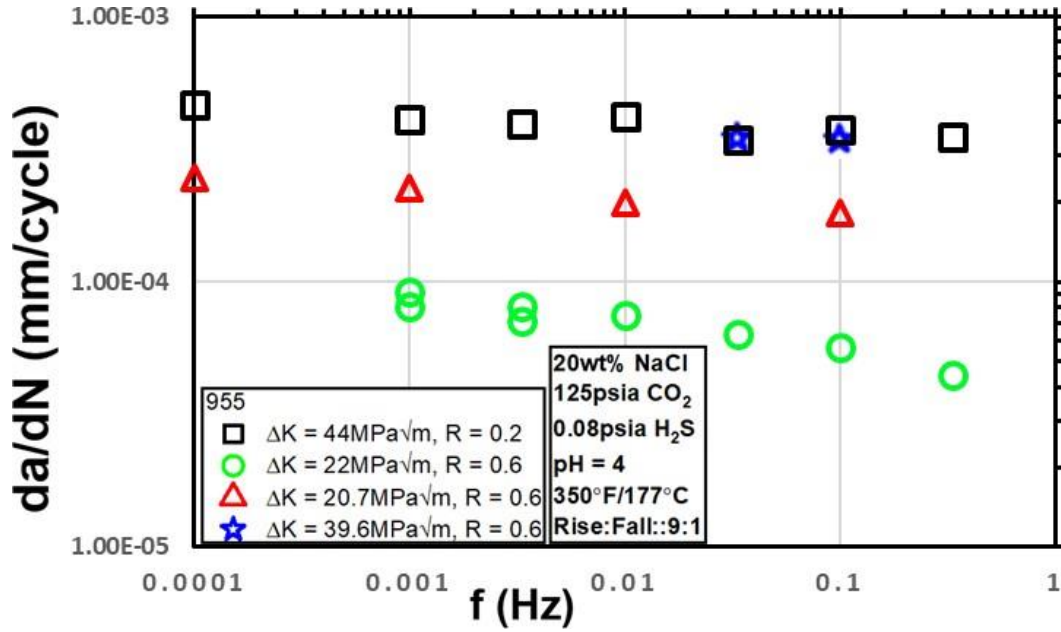


Figure 13: FCGR frequency scans on 955 (2808-CL4) in sour environment at 350°F (177°C) over a range of ΔK values.

Table 10: Color coded numerical values for Figure 13

Kmax	Kmin	f (Hz)	da/dt (mm/s)	Da (in)	Comments	DK (ksiin)	da/dN (mm/cycle)
50	10	0.33333	6.05E-04	0.00133		40	1.81E-03
50	10	0.33333	1.17E-04	0.01056	'B=0.4722"	40	3.52E-04
50	10	0.1	3.73E-05	0.00677	'9/1'	40	3.73E-04
50	10	0.03333	1.13E-05	0.00508	'27/3'	40	3.40E-04
50	10	0.01	4.19E-06	0.00313	'90/10'	40	4.19E-04
50	10	3.33E-03	1.31E-06	0.00312	'270/30'	40	3.94E-04
50	10	1.00E-03	4.09E-07	5.64E-03	'900/100'	40	4.09E-04
50	10	1.00E-04	4.61E-08	0.00291	'9000/1000'	40	4.61E-04
50	30	3.33E-01	1.48E-05	0.05391	'Change to R = 0.6'	20	4.45E-05
50	30	0.1	5.63E-06	0.00335	'Change to 9/1'	20	5.63E-05
50	30	0.03333	2.11E-06	0.00585	'Change to 27/3'	20	6.34E-05
50	30	0.01	2.46E-07	0.01304	'Change to 90/10'	20	2.46E-05
50	30	1.00E-02	7.47E-07	1.69E-03	'90-10 rise fall'	20	7.47E-05

Kmax	Kmin	f (Hz)	da/dt (mm/s)	Da (in)	Comments	DK (ksiin)	da/dN (mm/cycle)
50	30	3.33E-03	2.68E-07	1.48E-05	'270/30'	20	8.05E-05
50	30	3.33E-03	2.36E-07	3.40E-03	'restart'	20	7.09E-05
50	30	1.00E-03	8.03E-08	2.41E-04	'900/100'	20	8.03E-05
50	30	0.001	3.17E-08	0.00219	'power outage restart: 900/100'	--	--
50	30	1.00E-03	9.22E-08	0.0044	'restart'	20	9.22E-05
50	30	1.00E-04	-4.86E-10	2.65E-05	'9000/1000'	--	--
72	43.2	1.00E-04	-4.85E-04	0.00157	'Kmax =72'	28.8	-4.85E+00
72	43.2	0.1	1.82E-05	0.00788	'9/1'	28.8	1.82E-04
72	43.2	0.01	1.98E-06	1.01E-03	'90/10'	28.8	1.98E-04
72	43.2	1.00E-03	2.24E-07	0.00236	'900/100'	28.8	2.24E-04
72	43.2	1.00E-04	2.45E-08	-7.84E-04	'9000s holds'	28.8	2.45E-04
90	54	0.1	3.40E-05	0.00997	'Kmax to 90'	36	3.40E-04
90	54	0.03333	1.14E-05	8.72E-04	'27/3'	36	3.42E-04

The above set of results in sour service indicate that all the PH nickel-based alloys studied here (725, 945X, 955) in the sour environment(s) of interest do not appear to exhibit susceptibility to environmentally assisted corrosion fatigue. In addition, there was no evidence of stable static crack growth rate in any of these materials up to K values of 90 ksi√in (99 MPa√m).

In the presence of a high chloride concentration at elevated temperatures, the conditions that stabilize sustained metal ion dissolution and hydrolysis leading to local acidification are likely to lead to conditions where cracking can be sustained. There is evidence which suggests that the susceptibility to environmentally assisted cracking is related to susceptibility to localized corrosion. Crack growth rates were found to increase sharply and K_{th} values decreased sharply when the corrosion potential was at or below the repassivation potential[1]. These observations are consistent with those in literature as well as with the frame work that conditions where the repassivation potential is comparable to or lower than the corrosion potential is needed for sustained crack growth[1].

5.2.4 C22HS (Specimen ID – 2785-CL3)

FCGR frequency scans at various ΔK 's and R-ratios are summarized in Figure 14. There is no effect of frequency on the fatigue crack growth over the range of ΔK 's explored. The initial set of frequency scan at 40 ksi√in (44 MPa√m) and 20 ksi√in (22 MPa√m) were performed at a K_{max} of 50 ksi√in (55

MPa√m). The K_{max} was then increased from 50 ksi√in (55 MPa√m) to 72 ksi√in (79.2 MPa√m) and frequency scans were performed over a range of frequencies. The lack of frequency dependence over a wide range of frequencies clearly suggests that there is little or no environmental effect on the corrosion fatigue behavior in this environment. This is not surprising given that C22HS is highly alloyed and in general is expected to exhibit excellent resistance to localized corrosion in these environments. It is interesting to note that even though C22HS has the highest yield strength of all the materials tested, there is no evidence of an environmental effect. The higher strength of C22HS does not appear to increase its susceptibility to environment assisted cracking. This suggests that the high alloying content of the C22HS, provides excellent resistance to localized corrosion and enables repassivation of the fresh metal surface.

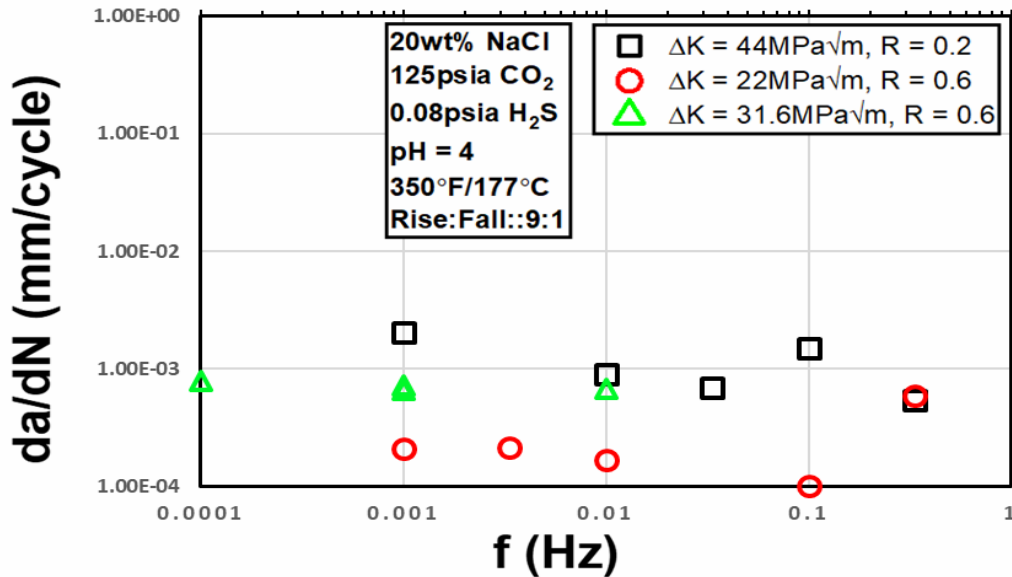


Figure 14: FCGR frequency scans on C22HS (2785-CL3) in sour environment at 350°F (177°C) over a range of ΔK values.

Table 11: Color coded numerical values for Figure 14

Kmax	Kmin	f (Hz)	da/dt (mm/s)	Da (in)	Comments	DK (ksiin)	da/dN (mm/cycle)
50	10	0.33333	1.80E-04	0.06215	'Beff=0.4892"	40	5.41E-04
50	10	0.1	1.48E-04	0.02616	'9/1'	40	1.48E-03
50	10	0.03333	2.29E-05	0.00828	'27/3'	40	6.87E-04
50	10	0.01	9.07E-06	0.00746	'90/10'	40	9.07E-04
50	10	0.001	2.04E-06	0.01032	'270/30'	40	2.04E-03
50	10	1.00E-04	-5.36E-07	0.02253	'9000/1000'	40	-5.36E-03
50	30	1.00E-04	3.18E-05	4.77E-04	'Kmax=50'	20	3.18E-01
50	30	0.33333	1.95E-04	0.00649	'2.7/0.3'	20	5.85E-04

Kmax	Kmin	f (Hz)	da/dt (mm/s)	Da (in)	Comments	DK (ksiin)	da/dN (mm/cycle)
50	30	1.00E-01	1.01E-05	0.00922	'9/1'	20	1.01E-04
50	30	0.01	1.67E-06	0.00272	'90/10'	20	1.67E-04
50	30	0.00333	7.16E-07	0.00231	'270/30'	20	2.15E-04
50	30	0.001	2.10E-07	0.00308	'900/100'	20	2.10E-04
50	30	1.00E-04	4.17E-08	1.14E-03	'restart'	20	4.17E-04
72	43.2	1.00E-04	1.56E-05	9.09E-04	'Kmax to 72'	28.8	0.15606
72	43.2	1.00E-01	-4.42E-05	6.70E-04	'9/1'	28.8	-4.42E-04
72	43.2	1.00E-02	6.74E-06	1.19E-02	'90/10'	28.8	6.74E-04
72	43.2	0.001	7.27E-07	0.00173	'900/100'	28.8	7.27E-04
72	43.2	1.00E-04	7.85E-08	0.00137	'9000/1000'	28.8	7.85E-04
72	43.2	1.00E-03	6.64E-07	0.00253	'900/100'	28.8	6.64E-04
72	43.2	1.00E-04	4.66E-08	0.00192	'9000s holds'	28.8	4.66E-04

Attempts were made to stabilize static crack growth rate behavior in sour service for C22HS at 72 ksi√in (79.2 MPa√m), via the introduction of hold times when cycling at low frequencies. The resulting crack length vs time at 72 ksi√in (79.2 MPa√m) is shown in Figure 15. The changes made in the test during this period are indicated in the plot with vertical comments. The comments along with the time stamp are located on the plot when the change was made. The growth rate appears to decay with time and exhibits very low values in the range of 2×10^{-8} mm/s. Hence no further attempt was made to stabilize static crack growth rate in this specimen.

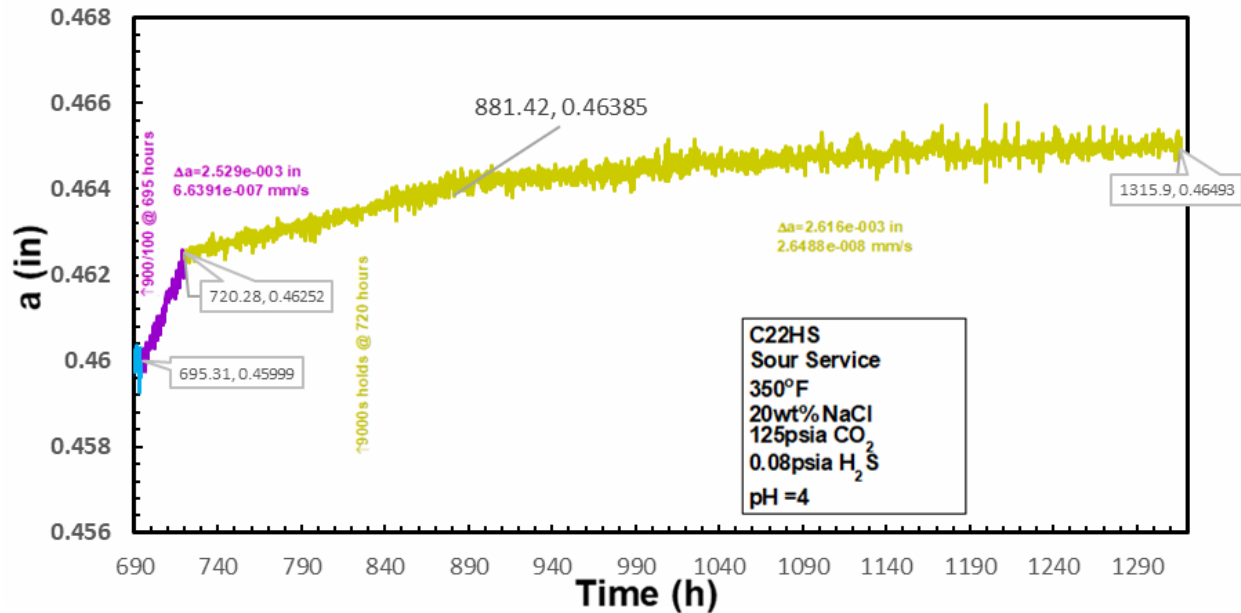


Figure 15: Crack length vs time for C22HS (2785-CL3) in sour environment at 350°F (177 C) 72 ksi√in (79.2 MPa√m), R = 0.6 and 9000 s holds.

5.2.5 825 (Specimen ID 2833 — CL4)

FCGR frequency scans at various ΔK 's and R-ratios for 825 are summarized in Figure 16. A set of initial tests were performed at higher values of K_{max} (50 ksi√in (55 MPa√m)), however, rapid crack extension was observed, hence subsequent FCGR frequency scan was performed at 25 ksi√in (27.5 MPa√m). The test was performed at an R-ratio of 0.2 at a ΔK of 20 ksi√in (22 MPa√m). The results are shown in Figure 16. The results indicate that under these conditions, there is no significant effect of frequency on the FCGR. This suggests that under these conditions, there is no environmental effect. Under the conditions tested, it appears that 825 is more susceptible to cracking at 50 ksi√in (55 MPa√m), which is likely associated with the fact that it has the lowest alloying content of all the materials evaluated. However, at the lower value of ΔK (20 ksi√in/20 MPa√m), there was no effect of frequency under the conditions evaluated.

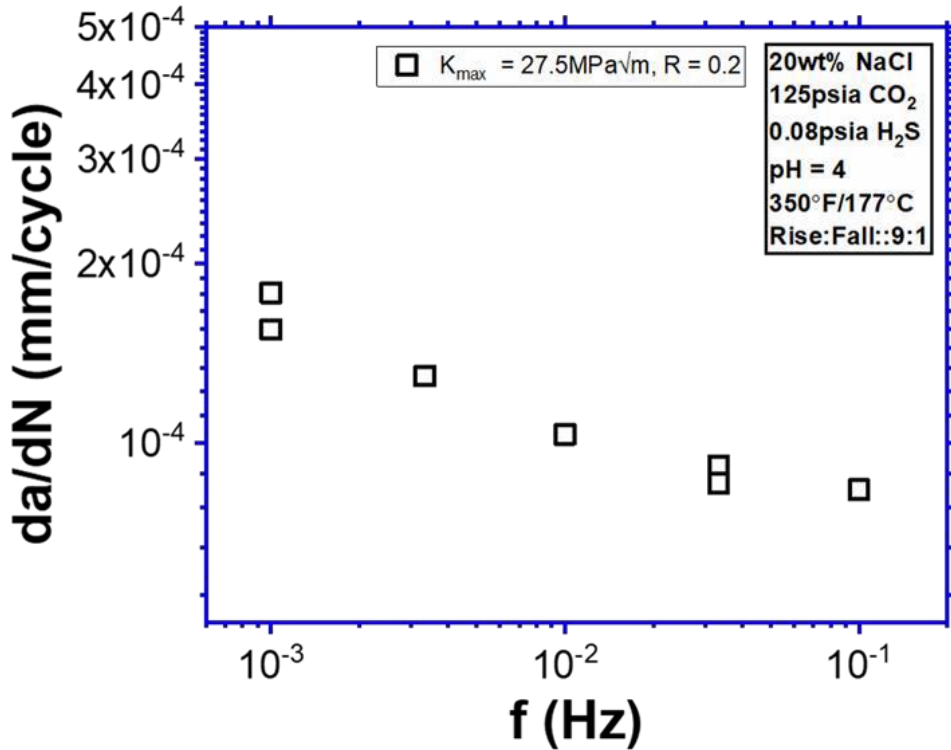


Figure 16: FCGR frequency scans on 825 (2835-CL4) in sour environment at 350°F (177°C) at 20 ksi/in (22 MPa√m).

Table 12: Numerical values for Figure 16

Kmax	Kmin	f (Hz)	da/dt (mm/s)	Da (in)	Comments	Rise Time (s)	Fall Time (s)	DK (ksiin)	da/dN (mm/cycle)
25	5	0.1	8.34E-06	0.02404	'Beff=0.472 5"	9	1	20	8.34E-05
25	5	0.03333	3.05E-06	0.01191	'27/3'	27	3	20	9.14E-05
25	5	0.01	6.58E-08	0.00329	'90/10'	90	10	20	6.58E-06
25	5	0.03333	2.85E-06	0.00887	'RESTART'	27	3	20	8.55E-05
25	5	0.01	1.03E-06	0.00495	'90/10'	90	10	20	1.03E-04
25	5	0.00333	4.31E-07	0.00169	'270/30'	270	30	20	1.29E-04
25	5	1.00E-03	1.55E-07	0.0012	'900/100'	900	100	20	1.55E-04

In summary, the sour service fatigue behavior of four of the five materials (725/945X/955 and C22HS) evaluated in this study do not show any susceptibility to environmental effects. Specifically, 725, 945X, 955, and C22HS do not exhibit any evidence of static crack growth rate up to the limit of the specimen. This suggests that most of these materials are very resistant to environmental effects in the tested environment. The only exception was the cracking behavior observed on 825 at 50 ksi√in (55 MPa√m). The resistance to environmental assisted fatigue and static crack growth under these conditions is consistent with the high alloying content of the materials evaluated. The absence of environmental effects will allow using the in-air properties over a range of ΔK for fatigue applications.

5.3 Seawater + CP

Environmentally assisted FCGR was measured in seawater + CP, since it is anticipated that subsea components, will experience cathodic polarization. High strength nickel-based alloys are extremely corrosion resistance and have excellent resistance to localized corrosion as evidenced by the high CCT values at +700 mV SCE. However, typical subsea production systems do contain significant number of steel components, which are subject to cathodic protection to prevent corrosion. In general, while every attempt is made to isolate high strength nickel-based alloys from carbon steel, it is not always practical, and the isolation is likely less than perfect. Hence, in design it is important to consider the effect of cathodic protection on the FCGR, as well as the static crack growth rate. The data developed can be used for developing design specific flaw acceptance criteria, and/or quantitatively comparing the performance of various materials.

5.3.1 725 (Specimen ID 2810-LR1)

The effect of ΔK and frequency were studied on 725 in seawater + CP at -1050 mV SCE. The results of the frequency scans are shown in Figure 17. FCGR at ΔK 's of 40 ksi√in (44 MPa√m) and 20 ksi√in (22 MPa√m) at a K_{max} of 50 ksi√in (55 MPa√m) increases by about 30 times as the frequency decreases from 300 mHz to 0.1 mHz, and there is no evidence of a plateau in FCGR. FCGR with 9000 s hold time (0.1 mHz) is about 7-8 times higher than the values obtained at 0.1 mHz under pure cycling. FCGR with 86400 s hold periods is about 10 times higher than obtained under 9000 s hold periods. The above data suggest static crack growth rate at a K_{max} of 50 ksi√in (55 MPa√m) is significant under these conditions.

To quantify the effect of static crack growth rate at a 50 ksi√in (55 MPa√m), the test was transitioned from the hold periods to constant K. This resulted in stable crack growth rate of 3.5×10^{-6} mm/s under constant K conditions as seen in Figure 18. The changes made in the test during this period are indicated in the plot with vertical comments. The comments along with the time stamp are located on the plot when the change was made. The K value was then decreased from 50 ksi√in (55 MPa√m) to 45 ksi√in (49.5 MPa√m) using a decreasing K profile described in the experimental section. The crack growth rate associated with the decreasing K profile was 8.2×10^{-7} mm/s, which is ~4 times lower than the crack growth rate obtained during the constant K portion of the test. When the test was transitioned to constant K at 45 ksi√in (49.5 MPa√m) the crack growth rate measured was 2.8×10^{-6} mm/s, which is higher than the crack growth rate during the decreasing K portion. Similar behavior was observed when K was decreased to lower K values as is evident in Figure 18. The above results suggest that static crack growth is not only a strong function of K but also of the K- gradient. These results are summarized in Figure 19, which clearly shows that the crack growth rate under a decreasing K profile is about 3-4 times lower than at constant K.

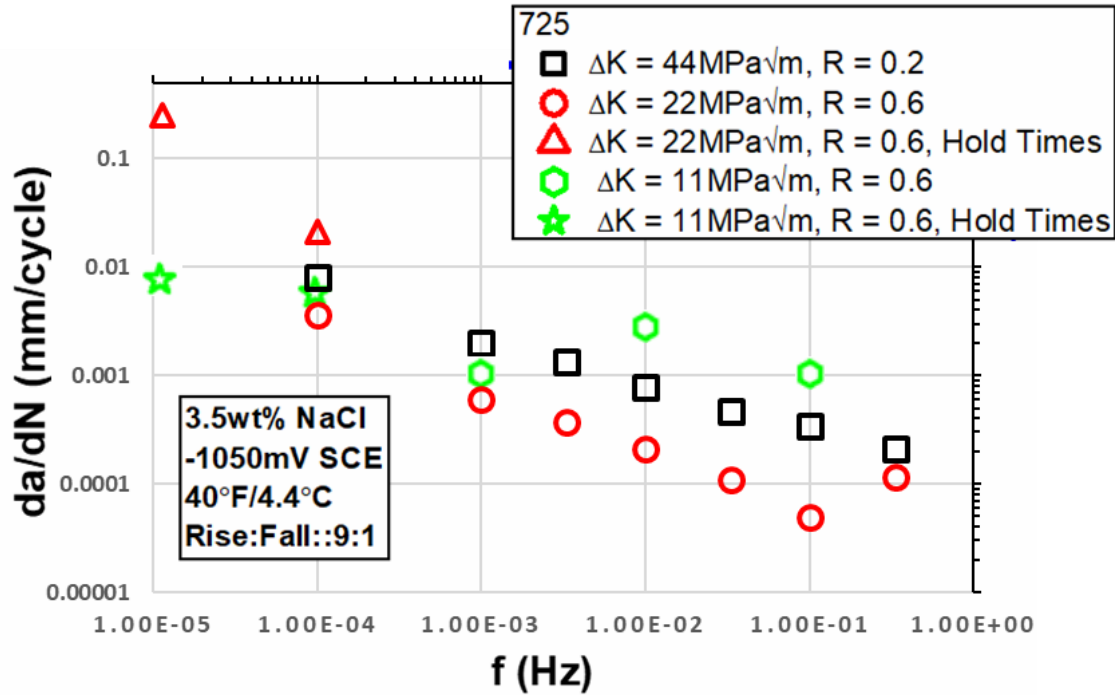


Figure 17: FCGR as a function of ΔK and frequency for 725 (2810-LR1) in seawater + CP at -1050 mV SCE.

Table 13: Color coded numerical values for Figure 17

f (Hz)	da/dt (mm/s)	Da (in)	Comments	da/dN (mm/cycle)	K (ksiin0.5)	da/dt (mm/s)	K (ksiin0.5)	da/dt (mm/s)
0.3333	6.93E-05	0.0047	□	2.08E-04	50	3.51E-06	47.67	8.17E-07
0.1	3.40E-05	0.0039	1-Sep	3.40E-04	45.3463	2.78E-06	42.74	4.75E-07
0.0333	1.53E-05	0.0036	27/3	4.59E-04	39.90258	1.64E-06	37.42	3.66E-07
0.01	7.79E-06	0.003	90/10	7.79E-04	34.30429	1.12E-06	32.63	6.40E-08
0.0033	4.39E-06	0.008	270/30	0.00133	30.23802	7.25E-07		
1.00E-03	2.00E-06	0.0035	900/100	0.002	25	8.83E-08		
1.00E-04	8.11E-07	8.30E-03	Change to 9000/1000	0.00811				
3.33E-01	3.90E-05	0.0031	2.7/0.3	1.17E-04				
1.00E-01	4.95E-06	0.0142	1-Sep	4.95E-05				
0.0333	3.60E-06	0.0035	Change to 27/3	1.08E-04				
0.01	2.08E-06	0.005	90/10	2.08E-04				
0.0033	1.24E-06	0.004	270/30	3.76E-04				
1.00E-03	6.08E-07	1.90E-03	900/100	6.08E-04				

f (Hz)	da/dt (mm/s)	Da (in)	Comments	da/dN (mm/cycle)	K (ksiin ^{0.5})	da/dt (mm/s)	K (ksiin ^{0.5})	da/dt (mm/s)
1.00E-04	3.65E-07	5.70E-03	Change to 9000/1000	0.00365				
1.00E-04	2.13E-06	1.06E-02	Introduce 9000s holds	0.02134				
1.14E-05	2.85E-06	1.16E-02	begin 86400s hold	0.24915				
0.1	1.04E-04	0.0099	'restart cycling at 9/1'	0.00104				
1.00E-02	2.82E-05	0.00382	'change to 90/10'	0.00282				
1.00E-03	1.02E-06	3.65E-03	'900/100'	0.00102				
1.00E-04	6.27E-07	0.00727	'begin 9000s holds'	0.00627				
1.14E-05	9.41E-08	0.00296	'Change to 1day holds'	0.00822				

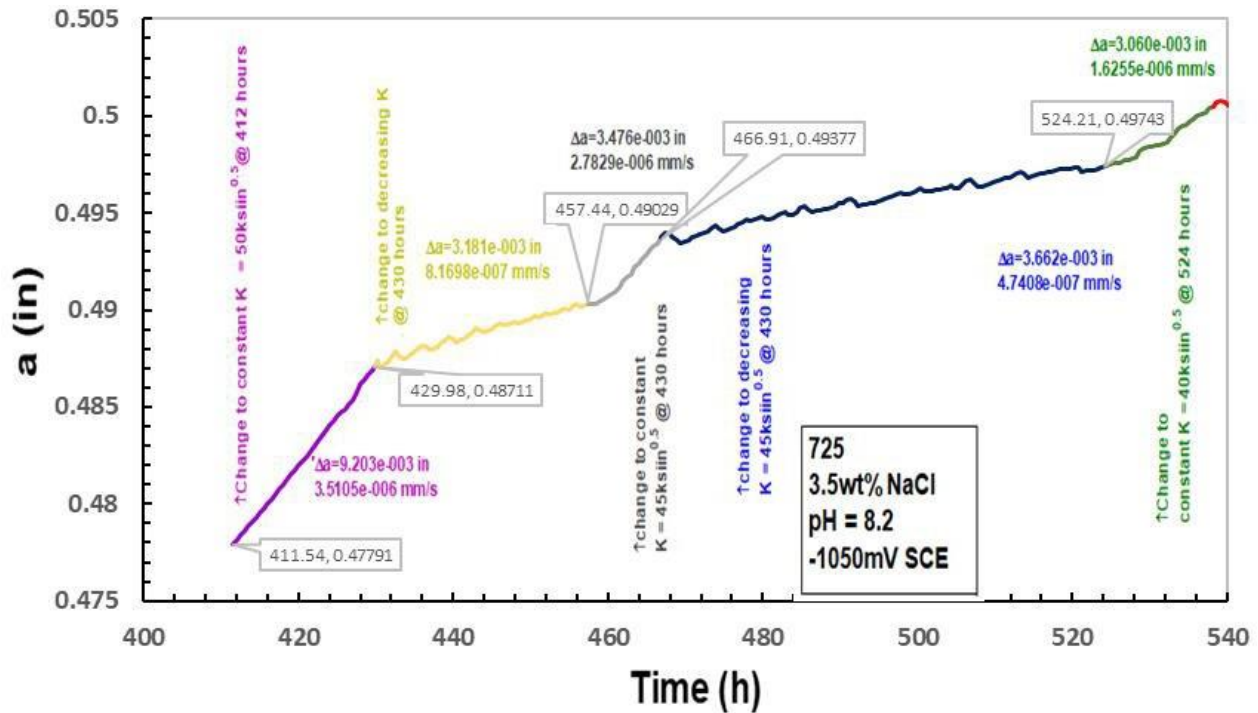


Figure 18: Crack length vs time under constant K and varying K for 725 (2810-LR1) in seawater + CP at -1050 mV SCE.

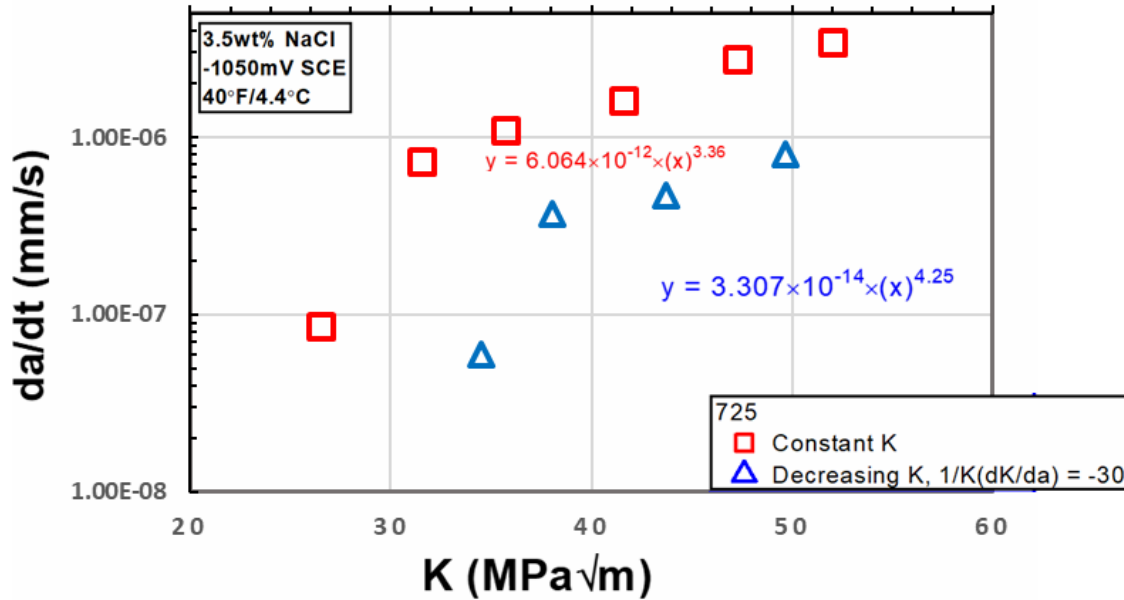


Figure 19: Crack growth rate as function of K and loading mode for 725 (2810-LR1) in seawater at -1050 mV SCE.

Table 14: Color coded numerical values for Figure 19

da/dN (mm/cycle)	K (MPa√m)	1.1*K	da/dt (mm/s)	K (MPa√m)	1.1*N	da/dt (mm/s)
2.07E-04	51.98	57.178	3.46E-06			
3.38E-04	47.29	52.019	2.74E-06			
4.57E-04	41.6	45.76	1.60E-06			
7.75E-04	35.7	39.27	1.11E-06			
0.00131	31.55	34.705	7.35E-07			
0.00198	26.5	29.15	8.63E-08			
				49.69	54.659	8.06E-07
				43.75	48.125	4.67E-07
				38.05	41.855	3.68E-07
				34.48	37.928	5.91E-08

The K_{th} values under constant K conditions appear to be at about 25 ksi√in (27.5 MPa√m) based on the sharp change in crack growth rate. On the same basis under decreasing K the K_{th} would be 32 ksi√in (35.2 MPa√m). This would suggest that under increasing K, the measured K_{th} would likely be lower; however, it is important to note that under increasing K conditions it has been shown that the resolvable crack growth rate is typically on the order of about $4-6 \times 10^{-7}$ mm/s which essentially is the limit of the value of K at which K_{th} can be determined. The values of crack growth rate at K_{th} under constant K conditions in this case are about 8×10^{-8} mm/s. However, it should be noted that a sharp change in crack growth rate in itself is not an ideal basis for determining K_{th} . It is important to attempt to characterize the crack growth rate behavior at lower values of K since it has been shown that slow

stable crack growth rate on the order 3×10^{-9} to 10^{-8} mm/s can be sustained in precipitation hardened alloys under cathodic polarization[7].

5.3.2 945X (Specimen ID 2805-LR1)

The effect of frequency and ΔK on the FCGR behavior of 945X in seawater under cathodic polarization of -1050 mV SCE is shown in Figure 20. 945X exhibits little or no frequency dependence at a K_{max} of 50 ksi \sqrt{in} (55 MPa \sqrt{m}) and a ΔK corresponding to both 40 ksi \sqrt{in} (44 MPa \sqrt{m}) and 20 ksi \sqrt{in} (22 MPa \sqrt{m}) in the range of 300 mHz to 30 mHz. However, at frequencies below 30 mHz, FCGR increases by about 3 times as the frequency decreases from 30 mHz to 0.1 mHz. Over all there is about 5 fold increase in FCGR as the frequency decreases from 300 mHz to 0.1 mHz. This represents a relatively shallow dependence on frequency compared to the 725 which exhibited about a 30x change in FCGR under same conditions.

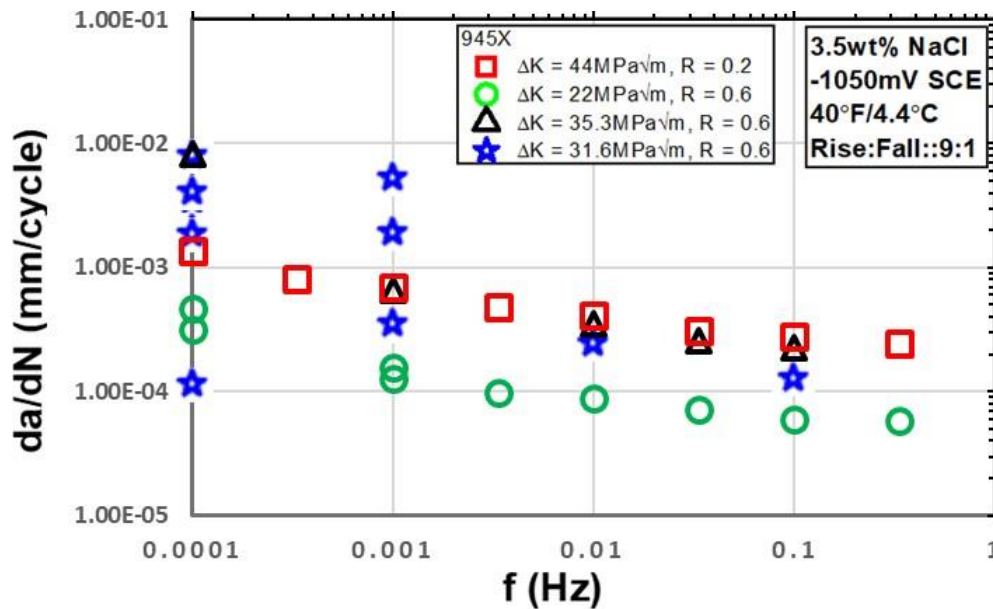


Figure 20: FCGR as a function of ΔK and frequency for 945X (2805-LR1) in seawater + CP at -1050 mV SCE.

Table 15: Color coded numerical values for Figure 20

Kmax	Kmin	f (Hz)	da/dt (mm/s)	Da (in)	Comments	da/dN (mm/cycle)
80	48	0.1	2.23E-05	0.00734	[]	2.23E-04
80	48	0.03333	8.65E-06	0.00304	'Change to 30mHz'	2.59E-04
80	48	0.01	3.49E-06	0.00203	'90/10'	3.49E-04
80	48	0.001	6.63E-07	0.0041	'Change to 1mHz'	6.63E-04

80	48	1.00E-04	8.24E-07	0.00317	'Change to 9000s hold'	0.00824
----	----	----------	----------	---------	------------------------	---------

Kmax	Kmin	f (Hz)	da/dt (mm/s)	Da (in)	Comments	da/dN (mm/cycle)
50	10	0.33333	8.05E-05	0.00536	'2.7/0.3 start'	2.42E-04
50	10	0.1	2.75E-05	0.00468	'9/1'	2.75E-04
50	10	0.03333	1.02E-05	0.00358	'changed to 27/3'	3.05E-04
50	10	0.01	4.07E-06	0.00343	'90/10'	4.07E-04
50	10	0.00333	1.62E-06	0.00286	'270/30'	4.85E-04
50	10	0.001	6.97E-07	0.00303	'900/100'	6.97E-04
50		3.33E-04	2.73E-07	-0.00304	'2700/300'	8.19E-04
50	10	1.00E-04	1.37E-07	0.00681	'Change to 0.1mHz'	0.00137
50	30	0.33333	1.95E-05	0.00457	'2.7/0.3'	5.85E-05
50	30	0.1	6.01E-06	0.00337	'9/1'	6.01E-05
50	30	0.03333	2.42E-06	0.00206	'27/3'	7.27E-05
50	30	0.01	8.92E-07	0.00134	'90/10'	8.92E-05
50	30	0.00333	3.26E-07	8.80E-04	'Change to 3mHz'	9.79E-05
50	30	1.00E-03	1.28E-07	0.00203	'900/100'	1.28E-04
50	0	1.00E-04	3.14E-08	0.00213	'9000/1000'	3.14E-04
50	30	0.001	1.56E-07	0.00163	'900/100'	1.56E-04
50	30	1.00E-04	4.67E-08	-1.92E-04	'Change to 9000s holds'	4.67E-04
72	43.2	0.001	3.30E-07	0.00152	'Kmax=72'	3.30E-04
72	43.2	1.00E-04	1.27E-06	5.40E-04	'9000s holds'	--
72	43.2	0.1	1.23E-05	0.00608	'9/1'	1.23E-04
72	43.2	0.01	2.36E-06	0.00224	'90/10'	2.36E-04
72	43.2	1.00E-03	3.45E-07	0.00632	'900/100'	3.45E-04
72	43.2	1.00E-04	1.13E-08	-0.00562	'Insert 9000s holds'	1.13E-04
80	48	1.00E-04	7.82E-07	0.00779	'Change to 80/48'	0.00782
80	48	1.14E-05	5.95E-07	0.00132	'1day holds'	0.052
80	48	1.16E-07	1.22E-06	0.00374	'Constant K'	10.5156
72.35897	43.41538	1.16E-07	3.30E-07	0.00346	'Change to decreasing K'	2.84816
71.92457	43.15474	1.16E-07	5.55E-07	0.00178	'Change to constant K'	4.78524

Kmax	Kmin	f (Hz)	da/dt (mm/s)	Da (in)	Comments	da/dN (mm/cycle)
71.92	43.15	1.16E-07	5.19E-07	0.00939	'change to decreasing K'	4.4709
71.92	43.15	0.001	5.18E-06	0.01036	'Change to 1mHz'	0.00518
71.92	43.15	1.00E-04	3.40E-07	2.27E-04	'9000s holds'	0.0034
71.92	43.15	1.20E-08	1.36E-06	0.00116	'constant K'	113.61902
71.92	43.15	1.00E-04	1.97E-07	2.31E-04	'Change to 9000s holds'	0.00197
71.92	43.15	1.14E-05	4.28E-08	2.00E-05	'Change to 1day holds'	0.00374
71.92	43.15	1.00E-04	3.93E-07	7.71E-04	'Change to 9000s holds and -1150mV	0.00393
80	48	0.001	1.84E-06	0.00431	'Change to 80/48 and -1050mV 1mhz'	0.00184
80	48	1.00E-04	1.80E-07	-0.00441	'change to 9000s hold'	0.0018
80	48	1.14E-05	6.66E-08	-1.79E-04	'1 day holds'	0.00582
82	49.2	1.14E-05	5.03E-07	0.00559	'Change to kmax = 82'	0.04394
82	49.2	1.16E-07	9.35E-07	0.00352	'Constant K'	8.05729
73.38105	44.02863	1.16E-07	1.26E-07	0.0045	'Change to decreasing K/C = 30/Da = 0.2mills'	1.09006
71.20612	42.72367	1.16E-07	5.70E-07	0.00497	'Change to constant K'	4.91766
71.20612	42.72367	1.16E-07	3.04E-06	0.00266	'Change to -1150mV SCE'	26.17437
71.20612	42.72367	1.16E-07	4.36E-06	0.00966	'Change to decreasing K'	37.62457
71.20612	42.72367	1.16E-07	2.52E-06	0.00849	'Change to -1100mV SCE'	21.69529
71.20612	42.72367	1.16E-07	1.50E-06	0.0063	'Change to -1050mV SCE'	12.90416
71.20612	42.72367	1.16E-07	5.11E-07	0.00219	'Change to -1000mV SCE'	4.40702
71.20612	42.72367	1.16E-07	2.21E-07	0.0022	'Change to -950mV SCE'	1.9087
71.20612	42.72367	1.16E-07	9.24E-08	0.0025	'change to -900mV SCE'	0.79666
71.20612	42.72367	1.16E-07	2.03E-08	7.81E-04	'-850mV vs SCE'	0.17477

FCGR exhibits a relative sharp increase at 0.1 mHz and an R = 0.6 both at a K_{max} of 80 ksi \sqrt{in} (88 MPa \sqrt{m}) and 72 ksi \sqrt{in} (79.2 MPa \sqrt{m}). The increase in FCGR is shallow in the frequency range of 100 mHz to 1 mHz with about a 2-3 times increase. However, at 0.1 mHz corresponding to 9000 s hold

periods there is a 10 fold increase in FCGR compared to the values 1 mHz. This suggests that there is likely a significant contribution from static crack growth rate under these conditions.

A transition to constant K at 80 ksi√in (80 MPa√m) resulted in a static crack growth rate of 1.2×10^{-6} mm/s as seen in Figure 21. The changes made in the test during this period are indicated in the plot with vertical comments. The comments along with the time stamp are located on the plot when the change was made.

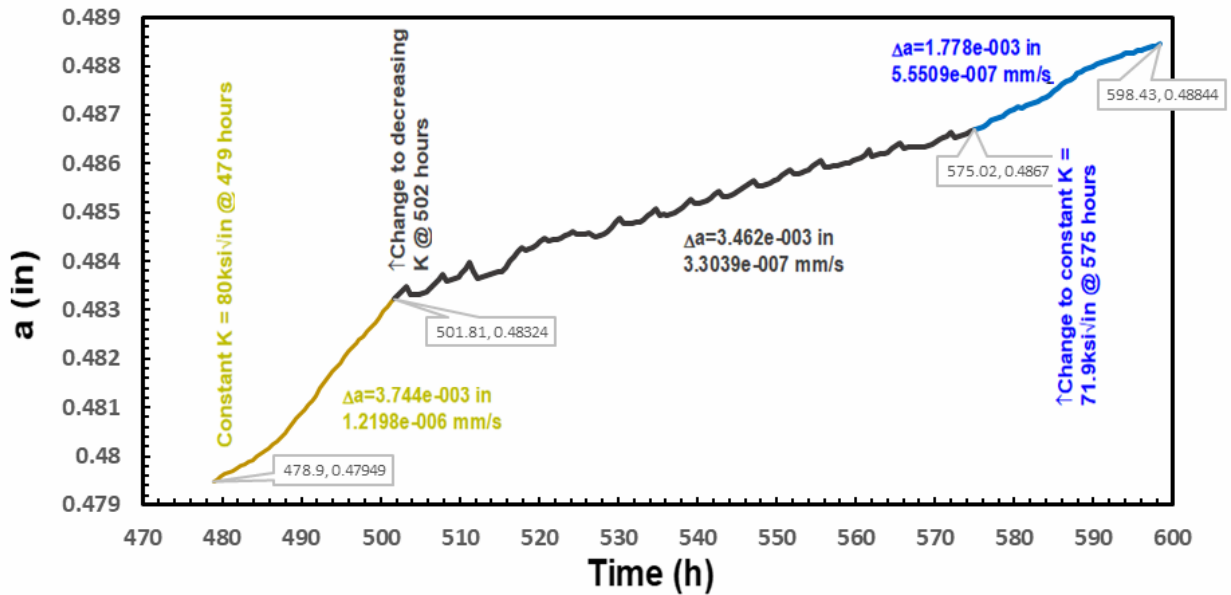


Figure 21: Crack length vs time under constant K and varying K for 945X (2805-LR1) in seawater + CP at -1050 mV SCE.

The crack growth rate under a decreasing K-gradient decreases about 4 times. However, on transitioning back to constant K conditions at about 72 ksi√in (79.2 MPa√m), the crack growth rate is 5.5×10^{-7} mm/s which is only about 1.5 times higher than under decreasing K conditions. This behavior appears to be different from the observed behavior on 725. This segment of the experiment was repeated by going to constant K at 82 ksi√in (90.2 MPa√m) followed by applying a decreasing K profile to 71.2 ksi√in (78.3 MPa√m) at which point the test was transitioned to constant K as shown in Figure 22. The changes made in the test during this period are indicated in the plot with vertical comments. The comments along with the time stamp are located on the plot when the change was made. The crack growth rate at 82 ksi√in (90.2 MPa√m) is 9.3×10^{-7} mm/s and under decreasing K profile was 1.2×10^{-7} mm/s which is 3 times lower than measured in the previous segment under identical conditions. The crack growth rate at constant K of 71.2 ksi√in (78.3 MPa√m) is 5.7×10^{-7} mm/s which is consistent with the previous observed crack growth rate. The sharp decrease in crack growth rate by a factor of 2 for about 10% change in K suggests that the K_{th} is in the range of about 72 ksi√in (79.2 MPa√m).

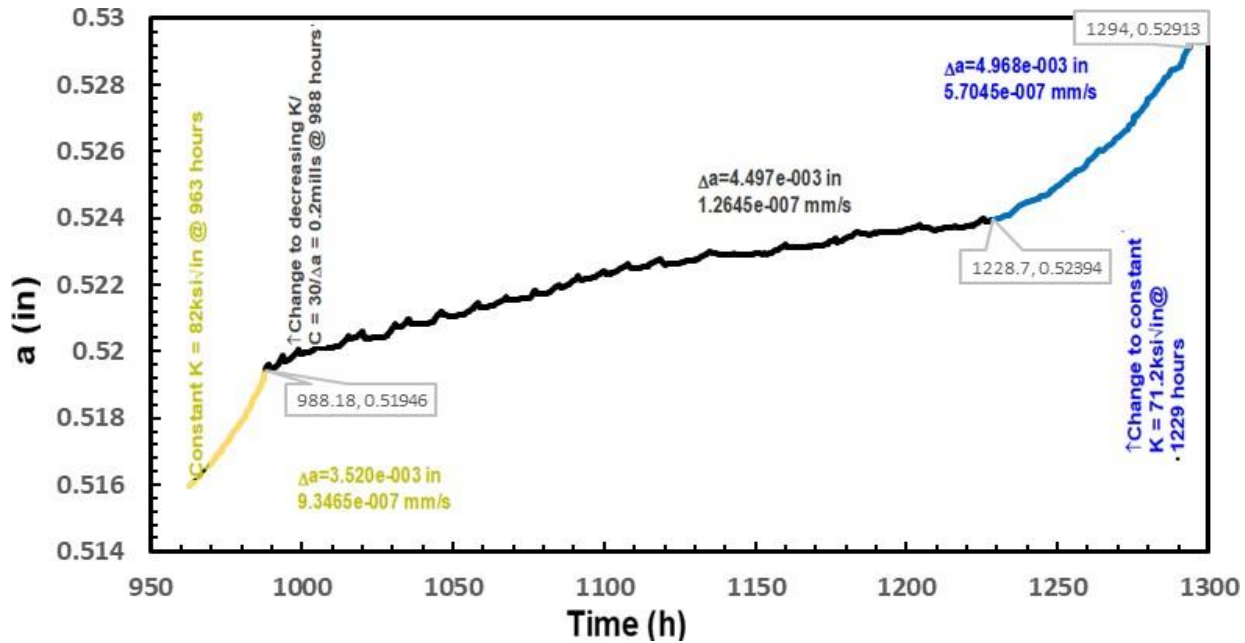


Figure 22: Crack length vs time under constant K and varying K for 945X (2805-LR1) in seawater + CP at -1050 mV SCE.

The resulting K vs CGR is shown in Figure 23. As discussed above there is a relatively sharp decrease in crack growth rate over a narrow range of K values suggesting that K_{th} is in the range of about 72 $\text{ksi}\sqrt{\text{in}}$ (79.2 $\text{MPa}\sqrt{\text{m}}$). Similar to the observations on 725 there is a significant effect of loading profile on the measured crack growth rate. Since the specimen did not generate data over a wide range of K values, it was decided to explore the effect of applied potential on the measured crack growth rate at 71.2 $\text{ksi}\sqrt{\text{in}}$ (78.3 $\text{MPa}\sqrt{\text{m}}$) as shown in Figure 24. The changes made in the test during this period are indicated in the plot with vertical comments. The comments along with the time stamp are located on the plot when the change was made. The crack growth rate decreases from about 4×10^{-6} mm/s at -1150 mV SCE to 1.5×10^{-6} mm/s at -1050 mV SCE. However, from -1050 mV SCE to -850 mV SCE the decrease in crack growth rate is much more significant decreasing to 2×10^{-8} mm/s at -850 mV SCE.

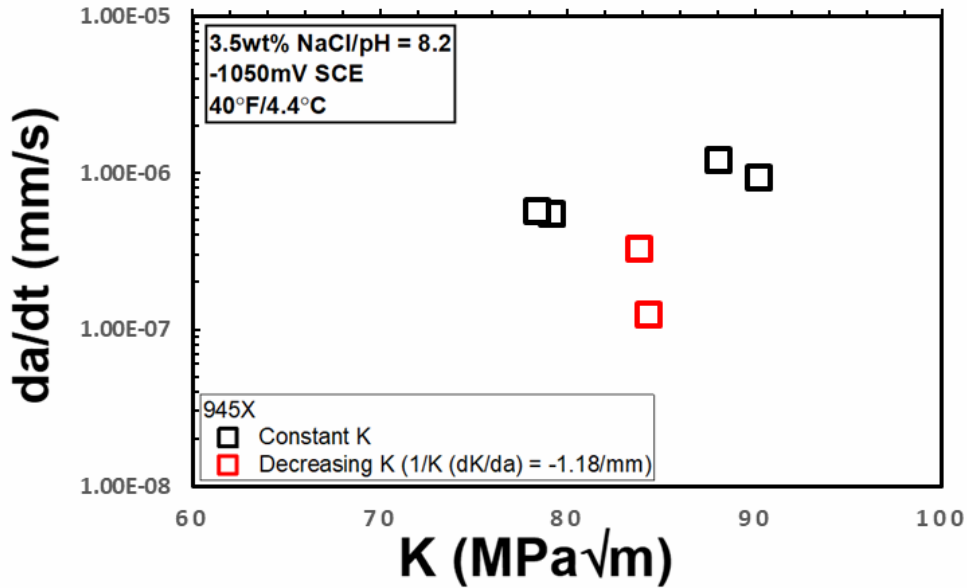
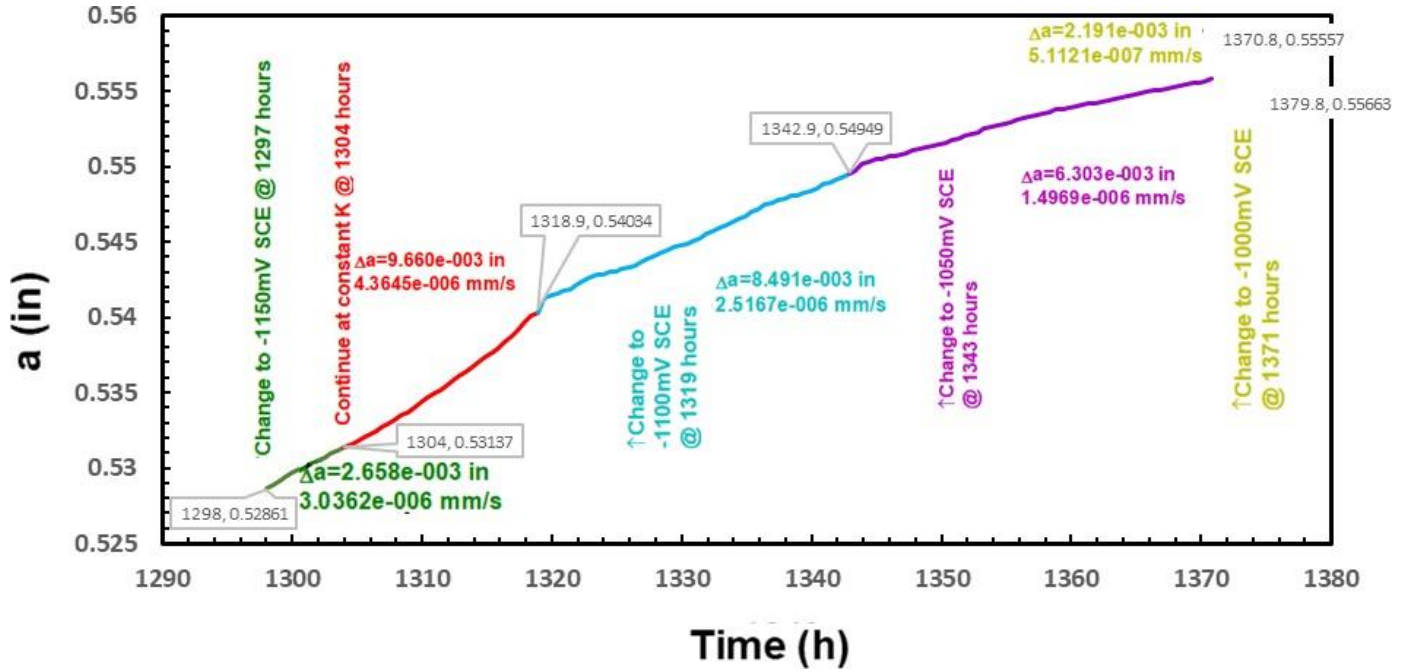


Figure 23: K vs CGR for 945X under constant K as well as decreasing K.

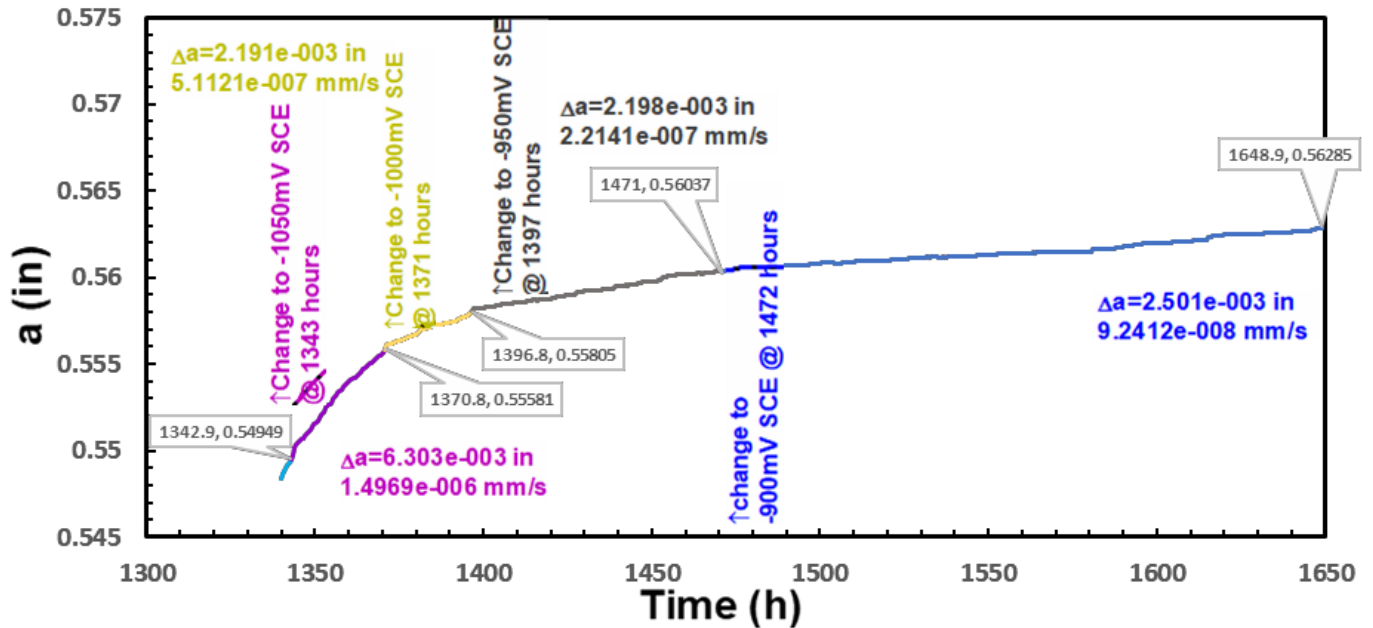
Table 16: Color coded numerical values for Figure 23

K (MPa√m)	da/dt (mm/s)	1.1*A	K (MPa√m)	1.1*D	da/dt (mm/s)	Eapp (mV SCE)	CGR (mm/s)	log(CGR)
80	1.22E-06	88				-1150	4.36E-06	-5.36007
79	7.85E-07	--				-1100	2.47E-06	-5.6068
80	1.22E-06	88				-1050	1.50E-06	-5.82481
71.92457	5.55E-07	79.11703				-1000	5.11E-07	-6.2914
82	9.35E-07	90.2				-950	2.21E-07	-6.65481
71.20612	5.70E-07	78.32673				-900	9.24E-08	-7.03427
			76.15	83.765	3.30E-07	-1150	4.36E-06	-5.36007
			76.6	84.26	1.26E-07	-1100	2.47E-06	-5.6068

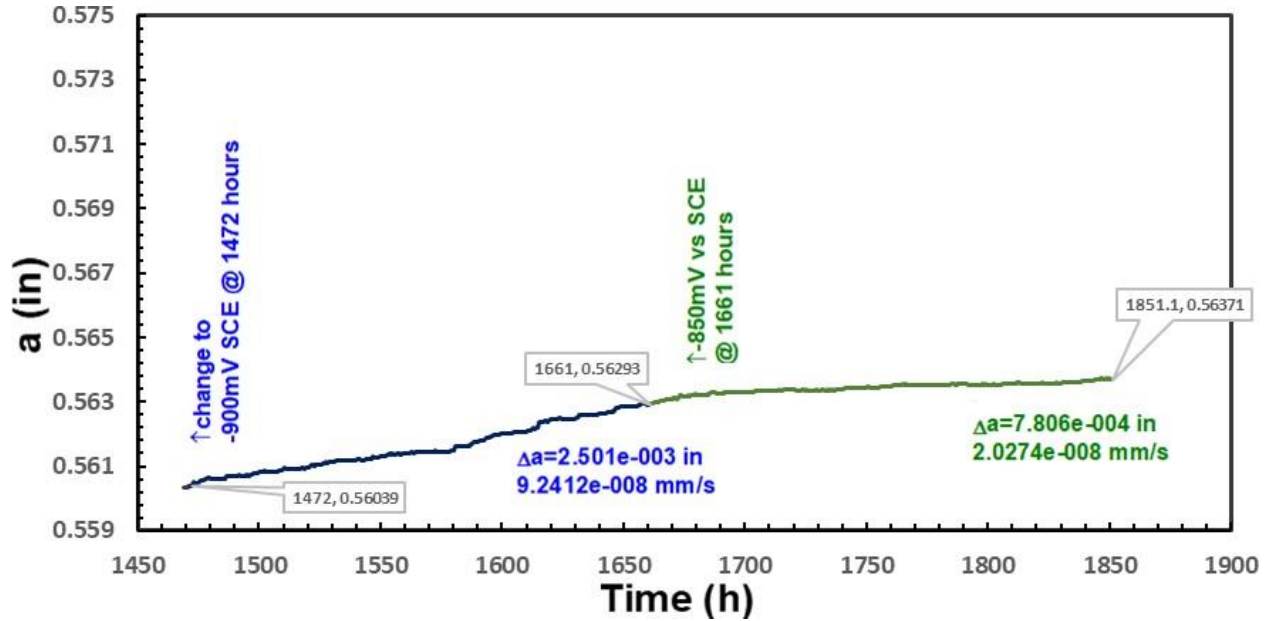
A summary of the crack growth rate as a function of applied potential is shown below in Figure 25. It is clear, that the crack growth rate has a shallow dependence at the high applied potentials, but there is a sharp change in the crack growth rate at -1000 mV SCE. However, at in the range of -1000 mV to -900 mV SCE the change in crack growth rate is linear dropping by about 4 times. However, at -850 mV SCE, there is a shape change in the crack growth rate. The crack growth rate at -850 mV SCE is about 5 times lower than the value at -900 mV SCE. It is likely that at the higher potentials there is a significant IR drop down the crack which limits the crack tip potential explaining the weak dependence of crack growth rate on potential, this behavior is consistent with the observations on steel[8]. It is also likely that at -850 mV SCE, the overvoltage for hydrogen at the crack tip is very low and hence very limited hydrogen is generated to sustain crack advance, which likely explains the low crack growth rate. In the intermediate potential, it is likely that the crack growth rate is related to the crack tip hydrogen generation rates.



a) Crack length vs time from -1150 mV SCE to -1000 mV SCE



b) Crack length vs time from -1050 mV SCE to -950 mV SCE



d) Crack length vs time from -900 mV SCE to -850 mV SCE.

Figure 24: Crack length as a function of time for 945X (2805-LR1) at a K value of 71.2 ksi√in (78.3 MPa√m) over a range of applied potential.

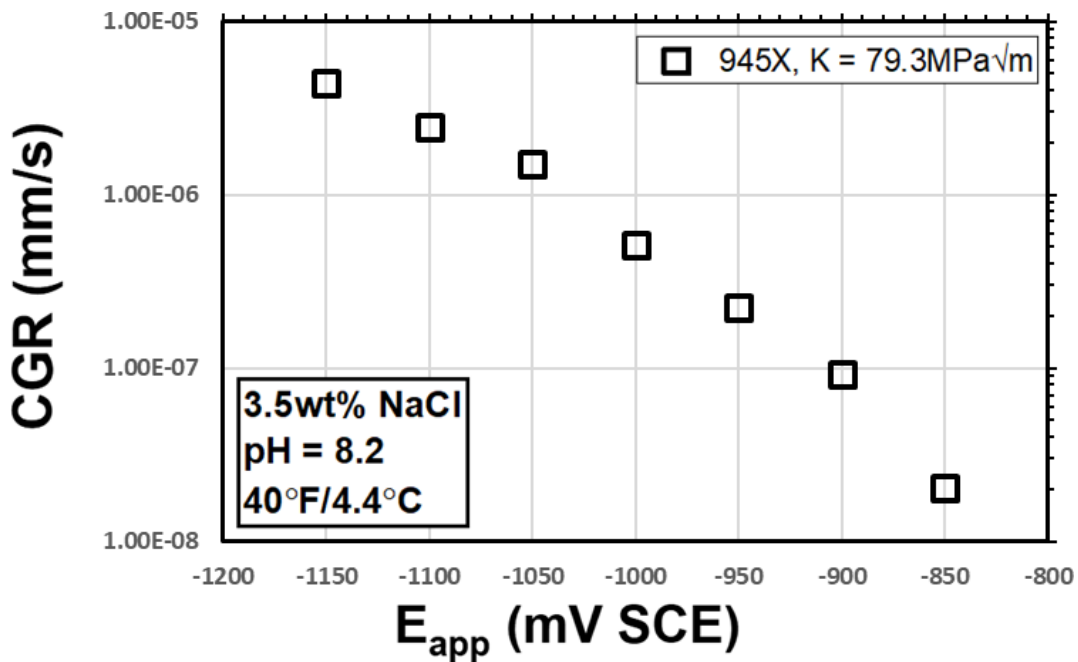


Figure 25: CGR of 945X (2805-LR1) as a function of applied potential at 71.2 ksi√in (78.3 MPa√m).

Table 17: Numerical values for Figure 25

K (MPa√m)	da/dt (mm/s)	1.1*A	K (MPa√m)	1.1*D	da/dt (mm/s)	E _{app} (mV SCE)	CGR (mm/s)	log(CGR)
80	1.22E-06	88	76.15	83.765	3.30E-07	-1150	4.36E-06	-5.36007
79	7.85E-07	--	76.6	84.26	1.26E-07	-1100	2.47E-06	-5.6068
80	1.22E-06	88				-1050	1.50E-06	-5.82481
71.92457	5.55E-07	79.11703				-1000	5.11E-07	-6.2914
82	9.35E-07	90.2				-950	2.21E-07	-6.65481
71.20612	5.70E-07	78.32673				-900	9.24E-08	-7.03427
						-850	2.03E-08	-7.69307

5.3.3 955 (Specimen ID 2808-LR3/LR5)

The effect of ΔK and frequency on 955 in seawater and CP is shown below in Figure 26. The results indicate that at a constant K_{max} of 50 ksi√in (55 MPa√m) and at a ΔK of 40 ksi√in (44 MPa√m) FCGR increases by about 10-fold as the frequency decreases from 0.3 Hz to 0.1 mHz, which is lower than 725 but higher than that observed for 945X. At a lower ΔK of 20 ksi√in (22 MPa√m) there is a shallow increase in FCGR up to 1 mHz; however, at 0.1 mHz the FCGR is about 30 times higher than that 0.3Hz, which is similar to 725. The lack of a plateau in FCGR suggests that there may be evidence of static crack growth rate. Frequency scan tests performed at an $R = 0.6$ and K_{max} of 60 ksi√in (66 MPa√m), and 80 ksi√in (88 MPa√m), are also shown on Figure 26. At a ΔK of 24 ksi√in/26.4 MPa√m (K_{max} of 60 ksi√in/66 MPa√m) FCGR has a shallow dependence on frequency, an attempt was made to introduce 9000 s hold periods, which did not result in stable crack propagation. However, at K_{max} of 80 ksi√in (88 MPa√m) there is a sharp increase in FCGR at 0.1 mHz (associated with 9000 s hold periods). This was associated with static crack growth and confirmed by transitioning to constant K as seen in Figure 27. The changes made in the test during this period are indicated in the plot with vertical comments. The comments along with the time stamp are located on the plot when the change was made. The crack was then transitioned to a higher potential of -1150 mV SCE, which was followed by commencing a decreasing K profile. Under constant K conditions changing the applied potential from -1050 mV SCE to -1150 mV SCE resulted in the crack growth rate from 1×10^{-6} mm/s to 2.77×10^{-6} mm/s. Under decreasing K profile, the CGR decreased by a factor of 10 to 2.77×10^{-7} mm/s. At this stage the reference electrode malfunctioned, and the reference electrode had to be changed.

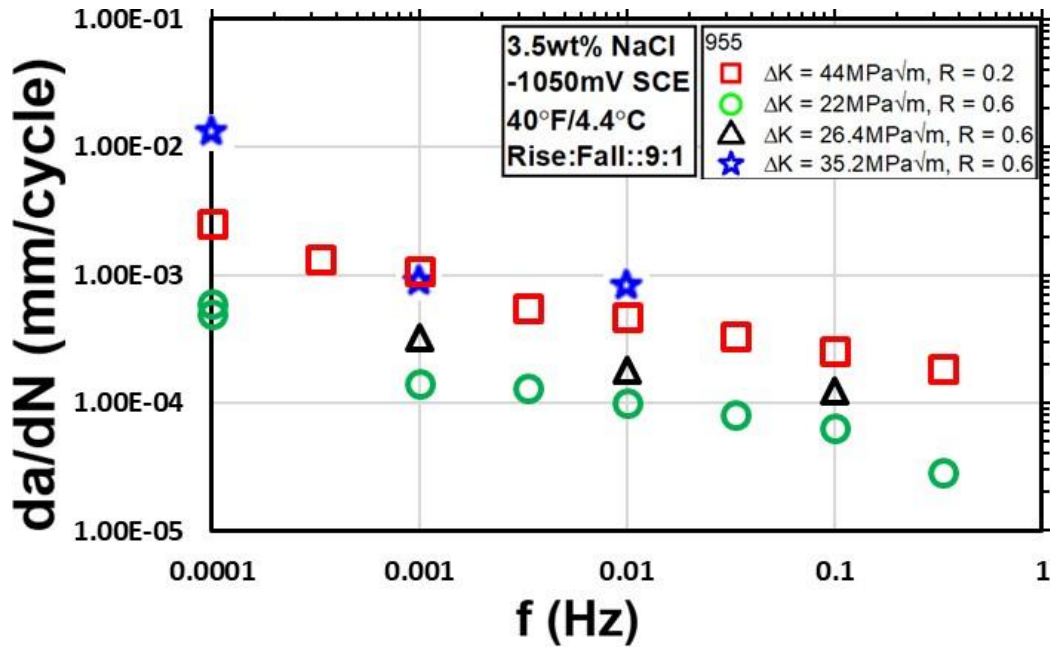


Figure 26: FCGR as a function of frequency and ΔK of 955 (2808-LR3) in seawater under cathodic polarization of -1050 mV SCE.

Table 18: Color coded numerical values for Figure 26

Kmax	Kmin	f (Hz)	da/dt (mm/s)	Da (in)	Comments	DK (ksiin)	da/dN (mm/cycle)
60	36	0.1	1.24E-05	0.00588	[]	24	1.24E-04
60	36	0.01	1.80E-06	0.00595	'Change to 90/10'	24	1.80E-04
60	36	1.00E-03	3.22E-07	0.00107	'900/100'	24	3.22E-04
60	36	1.00E-04	-1.01E-06	-9.06E-04	'Change to 9000s holds'	24	-0.0101
50	10	0.33333	6.23E-05	0.00654	'B=0.4769"	40	1.87E-04
50	10	0.1	2.51E-05	0.00582	'9/1'	40	2.51E-04
50	10	0.03333	1.11E-05	0.00227	'27/3'	40	3.33E-04
50	10	0.01	4.75E-06	0.00497	'90/10'	40	4.75E-04
50	10	0.00333	1.84E-06	0.00235	'270/30'	40	5.51E-04
50	10	1.00E-03	1.06E-06	0.00488	'900/100'	40	0.00106
50	10	3.33E-04	4.42E-07	-6.88E-04	'2700/300'	40	0.00133
50	10	1.00E-04	2.55E-07	0.00613	'Change to 9000/1000'	40	0.00255
50	30	0.33333	9.62E-06	0.01522	'Change to R = 0.6/2.7 - 0.3'	20	2.89E-05

Kmax	Kmin	f (Hz)	da/dt (mm/s)	Da (in)	Comments	DK (ksiin)	da/dN (mm/cycle)
50	30	0.1	6.40E-06	0.01247	'Change to 9/1'	20	6.40E-05
50	30	0.03333	2.66E-06	0.00263	'Change to 27/3'	20	7.97E-05
50	30	0.01	1.00E-06	0.00169	'Change to 90/10'	20	1.00E-04
50	30	0.00333	4.35E-07	0.00445	'Change 270/30'	20	1.30E-04
50	30	0.001	1.43E-07	0.00178	'Change to 900/100'	20	1.43E-04
50	30	1.00E-04	5.98E-08	-8.92E-04	'9000s holds'	20	5.98E-04
50	30	1.00E-04	4.98E-08	0.00332	'Change to 9000/1000'	20	4.98E-04
80	48	0.01	8.00E-06	0.00693	'Change to 80/48'	32	8.00E-04
80	48	0.001	8.59E-07	0.00158	'900/100'	32	8.59E-04
80	48	1.00E-04	1.27E-06	0.00355	'Change to 9000s holds'	32	0.0127

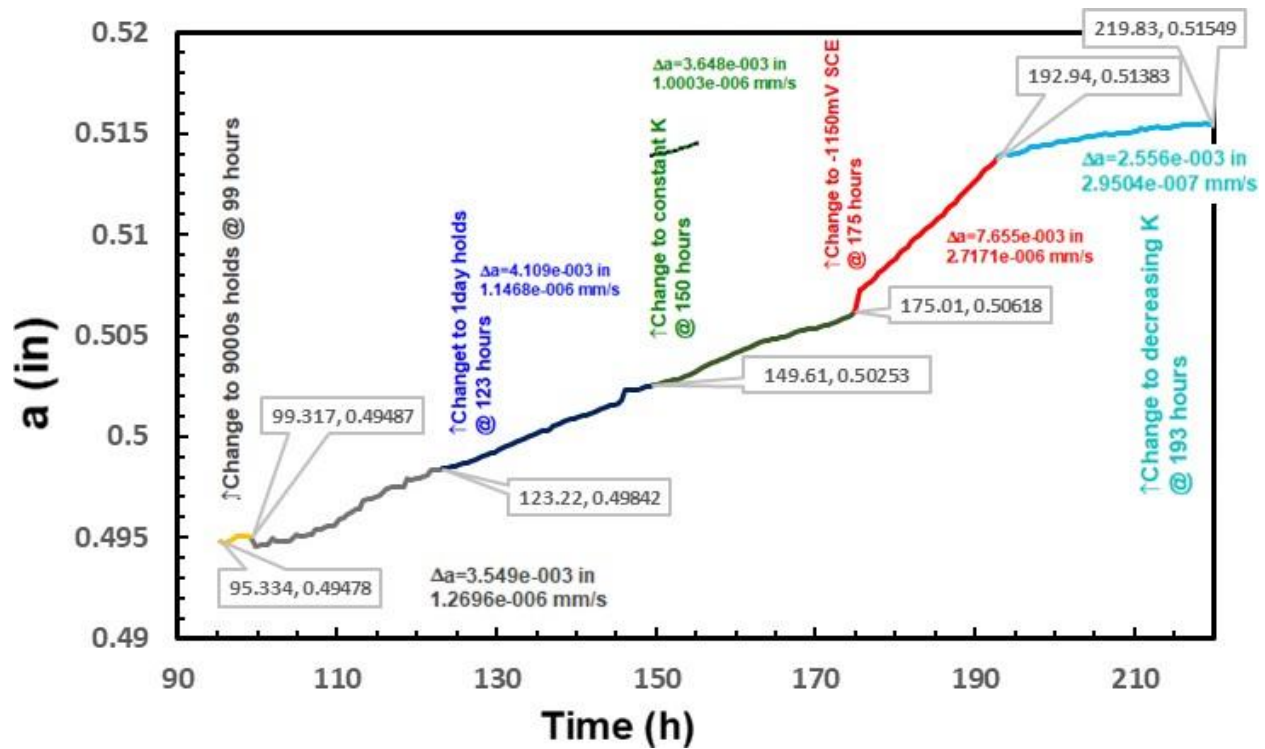


Figure 27: Crack length vs time for 955 (2808-LR3) at constant K and under decreasing K conditions.

In order to get the crack reactivated, the K value was increased 84 ksi√in (92.4 MPa√m) and the crack was transitioned to constant K as described in the experimental section. The applied potential was varied to characterize the effect of applied potential on the measured crack growth rate as seen in Figure 28. This sample reached the end of the available ligament and hence another sample was used to study the effect of K on the crack growth rate.

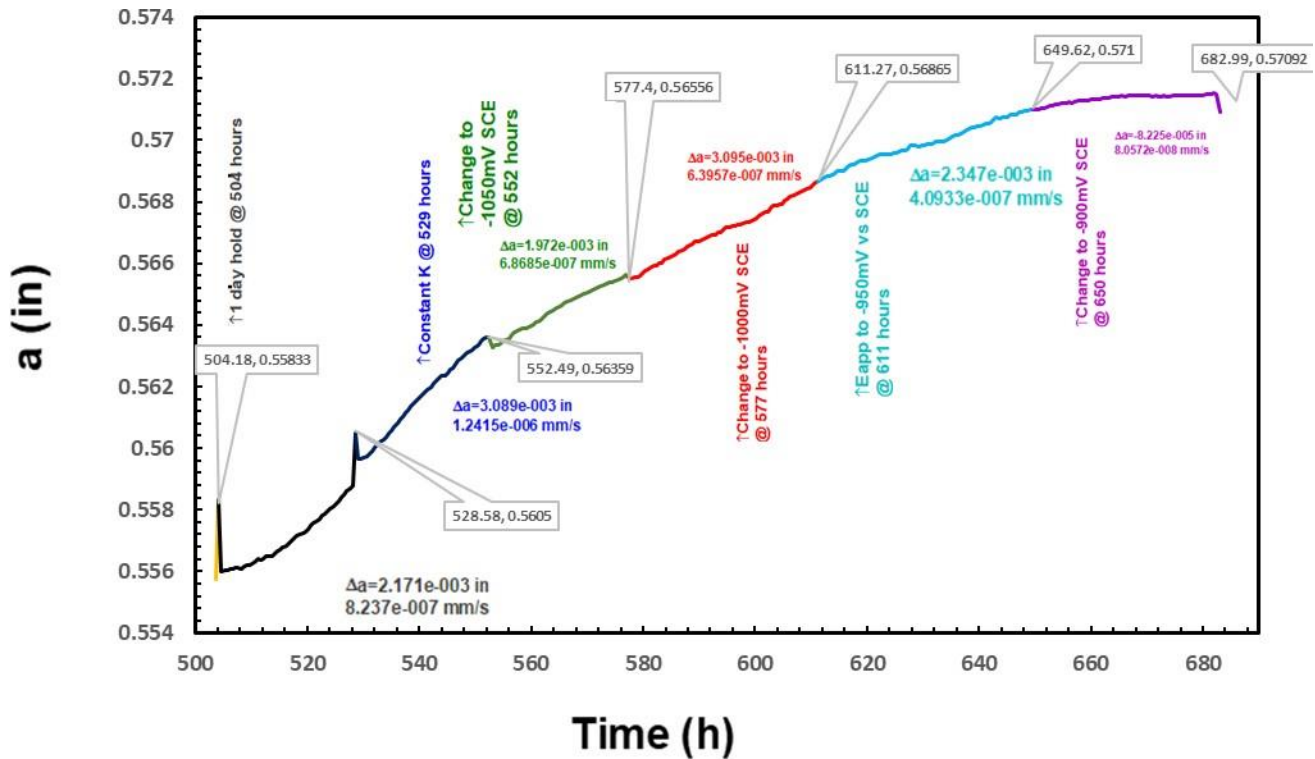


Figure 28: Crack length vs time for 955 (2808-LR3) as a function of applied potential at $K = 84 \text{ ksi}\sqrt{\text{in}}$ ($92.4 \text{ MPa}\sqrt{\text{m}}$).

The new sample was initiated under cycling at a K_{max} of $72 \text{ ksi}\sqrt{\text{in}}$ ($79.2 \text{ MPa}\sqrt{\text{m}}$) at -1200 mV SCE followed by increasing hold periods from 9000 s before transitioning to constant K . The potential was then stepped down from -1200 mV SCE to -950 mV SCE as shown in Figure 29. The changes made in the test during this period are indicated in the plot with vertical comments. The comments along with the time stamp are located on the plot when the change was made. The effect of applied potential on crack growth rate at several different values of K is shown in Figure 30. There is a strong effect of applied potential at $72 \text{ ksi}\sqrt{\text{in}}$ ($79.2 \text{ MPa}\sqrt{\text{m}}$) with the CGR decreasing from about $2 \times 10^{-6} \text{ mm/s}$ to about $8.7 \times 10^{-7} \text{ mm/s}$ as the potential is decreased from -1200 mV SCE to -1100 mV SCE . When the potential is decreased from -1100 mV SCE to -950 mV SCE there is a sharp decrease in crack growth rate to $6.5 \times 10^{-8} \text{ mm/s}$. At $84 \text{ ksi}\sqrt{\text{in}}$ ($92.4 \text{ MPa}\sqrt{\text{m}}$) the crack growth rate decreases from $1.2 \times 10^{-6} \text{ mm/s}$ to $4.3 \times 10^{-7} \text{ mm/s}$ as the potential decreases from -1100 mV SCE to -950 mV SCE . There is a sharp decrease in crack growth to $8 \times 10^{-8} \text{ mm/s}$ when the potential was changed to -950 mV SCE . The effect of K on crack growth rate for 955 at -1050 mV SCE is shown in Figure 31. No stable crack growth rate was observed at $60 \text{ ksi}\sqrt{\text{in}}$ and for reference a growth rate of 10^{-8} mm/s is indicated on the graph.

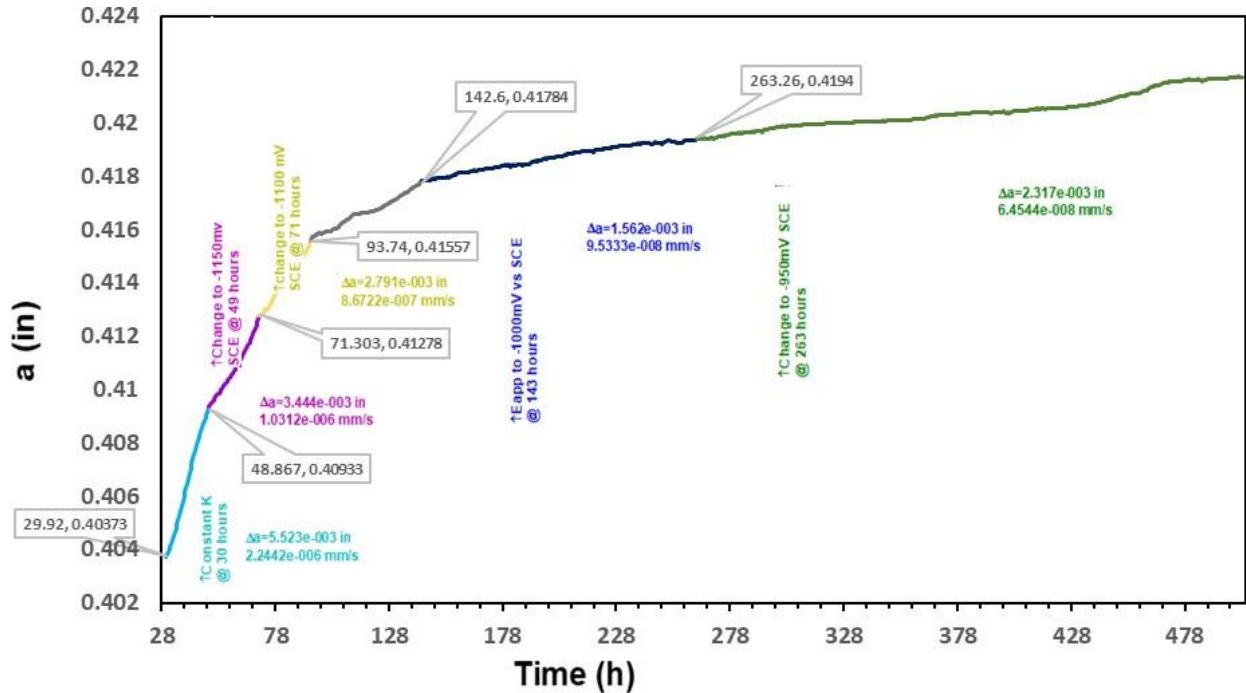


Figure 29: Crack length vs time for 955 (2808-LR5) as a function of applied potential at 72 ksi√in (79.2 MPa√m).

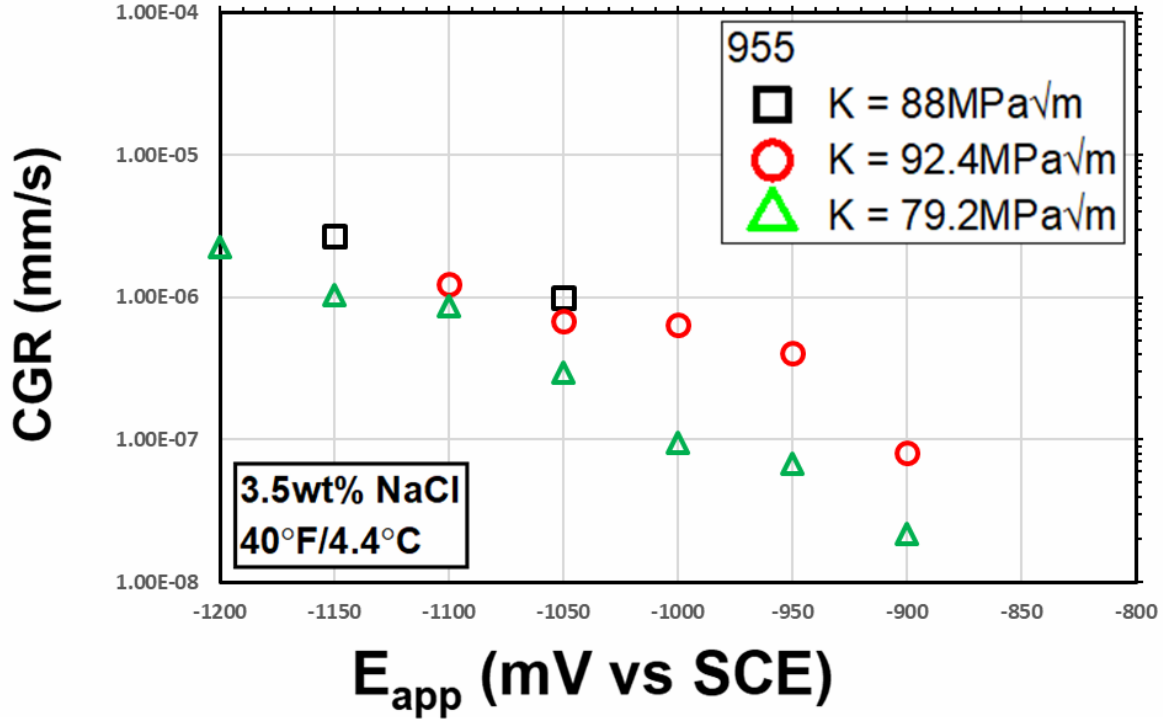


Figure 30: Effect of applied potential on crack growth rate for 955 over a range of K values.

Table 19: Color coded numerical values for Figure 30 (two tables)

Eapp	CGR (mm/s) K = 72MPa√m	log(CGR)	CGR (mm/s) K = 65.18MPa√m
-1200	2.24E-06	-5.64893	2.13E-06
-1150	1.03E-06	-5.98665	1.36E-06
-1100	8.67E-07	-6.06187	1.14E-06
-1050	2.93E-07	-6.53278	3.89E-07
-1000	9.53E-08	-7.02076	2.82E-07
-975	--	--	1.23E-07
-950	6.82E-08	-7.16647	--
-900	2.18E-08	-7.66254	--

K (MPa√m)	Eapp (mV SCE)	CGR (mm/s)	CGR (mm/s)	CGR (mm/s)
	-1050mV SCE		80MPa√m	K = 84MPa√m
80	1.00E-06	-1150	2.72E-06	
72.8	--	-1100	--	
		-1050	1.00E-06	
72.8	--	-1100	--	1.24E-06
		-1050		6.87E-07
		-1000		6.40E-07
		-950		4.09E-07
		-900		8.06E-08

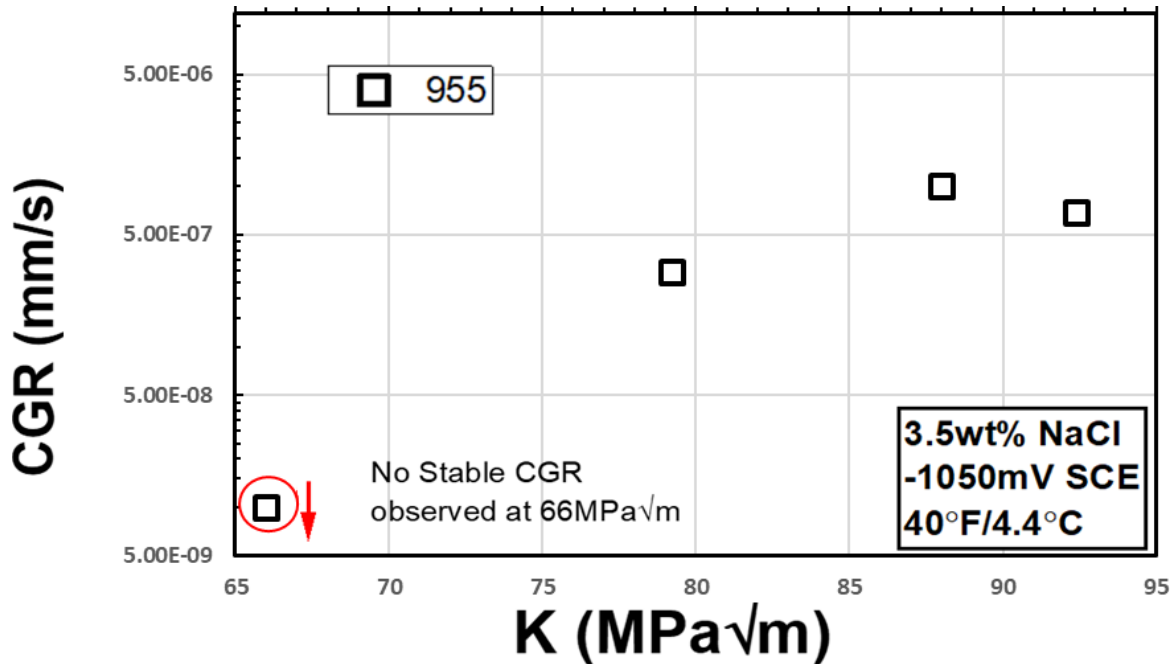


Figure 31: CGR as a function of K for 955 at -1050 mV SCE.

Table 20: Numerical values for Figure 31

K (MPa√m)	CGR (mm/s)	
	-1050mV SCE	-1150mV SCE
60	1.00E-08	--
72	2.93E-07	1.03E-06
80	1.00E-06	2.72E-06
84	6.87E-07	--

5.3.4 C22HS (Specimen ID 2785-LR4)

The effect of ΔK and frequency on the FCGR behavior of C22HS, at a K_{max} of 50 ksi√in (55 MPa√m), is shown below in Figure 32. The results of the frequency scan indicate that there is no significant effect of frequency on the FCGR behavior, over a range of ΔK at -1050 mV SCE. The lack of frequency dependence suggests that the material is not susceptible to environmentally assisted cracking under these conditions. This is in contrast to the behavior of the precipitation hardened alloys, all of which exhibited susceptibility to environmentally assisted cracking as evidenced by increasing FCGR with decreasing frequency. To explore the response of C22HS, the K_{max} value was increased from 50 ksi√in (55 MPa√m) to 72 ksi√in (79.2 MPa√m) and the potential decreased to -1200 mV SCE. The K value was increased to 90 ksi√in (99 MPa√m), and under these conditions, FCGR exhibited at 4 - 6 time increases as the frequency was reduced from 0.3 Hz to 0.1 mHz.

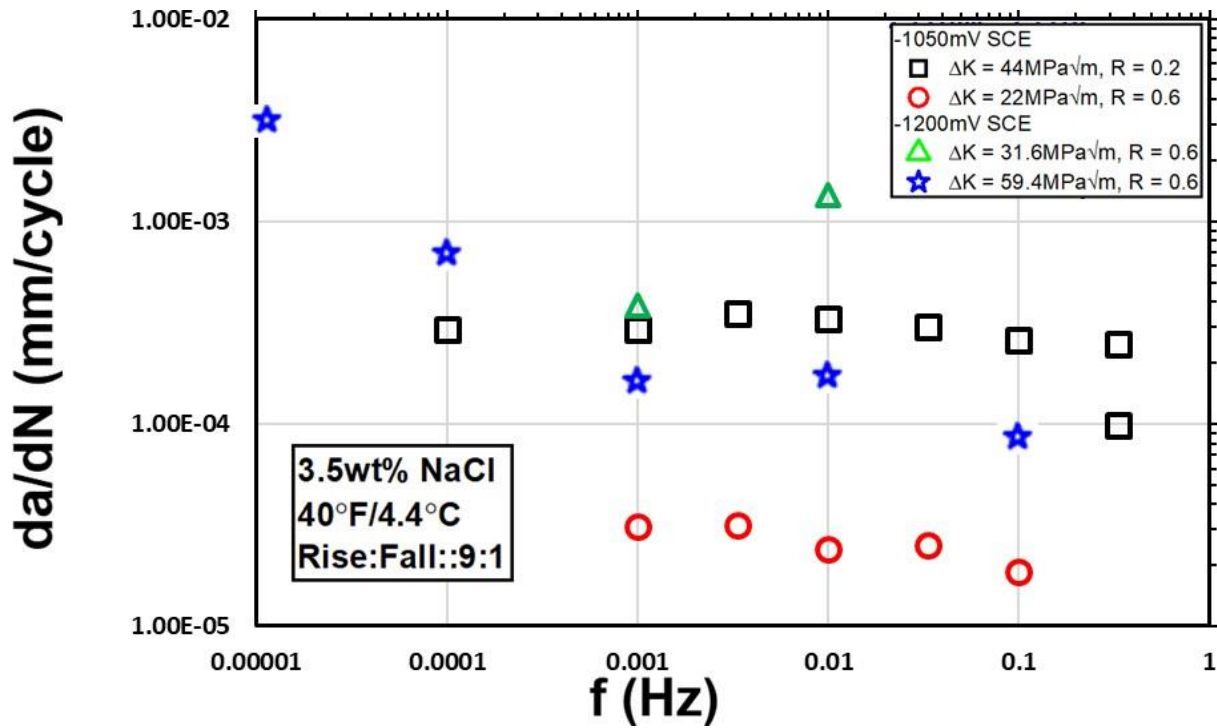


Figure 32: FCGR as a function of frequency for C22HS (2785-LR4) over a range of ΔK values, and potentials

Table 21: Color coded numerical values for Figure 32

f (Hz)	da/dt (mm/s)	Da (in)	Comments	Rise Time (s)	Fall Time (s)	Hold Time (s)	DK (MPa√m)	da/dN (mm/cycle)
0.33333	8.21E-05	0.0103	'B=0.4782"	2.7	0.3	0	40	2.46E-04
0.1	2.60E-05	0.00476	'9/1'	9	1		40	2.60E-04
0.03333	1.01E-05	0.00337	'27/3'	27	3		40	3.03E-04
0.01	3.27E-06	0.00184	'90/10'	90	10		40	3.27E-04
0.00333	1.17E-06	0.00353	'270/30'	270	30		40	3.51E-04
0.001	2.94E-07	0.00323	'900/100'	900	100		40	2.94E-04
1.00E-04	2.91E-08	-0.00491	'9000/1000'	9000	1000		40	2.91E-04
0.01	1.35E-05	0.00185	[]				28.8	0.00135
1.00E-03	3.83E-07	0.00204	'900/100'				28.8	3.83E-04
0.1	8.38E-06	0.00799	'Kmax to 90'				36	8.38E-05
0.01	1.68E-06	0.00373	'90/10'				36	1.68E-04
0.001	1.60E-07	0.00309	'Change to 900/100'				36	1.60E-04

f (Hz)	da/dt (mm/s)	Da (in)	Comments	Rise Time (s)	Fall Time (s)	Hold Time (s)	DK (MPa√m)	da/dN (mm/cycle)
1.00E-04	6.80E-08	9.94E-04	'begin 9000s holds'				36	6.80E-04
1.14E-05	3.54E-08	0.00178	'Change to 1 day holds'				36	0.0031
1.16E-07	2.79E-08	0.0014	'Constant K'				36	0.24089
1.16E-07	-6.10E-09	-1.36E-04	'Change to increasing K'				36	-0.05261
0.33333	3.28E-05	0.01015	'change to R=0.6'				20	9.83E-05
0.1	1.86E-06	0.00287	'changed to 9/1'				20	1.86E-05
0.03333	8.39E-07	0.00164	'27/3'				20	2.52E-05
0.01	2.42E-07	0.00208	'90/10'				20	2.42E-05
0.00333	1.05E-07	0.00115	'Change to 270/30'				20	3.14E-05
0.001	3.12E-08	3.28E-05	'900/100'				20	3.12E-05

An attempt was made to transition the crack to constant K conditions to understand if stable crack growth rate could be sustained under these conditions. The result of the crack length versus time and the transition to constant K is shown in Figure 33. The changes made in the test during this period are indicated in the plot with vertical comments. The comments along with the time stamp are located on the plot when the change was made. It is evident that there is some transient crack growth rate when going from 1 day hold periods, to constant K. However, it appears that the growth rate decays sharply with time and appears to flat line suggesting little or no crack advance. The test was not continued given the fact that no crack growth rate was observe even at -1200 mV SCE, which is significantly more cathodic the potentials from typical Al anodes that would be used in subsea applications.

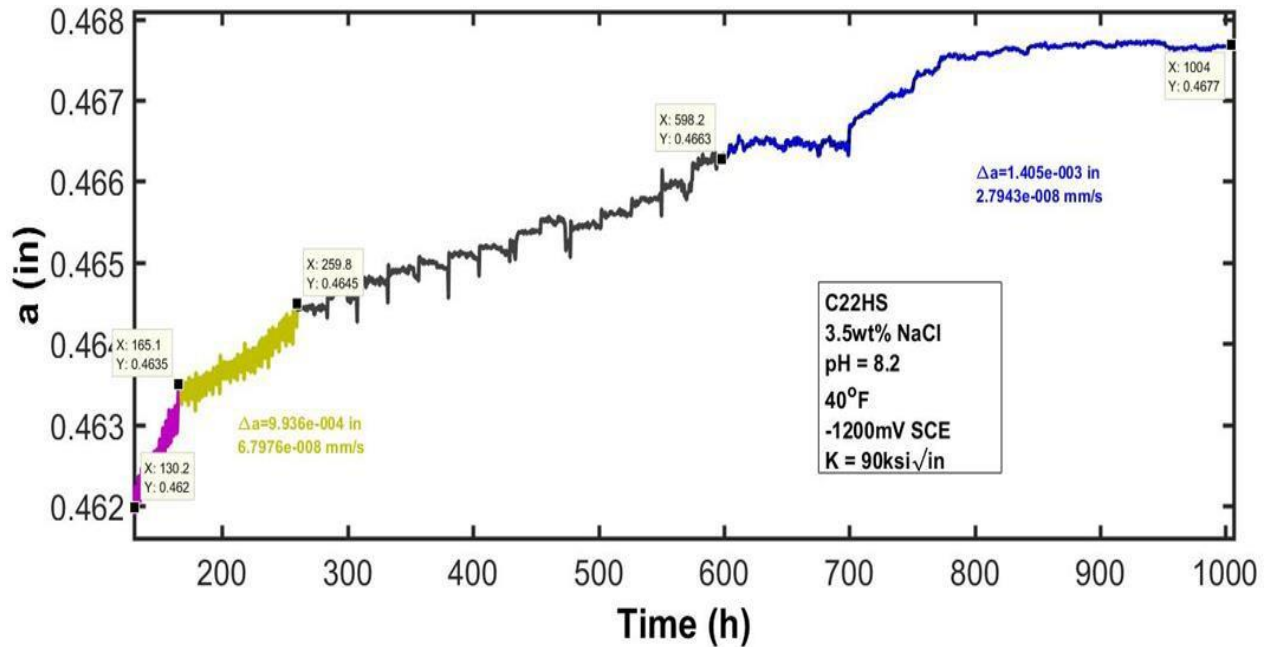


Figure 33: Crack growth rate at constant K of 90 ksi√in (99 MPa√m) and -1200 mV SCE for C22HS (2785-LR1).

5.3.5 825 (Specimen ID 2833-CL3)

The FCGR behavior of 825 as a function of frequency at two different ΔK at a K_{max} of 50 ksi√in (55 MPa√m) is shown below in Figure 34. There is no strong environmental effect under the tested conditions as reflected by the fact that the FCGR does not exhibit a frequency dependence. The behavior of 825, which is a cold worked alloy, is different compared that observed for the precipitation hardened alloys 725, 945X, and 955. However, it is similar to the behavior of C22HS, which is also a cold worked alloy.

The sample was then transitioned to a K_{max} of 60 ksi√in (66 MPa√m) to evaluate if it was possible to stabilize static crack growth. To establish static crack growth conditions, 9000 s holds periods were applied as shown in Figure 35. The changes made in the test during this period are indicated in the plot with vertical comments. The comments along with the time stamp are located on the plot when the change was made. The potential of the sample was then stepped to -1150 mV SCE to facilitate the transition, following which 1 day hold periods were introduced. As seen in Figure 35, the growth rate during the 1-day holds is low, and all the crack extension is during the reloading event once a day. During the hold periods, the voltage signal decays suggesting that there is no stable crack extension. Hence, no transition to constant K was made. No further increases in K were made and the test was terminated.

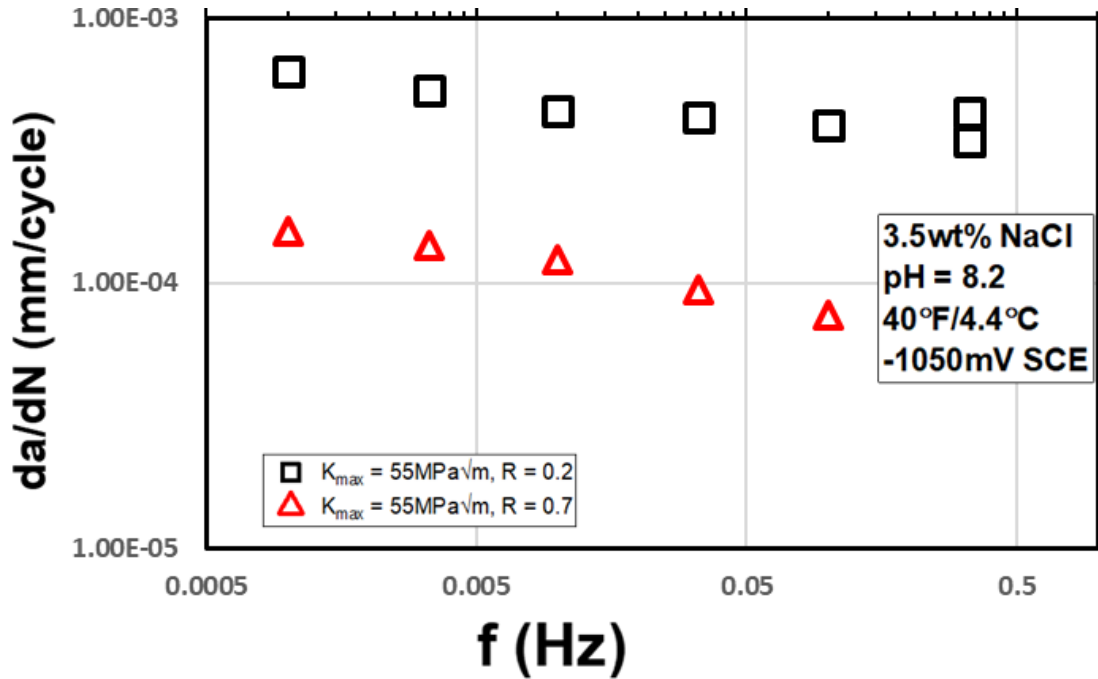


Figure 34: FCGR as a function of frequency for 825 (2833-CL3) over a range of K values.

Table 22: Numerical values for Figure 34

Kmax	Kmin	f (Hz)	da/dt (mm/s)	Da (in)	Comment _s	DK (MPa√m)	da/dN (mm/cycle)
50	10	0.33333	1.46E-04	1.15E-04	[]	40	4.39E-04
50	10	0.33333	1.15E-04	0.00519	'B=0.4692"	40	3.46E-04
50	10	0.1	3.92E-05	0.00422	'9/1'	40	3.92E-04
50	10	0.03333	1.42E-05	0.00353	'27/3'	40	4.25E-04
50	10	0.01	4.46E-06	0.00481	'90/10'	40	4.46E-04
50	10	0.00333	1.78E-06	0.0027	'270/30'	40	5.35E-04
50	10	0.001	6.29E-07	0.0018	'900/100'	40	6.29E-04
50	30	0.33333	1.61E-05	0.00512	'Change to R=0.6'	20	4.83E-05
50	30	0.1	7.64E-06	0.00295	'9/1'	20	7.64E-05
50	30	0.03333	3.16E-06	0.00976	'27/3'	20	9.48E-05
50	30	0.01	1.22E-06	0.00462	'90/10'	20	1.22E-04
50	30	0.00333	4.62E-07	0.00301	'270/30'	20	1.38E-04
50	30	1.00E-03	1.56E-07	0.00342	'Change to 900/100'	20	1.56E-04

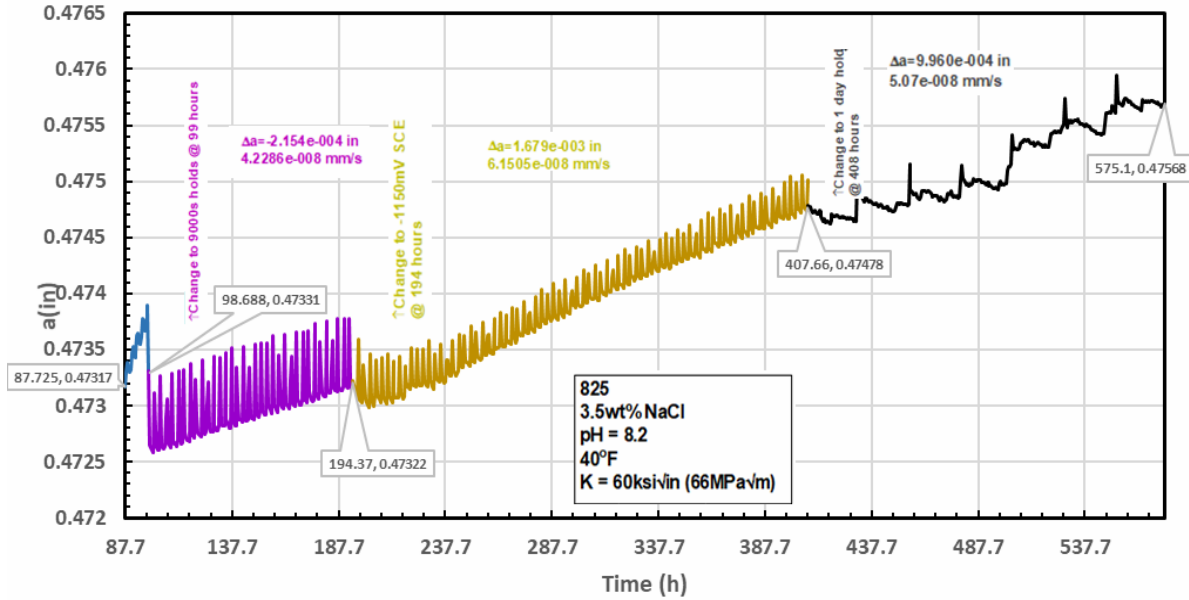
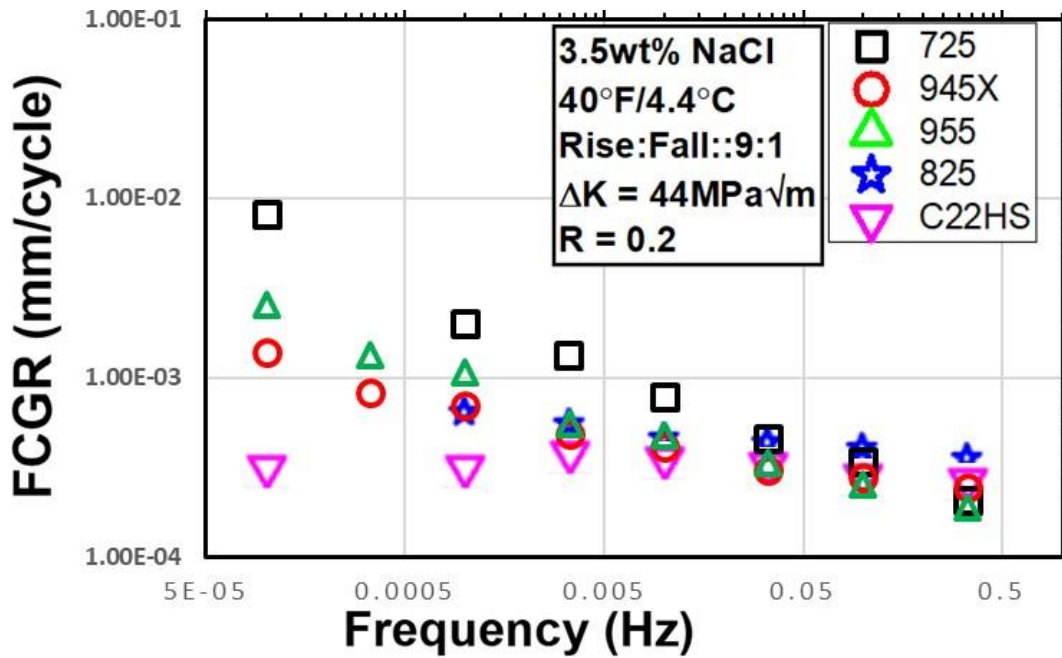
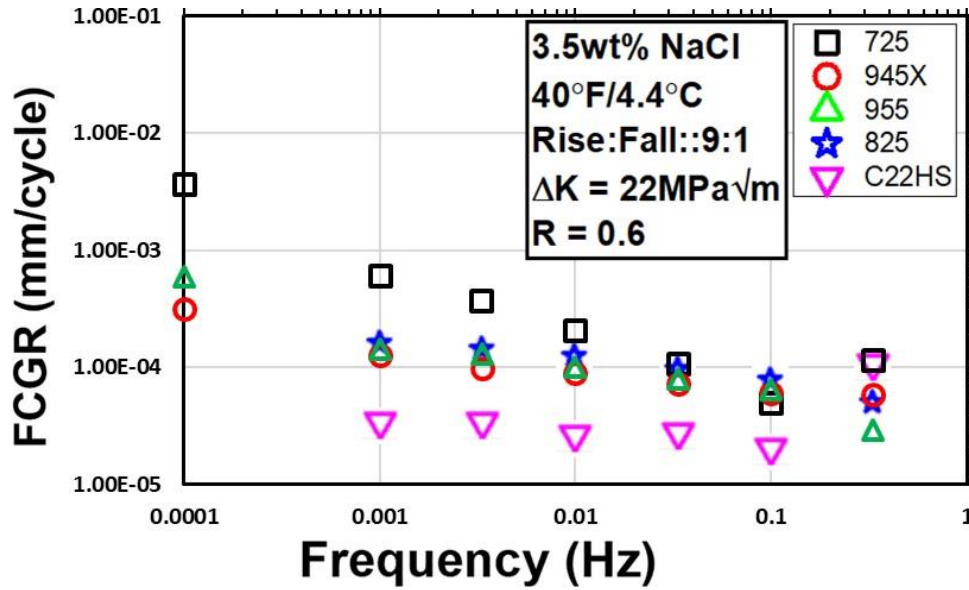


Figure 35: Crack length vs time for 825 (2833-CL3) at 60 ksi in (66 MPa√m) to determine behavior under constant K conditions.

A comparison of the FCGR behavior as a function of frequency at two different ΔK values for all the alloys is shown in Figure 36. The results clearly indicate that the FCGR of the cold worked alloys are largely independent of frequency. However, the FCGR of the PH nickel-based alloys exhibit a strong dependence on frequency. This is discussed in more detail in the discussion section.



a) Rate for various alloys under CP at an R- ratio of 0.2 and ΔK of 44 MPa√m
Effect of frequency on the fatigue crack growth.



b) Effect of frequency on the fatigue crack growth rate for various alloys under CP at a R-ratio of 0.6 and ΔK of $22\text{MPa}\sqrt{\text{m}}$.

Figure 36: Comparison of the FCGR as a function of frequency at two different ΔK values for all the alloys evaluated under cathodic polarization.

Table 23: Color coded numerical values for Figure 36a

FCGR (mm/cycle) DK = 40/R = 0.2	FCGR (mm/cycle) DK = 20/R = 0.6	Frequency (Hz)
2.08E-04	1.17E-04	0.3333
3.40E-04	4.95E-05	0.1
4.59E-04	1.08E-04	0.0333
7.79E-04	2.08E-04	0.01
0.00133	3.76E-04	0.0033
0.002	6.08E-04	0.001
0.00811	0.00365	1.00E-04
2.42E-04	5.85E-05	0.33333
2.75E-04	6.01E-05	0.1
3.05E-04	7.27E-05	0.03333
4.07E-04	8.92E-05	0.01
4.85E-04	9.79E-05	0.00333
6.97E-04	1.28E-04	0.001

FCGR (mm/cycle) DK = 40/R = 0.2	FCGR (mm/cycle) DK = 20/R = 0.6	Frequency (Hz)
8.19E-04	--	3.33E-04
0.00137	3.14E-04	1.00E-04
1.87E-04	2.89E-05	0.33333
2.51E-04	6.40E-05	0.1
3.33E-04	7.97E-05	0.03333
4.75E-04	1.00E-04	0.01
5.51E-04	1.30E-04	0.00333
0.00106	1.43E-04	1.00E-03
0.00133	--	3.33E-04
0.00255	5.98E-04	1.00E-04
3.46E-04	4.83E-05	0.33333
3.92E-04	7.64E-05	0.1
4.25E-04	9.48E-05	0.03333
4.46E-04	1.22E-04	0.01
5.35E-04	1.38E-04	0.00333
6.29E-04	1.56E-04	0.001
2.46E-04	9.83E-05	0.33333
2.60E-04	1.86E-05	0.1
3.03E-04	2.52E-05	0.03333
3.27E-04	2.42E-05	0.01
3.51E-04	3.14E-05	0.00333
2.94E-04	3.12E-05	0.001
2.91E-04		1.00E-04

Table 24: Color coded numerical values for Figure 36b

(mm/cycle) DK = 40/R = 0.2	(mm/cycle) DK = 20/R = 0.6	
2.08E-04	1.17E-04	0.3333
3.40E-04	4.95E-05	0.1
4.59E-04	1.08E-04	0.0333
7.79E-04	2.08E-04	0.01
0.00133	3.76E-04	0.0033
0.002	6.08E-04	0.001
0.00811	0.00365	1.00E-04
2.42E-04	5.85E-05	0.33333
2.75E-04	6.01E-05	0.1

(mm/cycle) DK = 40/R = 0.2	(mm/cycle) DK = 20/R = 0.6	
3.05E-04	7.27E-05	0.03333
4.07E-04	8.92E-05	0.01
4.85E-04	9.79E-05	0.00333
6.97E-04	1.28E-04	0.001
8.19E-04	--	3.33E-04
0.00137	3.14E-04	1.00E-04
1.87E-04	2.89E-05	0.33333
2.51E-04	6.40E-05	0.1
3.33E-04	7.97E-05	0.03333
4.75E-04	1.00E-04	0.01
5.51E-04	1.30E-04	0.00333
0.00106	1.43E-04	1.00E-03
0.00133	--	3.33E-04
0.00255	5.98E-04	1.00E-04
3.46E-04	4.83E-05	0.33333
3.92E-04	7.64E-05	0.1
4.25E-04	9.48E-05	0.03333
4.46E-04	1.22E-04	0.01
5.35E-04	1.38E-04	0.00333
6.29E-04	1.56E-04	0.001
2.46E-04	9.83E-05	0.33333
2.60E-04	1.86E-05	0.1
3.03E-04	2.52E-05	0.03333
3.27E-04	2.42E-05	0.01
3.51E-04	3.14E-05	0.00333
2.94E-04	3.12E-05	0.001
2.91E-04		1.00E-04

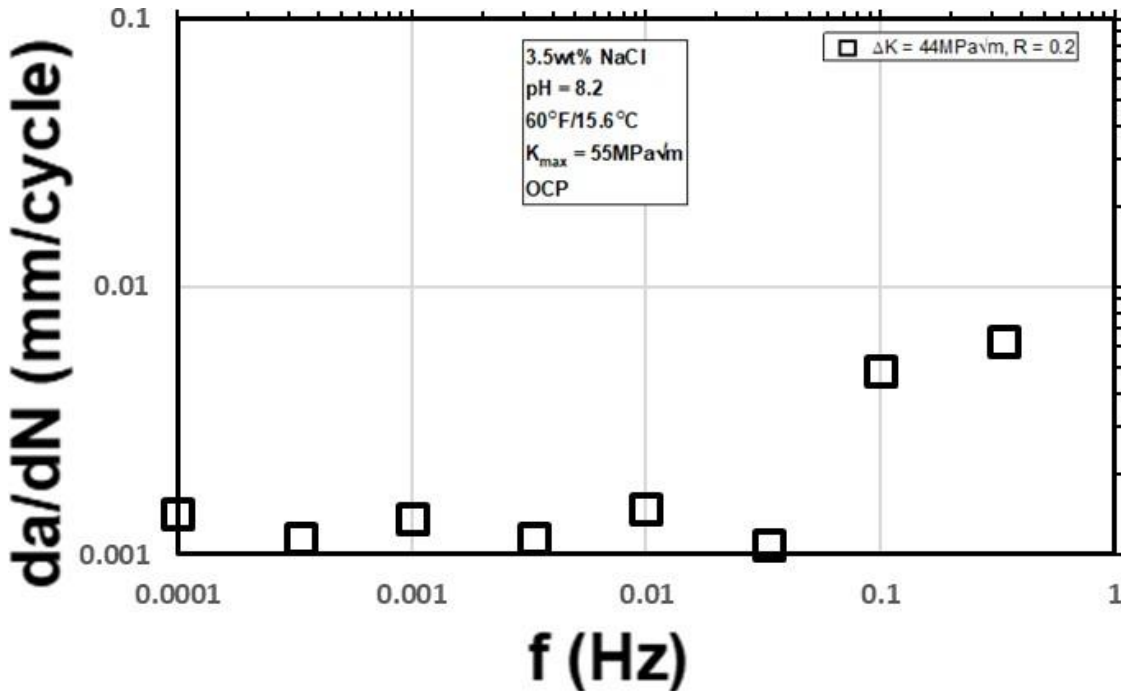
5.4 Seawater Under OCP

The corrosion fatigue behavior of the various alloys was also evaluated under open circuit conditions. The intent of performing tests at open circuit conditions was to understand the behavior in the absence of any applied potential. This scenario can occur, if systems are electrical isolated from steel components for which the cathodic protection system is designed. It is also possible that in cases the anodes may deplete in time and the systems may no longer be experiencing cathodic potentials. If these materials are used in top side components, they may never be subject to cathodic protection.

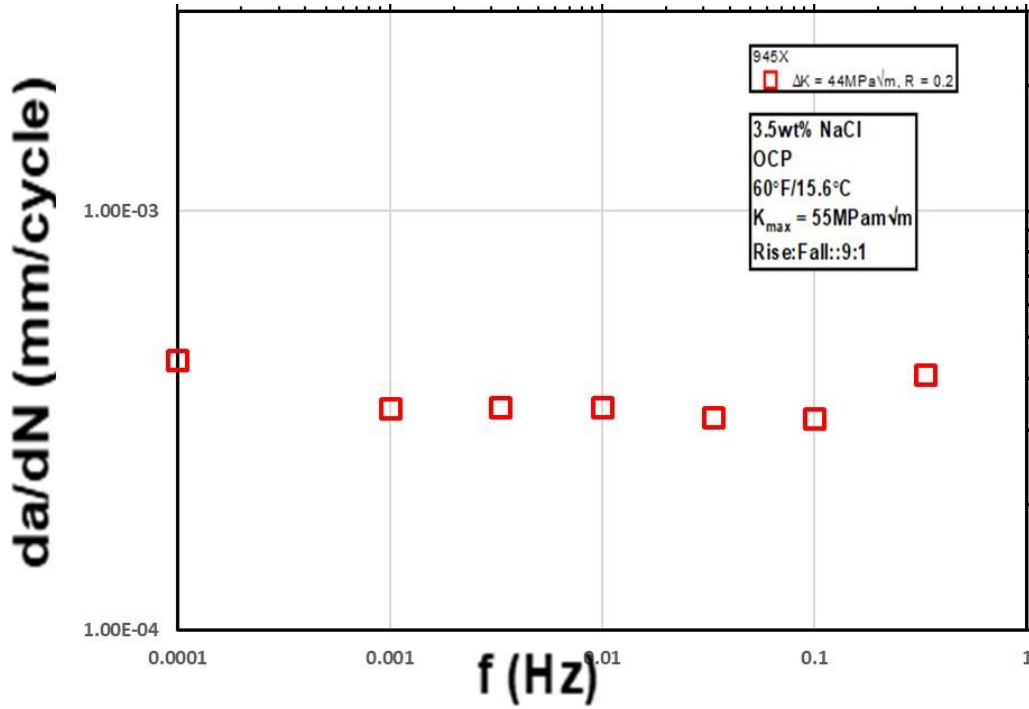
In this context, the mechanism of corrosion fatigue at open circuit conditions would likely be driven by the presence of chlorides, and not by a Hydrogen Embrittlement (HE) mechanism that is evident

at the applied cathodic potentials. The measurement of the critical crevice temperature, which indicates susceptibility to localized corrosion would be an appropriate frame work in which to understand the corrosion fatigue results at OCP.

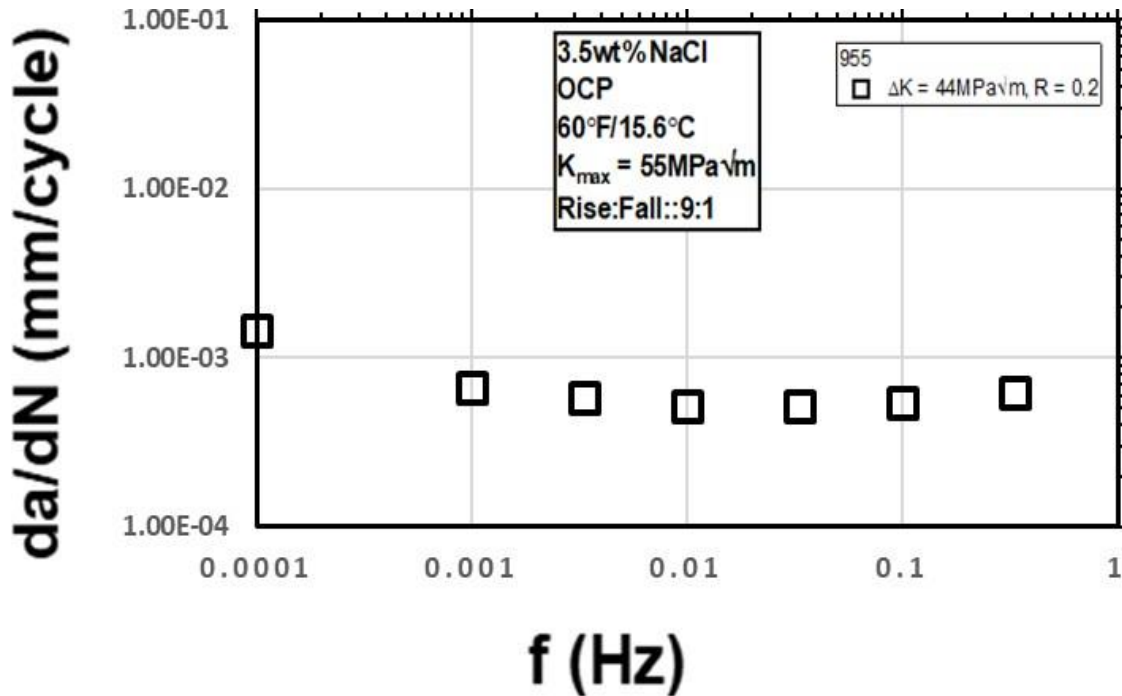
The FCGR behavior as a function of frequency for the precipitation hardened alloys, 725, 945X, and 955 is shown below in Figure 37. The FCGR is largely independent of ΔK over a wide range of frequencies, suggesting that there is little or no environmental effect. This behavior is consistent with the observation that the critical crevice temperature for all the alloys is higher than 24°C, which is significantly higher than 15.6°C the temperature at which these tests were performed. It is also important to note that the critical crevice temperature was determined at an applied potential of +700mV SCE, which is also significantly higher the open circuit potential of these alloys.



a) 725 (2810-LR1)



b) 945X (2805-LR1)



c) 955 (2808-LR3)

Figure 37: FCGR as a function of frequency for the precipitation hardened alloys (725, 945X, and 955) at OCP.

Table 25: Numerical values for Figure 37a

Kmax	Kmin	f (Hz)	da/dt (mm/s)	Da (in)	Comments	da/dN (mm/cycle)
50	10	0.33333	0.00207	0.02248	'Begin OCP @ 60F'	0.00622
50	10	0.1	4.89E-04	0.01482	'9/1'	0.00489
50	10	0.03333	3.65E-05	0.01705	'27/3'	0.00109
50	10	0.01	1.49E-05	0.00489	'90/10'	0.00149
50	10	0.00333	3.83E-06	0.00244	'270/30'	0.00115
50	10	0.001	1.36E-06	0.00349	'900/100'	0.00136
50	10	3.33E-04	3.82E-07	0.00162	'2700/300'	0.00115
50	10	1.00E-04	1.42E-07	0.00152	'Change to 0.1mHz'	0.00142

Table 26: Numerical values for Figure 37b

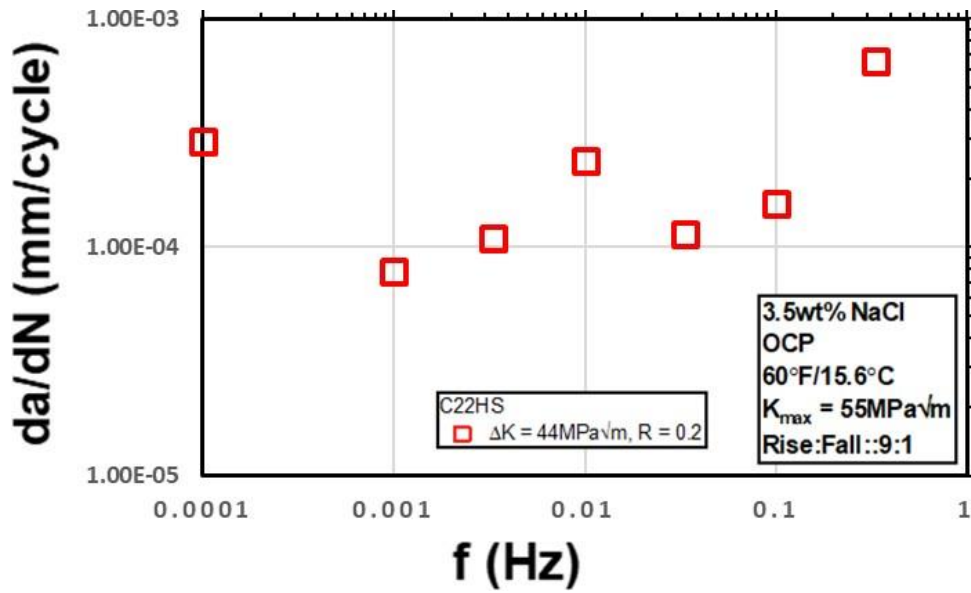
Kmax	Kmin	f (Hz)	da/dt (mm/s)	Da (in)	Comments	da/dN (mm/cycle)
50	10	0.33333	1.36E-04	0.00755	'Begin OCP @ 60F'	4.08E-04
50	10	0.1	3.21E-05	0.0054	'9/1'	3.21E-04
50	10	0.03333	1.07E-0	0.00429	'27/3'	3.22E-04
50	10	0.01	3.42E-06	0.00429	'90/10'	3.42E-04
50	10	0.00333	1.14E-06	0.00288	'270/30'	3.41E-04
50	10	0.001	3.39E-07	0.00178	'Change to 1mHz'	3.39E-04
50	10	1.00E-04	4.42E-08	0.00101	'Change to 0.1mHz'	4.42E-04

Table 27: Numerical values for Figure 37c

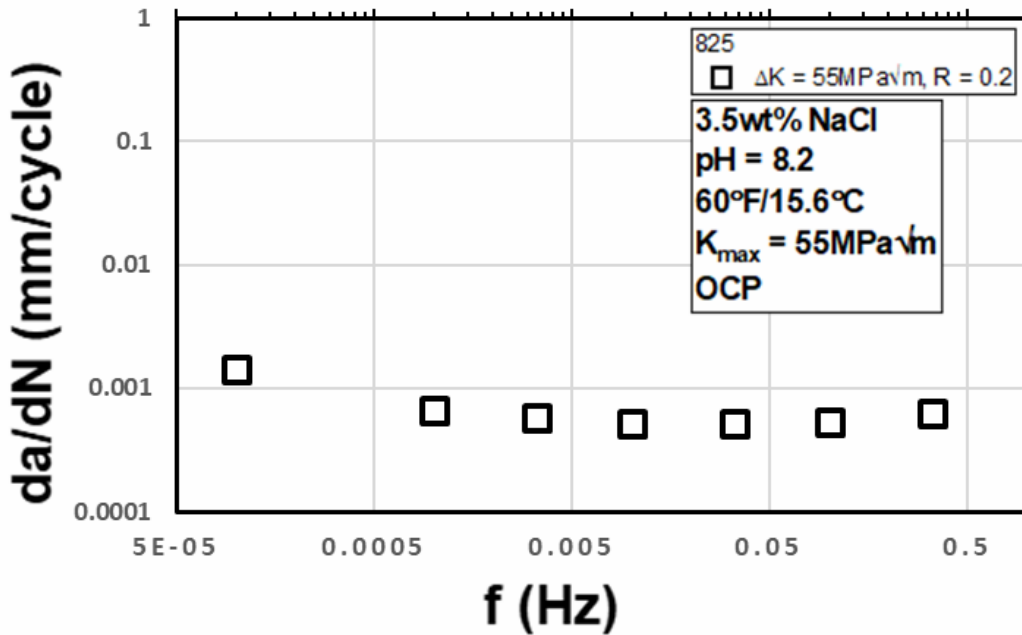
Kmax	Kmin	f (Hz)	da/dt (mm/s)	Da (in)	Comments	DK (MPa√m)	da/dN (mm/cycle)
50	10	0.33333	2.08E-04	0.0042	'B=0.4692"	40	6.24E-04
50	10	0.1	5.38E-05	0.0118	'9/1'	40	5.38E-04
50	10	0.03333	1.74E-05	0.0055	'27/3'	40	5.23E-04
50	10	0.01	5.21E-06	0.00316	'90/10'	40	5.21E-04
50	10	0.00333	1.94E-06	0.00444	'270/30'	40	5.83E-04
50	10	0.001	6.68E-07	0.00215	'900/100'	40	6.68E-04
50	10	1.00E-04	1.44E-07	0.00171	'9000/1000'	40	0.00144

The results of the FCGR behavior of the coldworked alloys is shown below in Figure 38. Similar to The behavior of the precipitation hardened alloys, the cold worked nickel-based alloys at OCP do not exhibit any frequency dependence suggesting no evidence of environmental assisted FCGR. Similar to the PH nickel-based alloys, C22HS, and 825 exhibited significantly higher critical crevice

temperature compared to the test temperature of 15.6°C, thus making it unlikely that any environmentally assisted fatigue would be stabilized.



a) C22HS (2785-LR4)



b) 825 (2833-CL3)

Figure 38: FCGR as a function of frequency for the precipitation hardened alloys (C22HS, and 825) at OCP.

Table 28: Numerical values for Figure 38a

Rise Time (s)	Fall Time (s)	DK (MPa√m)	da/dN (mm/cycle)
		40	6.48E-04
		40	1.55E-04
		40	1.13E-04
		40	2.40E-04
		40	1.10E-04
		40	7.80E-05
9000	1000	40	2.91E-04

Table 29: Numerical values for Figure 38b

da/dt (mm/s)	Da (in)	Comments	DK (MPa√m)	da/dN (mm/cycle)
2.08E-04	0.0042	'B=0.4692'''	40	6.24E-04
5.38E-05	0.0118	'9/1'	40	5.38E-04
1.74E-05	0.0055	'27/3'	40	5.23E-04
5.21E-06	0.00316	'90/10'	40	5.21E-04
1.94E-06	0.00444	'270/30'	40	5.83E-04
6.68E-07	0.00215	'900/100'	40	6.68E-04
1.44E-07	0.00171	'9000/1000'	40	0.00144

A summary comparison of the behavior of all the alloys in seawater under OCP conditions is shown in Figure 39. The results clearly indicate that the FCGR has little or no frequency dependence in all the alloys consistent with no environmental effect under these conditions.

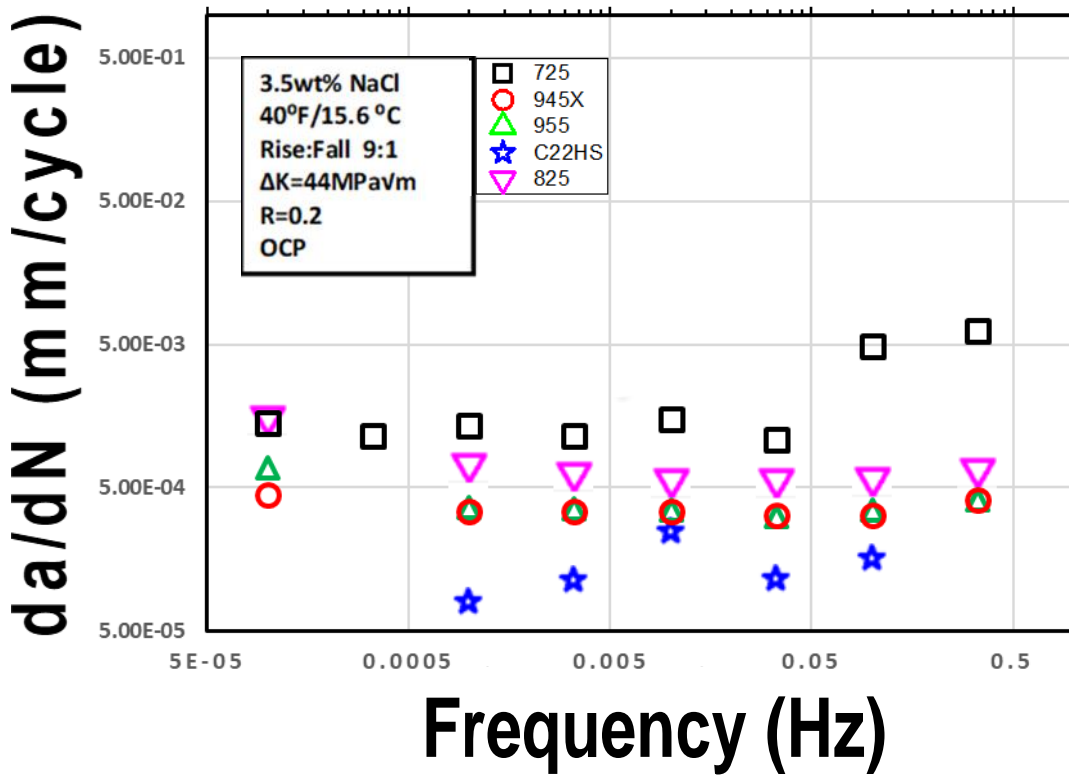


Figure 39: FCGR as a function of frequency for all the alloys in seawater under OCP conditions.

Table 30: Color coded numerical values for Figure 39

Frequency (Hz)	da/dN (mm/cycle)
0.33333	0.00622
0.1	0.00489
0.03333	0.00109
0.01	0.00149
0.00333	0.00115
0.001	0.00136
3.33E-04	0.00115
1.00E-04	0.00142
0.33333	4.08E-04
0.1	3.21E-04
0.03333	3.22E-04
0.01	3.42E-04
0.00333	3.41E-04
0.001	3.39E-04

1.00E-04

4.42E-04

Frequency (Hz)	da/dN (mm/cycle)
0.33333	4.12E-04
0.1	3.50E-04
0.03333	3.18E-04
0.01	3.47E-04
0.00333	3.53E-04
1.00E-03	3.66E-04
1.00E-04	6.84E-04
0.33333	6.48E-04
0.1	1.55E-04
0.03333	1.13E-04
0.01	2.40E-04
0.00333	1.10E-04
0.001	7.80E-05
0.33333	6.24E-04
0.1	5.38E-04
0.03333	5.23E-04
0.01	5.21E-04
0.00333	5.83E-04
0.001	6.68E-04
1.00E-04	0.00144

6 DISCUSSION

6.1 Fatigue Crack Growth of PH Nickel Alloys

It is clear from the data presented earlier that all the PH nickel-based alloys are susceptible to environmentally assisted cracking in seawater under cathodic polarization. The environmental effects are more pronounced at low frequencies. FCGR vs ΔK for the alloys tested at 1 mHz and 0.1 mHz are shown below in Figure 40. The results for $R = 0.6$ are plotted and indicate that FCGR at 0.1 mHz is higher than at 1 mHz. The values at 0.1 mHz are about 20 times higher than the in-air values (as represented by the BS7910 curves for steel[9]). It is interesting to note that the FCGR values for 725 are about 20 times higher than the in-air values at 20 ksi $\sqrt{\text{in}}$ (22 MPa $\sqrt{\text{m}}$), while FCGR of 955 and 945X at 20 ksi $\sqrt{\text{in}}$ (22 MPa $\sqrt{\text{m}}$) are about 5.5 and 3.5 times higher respectively. FCGR at 32 ksi $\sqrt{\text{in}}$ (35.2 MPa $\sqrt{\text{m}}$) for both 955 and 945X are about 20 times higher than the in-air values.

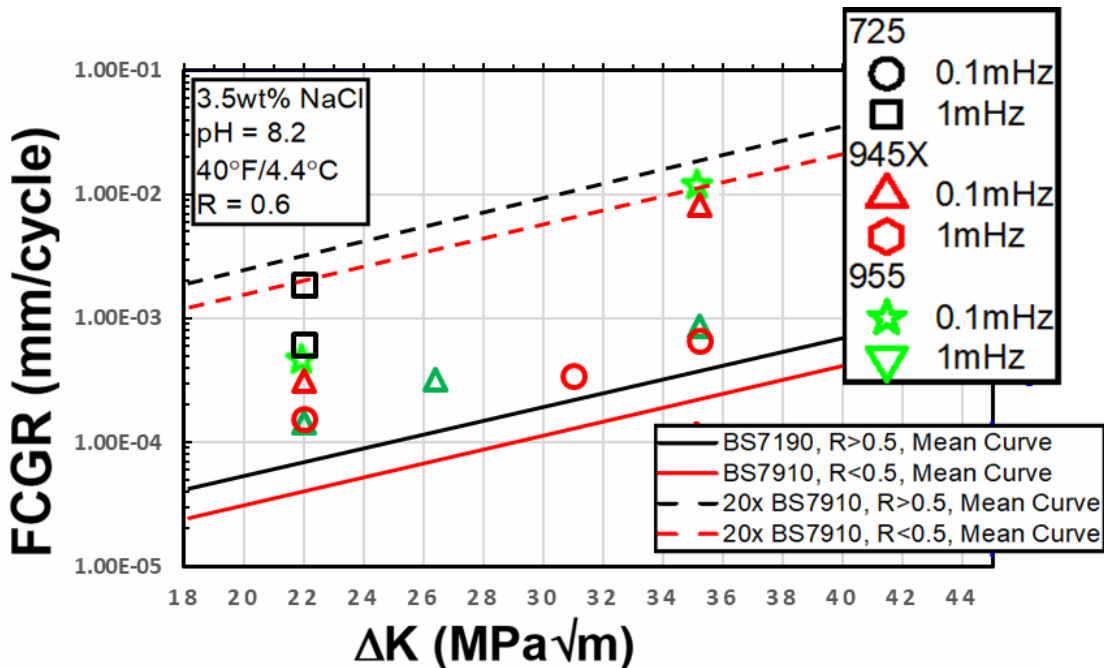


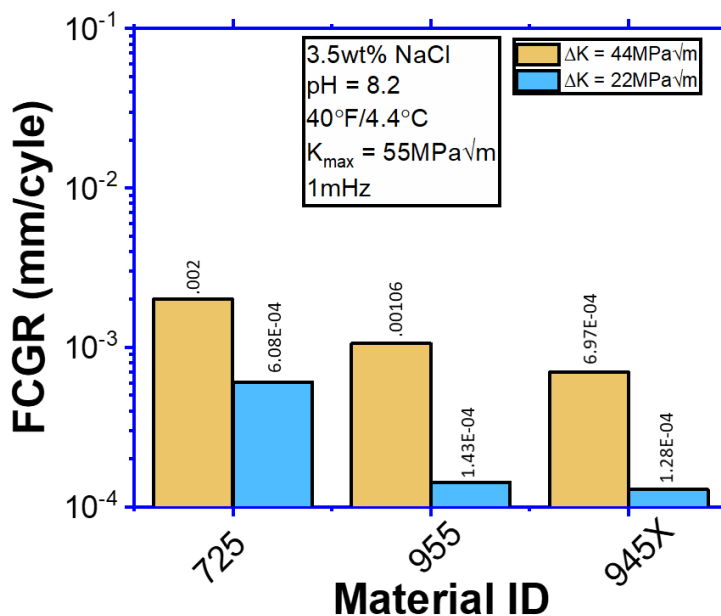
Figure 40: FCGR as a function of ΔK for 725, 955, and 945X at 1 mHz and 0.1 mHz.

Table 31: Color coded numerical values for Figure 40

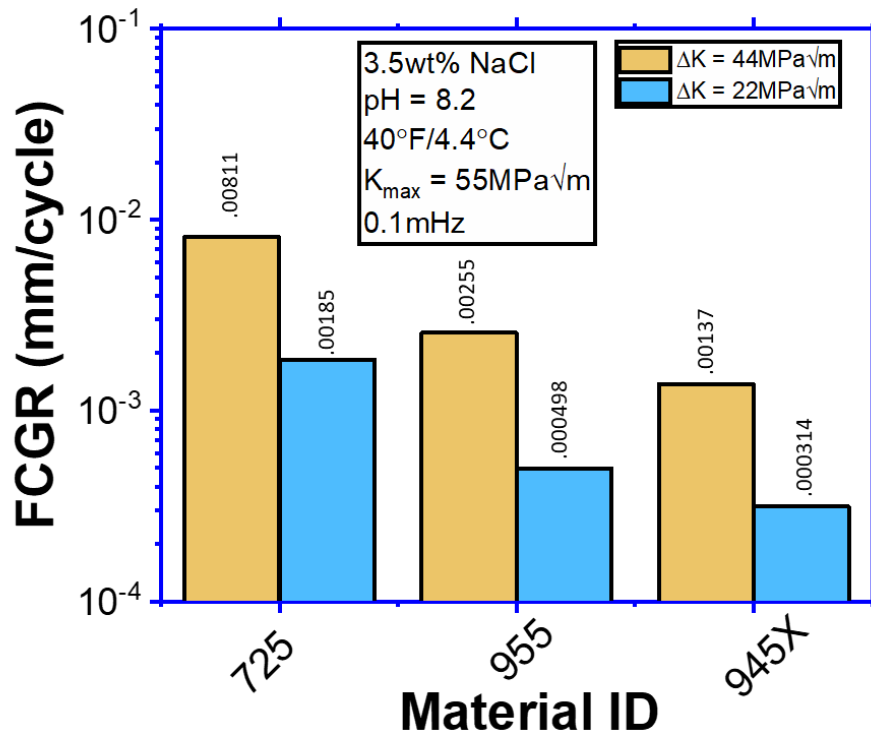
FCGR (mm/cycle)	DK (MPa $\sqrt{\text{m}}$)	FCGR (mm/cycle)	FCGR (mm/s)
0.1mHz	1.1*B	1mHz	1mHz
--	40	--	<u>0.002</u>
<u>0.00811</u>	20	22	<u>6.08E-04</u>
<u>0.00185</u>	20	22	<u>0.00185</u>

	DK (MPa√m)		FCGR (mm/cycle)		FCGR (mm/s)
	0.1mHz		1.1*B	1mHz	1mHz
	0.00137	40	--	6.97E-04	--
	3.14E-04	20	22	1.56E-04	--
	0.00824	32	35.2	6.63E-04	
	1.13E-04	28.2	31.02	3.45E-04	
	0.00255	40	--	0.00106	--
	4.98E-04	20	22	1.43E-04	--
	--	24	26.4	3.22E-04	--
	0.0127	32	35.2	8.59E-04	
	--	--	--	--	

A comparison of the FCGR at 1mHz and 0.1mHz for the three alloys is shown below at a K_{max} of 50 ksi√in (55 MPa√m) and ΔK of 20 ksi√in (22 MPa√m) and 40 ksi√in (44 MPa√m) (Figure 41). The results clearly indicate that 725 is significantly more susceptible than 955, which in turn is more susceptible than 945X. The effect is evident at both 40 ksi√in (44 MPa√m) and 20 ksi√in (22 MPa√m) as well as 1 mHz and 0.1 mHz. The difference is more pronounced at the higher R-ratio corresponding to 20 ksi√in (22 MPa√m). The difference in behavior is likely due to the different values of K_{max} at which static crack growth is significant. 725 clearly exhibited steady state crack growth rate in the range of 25 to 50 ksi√in (27.5 to 55 MPa√m), while 955 did not exhibit static crack growth even at 60 ksi√in (66 MPa√m). The difference in behavior of the different alloys could be associated with the fact that 725 is known to have sigma phase on the grain boundaries which has been suggested to increase susceptibility to HE[4, 5]. This may be a likely reason for the increased susceptibility for 725 compared to 955 and 945X.



a) FCGR of 725, 955, and 945X at ΔK values of 22 and 44 MPa√m and 1 mHz



b) FCGR of 725, 955, and 945X at ΔK values of 22 and 44 MPa m^{1/2} and 0.1 mHz.

Figure 41: FCGR as a function of ΔK for 725, 955, and 945X at 1 mHz and 0.1 mHz in seawater under cathodic polarization at -1050 mV SCE.

6.2 Static Crack Growth Rate of PH Nickel Alloys

A summary of the static crack growth behavior of the various PH nickel alloys under seawater + CP conditions, developed in this program as well as data in literature on 718 and 625+ are added for reference are shown in Figure 42.

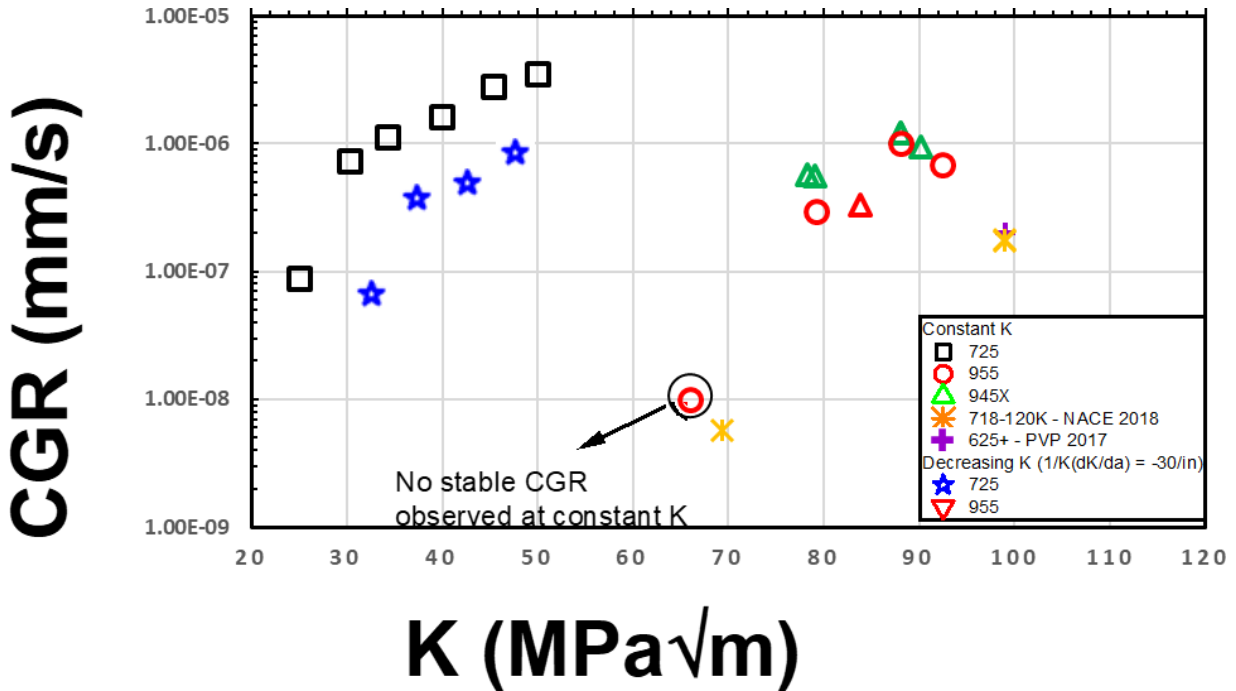


Figure 42: Crack growth rate as a function of K at constant K and under decreasing K for 725, 955, 945X, 718, and 625+ in 3.5 wt% NaCl at -1050 mV SCE.

Table 32: Numerical values for Figure 42

K (MPa√m)		CGR (mm/s) -1050mV SCE/Constan t K	K (MPa√m)		CGR (mm/s) -1050mV SCE/Decreasin g K	DNVGL Log ID
1.1*A			1.1*D			
50	55	3.51E-06	47.67	52.437	8.17E-07	2810
45.3463	49.88093	2.78E-06	42.74	47.014		
39.90258	43.89283	1.64E-06	37.42	41.162	3.66E-07	
34.30429	37.73472	1.12E-06	32.63	35.893	6.40E-08	
30.23802	33.26182	7.25E-07				
25	27.5	8.83E-08				
80	88	1.00E-06				
84	92.4	6.87E-07				
72	79.2	2.93E-07				
60	66	1.00E-08				
80	88	1.22E-06	76.15	83.765	3.30E-07	2805
79	--	7.85E-07	76.6	84.26	1.26E-07	
80	88	1.22E-06				

K (MPa√m)		CGR (mm/s) -1050mV SCE/Constant K	K (MPa√m)		CGR (mm/s) -1050mV SCE/Decreasing K	DNVGL Log ID
1.1*A			1.1*D			
71.92457	79.11703	5.55E-07				
82	90.2	9.35E-07				
71.20612	78.32673	5.70E-07				
90	99	1.72E-07				
90	99	1.76E-07				
63	69.3	5.68E-09				
90	99	2.00E-07				

It is clear from the data that 725 is significantly more susceptible to H embrittlement than 955 and 945X. Under constant K conditions, a K value of 30 ksi√in (33 MPa√m) is needed to sustain a crack growth rate of 10⁻⁶ mm/s while K values of about 80 ksi√in (88 MPa√m) are needed to sustain similar crack growth rates in 955 and 945X. There doesn't appear to be any significant difference between the behavior of 955 and 945X at these levels of crack growth rate. It is also interesting to note that for both 718 and 625+ even at 90 ksi√in (99 MPa√m) the crack growth rate is only about 2×10⁻⁷ mm/s. The higher susceptibility of 725 is consistent with recent work performed on 725 which exhibited significant susceptibility (~45% reduction in threshold stress) to environmentally assisted cracking. This is in contrast to behavior of 625+, a similar alloy (with slightly higher Ni content) which exhibited only a 20% reduction in the threshold stress[4]. The higher resistance of 625+ to HE is also supported by observations of significantly slower crack growth rate at 90 ksi√in (99 MPa√m)[10] as well as measured K_{th} values which are higher under comparable values of cathodic polarization[11]. The increased susceptibility of 725 compared to a similar alloy of 625+ was attributed to formation of sigma phase along grain boundaries. The observed high crack growth rate and low value of K_{th} for 725 is likely due to decoration of sigma phase along the grain boundary.

Crack growth rate measured at constant K for 725 is higher than that measured under decreasing K by about a factor of 3-4 over a wide range of K, which is similar to the behavior observed for 955 albeit at higher values of K. The effect of K-gradient/loading mode on the crack growth rate has been observed in earlier work for seawater + CP conditions for similar precipitation hardened alloys like 718[7] and K-500[12]. However, in prior work the effect of a positive K-gradient was explored, which indicated that under an increasing K profile, crack growth rate values were significantly higher than under a constant K profile[7]. The role of constant K/load was explored in K-500 by transitioning a rising displacement test to constant load, which resulted in not only a sharp decrease in crack growth rate but also led to what appeared to be ductile tearing suggesting that the crack propagation was not environmentally assisted[12]. The effect of decreasing K-rate under cathodic polarization on crack growth rate, was explored on a single test by varying K-rate over several orders of magnitude[13]. The crack growth rate of 718 varied sharply with K-rate and at very low K-rate (~0.05 MPa√m/h) exhibited evidence of slip band based transgranular cracking[13]. However, with careful transitioning and testing under constant K conditions there was evidence of mixed mode of cracking exhibiting both intergranular as well as slip band based transgranular cracking[7].

The effect of K-gradient on the crack growth rate behavior is not confined to PH nickel alloys and similar observations have been made in hydrogen charged F22[14] as well as in line pipe steels in high pressure hydrogen[15].

6.2.1 Effect of Applied Potential

The effect of applied potential on the crack growth rate behavior of 955 and 945X are summarized in Figure 43. The crack growth rate of 955 is significantly lower than 945X at ~ 72 ksi $\sqrt{\text{in}}$ (79.2 MPa $\sqrt{\text{m}}$). Over the range of applied potential from -1150 mV to -900 mV SCE, the crack growth rate of 945X is about 5 times higher than that of 955 and the ratio appears to be largely independent of applied potential. It is interesting to note that at higher values of K (~ 80 to 84 ksi $\sqrt{\text{in}}$ (88 to 92.4 MPa $\sqrt{\text{m}}$)) for 955 the crack growth rate is higher and in the potential range of -1050 mV to -950 mV SCE the crack growth rate is largely independent of applied potential. The effect of applied potential on crack growth rate has been evaluated in K-500 under rising displacement conditions[12, 16]. At 50 MPa $\sqrt{\text{m}}$ there was no significant effect of applied potential on the crack growth rate in the range of -1150 mV to -1000 mV SCE[12]. A ~ 5 -7 times change in crack growth rate was observed as the potential varied from -1000 mV to -800 mV SCE before exhibiting threshold behavior at -750 mV SCE[12].

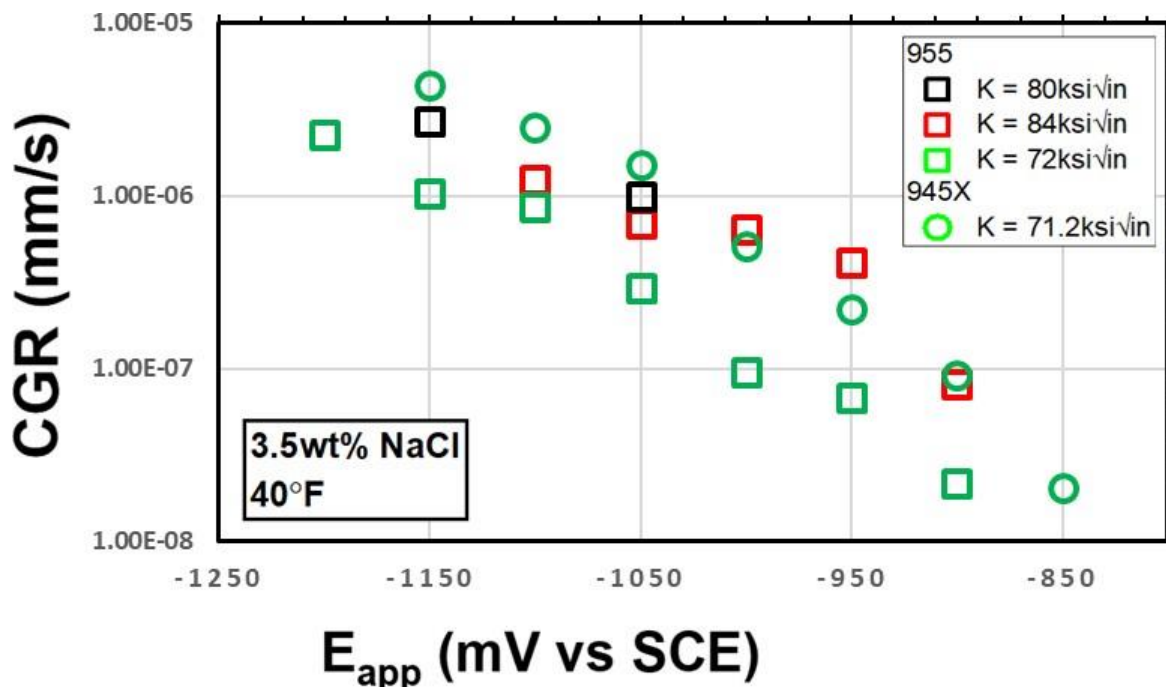


Figure 43: Effect of applied potential on crack growth rate for 955 and 945X.

Table 33: Numerical values for Figure 43

K (KSI√in)	CGR (mm/s) -1050mV SCE	E _{app} (mV SCE)	CGR (mm/s) 80MPa√in	CGR (mm/s) K = 84MPa√in
80	1.00E-06	-1150	2.72E-06	
72.8	--	-1100	--	
		-1050	1.00E-06	
72.8	--	-1100		1.24E-06
		-1050		6.87E-07
		-1000		6.40E-07
		-950		4.09E-07
		-900		8.06E-08
80	4.36E-06	-1150		
79	2.47E-06	-1100		
80	1.50E-06	-1050		
71.92457	5.11E-07	-1000		
82	2.21E-07	-950		
71.20612	9.24E-08	-900		
	2.03E-08	-850		
72	2.24E-06	-1200		
72	1.03E-06	-1150		
72	8.67E-07	-1100		
72	2.93E-07	-1050		
72	9.53E-08	-1000		
	--	-975		
72	6.82E-08	-950		
72	2.18E-08	-900		

6.3 Implications for Oil and Gas Industry

The program performed herein was aimed at understanding the behavior of novel materials that could be used in O&G applications. The emphasis of this work was to understand the response of these materials in environments that are relevant to HPHT conditions. The intent was to develop quantitative data that can be used for design and/or life extension purposes. The development of quantitative data to assess damage also provides a frame work to make clear comparisons between the performances of these materials. The results of the program support the following summary of findings and recommendations:

6.3.1 Sour Service

In the sour environment tested over a range of loading conditions, it was found that four of the five high strength nickel-based alloys exhibited excellent resistance to environmentally assisted fatigue. 825 was the only alloy that exhibited some degree of susceptibility in sour environment. This was clearly evident from the fact that the FCGR did not exhibit a frequency dependence over a wide range of frequencies. Hence, even in conditions associated with start-up and shutdown, it is reasonable to suggest that there is unlikely to be any environmentally assisted fatigue response. Under similar loading conditions, four of the five materials exhibited similar FCGRs.

6.3.2 Seawater + CP

The precipitation hardened nickel based alloys however, did exhibit significant susceptibility to environmentally assisted fatigue in seawater + CP conditions. FCGR increased with decreasing frequency and there was no obvious evidence of a plateau at low frequencies, as has been observed for steels in sour service. This would suggest that when designing for very low frequency events, it is important to characterize not only the magnitude of the loads, but also the frequency of the cycle to make an accurate assessment of the FCGR to be used in design. The FCGR at low frequencies (0.1 mHz) for 725 was about 20 times higher than the mean BS7910[9] curve values for steel, while those for 945X and 955 were similar with about 7 times higher than the mean BS7910 curve values[9]. All the precipitation hardened alloys exhibited static crack growth rate under the conditions evaluated. 725 exhibited the highest static crack growth rate, while 955 exhibited the lowest static crack growth rate of all the PH nickel-based alloys. The static crack growth rate of 945X, and 955 is very sensitive to the applied potential, with the crack growth rates falling sharply at -900 to -850 mV SCE. This suggests that if low voltage anodes could be used for subsea applications, it is possible to consider the use of high strength materials like 945X, and 955. The use of 725 presents an interesting dilemma, since it has excellent performance in sour service environments even at 400°F but has extremely poor resistance to cracking in seawater + CP conditions. In scenarios where sour service behavior is critical, the CP design may have to be optimized to use of 725. It is interesting to note that cold worked nickel-based alloys C22HS, and 825 both exhibit excellent resistance to environmentally assisted fatigue and exhibit no evidence of any static crack growth rate under the conditions evaluated. It is possible to consider these materials in subsea applications. However, C22HS is relatively more expensive than the other alloys, and may not be available in the range of sizes that are desired. Cold worked material like 825 and potentially other variants could be considered for some applications. However, as in the case of C22HS it may be challenging to make large forgings with uniform through thickness properties out of cold worked material. It would be useful to consider evaluating some of the newly developed cold worked alloys to enhance the portfolio of alloys available for materials selection.

6.3.3 Seawater at OCP

All the materials evaluated here, have excellent resistance to localized corrosion as measured by the critical crevice temperature in 3.5 wt% NaCl at +700 mV SCE. These materials are unlikely to experience localized corrosion in seawater environments. The corrosion fatigue behavior in seawater under OCP is independent of frequency for all the materials (in the loading conditions studied). This suggests that none of these materials are susceptible to environmentally assisted fatigue (in the

loading conditions evaluated). In the absence of cathodic protection, environmentally assisted fatigue at OCP is expected to be driven by a chloride-SCC mechanism. The absence of environmentally assisted fatigue is consistent with the excellent resistance to localized corrosion. In choosing alloys that may not be subject to CP, like in top side applications, it is important to note that if process conditions are warm and seawater misting can occur, it is important to play close attention to the critical crevice temperature. Alloy selection would have to be based not only on the sour service process fluids (which tend to be deaerated) but also on the possibility of localized corrosion on the external surfaces from seawater misting.

In summary, materials selection for subsea applications is complex that requires multiple considerations. The basic material properties like yield strength, ductility, and charpy values play a significant role in the selection of materials for specific subsea applications. It is not only important to evaluate the performance of the material in a range of environment and loading conditions, but also to understand the resistance to localized corrosion, in making materials selection decision and design of various components. While the current program was focused on some of the key materials of interest, there is data in literature on the behavior of materials like 718-120K, and 150K. A comparison of the critical crevice temperature, and the K_{th} values in seawater + CP at -1050 mV SCE for the various materials tested in this program along with those of 718 is shown below in Table 6.

A few interesting trends emerge from the data, the resistance to localized corrosion is broadly consistent with the alloying elements (Cr, Mo, and Nb) with 718 exhibiting the lowest CCT, while C22HS exhibits the highest resistance. The relative ranking for resistance to localized corrosion resistance is

C22HS>725>955>825/945X>718

However, with respect to hydrogen embrittlement (HE) behavior, there is no obvious trend with either yield strength, or the composition. This suggests that microstructural effects play a significant role and need to be understood. The relative ranking for resistance of HE is

C22HS>718-150K>718-120K>945X/955>725

Table 34: Comparison of the K_{th} in seawater at -1050 mV SCE, and critical crevice temperature of various alloys tested in this program with 718-120K and 150K in seawater.

Material	YS (ksi)	CCT (+700mV SCE)	K_{th} (ksi√in) at -1050mV SCE	K_{th} (MPa√m) at -1050mV SCE
825	127	24.2	>60	>66
945X	149	23.6	50-60	55 - 66
718-120K	136	~20	66	72.6
718-150K	161	~20	90	99
955-140K	147	44.9	50-60	55 - 66
725	131	66.6	25	27.5
C22HS	190	>95C	>90	>99

718-150K has excellent resistance to HE in seawater at -1050 mV SCE, with K_{th} values similar to C22HS. There is very little information on the behavior of 718-150K in sour service conditions. However, given that the chemistry of the 150K is similar to that of the 120K, it is expected that the resistance to localized corrosion in sour environments is likely similar to that of 718-120K. The susceptibility to cracking is likely influenced not only by the resistance to localized corrosion but also

the yield strength, and microstructure. To develop a larger database of material properties, it would be useful to develop properties for 718-150K in sour service conditions.

Another, observation from this work was the superior resistance of the coldworked materials to HE under seawater + CP conditions. It is proposed that additional materials like ATI-830 (140K) be evaluated for HE resistance.

7 SUMMARY

Environmentally assisted cracking of high strength precipitation hardened (PH) nickel based alloys 725, 945X, 955, as well as cold worked C22HS, and 825 were evaluated in environments relevant to subsea high pressure and high temperature (HPHT) applications. The primary environments of interest in this effort were 3.5 wt% NaCl, at pH 8.2 with and without cathodic polarization (CP) at low temperatures, and sour production environments at elevated temperature and pressure. Materials were evaluated in the sour production environment at 350°F/400°F (177°C/204°C), with 125 psia CO₂ and 0.08 psia H₂S. Fatigue crack growth rate (FCGR) and static crack growth rate measurements were performed in both the environments. The results of the program are summarized below:

Sour Service

In sour environments, the alloys exhibited excellent resistance to environmentally assisted fatigue and stress corrosion cracking. FCGR in four of the five tested alloys at (725, 945X, 955, C22HS) did not exhibit a frequency dependence, when tested over a range of ΔK values. These alloys also did not exhibit any evidence of static crack growth rate up to a stress intensity factor (90 ksi $\sqrt{\text{in}}$ (99 MPa $\sqrt{\text{m}}$). However, 825 did exhibit susceptibility when tested at a K_{max} of 50 ksi $\sqrt{\text{in}}$ (55 MPa $\sqrt{\text{m}}$). At a lower K_{max} value of 25 ksi $\sqrt{\text{in}}$ (27.5 MPa $\sqrt{\text{m}}$) there was no evidence of environmental effect as evident from the FCGR being frequency independent over a range of frequencies.

Seawater + Cathodic Polarization

FCGR of all the PH nickel-based alloys under CP exhibits a strong dependence on frequency in the range of 0.3 Hz to 0.1 mHz, at two different values of ΔK (40 ksi $\sqrt{\text{in}}$ /44M Pa $\sqrt{\text{m}}$ and 20 ksi $\sqrt{\text{in}}$ /22 MPa $\sqrt{\text{m}}$). A comparison of the FCGR behavior suggests that 725 exhibited the highest susceptibility, while the FCGR of 955 and 945X were lower similar to each other but lower than 725. In all the PH nickel-based alloys, stable static crack growth rate (CGR) was observed. Static crack growth rate of 10⁻⁶ mm/s (under constant K conditions) was obtained on 725 at 50 ksi $\sqrt{\text{in}}$ (55 MPa $\sqrt{\text{m}}$). However, for 945X and 955, a static crack growth rate of 10⁻⁶ mm/s was observed at a higher K value of 80 ksi $\sqrt{\text{in}}$ (88 MPa $\sqrt{\text{m}}$) for 945X and 955. Applied potential in the range of -1050 mV to -850 mV SCE had a significant effect on the crack growth rate, with crack growth rate of 945X and 955 decreasing sharply with decreasing cathodic potential. The measured crack growth rate at -850mV SCE for 945X and 955 was very low on the order of 10⁻⁸ mm/s. In considering the use of high strength PH nickel-based alloys, it is recommended that methods to control the cathodic protection potential to values below - 1050 mV SCE be considered. FCGR of the cold worked nickel-based alloys C22HS, and 825 did not exhibit a frequency dependence. For both these alloys (C22HS and 825), there was no evidence of static crack growth. This suggests that under these conditions, C22HS and 825 were resistant to environmentally assisted fatigue and static crack growth.

Seawater at Open Circuit Potential (OCP)

The resistance to seawater exposure in the absence of cathodic protection, was evaluated, by performing critical crevice temperature tests in 3.5 wt% NaCl. The critical crevice temperature increased with increasing alloy content of Chromium (Cr), Molybdenum (Mo), and Tungsten (W). Alloy 825, and 945X exhibited the lowest critical crevice temperature, at ~24°C. Increasing Cr, Mo, and W content resulted in increasing critical crevice temperature. C22HS did not exhibit any evidence of crevice attack even at temperatures as high as 95°C. The resistance to environmentally assisted

fatigue behavior was also evaluated at OCP for all the alloys at 15.6°C (60°F). The FCGR did not vary with frequency in any of the materials, consistent with excellent resistance to environmentally assisted fatigue at OCP.

8 REFERENCES

- [1] R. Thodla, L. Cao, J. Hawk, and M. Ziomek-Moroz, "Relationship Between Localized Corrosion and Stress Corrosion Cracking of Nickel Based Alloys in HPHT Oil and Gas Environments," in *CORROSION 2016*, 2016: NACE International.
- [2] T. Cassagne, M. Bonis, D. Hillis, and C. Duret, "Understanding Field Failures of Alloy 718 Forging Materials in HPHT wells," presented at the EUROCORR, 2008.
- [3] P. Nice, R. Strong, W. M. Bailey, G. Rørvik, J. H. Olsen, and T. G. Mobberley, "Hydrogen embrittlement failure of a precipitation hardened nickel alloy subsurface safety valve component installed in a North Sea seawater injection well," in *CORROSION 2014*, 2014: NACE International.
- [4] M. Iannuzzi, M. M. Morra, A. H. Qvale, T. Frydenberg, I. Osen, and R. M. Thompson, "Hydrogen Stress Cracking of Nickel Alloy UNS N07725 — Part II: Correlation between Microstructure and Hydrogen Stress Cracking Resistance of Ni-Cr-Mo-Nb age hardened alloys," presented at the CORROSION, Phoenix, 2018.
- [5] M. Iannuzzi, M. M. Morra, A. H. Qvale, T. Frydenberg, I. Osen, and R. M. Thompson, "Hydrogen Stress Cracking of Nickel Alloy UNS N07725 — Part I: A Field Failure Investigation and Potential Impact on Future Quality Control," presented at the CORROSION, Phoenix, 2018.
- [6] *ASTM E647 — Standard Test Method for Measurement of Fatigue Crack Growth Rates*, 2015.
- [7] R. Thodla, "Environmentally Assisted Cracking of High Strength Nickel Based Alloys Under Cathodic Protection," in *CORROSION 2018*, 2018: NACE International.
- [8] A. Turnbull and A. T. May. (1983) Cathodic Protection of Crevices in BS 4360 50D Structural Steel in 3.5% NaCl and in Seawater. *Materials Performance*.
- [9] B. S. Institution, *Guide on methods for assessing the acceptability of flaws in metallic structures*. British Standard Institution, 1999.
- [10] R. Thodla, C. Holtam, and R. Saraswat, "Development of a Novel Test Method to Characterize Material Properties in Corrosive Environments for Subsea HPHT Design," in *ASME 2017 Pressure Vessels and Piping Conference*, 2017, pp. V005T05A005–V005T05A005: American Society of Mechanical Engineers.
- [11] M. Koul and E. Knudsen, "Environmentally Assisted Cracking Evaluation of a Large UNS N07725 Forging Under Cathodic Protection Conditions," *Corrosion*, vol. 68, no. 5, pp. 449–460, 2012.
- [12] R. P. Gangloff, H. M. Ha, J. T. Burns, and J. R. Scully, "Measurement and modeling of hydrogen environment-assisted cracking in Monel K-500," *Metallurgical and Materials Transactions A*, vol. 45, no. 9, pp. 3814–3834, 2014.
- [13] R. Thodla, B. C. Rollins, H. M. Scott, and C. Holtam, "Effect of Strain Rate on the Fatigue and Static Crack Growth Rate of UNS N07718 Under Cathodic Polarization," in *CORROSION 2017*, 2017: NACE International.
- [14] A. M. Al-Rumaih and R. P. Gangloff, "Measurement and Modeling of Temperature Dependent Internal Hydrogen Assisted Cracking in Cr-Mo Steel," in *International Hydrogen Conference (IHC 2012)*, 2014: ASME Press.
- [15] K. A. Nibur, B. P. Somerday, C. San Marchi, J. W. Foulk, M. Dadfarnia, and P. Sofronis, "The relationship between crack-tip strain and subcritical cracking thresholds for steels in high-pressure hydrogen gas," *Metallurgical and Materials Transactions A*, vol. 44, no. 1, pp. 248–269, 2013.
- [16] Z. D. Harris, J. D. Dolph, G. L. Pioszak, B. C. R. Troconis, J. R. Scully, and J. T. Burns, "The Effect of Microstructural Variation on the Hydrogen Environment — Assisted Cracking of Monel K-500," *Metallurgical and Materials Transactions A*, vol. 47, no. 7, pp. 3488–3510, 2016.

9 LIST OF VARIABLES AND ACRONYMS

List of Variables	
Δa	Increment in crack length (mm)
ΔK	Amplitude of Stress Intensity Factor (MPa \sqrt{m})
a	Crack length (mm)
a/W	Crack length to width
B	Specimen Thickness (mm)
C	Constant Representing K-profile (/mm)
dK/da	K-gradient (MPa $\sqrt{m/mm}$)
E_{app}	Applied Potential (mV)
f	Volume fraction of particles
K	Stress Intensity Factor (MPa \sqrt{m})
K_{max}	Maximum Value Stress Intensity Factor
K_{min}	Minimum Value Stress Intensity Factor
K_0	Initial Stress Intensity Factor (MPa \sqrt{m})
p	Partial Pressure (psia)
R	Ratio of K_{min}/K_{max}
W	Specimen width (mm)

List of Acronyms	
CP	Cathodic Polarization
CGR	Crac Growth Rate
DCPD	Direct Current Potential Drop
FCGR	Fatigue Crack Growth Rate
HE	Hydrogen Embrittlement
HPHT	High Pressure High Temperature
HRC	Hardness Rockwell C
OCP	Open Circuit Potential
PH	Precipitation Hardened
PTFE	Poly Tetra Fluro Ethylene
PREN	Pitting Resistance Equivalent Number
SCE	Saturated Calomel Electrode
YS	Yield Strength

About DNV GL

Driven by our purpose of safeguarding life, property and the environment, DNV GL enables organizations to advance the safety and sustainability of their business. We provide classification and technical assurance along with software and independent expert advisory services to the maritime, oil and gas, and energy industries. We also provide certification services to customers across a wide range of industries.

Operating in more than 100 countries, our 16,000 professionals are dedicated to helping our customers make the world safer, smarter and greener.

This page left intionally blank

APPENDIX C:

CORROSION TESTING REPORT (HONEYWELL CORROSION SOLUTIONS)

The following is the report for 6-, 12-, 18-, and 48-week testing conducted by Honeywell Corrosion Solutions. The report has been slightly reformatted but otherwise is as provided at the conclusion of testing and their analyses.

Report No. TS3333PH Rev2

Final Report: Extended Duration Corrosion Testing of Five Ni-base

HONEYWELL CORROSION SOLUTIONS (HCS)

11201 Greens Crossing Blvd.
Suite 700
Houston, TX 77067-4458
281.444.2282

Report No. TS3333PH Rev2

Project Final Report

**Extended Duration Corrosion Testing of Five Ni-base Corrosion
Resistant Alloys (CRAs) at 15,000 psig and 350°F**

July 11, 2019

Prepared for

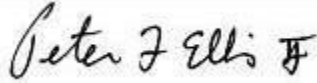
Mr. Maurice Peltier
Aiken Engineering

9720 Cypresswood Drive, Suite 340 Houston, TX 77070

This report documents work performed by Honeywell International, Inc. (Honeywell), Houston, TX, for Aiken Engineering, Houston, Texas, on behalf of Argonne National Laboratory and the U.S. Bureau of Safety and Environmental Enforcement (BSEE) under Aiken purchase order PN2456HCS-61-2017.

Prepared by:

Reviewed by:



Peter F. Ellis II
Lab Engineering Team Leader
Peter.ellis2@honeywell.com

Sridhar Srinivasan
Global Business Leader, Corrosion
Sridhar.srinivasan@honeywell.com

Final Report No. TS3333PH Rev2
Extended Duration Corrosion Testing of Five Ni-base
Corrosion Resistant Alloys at 15,000 psig and 350°F



Table of Contents

1.0	Introduction	1
2.0	Objective	1
3.0	Technical Approach	1
3.1	Cited Standards	1
3.2	Overview	2
3.3	Specimens and Mechanical Test Results Supplied by Westmoreland	3
3.4	Reagent and Gas Purity	3
3.5	Test Procedures	4
3.5.1	C-ring Strain-Deflection Calibration	4
3.5.2	VHP Autoclave Set-up	5
3.5.3	Solution Preparation	6
3.5.4	Specimen Preparation	6
3.5.5	Autoclave Loading	7
3.5.6	Replenishment	7
3.5.7	Test Shutdown and Specimen Recovery	8
3.5.8	Post-Test Analysis Procedure	8
4.0	Results	10
4.1	Westmoreland Test Results	10
4.1.1	Charpy V-Notch Impact Energy Tests	10
4.1.2	Uniaxial Tensile Test Results	10
4.2	Strain-Deflection Calibration Results	10
4.3	Test Solution pH Measurements	11
4.4	Actual vs Nominal Exposure Times at Temperature and Pressure	11
4.5	Test I (6-week exposure) Corrosion and Cracking Results	11
4.6	Test II (12-week exposure) Corrosion and Cracking Results	12
4.7	Test III (18-week exposure) Corrosion and Cracking Results	12
4.8	Test IV (48-week exposure) Corrosion and Cracking Results	12
5.0	Discussion	13
5.1	Alloy Composition and Anticipated Corrosion and SCC Behavior	13
5.2	Statistical Analysis of the Coupon Mass-Loss and Corrosion Rate Data	13
5.2.1	Side-by-Side Comparison of Mass-Loss and Corrosion Rates	13
5.2.2	Source of Scatter in Corrosion Rates of Duplicate Coupons	14
5.2.3	Lack of Discernable Corrosion Rate Trend with Time	15
5.3	C-ring Cracking Test Results	15
6.0	Conclusions	15

Final Report No. TS3333PH Rev2
Extended Duration Corrosion Testing of Five Ni-base
Corrosion Resistant Alloys at 15,000 psig and 350°F

List of Table and Figures

Table 1. Initially Specified Environmental Test Matrix and Replenishment Schedule	17
Table 2. Final Environmental Test Matrix and Replenishment Schedule Approved by the Sponsors	17
Table 3. Alloy Test Matrix per Autoclave Test	18
Table 4. Test Specimens Delivered by Westmorland	19
Table 5. CRA Composition Data	19
Table 6. Charpy V-Notch Impact Toughness Results Provided by Westmoreland	20
Table 7. Mechanical Test Results Provided by Westmoreland	21
Table 8. C-ring Strain-Deflection Calibration Data	22
Table 9. Adjusted Target C-ring Deflection Calculations	22
Table 10. pH Measurement Results during Tests I through IV	23
Table 11. Nominal vs. Actual Exposure Times at Temperature and Pressure	23
Table 12. Test I (6-Week Exposure) – Corrosion Rate and Pitting Results	24
Table 13. Test I (6-week exposure) – C-ring Test Results	24
Table 14. Test II (12-Week Exposure) – Corrosion Rate and Pitting Results	25
Table 15. Test II (12-week exposure) – C-ring Test Results	25
Table 16. Test III (18-Week Exposure) – Corrosion Rate and Pitting Results	26
Table 17. Test III (18-week exposure) – C-ring Test Results	26
Table 18. Test IV (48-Week Exposure) – Corrosion Rate and Pitting Results	27
Table 19. Test IV (48-week exposure) – C-ring Test Results	27
Table 20. Statistical Summary of Coupon Mass-Loss and Corrosion Rate Data	28
Table 21. Scatter Analysis Between Duplicate Coupons in the Same Test	28
Figure 1. The Three HCS Very High Pressure (VHP) Autoclaves	29
Figure 2. Specimen Test Rack Ready for Autoclave Insertion	30
Appendix A: Test I, Post-Exposure Specimen Photographs	31–40
Appendix B: Test II, Post-Exposure Specimen Photographs	41–50
Appendix C: Test III, Post-Exposure Specimen Photographs	51–56
Appendix D: Test IV, Post-Exposure Specimen Photographs	57–66

Disclaimer

Neither Honeywell nor any person acting on behalf of Honeywell:

- Assumes any liability for consequences or damages resulting from the use, misuse, or reliance upon the information disclosed in this report.

Final Report No. TS3333PH *Rev2*

Extended Duration Corrosion Testing of Five Ni-base

Corrosion Resistant Alloys at 15,000 psig and 350°F

- Makes any warranty or representations that the use of any information, apparatus, method, or process disclosed in this report may not infringe on privately-owned rights.

Final Report No. TS3333PH Rev2

Extended Duration Corrosion Testing of Five Ni-base

Corrosion Resistant Alloys at 15,000 psig and 350°F

1.0 Introduction

Acting through a third party (Aiken Engineering), the Sponsors, the Bureau of Safety and Environmental Enforcement (BSEE) and its proxy, Argonne National Laboratory (ANL) contacted Honeywell Corrosion Solutions (HCS) with a Request for Proposals to conduct four autoclave exposures of five nickel-based corrosion resistant alloys with low levels of H₂S in methane at total pressures of 15,000 psig at 350°F. HCS was contacted because its Technical Services Laboratory (TSL) has three autoclaves and the supporting safety and environmental protection infrastructure required to perform high-pressure, high temperature corrosion tests with highly toxic and flammable H₂S/CH₄ atmospheres at pressures up to 20,000 psig at temperatures up to 550°F.

This testing program was conceived by the Sponsors as a series of four extended duration cracking susceptibility tests of 6-, 12-, 24-, and 48-weeks as compared to the 30day test duration specified by NACE MR0175 ISO 15150-3 (2015), Annex B. Ultimately, the Sponsors shortened the duration of Test III from 24 weeks to 18 weeks to fit within the schedule of the larger test program of which the Honeywell Testing Program was but one element.

2.0 Objective

The original objective of the HCS Testing Program was to conduct 6-, 12-, 24-, and 48week autoclave exposures of five nickel-based corrosion resistant alloys (CRAs) in 20 wt% NaCl brine with 0.05 psia H₂S in methane at autoclave total pressures of 15,000 psig at 350°F, determining both the corrosion behavior (weight-loss corrosion rate, pitting susceptibility, and crevice corrosion susceptibility) and the stress corrosion cracking (SCC) behavior, using corrosion coupons and NACE TM0177 Method C C-ring specimens, respectively.

The modified objective of the HCS Testing Program was to conduct 6-, 12-, 18-, and 48week autoclave exposures of the same alloys under the same test conditions.

3.0 Technical Approach

3.1 Cited Standards

1. ANSI/NACE MR0175/ISO 15156-3:2015, "Petroleum, Petrochemical, and Natural Gas Industries – Materials for use in H₂S-containing environments in oil and gas production – Part 3: Cracking-resistant CRAs (corrosion-resistant alloys) and other alloys – Annex B (normative) Qualification of CRAs for H₂S Service by laboratory testing."
2. ANSI/NACE TM0177-2016 – "Laboratory Testing of Metals for Resistance to Sulfide Stress Cracking and Stress Corrosion Cracking in H₂S Environments, Method C (NACE C-ring Test)."
3. ASTM G1-2017, "Standard Practice for Preparing, Cleaning, and Evaluating Corrosion Test Specimens."

3.2 Overview

Table 1 shows the initially specified Environmental Test Matrix and Replenishment Schedule, while Table 2 shows the final schedule. Both tables show that the total exposures greater than six weeks were divided into six-week segments with brine and headspace gas replenishments between successive exposure segments. The brine charge for each exposure segment was 20 wt% NaCl brine prepared from reagent-grade NaCl and distilled water with the pH adjusted to 4.0 at room temperature and atmospheric pressure using dilute reagent-grade HCl. The chloride concentration of the resulting brine was 121,353 mg/kg (139,223 mg/L).

The autoclave headspace gas charge consisted of a certified mixed gas containing 3.3 ppmv H₂S, 8,325 ppmv CO₂, balance methane, resulting in nominal H₂S and CO₂ partial pressures of 0.050 and 125 psia, respectively, at 15,000 psig total pressure.

Table 3 shows that two weight-loss corrosion coupons of each of the five CRAs were exposed and evaluated for uniform (weight-loss) corrosion rate and pitting susceptibility. This table also shows each of the nickel-base CRAs, except Alloy 825⁴, was evaluated for susceptibility to stress corrosion cracking (SCC) in each exposure using NACE C rings (TM0177 Method C), one of the most widely used specimen configurations for environmentally assisted cracking (EAC) evaluation.

One C-ring of each of CRA except Alloy 825 was exposed in electrical isolation from other specimens or the autoclave walls, while the other was galvanically coupled to a pair of sacrificial carbon steel anodes in the form of carbon steel corrosion coupons.

Standard NACE MR0175 ISO 15150-3 (2015), Annex B addresses the following three modes of environmentally assisted cracking (EAC):

1. Stress Corrosion Cracking (SCC) proceeds by a high-temperature anodic active path-dissolution mechanism. Testing for SCC is performed by exposing stressed specimens to the environment in question at the maximum temperature.

⁴The specimens for the HCS testing program were machined by Westmoreland Mechanical Testing & Research, Inc. Ultimately, Westmoreland was unable to deliver the required Alloy 825 C-rings, and the Sponsors decided to proceed without the Alloy 825 C-rings.

Final Report No. TS3333PH Rev2

Extended Duration Corrosion Testing of Five Ni-base

Corrosion Resistant Alloys at 15,000 psig and 350°F

2. Sulfide Stress Cracking (SSC) is a low temperature stress cracking phenomenon driven by absorption of corrosion engendered atomic hydrogen into the metal lattice. Testing for SSC is performed by exposing stressed specimens to the environment in question at the specified temperature of 75°F.
3. Galvanic Hydrogen Stress Cracking (GHSC) is essentially an accelerated form of SSC that may occur when a CRA is galvanically coupled to carbon steel. Testing for GHSC is performed by exposing stressed specimens to the environment in question at the specified temperature of 75°F.

Thus, the C-rings exposed in these autoclaves all constituted tests for susceptibility to anodic active-path driven SCC. None provided indications of susceptibility to atomic hydrogen absorption driven cracking phenomena (SSC, GHSC). While the configurations of the CRA C-rings galvanically coupled to carbon steel coupons were identical to the configurations used for GHSC testing, these specimens could provide no information regarding GHSC susceptibility, which has a specified test temperature of 75°F.

3.3 Specimens and Mechanical Test Results Supplied by Westmoreland

Table 4 lists the test specimens provided by Westmoreland, Inc. (contracted by the Sponsors to supply test specimens to HCS). Note that the sponsors elected to forego exposure of Alloy 825 C-rings and only coupons of this alloy were exposed.

Table 5 summarizes the alloy composition data available for the supplied CRA specimens.

The nickel-base test coupons were nominally 1.5 inches long by 0.75-inches wide by 0.125 inches thick with a centered 0.255-inch diameter mounting hole. Westmoreland also provided forty X70 pipeline carbon steel coupons of the same dimensions to be used as anodes for the galvanically coupled SCC tests.

The OD of the C-rings was 1.5-inches with a width of 0.75 inches and a thickness of 0.10 inches with diametrically opposing 0.255-inch diameter mounting holes.

Westmoreland also performed the pre-requisite uniaxial mechanical testing required for proper loading of C-ring specimens, determining the actual 0.2% offset yield strengths at both 75°F and 350°F, referred herein as AYS_{75} and AYS_{350} as well as the strains corresponding to the AYS values, referred to as the critical strains. The resulting data are contained in Table 6.

3.4 Reagent and Gas Purity

The NaCl and HCl used for formulation of the brine were of analytical reagent (AR) purity.

Nitrogen was ultra-high purity (UHP) grade.

CO₂ was chemically pure (CP) grade.

The Certified Mixed Gas contained 3.3 ppmv H₂S, 8,325 ppmv CO₂, balance methane. At 15,000 psig total pressure, the nominal partial pressures of H₂S and CO₂ were 0.05 psia and 125 psia, respectively.

3.5 Test Procedures

3.5.1 C-ring Strain-Deflection Calibration

NACE TM0177 (2016) provides an equation to calculate the deflection required to apply a given stress to carbon and low alloy steels but specifically cautions that this equation is not applicable to many corrosion-resistant alloys, including nickel-base alloys. Instead, TM0777 (2016) prescribes an empirical method in which the critical strain is determined from a uniaxial tensile specimen at the specified test temperature. A strain-gauged C ring is then deflected until the outer-fiber strain at the apex equals the critical strain, and the required deflection is measured **Definitions**

- The critical strain is the strain corresponding to 100% of the yield stress in a uniaxial tensile specimen at the intended test temperature.
- The C-ring target deflection is the C-ring deflection required to impart the critical strain on the outer fibers of the apex of the C-ring specimen allowing for thermal relaxation of the C-ring upon heating from room temperature.

C-ring Strain-Deflection Calibration Procedure

The following procedure was used to determine the C-ring Target Deflections for this project

1. A circumferentially oriented strain gauge was mounted a on the apex of one C-ring of each material.
2. The strain-gauged C-ring of each material was assembled finger-tight with loading hardware and connected to a micro-strain meter.
3. The micro-strain meter was zeroed, and the C-ring was loaded in incremental steps, halting to measure the C-ring diameter when the measured strain corresponded to 20, 40, 60, 80, and 100% of the room temperature critical strain.
4. The resulting strain-deflection data array was curve-fitted in EXCEL using the "zero-intercept" option to derive the strain-deflection correlation equation. Table 7 shows the results for the four CRAs subjected to C-ring cracking tests.
5. The strain-deflection correlation equation was solved for the Critical Deflection, the deflection corresponding to the critical strain at 350°F.

Final Report No. TS3333PH Rev2

Extended Duration Corrosion Testing of Five Ni-base

Corrosion Resistant Alloys at 15,000 psig and 350°F

6. The C-ring deflection was adjusted to this Critical Deflection and the outer-fiber strain was recorded as the actual initial strain.
7. The C-ring was heat-soaked at 350°F for a minimum of 12 hours and the outer fiber strain was recorded.
8. The critical strain was subtracted from the final strain yielding the thermal relaxation term.
 - a. Negative thermal relaxation terms indicate that the coefficient of thermal expansion of the C-ring alloy is greater than that of the Alloy C-276 tensioning rod, causing the outer-fiber strain to decrease with increasing temperature.
 - b. Positive thermal relaxation terms indicate that the coefficient of thermal expansion of the C-ring alloy is less than that of the Alloy C-276 tensioning rod, causing the outer-fiber strain to increase with increasing temperature.
9. The strain values of the thermal relaxation factors were substituted into the strain deflection correlation equations to obtain the deflection adjustments required to compensate for heating the test C-rings from room temperature to 350°F.
10. The deflection adjustments were added to the Critical Deflections to obtain the Adjusted Target Deflections.

The results of the strain-deflection calibration process are summarized in tabular form in Section 4.2.

3.5.2 Very High Pressure (VHP) Autoclave Set-up

All tests were performed using the three HCS VHP autoclaves having a service pressure limit of 20,000 psig at temperatures up to 550°F. The chambers of these autoclaves have an ID of 3.25 inches and a depth of 20 inches and are lined with Alloy C-276. The gross chamber volume is 2.7 L and the liquid charge is 2 L.

Two of the three autoclaves were used for the actual exposures, while the third was used as a VHP gas accumulator.

Each autoclave was configured with a

- dip-tube used for liquid and gas entry and liquid extraction, a
- headspace vent port,
- 20,000 psig pressure transducers for continuous monitoring and recording of pressure during the tests, and
- Thermocouples for continuous monitoring and recording of the autoclave temperatures.

3.5.3 Solution Preparation

1. Brine of the composition shown in Table 2 was prepared in 2-L aliquots in 6-L deaeration flasks each equipped with a fritted glass bubbler tube, a headspace gas vent, and a deaerated brine extraction tube.
2. 459.1 ± 0.1 g of reagent grade NaCl was weighed out and quantitatively transferred into the deaeration flask along with a Teflon-coated magnetic stirring bar and 1835 mL of distilled water. The mixture was stirred until the salt dissolved.
3. The solution was deaerated by purging overnight with UHP nitrogen per HCS's Standard Deaeration Procedure which consistently yields dissolved oxygen (DO) concentrations of 3-5 ppb.
4. With continuing nitrogen purging, the solution pH was measured using a freshly calibrated pH probe and the solution was titrated to pH 4.0 using 10% HCl prepared from reagent-grade HCl and distilled water.
5. A 20-mL aliquot of the acidified brine was purged with chemically pure CO₂ for 30 minutes and the pH was measured and recorded as the initial CO₂-saturated pH.

3.5.4 Specimen Preparation

1. The CRA and X-70 steel coupons for each test were cleaned with toluene and dried with acetone.
2. The physical dimensions of the CRA coupons were then measured to the nearest 0.001 inch using four-place calibrated digital calipers.
3. Each CRA coupon was then weighed twice to the nearest 0.0001 g on a calibrated four-place analytical balance, verified by weighing two NIST-Traceable check weights before and after weighing the coupons. HCS quality guidelines required that the two weights for each CRA coupon agree within 0.0002 g. The two weights were averaged to obtain the initial weight of the coupon.
4. The SCC CRA C-rings for each Autoclave Run were assembled using 10-24 Alloy C-276 all-thread rod, flat Alloy C-276 washers, and 10-24 Alloy C-276 nuts. The all-thread rod within the span of the C-ring and the C-276 flat washers were all wrapped with Teflon tape.
5. The CRA coupons were mounted on the protruding ends of the all-thread rods of the SCC C-rings using Teflon shoulder washers to electrically isolate the coupons from the C-rings and test rack.
6. All exposed portions all-thread rod and the C-276 nuts were masked with Teflon tape.

Final Report No. TS3333PH Rev2

Extended Duration Corrosion Testing of Five Ni-base

Corrosion Resistant Alloys at 15,000 psig and 350°F

7. The galvanically coupled CRA C-rings were assembled similarly except that a pair of X-70 pipeline steel coupons were inserted on the all-thread rod between the sides of the C-rings and the Alloy C-276 washers so that they were tightly clamped against the outer surface of the C-ring, creating an intentional galvanic couple.
8. Shortly prior to the start of the autoclave exposure, the hardware of each C-ring was carefully tightened to the thermal relaxation compensated target deflection obtained from the strain-deflection calibration.
9. The assembled C-rings and Alloy corrosion coupons were mounted on a test rack as shown in Figure 2.

3.5.5 Autoclave Loading

1. A 20-ml sheet Teflon liner was inserted into the autoclave, followed by the test rack.
2. The autoclave was sealed and leak tested with UHP nitrogen at 18,500 psig.
3. The nitrogen was vented and the autoclave was evacuated with a laboratory vacuum pump.
4. The autoclave was pressurized to a few hundred psig with UHP nitrogen and evacuated with a laboratory vacuum pump, completing one Flush-and-Vacuum cycle. The Flush-and-Vacuum procedure was repeated twice more to remove any residual air from the autoclave.
5. The prepared deaerated solution for the test was transferred into the autoclave under a UHP nitrogen blanket, then purged *in-situ* with UHP nitrogen for 30 minutes as a precaution against inadvertent air contamination.
6. The solution was next purged *in situ* for 30 minutes at atmospheric pressure with Certified Mixed Gas (CMG) having the composition shown in Table 2 to saturate the solution with the mixed gas at atmospheric pressure.
7. The Autoclave was shut-in and heated to 350°F. Following a 30-minute stabilization hold, the autoclave was then pressurized to 15,000 psig using the same certified mixed gas.

3.5.6 Replenishment

The brine and gas charges of the autoclaves for the 12-week, 18-week, and 48-week exposures were replenished every six weeks per the following procedure.

1. The heating bands of the autoclave were automatically de-energized at 11:30 PM of the last day of each six-week cycle, and the autoclave was cooled to less than 140°F for safety.
2. The pressure was vented to a caustic scrubber until less than 100 psig remained in the autoclave.
3. The residual pressure was used to expel brine from the autoclave through a "pH block" housing a calibrated pressure-resistant pH probe, permitting measurement of solution pH without loss of acid-gases through air contact.
4. A 40-mL aliquot of this brine was captured and purged with UHP nitrogen for 10 minutes before measuring the final N₂-saturated pH using a freshly calibrated pH probe.
5. The same brine aliquot was purged with CP CO₂ for 10 minutes before measuring and recording the final CO₂-saturated pH.
6. The solution was pushed from the autoclave using UHP nitrogen and the autoclave was evacuated with a vacuum pump.
7. Two liters of brine was prepared as above and loaded into the autoclave under a nitrogen blanket.
8. The brine was purged *in situ* with UHP nitrogen for 30 minutes and the headspace was evacuated.
9. The solution was next purged *in situ* for 30 minutes at atmospheric pressure with Certified Mixed Gas to saturate the solution with the mixed gas at atmospheric pressure.
10. The autoclave was heated to 350°F and pressurized to 15,000 ± 500 psig with the Certified Mixed Gas.

3.5.7 Test Shutdown and Specimen Recovery

1. At the end of its specified total exposure period, each autoclave was de-energized and cooled to less than 140°F prior to venting the total pressure to approximately 100 psig.
2. The "Block pH" Final N₂-Saturated pH and Final CO₂-Saturated pH measurements were made as described above.
3. The remainder of the brine was expelled to a sour waste drum using UHP nitrogen. The autoclave was backfilled with tap water and this was also expelled to the sour waste drum.
4. The autoclave was opened, and the test rack was retrieved. The rack was flushed with tap water, rinsed with distilled water, and dried with acetone, halting all corrosion reactions.

3.5.8 Post-Test Analysis Procedure

1. The specimen tree was photographed prior to disassembly.

Final Report No. TS3333PH Rev2

Extended Duration Corrosion Testing of Five Ni-base

Corrosion Resistant Alloys at 15,000 psig and 350°F

2. The CRA C-rings and coupons were then photographed before cleaning. Note that the X-70 coupons were neither photographed or further processed as their corrosion behavior was not being evaluated.
3. The CRA coupons were cleaned using mildly abrasive scrubbing pads and a paste of granulated Alconox alkaline laboratory detergent and distilled water, rinsed with distilled water, and dried with acetone.
4. The coupons were weighed twice to the nearest 0.0001 g per the HCS Standard Weighing Procedure, and the two weights for each coupon were averaged to obtain Weight 2, Weight 1 being the initial pre-test weight.
5. Since the coupons were bright and shiny following non-aggressive cleaning, no further cleaning and weighing steps were required.
6. The weight-loss corrosion rates were calculated per equation 1 in ASTM Standard G1, i.e.,

$$CR = 8.76 \times 10^4 m_l/DAT \quad \text{Eq 1}$$

CR = corrosion rate

m_l = mass loss, mg

D = Alloy Density, mg/cm³

A – Coupon surface area, cm²

T – exposure time, hours to the nearest 0.01 hr

7. The coupons were subsequently examined by stereomicroscope at 10X and 45X for corrosion pits. If pits were observed, the areas and apparent depths of the largest pits were measured using an optical metallograph.
8. The C-rings were cleaned using mildly abrasive scrubbing pads and a paste of granulated Alconox alkaline laboratory detergent and distilled water, rinsed with distilled water, and dried with acetone.
9. The apexes of the C-rings were examined by visually for cracking. Any visibly cracked C-rings were identified and set aside.
10. The apexes of the remaining C-rings were examined by stereomicroscope at 10X and 45X and any C-rings exhibiting cracking were set aside.
11. The apexes of the remaining C-rings were examined on an optical metallograph at magnifications up to 200X. Any C-rings showing cracking of the apex were set aside.
12. The remaining C-rings were deemed to have resisted cracking.

The appearance of the apex of each C-ring was photo-documented as suitable magnification.

4.0 Results

4.1 Westmoreland Test Results

4.1.1 Charpy V-Notch Impact Energy Tests

The results of Charpy V-Notch Impact Energy Tests performed by Westmoreland on the five alloys are presented in Table 6.

4.1.2 Uniaxial Tensile Test Results

The results of uniaxial tensile tests performed by Westmoreland on Allot 725, Alloy 945X, Alloy AF955, and C-22HS are summarized in Table 7. The results in this table were used in the preparation of Tables 8 and 9.

4.2. Strain Deflection Calibration Results

The procedures for determination of the strain-deflection correlation equation coefficients and target C-ring deflections were discussed in Section 3.5.1.

Table 8 shows the C-ring strain-deflection calibration data for Alloys 725, 945X, 955, and C-22HS and the resulting strain-deflection correlation terms. These terms fit the equation

$$\text{Deflection} = a(\text{strain}) + b \quad \text{Eq 2}$$

The term "b" is zero in all cases because the "zero-Intercept" option of the Microsoft® Excel spreadsheet used in generation of the table was enabled.

Table 9 summarizes the calculation of the Adjusted Target Deflections for the test C-rings.

Final Report No. TS3333PH Rev2

Extended Duration Corrosion Testing of Five Ni-base

Corrosion Resistant Alloys at 15,000 psig and 350°F

4.3 Test Solution pH Measurements

The test solution pH measurements obtained during Tests I through IV are compiled in Table 10.

It was neither physically possible to measure the *in-situ* pH of the test solution in the autoclaves at 350°F and 15,000 psig, nor to calculate the *in situ* pH values using the best commercially available ionic-thermodynamic models. The "Block pH" measurements were made at approximately 140°F and 100 psig on brine flowing from the autoclave without air exposure. The relationships between these pH values and the *in situ* pH values are not known.

The N₂-Saturated pH values represent the pH of the brine devoid of acid gases from both ambient atmospheric exposure and the autoclave test atmosphere. The solution preparation procedure, Section 3.5.3, specified that the initial N₂-saturated pH of the brine be adjusted to 4.0 with HCl. Table 10 shows that the average initial N₂-saturated pH was 4.02 with a range of 3.95 to 4.10. In contrast, the average final N₂-saturated pH was 5.07 with a range of 2.95 to 8.20

ANSI/NACE MR0175/ISO 15156-3:2015, Annex B, recommends the CO₂-Saturated pH over the N₂-Saturated pH as being more indicative of actual autoclave conditions. The average initial CO₂-Saturated pH was 3.43 with a range of 3.01 to 4.28, while the average final CO₂-Saturated pH was 3.86 with a range of 2.75 to 5.11.

4.4 Actual vs Nominal Exposure Times at Temperature and Pressure

The actual accumulated exposure times at temperature (350 ± 5°F) and pressure (15,000 ± 500 psig) are compared with the nominal exposure times at temperature and pressure in Table 11. The actual accumulated exposure times at temperature and pressure were used when calculating the weight-loss corrosion rates.

4.5 Test I (6-week exposure) Corrosion and Cracking Results.

The results of the weight-loss corrosion rate determinations and assessments of pitting susceptibilities are summarized in Table 12. The mass losses of the individual coupons ranged from 1.2 to 2.1 mg. The mass-loss corrosion rates of the CRAs ranged from 0.653 to 1.218 μm/yr with a median rate of 0.862 μm/yr. These corrosion rates were consistent with nickel-based, Cr-Mo alloys in the passive state, and none of the coupons showed evidence of pitting.

The results of the C-ring cracking susceptibility tests are summarized in Table 13. Each of the two Alloy 945X C-rings was visibly cracked across the width of the specimen. The C-rings of Alloys 725, 955, and C-22HS all resisted cracking in this 6-week exposure test.

Appendix A contains photo documentation of the post-exposure appearances of the coupons and C-rings both before and after cleaning.

4.6 Test II (12-week exposure) Corrosion and Cracking Results.

The results of the weight-loss corrosion rate determinations and assessments of pitting susceptibilities are summarized in Table 14. The mass losses of the individual coupons ranged from 0.2 to 1.3 mg. The mass-loss corrosion rates of the CRAs ranged from 0.058 to 0.383 μm/yr with a median rate of 0.0254 μm/yr. These corrosion rates were consistent with nickel-based, Cr-Mo alloys in the passive state, and none of the coupons showed evidence of pitting.

The results of the C-ring cracking susceptibility tests are summarized in Table 15. The C-rings of Alloys 725, 945X, 955, and C-22HS all resisted cracking in this 12-week exposure test.

Appendix B contains photo documentation of the post-exposure appearances of the coupons and C-rings both before and after cleaning.

4.7 Test III (18-week exposure) Corrosion and Cracking Results.

The results of the weight-loss corrosion rate determinations and assessments of pitting susceptibilities are summarized in Table 16. The mass losses of the individual coupons ranged from 0.2 to 0.7 mg. The mass-loss corrosion rates of the CRAs ranged from 0.036 to 0.138 μm/yr with a median rate of 0.087 μm/yr. These corrosion rates were consistent with nickel-based, Cr-Mo alloys in the passive state, and none of the coupons showed evidence of pitting.

The results of the C-ring cracking susceptibility tests are summarized in Table 17. The C-rings of Alloys 725, 945X, 955, and C-22HS all resisted cracking in this 18-week exposure test.

Appendix C contains photo documentation of the post-exposure appearances of the coupons and C-rings both before and after cleaning.

4.8 Test IV (48-week exposure) Corrosion and Cracking Results.

The results of the weight-loss corrosion rate determinations and assessments of pitting susceptibilities are summarized in Table 18. The mass-losses of the individual coupons ranged from 0.7 to 5.0 mg. The mass-loss corrosion rates of the CRAs ranged from 0.048 to 0.366 μm/yr, with a median rate of 0.118 μm/yr. All the corrosion rates were consistent with nickel-based, Cr-Mo alloys in the passive state, and none of the coupons showed evidence of pitting.

The results of the C-ring cracking susceptibility tests are summarized in Table 19. The C-rings of Alloys 725, 945X, 955, and C-22HS all resisted cracking in this 48-week exposure test.

Final Report No. TS3333PH Rev2

Extended Duration Corrosion Testing of Five Ni-base

Corrosion Resistant Alloys at 15,000 psig and 350°F

Appendix D contains photo documentation of the post-exposure appearances of the coupons and C-rings both before and after cleaning.

5.0 Discussion

5.1 Alloy Composition and Anticipated Corrosion and SCC Behavior

All five of the alloys in this study are classified as nickel-base alloys. Four of the five alloys tested contain more than 50 wt% nickel. While the fifth, Alloy 825, contains 38.37 wt% nickel, nickel is still the predominant element, and Alloy 825 is also classified as a nickel-base alloy. The nickel contents of these alloys mean that their microstructures are 100% austenitic (face-centered cubic) at room temperature.

All of the tested alloys also contain more than 13 wt% chromium as well as varying, significant additions of molybdenum. The presence of chromium, reinforced by molybdenum, spontaneously form nanometer-thick kinetically protective passivation films on the alloys' surfaces upon contact with air or water. Under the correct conditions, these passivation films, which are also responsible for the "stainless" behavior of stainless steels, are spontaneously self-repairing on micro-second time scales, resulting in extremely low corrosion rates. If the chemical environment is so severe that self-repair of microdamage to the passivation film cannot occur, the damaged area corrodes rapidly while the surrounding surface remains passivated, forming a pit.

5.2 Statistical Analysis of the Coupon Corrosion Mass-Loss and Corrosion Rate Data

5.2.1 Side-by-Side Comparisons of Mass-Loss and Corrosion Rates

Table 20 provides side-by-side comparisons of the corrosion rates of the five pairs of corrosion coupons exposed in each of the four autoclave tests, in terms of:

- actual mass loss in milligrams (mg), and
- corrosion rates of the individual coupons in micrometers/year ($\mu\text{m}/\text{yr}$).

This table also includes statistical analytical summaries of the two data sets, showing that

1. The combined coupon mass-losses from the four tests ranged from 0.2 to 5.0 mg with a median of 1.05 mg, a mean of 1.24 mg, and a standard deviation of 0.98 mg.
2. The resulting corrosion rates ranged from 0.035 to 1.177 $\mu\text{m}/\text{yr}$ with a median of 0.131 $\mu\text{m}/\text{yr}$, a mean of 0.335 $\mu\text{m}/\text{yr}$, and a standard deviation of 0.319 $\mu\text{m}/\text{yr}$. For perspective, NACE-International classifies corrosion rates up to 25.4 $\mu\text{m}/\text{yr}$ as "very low"⁵.

Inspection of the side-by-side corrosion rate data showed both high scatter in the corrosion rates of duplicate coupons in the same test and no visible trend of corrosion rates with increasing cumulative exposure durations.

5.2.2 Source of Scatter in Corrosion Rates of Duplicate Coupons

The absolute differences in corrosion rates of duplicate coupons of the same alloy in the same test were calculated per Equation 3.

$$\begin{aligned} \text{Absolute Difference } (\mu\text{m}/\text{yr}) &= |CR_1 - CR_2| && \text{Eq 3} \\ CR_1 &= \text{Corrosion rate of first coupon} \\ CR_2 &= \text{Corrosion rate of second coupon} \end{aligned}$$

The relative differences in the corrosion rates of duplicate coupons of the same alloy in the same test were calculated per Equation 4 and compiled in the lower (orange) section of Table 21.

$$\text{Relative Difference } (\%) = |CR_1 - CR_2| / [(CR_1 + CR_2) / 2] \quad \text{Eq 4}$$

Because the coupons were weighed on a 4-place analytical balance, the theoretical mass-difference detection limit was 0.1 mg. For the nickel alloys tested, this meant that the minimum detectable difference in corrosion rate is 0.056 $\mu\text{m}/\text{yr}$. The relative differences in the corrosion rates of duplicate coupons in the same test were inherently large because all of the absolute differences in Table 21 were within six times the minimum detectable difference in corrosion rates.

5.2.3 Lack of Discernable Corrosion Rate Trend with Time

It is generally the case that corrosion rates in autoclave tests decrease with time, but no such trend was apparent in the current study due to two confounding factors.

⁵ R. James Landrun, Fundamentals of Designing for Corrosion Control, NACE-International, Houston, TX, 1989, p 47.

Final Report No. TS3333PH Rev2

Extended Duration Corrosion Testing of Five Ni-base

Corrosion Resistant Alloys at 15,000 psig and 350°F

- **Factor 1.** The first confounding factor was the inherent uncertainty (scatter) of the corrosion rate data between duplicate coupons in the same test because the individual mass losses were very close to the detection limit of the four-place analytical scale used to make the mass-loss determination.
- **Factor 2.** The environments of Tests II, III, and IV were replenished at six-week intervals to help maintain somewhat steady-state conditions for the C-ring cracking tests. A trend of decreasing corrosion rates with increasing exposure time might have been observed without the periodic replenishments of the test solution and headspace gases in Tests II, III, and IV. However, from an environmental severity standpoint:
 - The specimens of Test I were exposed to the conditions specified in Table 1 for nominally 6 weeks.
 - The specimens of Test II were nominally exposed to the conditions in Table 1 for two consecutive 6-week periods.
 - The specimens of Test III were nominally exposed to the conditions in Table 1 for three consecutive 6-week periods.
 - The specimens of Test IV nominally exposed to the conditions in Table 1 for eight consecutive 6-week periods.

A trend of decreasing corrosion rates with increasing exposure time might have been observed without the periodic replenishments of the test solution and headspace gases in Tests II, III, and IV.

However, because of replenishment, the specimens of Test II were exposed to two consecutive 6-week exposures rather than one 12-week exposure; the specimens of Test III were exposed to three consecutive 6-week exposures rather than one 18-week exposure; and the specimens of Test IV were exposed to eight consecutive 6-week tests rather than one 48-week week exposure. To Honeywell's knowledge, the effect of periodic environment replenishment on corrosion rate trends with time has not been characterized. Thus, it is not known whether a trend of decreasing corrosion rate with time would be apparent under these replenishment regimes even under ideal conditions.

5.3 C-ring Cracking Test Results

Both Alloy 945X C-rings cracked in Test I (6-week exposure) but did not crack in Tests II (12-week exposure), III (18-week exposure), or IV (48-week exposure). There was no discernable difference in the C-ring loading procedures of the four tests to account for this anomalous behavior, and none of the other C-rings cracked in any of the four tests.

6.0 Conclusions

Corrosion Coupon Tests

1. The coupon mass losses varied from 0.2 to 5 mg with a median of 1.05 mg, a mean of 1.24 mg, and a standard deviation of 0.98 mg. The difference between the median and mean values suggests that the data is geometrically distributed.
2. The corrosion rates calculated from the corrosion mass losses varied from 0.035 $\mu\text{m}/\text{yr}$ to 1.18 $\mu\text{m}/\text{yr}$, with a median of 0.131 $\mu\text{m}/\text{yr}$, a mean of 0.335 $\mu\text{m}/\text{yr}$, and a standard deviation of 0.319 $\mu\text{m}/\text{yr}$.
3. These are extraordinarily low corrosion rates given that NACE-International interprets 25.4 $\mu\text{m}/\text{yr}$ (1 mpy) as "very low." The almost total lack of corrosion is most likely due to spontaneously self-generating and self-repairing passivation films on the coupon surfaces.
4. No evidence of pitting corrosion was observed for any of the CRA coupons tested.

C-ring Cracking Tests

1. The C-ring exposures at 350°F in these autoclave tests represented tests for evaluation of susceptibilities of the CRAs to anodic active-path driven SCC. *None can be construed as measuring susceptibility to atomic hydrogen absorption driven cracking phenomena (SSC, GHSC).* While the configurations of the CRA C-rings galvanically coupled to carbon steel coupons were identical to the configurations used for GHSC testing, these specimens provided no information regarding GHSC susceptibility, which has a specified test temperature of 75°F.
2. The two Alloy 945X C-rings from the 6-week exposure test exhibited obvious cracking, though the C-rings of the other CRA's in this test resisted cracking, as did all the CRA C-rings in the 12-, 18-, and 48-week tests. Honeywell concludes that the failure of the two Alloy C-276 C-rings in the 6-week test were anomalous, and that Alloys 725, 945X, 955X and C-22HS were all resistant to SCC at 350°F in 20 wt% NaCl brine under a methane atmosphere at 15,000 psig containing 0.05 ppm H_2S and 125 psia CO_2 .
3. No indications of pitting attack were observed on any of the C-ring specimens.

Final Report No. TS3333PH Rev2

Extended Duration Corrosion Testing of Five Ni-base

Corrosion Resistant Alloys at 15,000 psig and 350°F

Table 1. Initially Specified Environmental Test Matrix and Replenishment Schedule

Test	Nominal Duration at Temp. and Press. (weeks)	Brine Charge	Gas Charge	Replenishment Procedure	Replenishment Schedule
I	6	20.00 wt% NaCl brine w pH 4.0 at atmospheric pressure and room temperature. 121,353 mg/kg (139,223 mg/L) chloride	3.3 ppmv H ₂ S, 8,325 ppmv CO ₂ , bal CH ₄ at 350°F and 15,000 psig (0.050 psia H ₂ S and 125 psia CO ₂).	Cool and hold at 140°F. Expel autoclave contents. Replace brine charge with fresh deaerated brine. Reheat to 350°F. Replenish gas charge.	None
II	12				6-weeks
III	24				6-, 12, and 18-weeks
IV	48				6-, 12-, 18-, 24-, 30-, 36-, and 48-weeks

Table 2. Final Environmental Test Matrix and Replenishment Schedule Approved by the Sponsors

Test	Nominal Duration at Temp. and Press. (weeks)	Brine Charge	Gas Charge	Replenishment Procedure	Replenishment Schedule	Total Exposure Duration Including Replenishments and One-day Cooldown at End-of-Test
I	6	20.00 wt% NaCl brine w pH 4.0 at atmospheric pressure and room temperature. 121,353 mg/kg (139,223 mg/L) chloride	3.3 ppmv H ₂ S, 8,325 ppmv CO ₂ , bal CH ₄ at 350°F and 15,000 psig (0.050 psia H ₂ S and 125 psia CO ₂).	Cool and hold at 140°F. Expel autoclave contents. Replace brine charge with fresh deaerated brine. Re-heat to 350°F. Replenish gas charge.	None	43
II	12				6-weeks	81
III	18				6-, and 12-weeks	128
IV	48				6-, 12-, 18-, 24-, 30-, 36-, and 48-weeks	349

Table 3. Alloy Test Matrix per Autoclave Test

Material	HON Traceability #	Specimens	Test
Alloy 725	14147	2 CRA Coupons [1]	Corrosion rate and pitting
		1 CRA C-ring [2]	Stress Corrosion Cracking (SCC)
		1 CRA C-ring galvanically coupled to two carbon steel anode coupons [3].	Galvanically affected SCC [4]
Alloy 955	14148	2 CRA Coupons	Corrosion rate and pitting
		1 CRA C-ring	SCC
		1 CRA C-ring galvanically coupled to two carbon steel anode coupons [3].	Galvanically affected SCC
Alloy 945X	14149	2 CRA Coupons	Corrosion rate and pitting
		1 CRA C-ring	SCC
		1 CRA C-ring galvanically coupled to two carbon steel anode coupons.	Galvanically affected SCC
Alloy C-22HS	14150	2 CRA Coupons	Corrosion rate and pitting
		1 CRA C-ring	SCC
		1 CRA C-ring galvanically coupled to two carbon steel anode coupons.	Galvanically affected SCC
Alloy 825	14151	2 CRA Coupons [5]	Corrosion rate and pitting

Notes

[1] 1.5-inch by 0.75-inch by 0.125 inch rectangular CRA coupon with a centered 0.255-inch mounting hole and 120-grit wet polish per ASTM Standard G1. Evaluated for weight-loss (uniform) corrosion and pitting per ASTM G1 and ASTM G46, respectively.

[2] NACE TM0177 Method C C-ring 1.5-inches in OD by 0.75-inch wide by 0.020 inches thick, loaded to outer fiber strain corresponding to the strain of a uniaxial tensile specimen at the 0.2%-offset yield stress at 350°F.

[3] NACE TM0177 Method C C-ring 1.5-inches in OD by 0.75-inch wide by 0.020 inches thick, clamped by the C-ring hardware between two carbon steel coupons, as described above, and loaded to outer fiber strain corresponding to the strain of a uniaxial tensile specimen at the 0.2%-offset yield stress at 350°F. The carbon steel coupons served as sacrificial anodes and were discarded after exposure without analysis. [4] These tests may provide an indication of the effect on SCC susceptibility of galvanically coupling the CRA to carbon steel, but do not constitute a test for susceptibility to Galvanic Hydrogen Stress Cracking (GHSC). As defined by NACE RM0175 ISO15156-3 (2015), Annex B, GHSC is a low-temperature phenomenon for which the specified test temperature is 75°F.

[5] While the original plan was to expose Alloy 825 C-rings, the inclusion of Alloy 825 C-rings was cancelled due to problems with timely delivery of the specimens.

Final Report No. TS3333PH Rev2

Extended Duration Corrosion Testing of Five Ni-base

Corrosion Resistant Alloys at 15,000 psig and 350°F

Table 4. Test Specimens Delivered by Westmorland

Material	HON #	Plan		Actual	
		C-rings	Coupons	C-rings	Coupons
Alloy 725	14147	10	8	10	8
Alloy 955	14148	10	8	10	8
Alloy 945X	14149	10	8	10	8
Alloy C-22HS	14150	10	8	10	8
Alloy 825	14151	10	8	0*	8
X70 pipeline steel	14152	0	40	0	40

* The Project Sponsors elected to proceed without the Alloy 825 C-rings

Table 5. CRA Composition Data

	C-22HS	725	945X	825	AF955
Compositions Provided by the Sponsor, wt%					
C	0.003	0.015	0.011	0.01	0.015
Si	0.015	0.04	0.07	0.4	0.09
Mn	0.25	0.03	0.08	0.75	0.08
P	<0.01	0.003	0.01	0.017	0.009
S	<0.001	0.0006	0.001	0.0002	0.0002
Cr	20.5	20.7	20.8	22.35	21.6
Mo	16.6	8.01	3.26	3.08	5.9
Ni	61.0	57.5	53.3	38.37	57.4
Al	0.23	0.32	0.11	0.12	0.43
B	0.006	0.0035			0.0043
Co	<0.05	0.05	0.3		0.01
Cu		<0.01	1.99	1.86	0.037
Pb		<0.00001			
Ti	<0.01	1.56	1.52	0.83	0.86
Bi		0.0003			
Ca		0.0003	0.003		
Mg	0.034	<0.00005	0.0004		
Se		<0.00005			
Ta	<0.1	0.004	0.01		
Fe	1.1	Bal	14.4	32	8.7
Nb+Ta	0.18	3.544	4.06		4.80

Table 6. Charpy V-Notch Impact Toughness Results Provided by Westmoreland

Alloy	Charpy Test Number	Temp (°F)	Impact Energy (ft-lb)	Mils Lat Exp	% Shear Fracture
725	1	73	66	32	20
	2		72	36	20
	3		65	31	20
	4	32	74	34	25
	5		68	32	20
	6		68	27	20
945X	1	73	101	42	25
	2		105	48	25
	3		96	47	25
	4	32	112	47	30
	5		106	44	25
	6		99	53	25
955	1	73	91	41	20
	2		92	43	20
	3		85	41	20
	4	32	96	43	20
	5		95	41	20
	6		98	46	25
C-22HS	1	73	140	59	100
	2		131	56	100
	3		120	52	100
	4	32	105	38	65
	5		107	45	65
	6		105	44	65
825	1	73	182	66	100
	2		176	63	100
	3		179	66	100
	4	32	192	70	100
	5		171	65	100
	6		179	68	100

Table 7. Mechanical Test Results Provided by Westmoreland

Alloy	Temp.	UTS (ksi)	0.2% YS (ksi)	Elong (%)	RA (%)	Critical Strain at YS (μ-in/in)	Average Critical Strain at YS	Average YS (ksi)

Final Report No. TS3333PH Rev2

Extended Duration Corrosion Testing of Five Ni-base

Corrosion Resistant Alloys at 15,000 psig and 350°F

							(μ -in/in)	
725	Room	190.7	129.5	38	50	5689*	6625	130.9
	Room	189.6	129.8	37	48	6489		
	Room	193.1	133.5	35	49	6760		
	350	179.4	122.4	36	51	6116	6115	123.5
	350	179.6	123.2	33	51	6031		
	350	181.3	124.8	34	53.5	6199		
945X	Room	181.0	149.5	24	35	7077	6990	148.5
	Room	189.2	148.2	31	49	6746		
	Room	184.3	147.9	32	50	7147		
	350	175.5	140.5	29	52	7375	6581	140.5
	350	176.7	140.9	30	54.5	6540		
	350	175.5	140.0	29	54	6622		
955	Room	186.3	148.0	34	52	7583	6832	147.3
	Room	185.3	146.6	34	50	6784		
	Room	182.9	147.2	34	55	6880		
	350	171.4	138.0	33	51.5	6408	6573	137.7
	350	168.3	137.5	35	57.5	6664		
	350	168.9	137.6	34	53.5	6647		
C-22HS	Room	182.8	176.2	21	71	9141	9120	184.8
	Room	183.4	178.4	20	70	9098		
	Room	205.4	199.9	16	61	8524		
	350	186.1	180.9	15	57	8074	8484	172.0
	350	174.4	168.8	17	67	8666		
	350	171.7	166.3	16	66.5	8301		
* Disregarded outlier								

Table 8. C-ring Strain-Deflection Calibration Data

CRA	Parameter	Percentage of Critical Strain						Correlation Terms	
		0	20	40	60	80	100		
725	μ -strain	0	1222	2442	3669	4904	6123	Term "a"	1.655E-05

Final Report No. TS3333PH Rev2

Extended Duration Corrosion Testing of Five Ni-base

Corrosion Resistant Alloys at 15,000 psig and 350°F

	Ring OD, in	1.501	1.4785	1.4585	1.437	1.4185	1.404	Term "b"	0
	Deflection, in	0	0.0225	0.0425	0.064	0.0825	0.097	R ²	0.994
945X	μ-strain	0	1317	2623	3955	5277	6568	Term "a"	1.639E-05
	Ring OD, in	1.5025	1.4815	1.457	1.4375	1.4145	1.397	Term "b"	0
	Deflection, in	0	0.021	0.0455	0.065	0.088	0.1055	R ²	0.9983
AF955	μ-strain	0	1322	2645	3938	5263	6582	Term "a"	1.646E-05
	Ring OD, in	1.497	1.474	1.4505	1.429	1.4085	1.3935	Term "b"	0
	Deflection, in	0	0.023	0.0465	0.068	0.0885	0.1035	R ²	0.9939
C-22HS	μ-strain	0	1696	3395	5096	6795	8467	Term "a"	1.67E-05
	Ring OD, in	1.498	1.4695	1.4415	1.408	1.385	1.36	Term "b"	0
	Deflection, in	0	0.0285	0.0565	0.09	0.113	0.138	R ²	0.9974

Table 9. Adjusted Target C-Ring Deflection Calculations

		CRA			
		725	945X	955	C-22HS
Critical Strain at 75°F	μ-strain	6625	6990	6832	9120
Critical Strain at 350°F	μ-strain	6115	6581	6573	8484
Critical Deflection	inch	0.101	0.108	0.108	0.141
Actual Initial Strain	μ-strain	6127	6553	6575	8480
Final Strain after Heat Soak	μ-strain	5495	5931	5889	8601
Thermal relaxation Term	μ-strain	-632	-622	-686	121
Deflection Adjustment	inch	0.007	0.009	0.008	-0.003
Adjusted Target Deflection	inch	0.108	0.117	0.116	0.138

Final Report No. TS3333PH Rev2

Extended Duration Corrosion Testing of Five Ni-base

Corrosion Resistant Alloys at 15,000 psig and 350°F

Table 10. pH Measurement Results during Tests I through IV

Test	Nominal Total Duration	Exposure Period	Beginning of Period		End of Period		
			N ₂ -Saturated pH	CO ₂ -Saturated pH	"Block" pH	N ₂ -Saturated pH	CO ₂ -Saturated pH
I	6-weeks	1	3.95	3.88	6.11	3.44	3.25
II	12-weeks	1	4.08	4.28	5.82	4.54	3.85
		2	3.97	3.45	5.90	6.29	5.02
		Average	4.03	3.87	5.86	5.42	4.44
III	18-weeks	1	4.00	3.88	5.75	3.98	3.82
		2	4.01	3.03	5.82	6.23	4.36
		3	4.08	4.28	5.80	6.58	4.09
		Average	4.03	3.73	5.79	5.60	4.09
IV	48-weeks	1	4.03	3.01	5.98	3.77	3.22
		2	4.01	3.10	6.17	2.95	2.88
		3	4.10	3.18	6.41	6.17	3.71
		4	3.97	3.06	6.87	6.35	4.79
		5	4.05	3.09	8.24	8.20	5.11
		6	4.00	3.21	3.63	3.55	2.75
		7	4.01	3.02	5.65	5.22	3.51
		8	4.00	3.09	5.52	4.36	3.09
		Average	4.02	3.10	6.06	5.07	3.63

Table 11. Nominal vs. Actual Exposure Times at Temperature and Pressure

Test	Test Description	Nominal Time at Temperature and Pressure	Actual Time at Temperature and Pressure	Variance (hours)	Variance (%)
I	6-Week Test	1008	1008	0	0
II	12-Week Test	2016	1988	-28	-1.39
III	18-Week Test	3024	3020	-4	-0.13
IV	48-Week Test	8064	8040	-24	-0.30

Table 12. Test I (6-Week Exposure) – Corrosion Rate and Pitting Results

CRA	Coupon ID	mass loss (mg)	Corrosion Rate (µm/yr)	Average Corrosion Rate (µm/yr)	Pitting Corrosion
-----	-----------	----------------	------------------------	--------------------------------	-------------------

Final Report No. TS3333PH Rev2

Extended Duration Corrosion Testing of Five Ni-base

Corrosion Resistant Alloys at 15,000 psig and 350°F

725	14147-C1	1.2	0.663	0.691	Not observed
725	14147-C2	1.3	0.720		
945X	14149-C1	2.1	1.177	1.009	Not observed
945X	14149-C2	1.5	0.842		
955	14148-C1	1.6	0.883	0.852	Not observed
955	14148-C2	1.5	0.821		
C-22HS	14150-C1	1.7	0.896	0.763	Not observed
C-22HS	14150-C2	1.2	0.631		
825	14151-C1	1.5	0.845	0.764	Not observed
825	14151-C2	1.2	0.682		

Table 13. Test I (6-week exposure) – C-ring Test Results

CRA	Cracking Mode Tested	C-ring Specimen Numbers	Galvanically Coupled to X-70 Pipeline Steel	Target Deflection of C-ring* (inch)	Actual Deflection (inch)	Pitting Observed	Cracking Observed
725	SCC	14147-R1	No	0.108	0.108	No	No
	GC-SCC	14147-R2	Yes	0.108	0.108	No	No
945X	SCC	14149-R1	No	0.117	0.117	No	Yes
	GC-SCC	14149-R2	Yes	0.117	0.117	No	Yes
955	SCC	14148-R1	No	0.116	0.116	No	No
	GC-SCC	14148-R2	Yes	0.116	0.116	No	No
C-22HS	SCC	14150-R1	No	0.138	0.138	No	No
	GC-SCC	14150-R2	Yes	0.138	0.138	No	No

* Calibrated to impress on the C-ring, the outer fiber strain corresponding to the strain of a uniaxial tensile specimen of the alloy at its 0.2%-offset yield stress at the test temperature.

Final Report No. TS3333PH Rev2

Extended Duration Corrosion Testing of Five Ni-base

Corrosion Resistant Alloys at 15,000 psig and 350°F

Table 14. Test II (12-Week Exposure) – Corrosion Rate and Pitting Results

CRA	Coupon ID	mass loss (mg)	Corrosion Rate (µm/yr)	Average Corrosion Rate (µm/yr)	Pitting Corrosion
725	14147-C3	1.1	0.309	0.266	Not observed
725	14147-C4	0.8	0.224		
945X	14149-C3	1.3	0.369	0.355	Not observed
945X	14149-C4	1.2	0.341		
955	14148-C3	1.2	0.336	0.196	Not observed
955	14148-C4	0.2	0.056		
C-22HS	14150-C3	0.4	0.107	0.187	Not observed
C-22HS	14150-C4	1.0	0.267		
825	14151-C3	0.7	0.201	0.201	Not observed
825	14151-C4	0.7	0.202		

Table 15. Test II (12-week exposure) – C-ring Test Results

CRA	Cracking Mode Tested	C-ring Specimen Numbers	Galvanically Coupled to X-70 Pipeline Steel	Target Deflection of C-ring (inch)	Actual Deflection (inch)	Pitting Observed	Cracking Observed
725	SCC	14147-R3	No	0.108	0.108	No	No
	GC-SCC	14147-R4	Yes	0.108	0.108	No	No
945X	SCC	14149-R3	No	0.117	0.117	No	No
	GC-SCC	14149-R4	Yes	0.117	0.117	No	No
955	SCC	14148-R3	No	0.116	0.116	No	No
	GC-SCC	14148-R4	Yes	0.116	0.116	No	No
C-22HS	SCC	14150-R3	No	0.138	0.138	No	No
	GC-SCC	14150-R4	Yes	0.138	0.138	No	No

Final Report No. TS3333PH Rev2

Extended Duration Corrosion Testing of Five Ni-base

Corrosion Resistant Alloys at 15,000 psig and 350°F

Table 16. Test III (18-Week Exposure) – Corrosion Rate and Pitting Results

CRA	Coupon ID	mass loss (g)	Corrosion Rate (µm/yr)	Average Corrosion Rate (µm/yr)	Pitting Corrosion
725	14147-C5	0.2	0.038	0.055	Not observed
725	14147-C6	0.4	0.077		
945X	14149-C5	0.6	0.116	0.093	Not observed
945X	14149-C7	0.4	0.078		
955	14148-C5	0.7	0.134	0.092	Not observed
955	14148-C6	0.3	0.057		
C-22HS	14150-C5	0.2	0.036	0.071	Not observed
C-22HS	14150-C6	0.6	0.110		
825	14151-C5	0.7	0.138	0.113	Not observed
825	14151-C6	0.5	0.097		

Table 17. Test III (18-week exposure) – C-ring Test Results

CRA	Cracking Mode Tested	C-ring Specimen	Galvanically Coupled to X-70 Pipeline Steel	Target Deflection of C-ring (inch)	Actual Deflection (inch)	Pitting Observed	Cracking Observed
725	SCC	14147-R5	No	0.108	0.037	No	No
	GC-SCC	14147-R6	Yes	0.108	0.074	No	No
945X	SCC	14149-R5	No	0.117	0.112	No	No
	GC-SCC	14149-R6	Yes	0.117	0.075	No	No
955	SCC	14148-R5	No	0.116	0.129	No	No
	GC-SCC	14148-R6	Yes	0.116	0.055	No	No
C-22HS	SCC	14150-R5	No	0.138	0.035	No	No
	GC-SCC	14150-R6	Yes	0.138	0.106	No	No

Final Report No. TS3333PH Rev2

Extended Duration Corrosion Testing of Five Ni-base

Corrosion Resistant Alloys at 15,000 psig and 350°F

Table 18. Test IV (48-Week Exposure) – Corrosion Rate and Pitting Results

CRA	Coupon ID	mass loss (mg)	Corrosion Rate (µm/yr)	Average Corrosion Rate (µm/yr)	Pitting Corrosion
725	14147-C7	2.0	0.138	0.104	Not observed
725	14147-C8	1.0	0.069		
945X	14149-C7	2.9	0.203	0.239	Not observed
945X	14149-C8	3.9	0.274		
955	14148-C7	1.0	0.069	0.080	Not observed
955	14148-C8	1.3	0.090		
C-22HS	14150-C7	0.7	0.046	0.056	Not observed
C-22HS	14150-C8	1.0	0.066		
825	14151-C7	2.8	0.198	0.276	Not observed
825	14151-C8	5.0	0.353		

Table 19. Test IV (48-week exposure) – C-ring Test Results

CRA	Cracking Mode Tested	C-ring Specimen Numbers	Galvanically Coupled to X-70 Pipeline Steel	Target Deflection of C-ring (inch)	Actual Deflection (inch)	Pitting Observed	Cracking Observed
725	SCC	14147-R7	No	0.108	0.108	No	No
	GC-SCC	14147-R8	Yes	0.108	0.108	No	No
945X	SCC	14149-R7	No	0.117	0.117	No	No
	GC-SCC	14149-R8	Yes	0.117	0.117	No	No
955	SCC	14148-R7	No	0.116	0.116	No	No
	GC-SCC	14148-R8	Yes	0.116	0.116	No	No
C-22HS	SCC	14150-R7	No	0.138	0.138	No	No
	GC-SCC	14150-R8	Yes	0.138	0.138	No	No

Final Report No. TS3333PH Rev2

Extended Duration Corrosion Testing of Five Ni-base

Corrosion Resistant Alloys at 15,000 psig and 350°F

Table 20. Statistical Summary of Coupon Mass-Loss and Corrosion Rate Data

Statistical Metric	CRA	Coupon	Test I	Test II	Test III	Test IV	Statistical Analysis Results		
Mass-Loss (mg)	725	1st	1.2	1.1	0.2	2.0	Min = 0.2 Max = 5.0 Median = 1.05 Mean = 1.24 Std-Dev = 0.98		
		2nd	1.3	0.8	0.4	1.0			
	945X	1st	2.1	1.3	0.6	2.9			
		2nd	1.5	1.2	0.4	3.9			
	955	1st	1.6	1.2	0.7	1.0			
		2nd	1.5	0.2	0.3	1.3			
	C-22HS	1st	1.7	0.4	0.2	0.7			
		2nd	1.2	1.0	0.6	1.0			
	825	1st	1.5	0.7	0.7	2.8			
		2nd	1.2	0.7	0.5	5.0			
	Corrosion Rate (µm/yr)	725	1st	0.663	0.309	0.037		0.037	Min = 0.035 Max = 1.177 Median = 0.131 Mean = 0.335 Std-Dev = 0.319
			2nd	0.720	0.224	0.074		0.074	
945X		1st	1.177	0.369	0.112	0.112			
		2nd	0.842	0.341	0.075	0.075			
955		1st	0.883	0.336	0.129	0.129			
		2nd	0.821	0.056	0.055	0.055			
C-22HS		1st	0.896	0.107	0.035	0.035			
		2nd	0.631	0.267	0.106	0.106			
825		1st	0.845	0.201	0.133	0.133			
		2nd	0.682	0.202	0.094	0.094			

Table 21. Scatter Analysis Between Duplicate Coupons in the Same Test

Statistical Metric	CRA	Test I	Test II	Test III	Test IV	Statistical Analysis Results
Absolute Difference Between Duplicate Coupons in the Same Test (mg)	725	0.059	0.089	0.038	0.072	Min = 0.001
	945X	0.347	0.030	0.038	0.074	Max = 0.347
	AF955	0.065	0.290	0.077	0.022	Median = 0.073
	C-22HS	0.275	0.166	0.074	0.021	Mean = 0.105
	825	0.169	0.001	0.040	0.161	Std-Dev = 0.098
Relative Difference Between Duplicate Coupons in the Same Test	725	8%	32%	67%	67%	Min = 0%
	945X	33%	8%	40%	29%	Max = 143%
	AF955	6%	143%	80%	26%	Median = 34%
	C-22HS	34%	86%	100%	35%	Mean = 45%
	825	22%	0%	33%	56%	Std-Dev = 36%

Final Report No. TS3333PH Rev2

Extended Duration Corrosion Testing of Five Ni-base
Corrosion Resistant Alloys at 15,000 psig and 350°F



Figure 1. The three Very High Pressure (VHP) Autoclaves Used for Experimental Evaluation of Cracking Susceptibility

Final Report No. TS3333PH Rev2

Extended Duration Corrosion Testing of Five Ni-base
Corrosion Resistant Alloys at 15,000 psig and 350°F



Alloy 825 coupons

Alloy C-22HS SCC C-ring and coupons

Alloy C-22HS GC-SCC C-ring with X-70 anodes

Alloy 725 SCC C-ring and coupons

Alloy 725 CG-SCC C-ring with X-70 anodes

Alloy 945X SCC C-ring and coupons

Alloy 945X GC-SCC C-ring with X-70 anodes

Alloy 955 SCC C-ring and coupons

Alloy 955 CG-SCC C-ring with X-70 anodes

Figure 2. Specimen Test Rack Ready for Autoclave Insertion

Final Report No. TS3333PH Rev2

Extended Duration Corrosion Testing of Five Ni-base
Corrosion Resistant Alloys at 15,000 psig and 350°F

Appendix A

Test I Post-Exposure Specimen Photographs

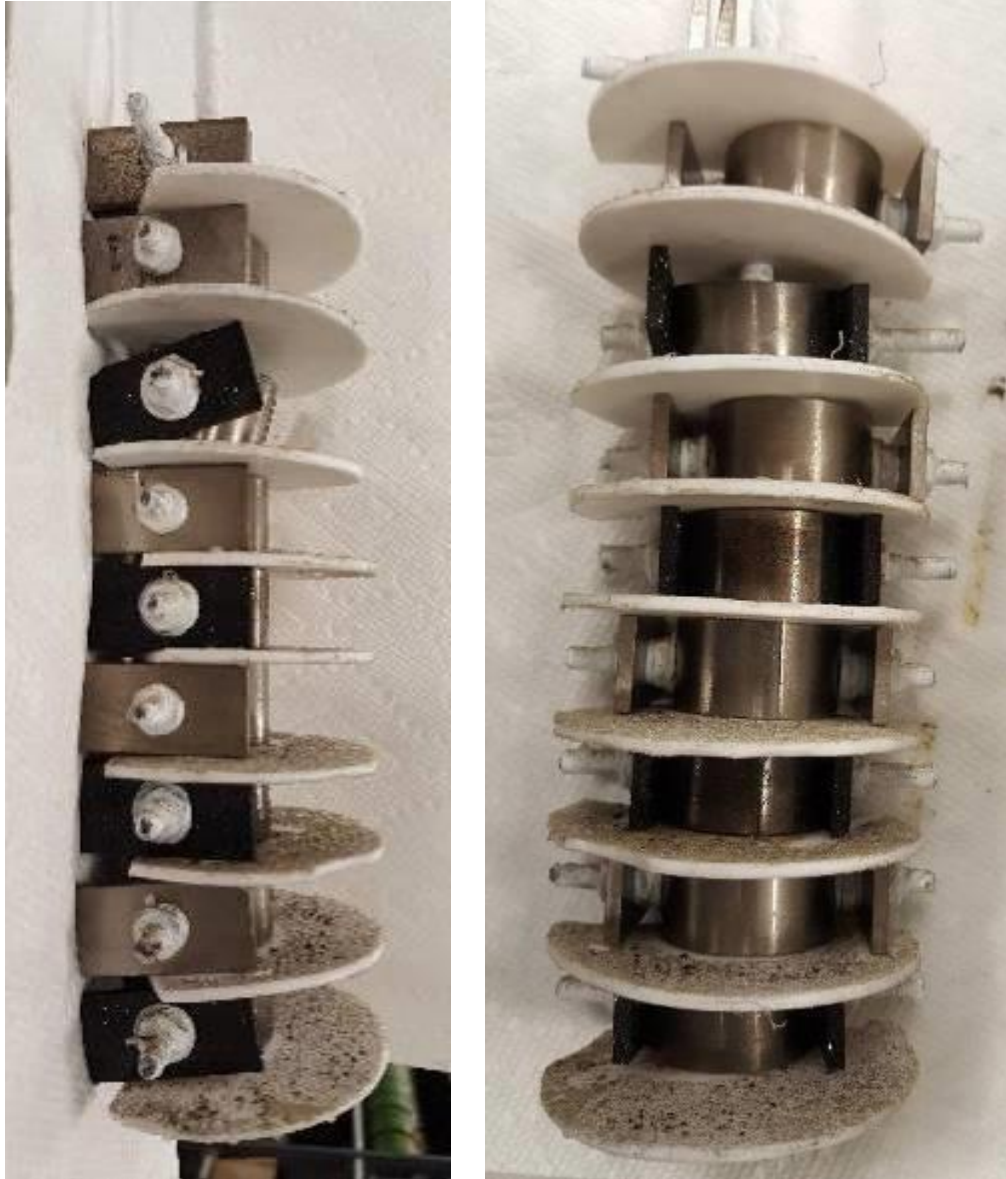
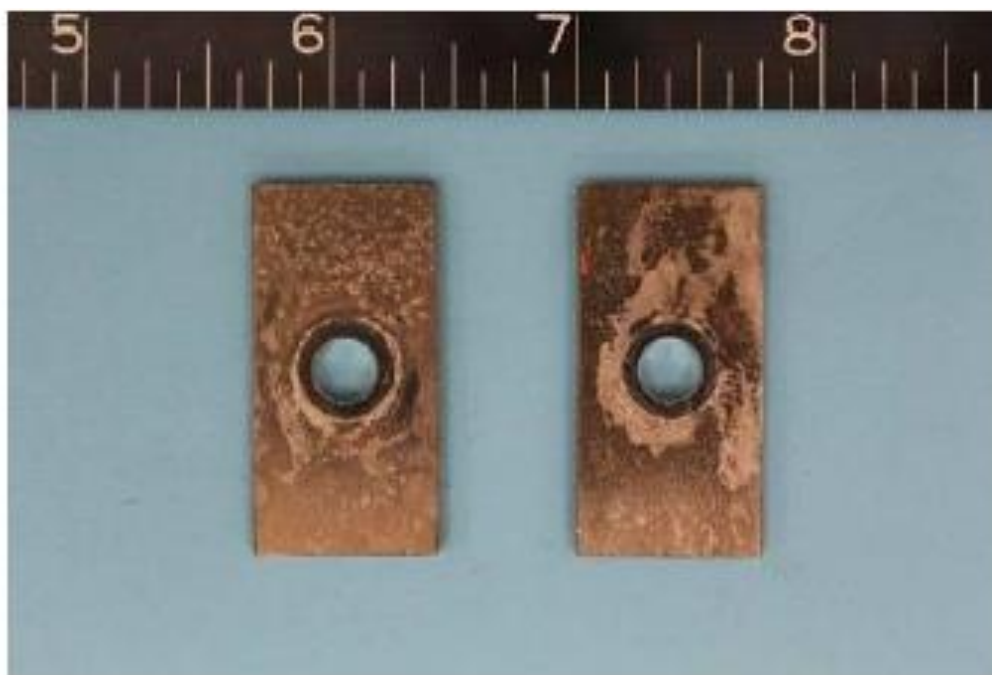


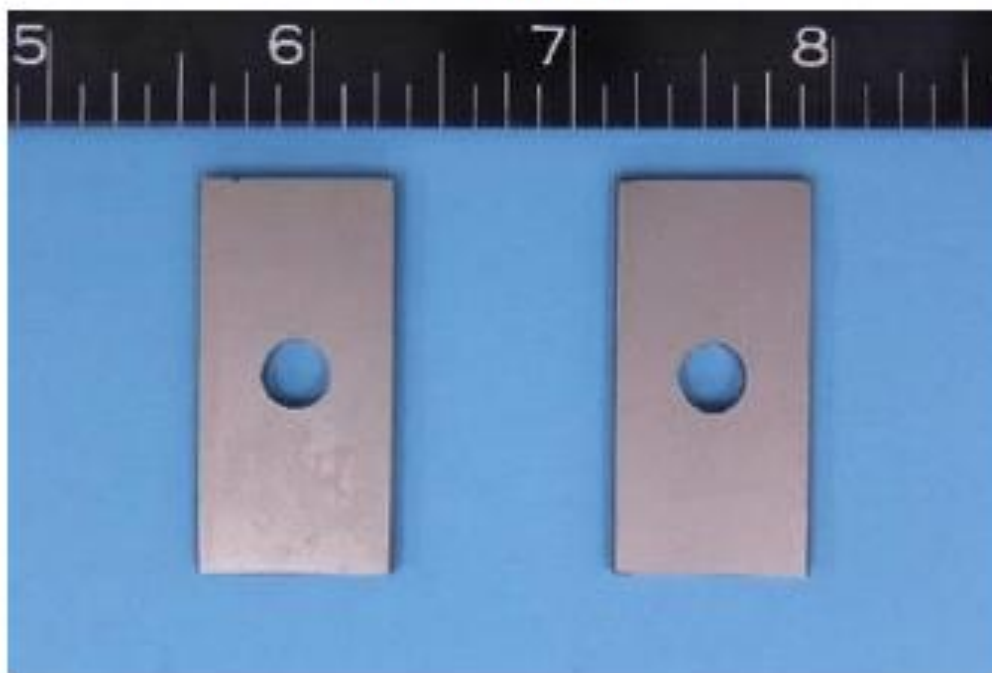
Figure A-1. Test Rack Upon Recovery.

Final Report No. TS3333PH Rev2

Extended Duration Corrosion Testing of Five Ni-base
Corrosion Resistant Alloys at 15,000 psig and 350°F



Before Cleaning

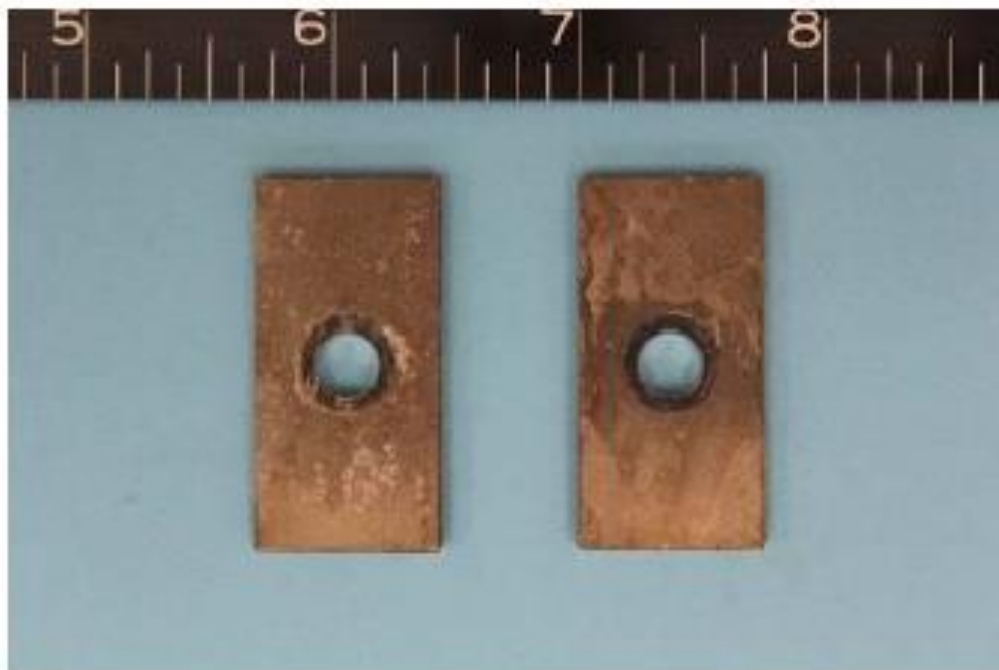


After Cleaning

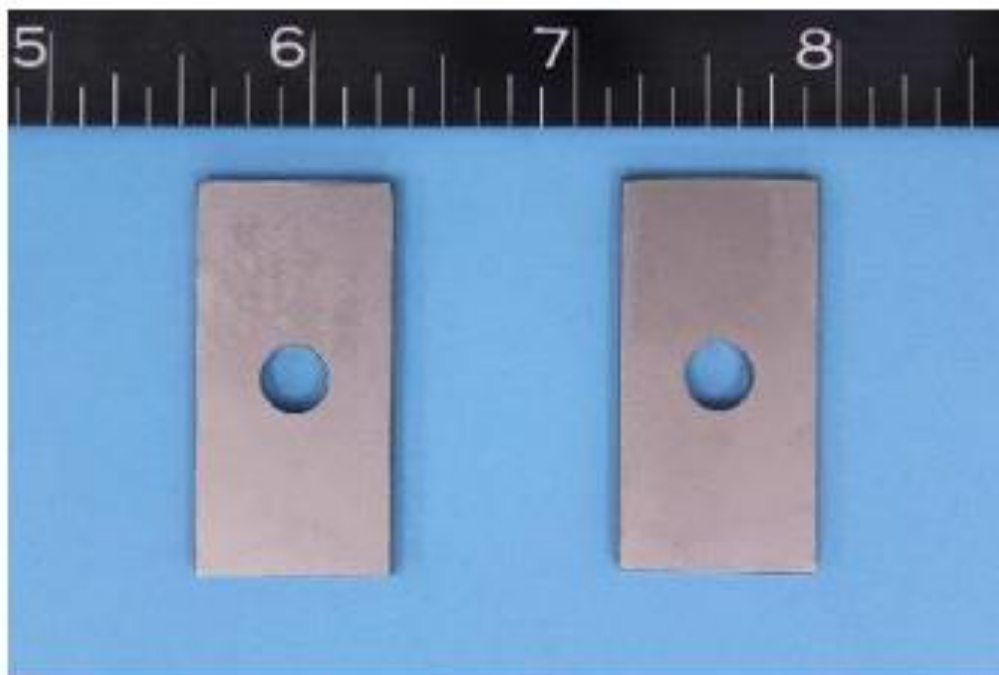
Figure A-2. Alloy 725 coupons, 6- week exposure, no pitting detected.

Final Report No. TS3333PH Rev2

Extended Duration Corrosion Testing of Five Ni-base
Corrosion Resistant Alloys at 15,000 psig and 350°F



Before Cleaning

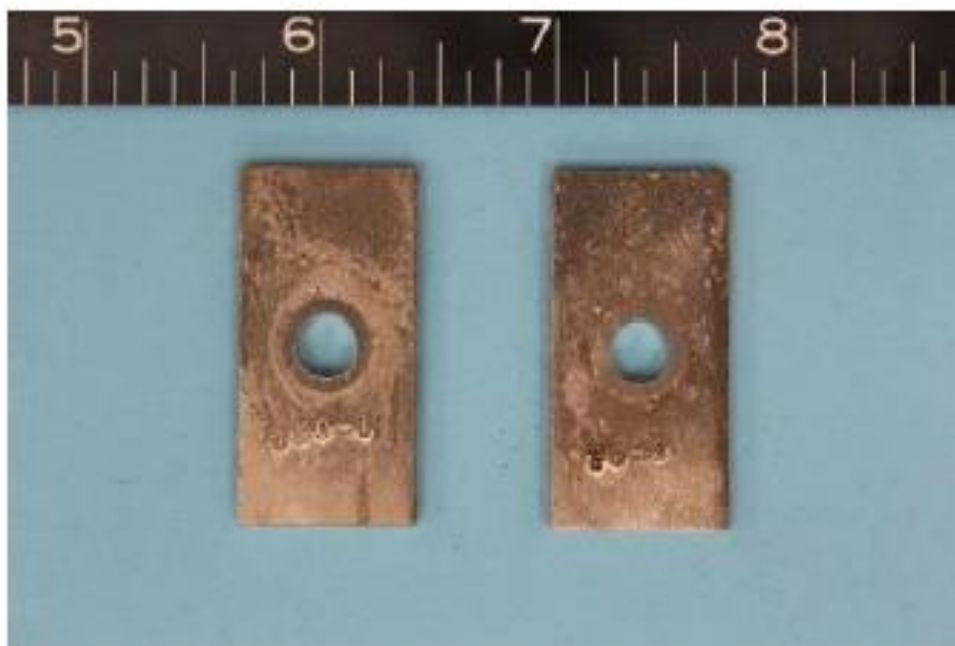


After Cleaning

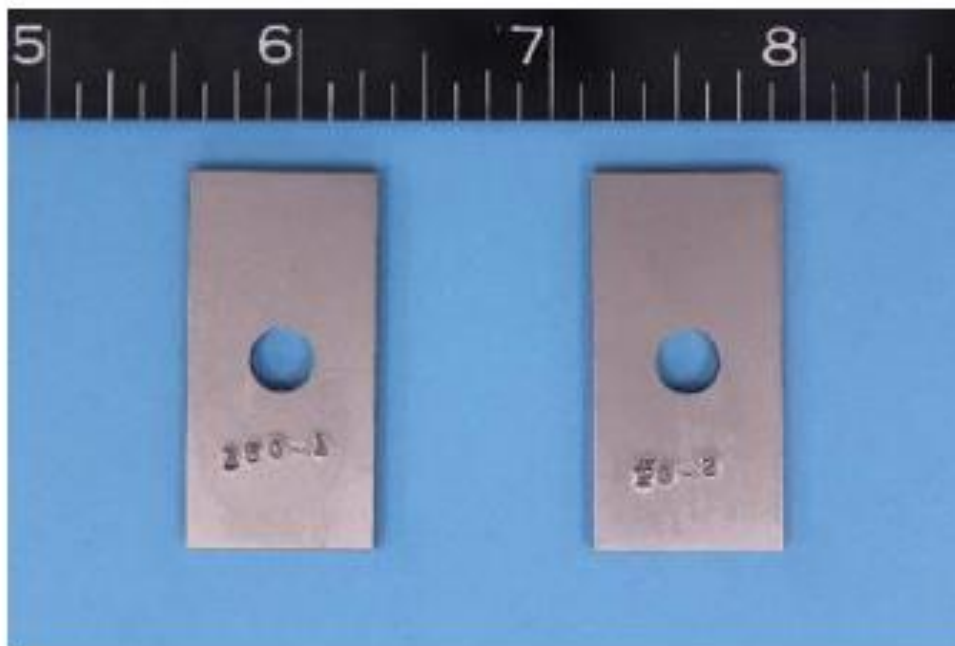
Figure A-3. Alloy 945X Coupons, 6-week exposure, no pitting detected.

Final Report No. TS3333PH Rev2

Extended Duration Corrosion Testing of Five Ni-base
Corrosion Resistant Alloys at 15,000 psig and 350°F



Before Cleaning

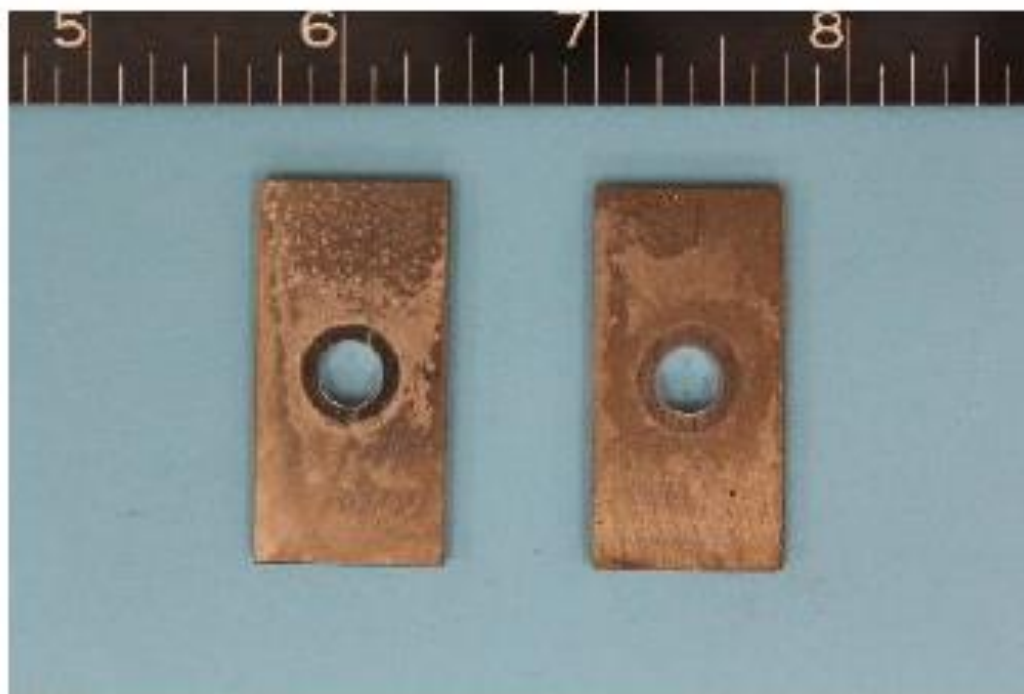


After Cleaning

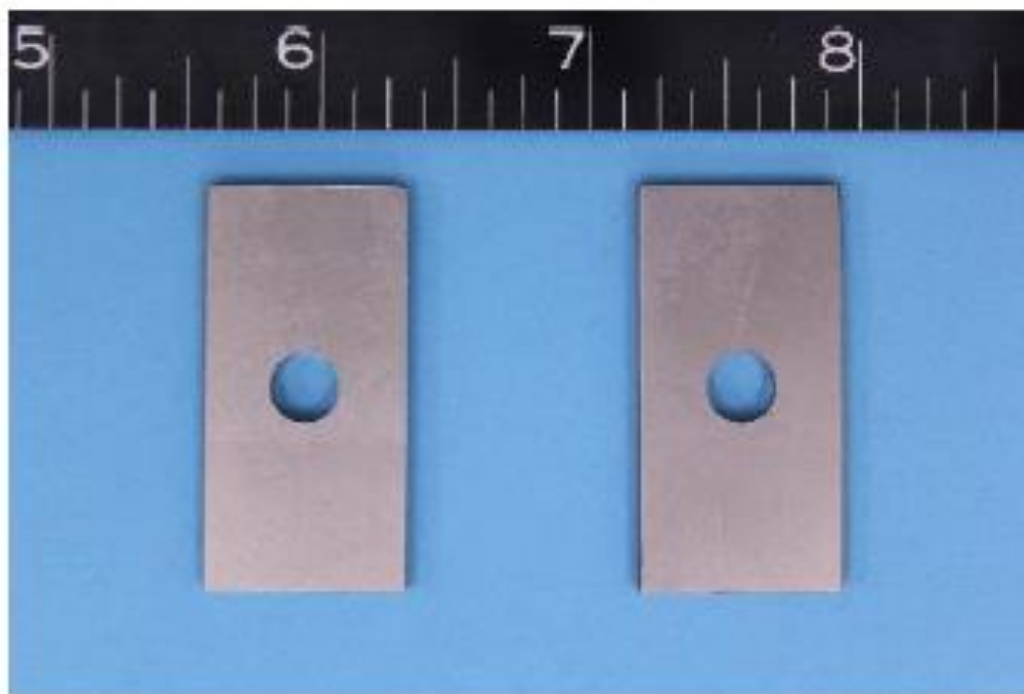
Figure A-4. Alloy 955 Coupons, 6-week exposure, no pitting detected.

Final Report No. TS3333PH Rev2

Extended Duration Corrosion Testing of Five Ni-base
Corrosion Resistant Alloys at 15,000 psig and 350°F



Before Cleaning



After Cleaning

Figure A-5. Alloy C-22HS coupons, 6-week exposure, no pitting detected.

Final Report No. TS3333PH Rev2

Extended Duration Corrosion Testing of Five Ni-base
Corrosion Resistant Alloys at 15,000 psig and 350°F

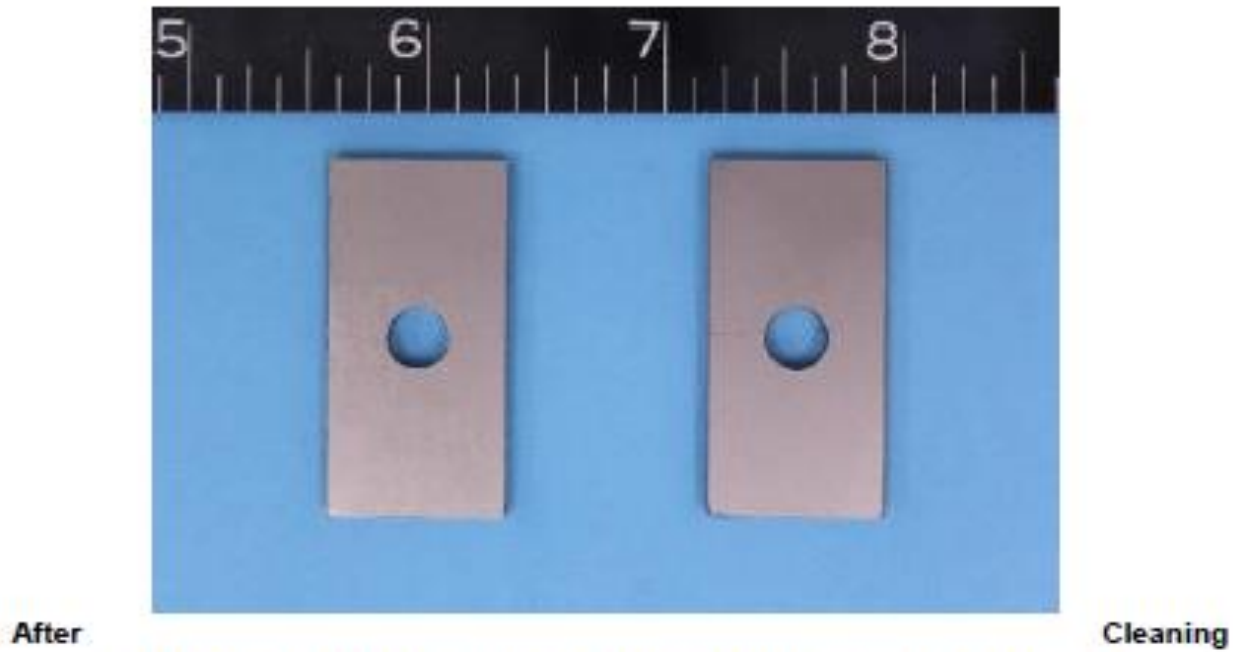
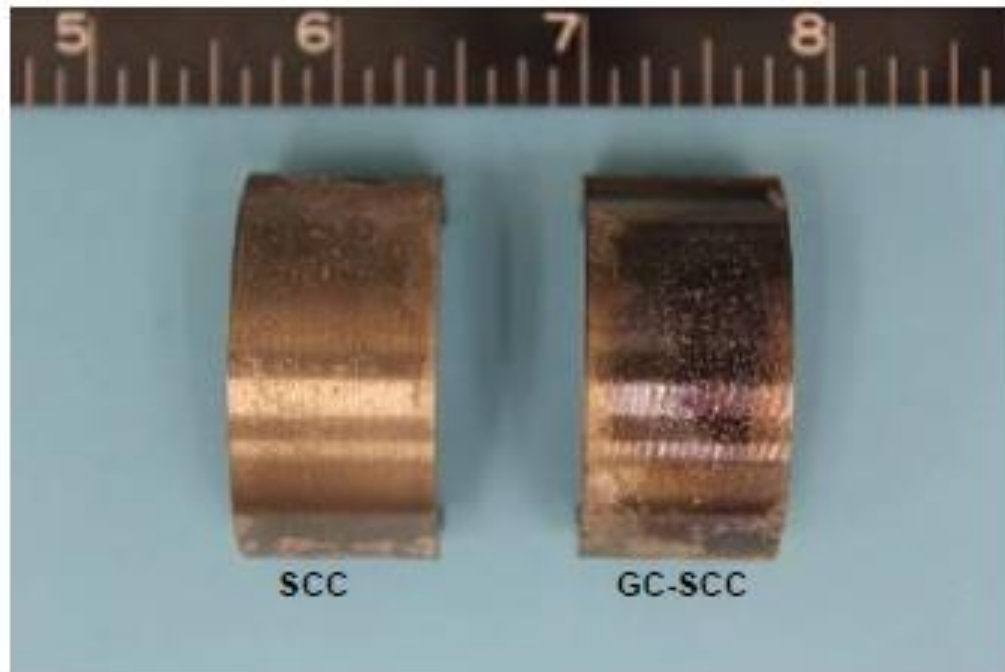


Figure A-6. Alloy 825 coupons, 6-week exposure, no pitting detected.

Final Report No. TS3333PH Rev2

Extended Duration Corrosion Testing of Five Ni-base
Corrosion Resistant Alloys at 15,000 psig and 350°F



Before Cleaning

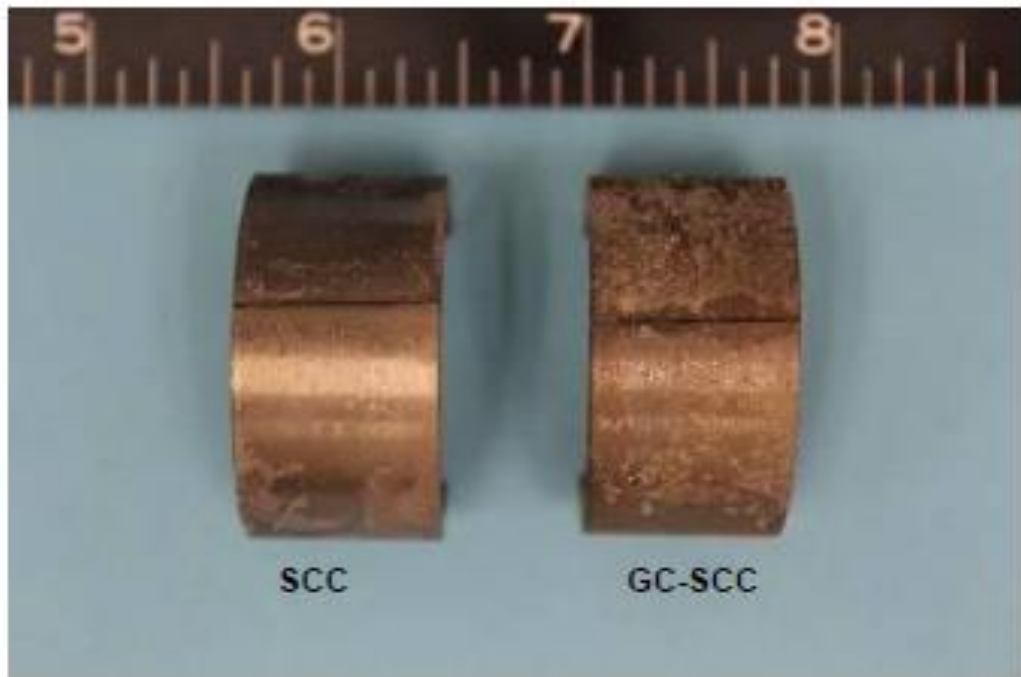


After Cleaning

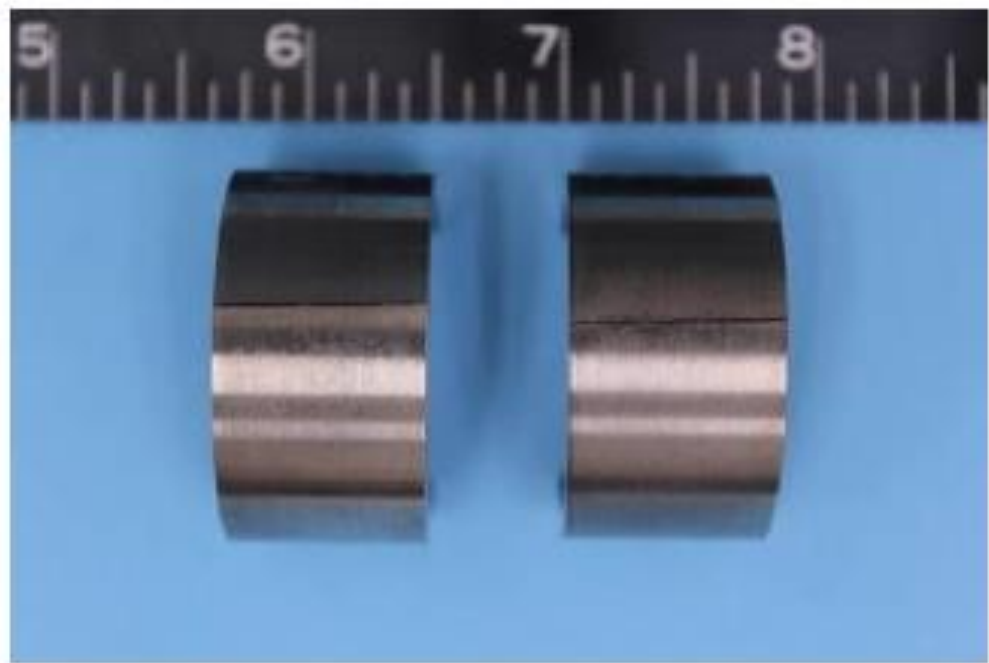
Figure A-7. Alloy 725 C-rings, 6-week exposure, no cracking detected.

Final Report No. TS3333PH Rev2

Extended Duration Corrosion Testing of Five Ni-base
Corrosion Resistant Alloys at 15,000 psig and 350°F



Before Cleaning

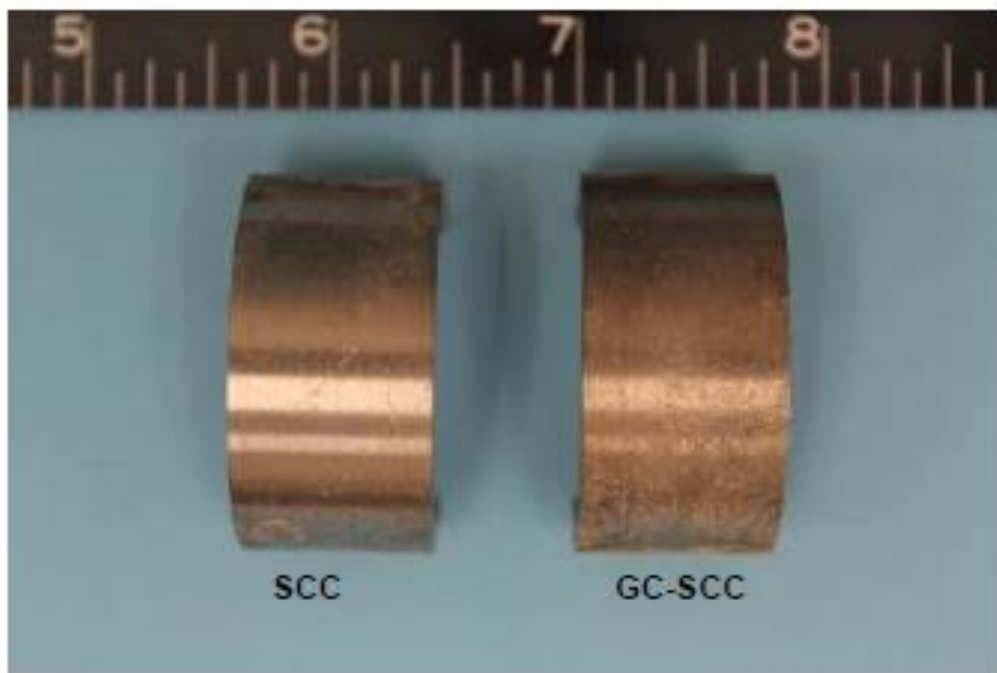


After Cleaning

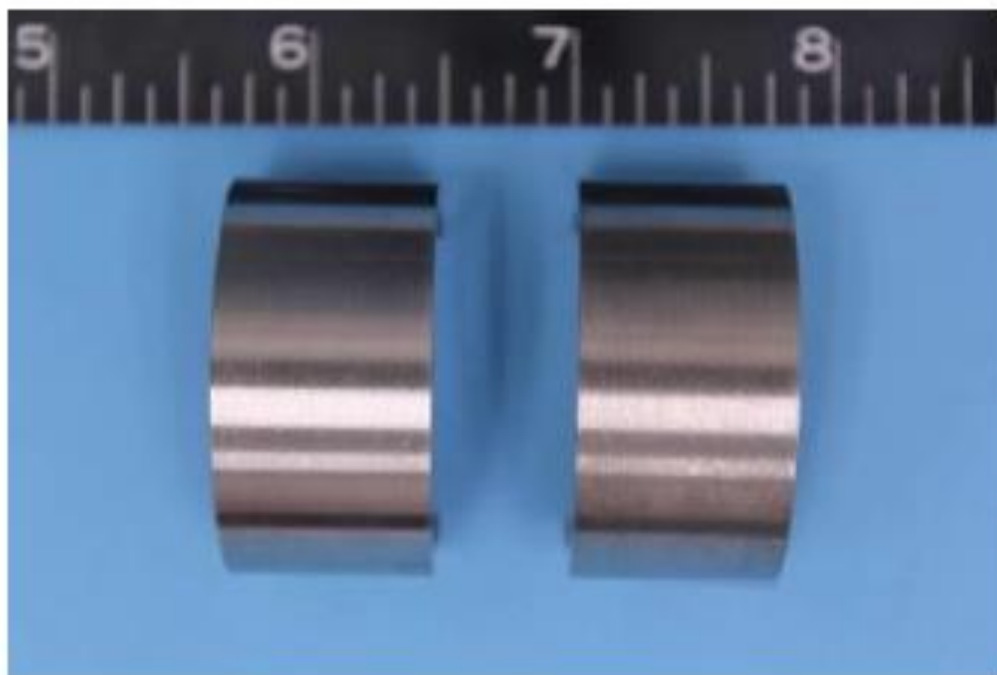
Figure A-8. Alloy 945X C-rings, 6-week exposure, both C-rings cracked.

Final Report No. TS3333PH Rev2

Extended Duration Corrosion Testing of Five Ni-base
Corrosion Resistant Alloys at 15,000 psig and 350°F



Before Cleaning

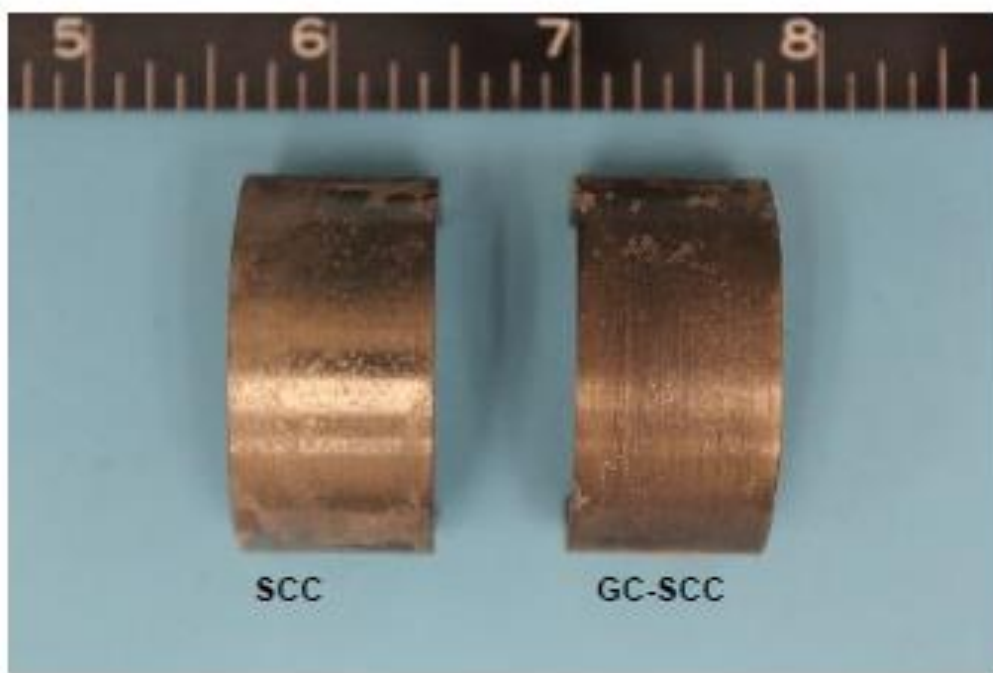


After Cleaning

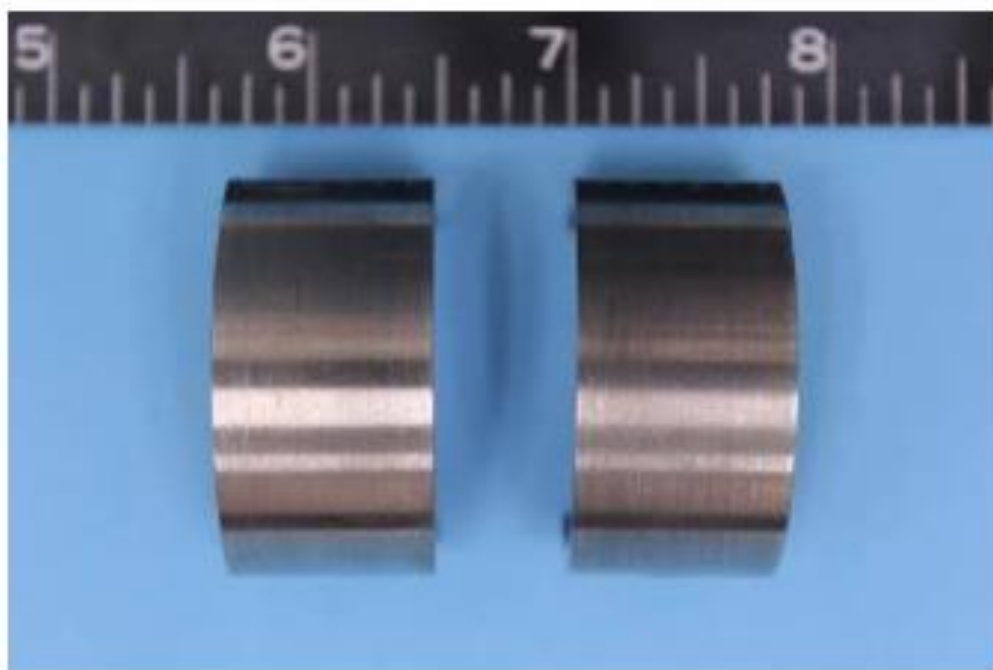
Figure A-9. Alloy 955 C-rings, 6-week exposure, no cracking detected.

Final Report No. TS3333PH Rev2

Extended Duration Corrosion Testing of Five Ni-base
Corrosion Resistant Alloys at 15,000 psig and 350°F



Before Cleaning



After Cleaning

Figure A-10. Alloy C-22HS C-rings, 6-Week exposure, no cracking detected.

Final Report No. TS3333PH Rev2

Extended Duration Corrosion Testing of Five Ni-base

Corrosion Resistant Alloys at 15,000 psig and 350°F

Appendix B

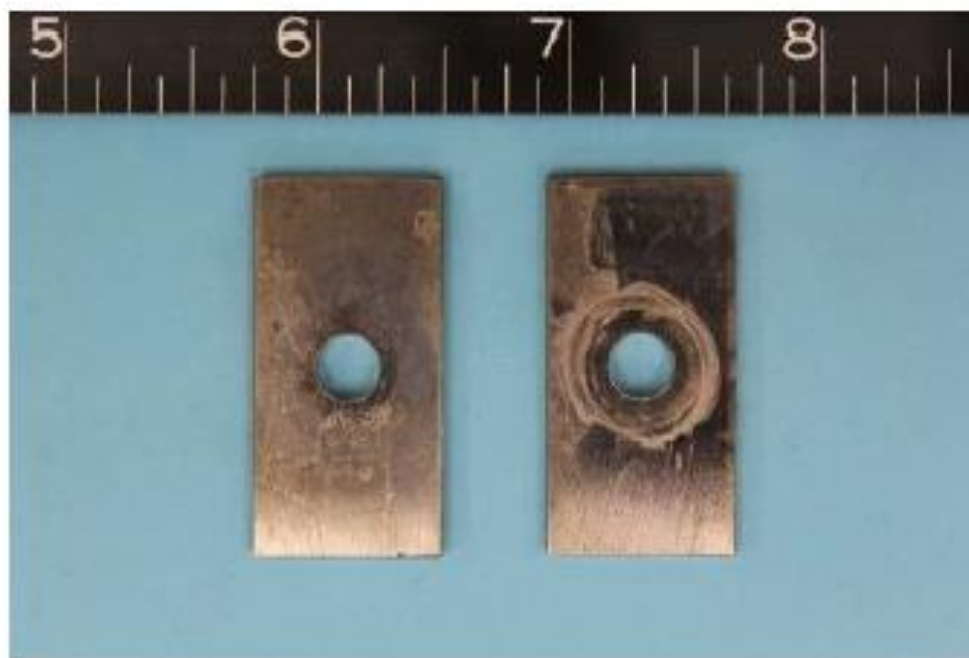
Test II Post-Exposure Specimen Photographs



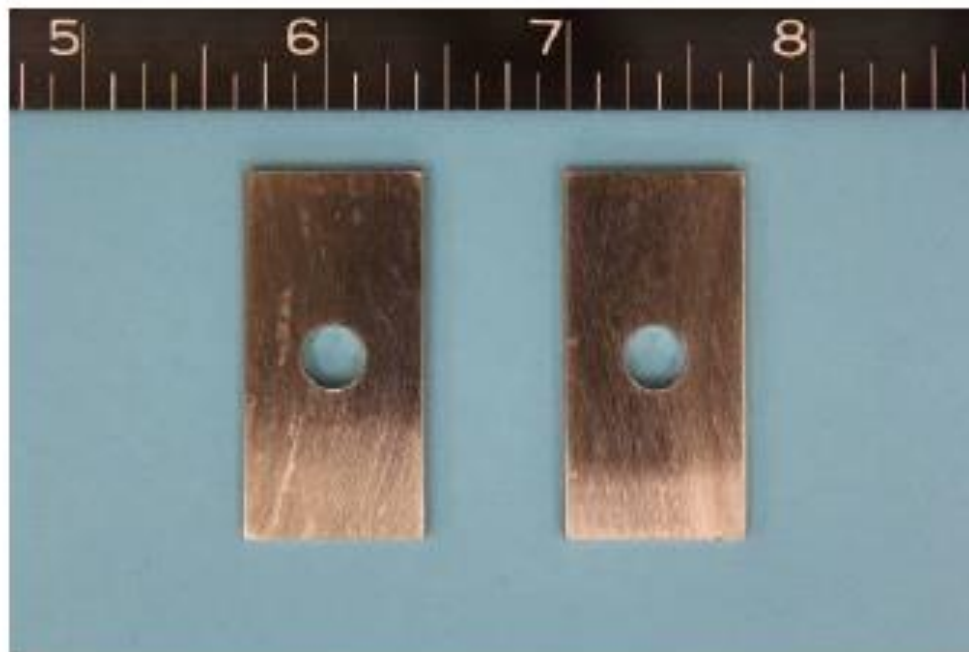
Figure B-1. Test Rack Upon Recovery.

Final Report No. TS3333PH Rev2

Extended Duration Corrosion Testing of Five Ni-base
Corrosion Resistant Alloys at 15,000 psig and 350°F



Before Cleaning

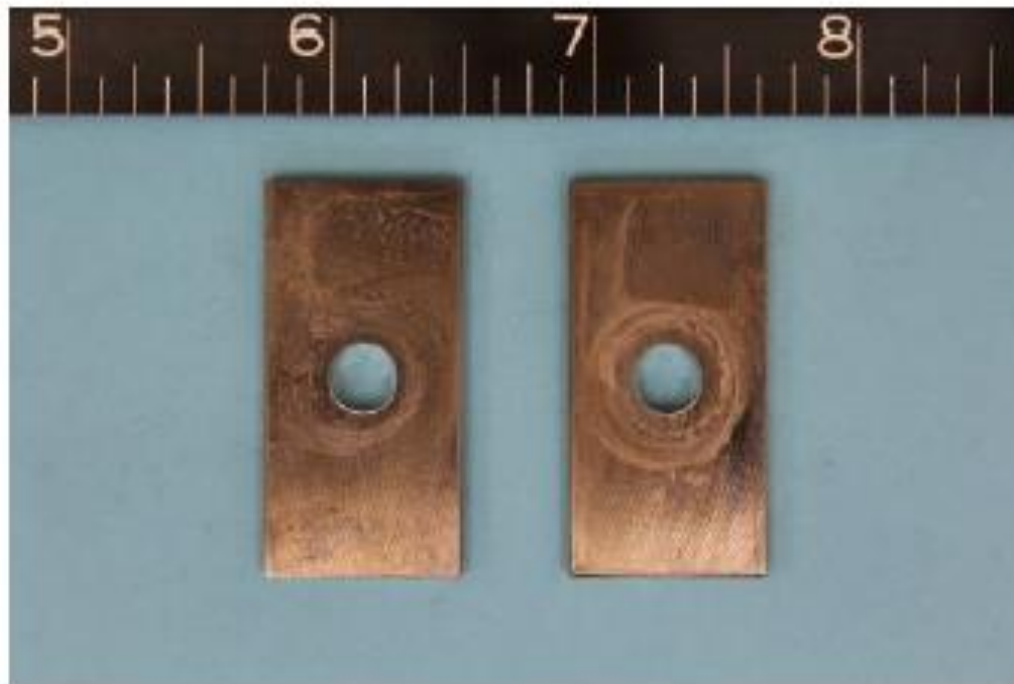


After Cleaning

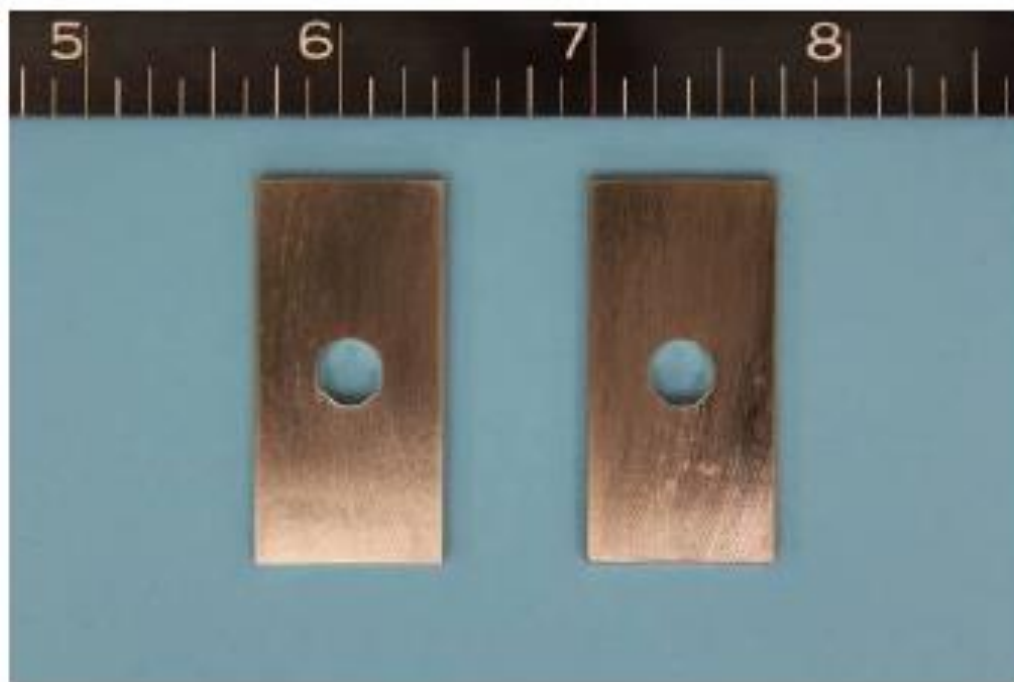
Figure B-2. Alloy 725 coupons, 12-week exposure

Final Report No. TS3333PH Rev2

Extended Duration Corrosion Testing of Five Ni-base
Corrosion Resistant Alloys at 15,000 psig and 350°F



Before Cleaning

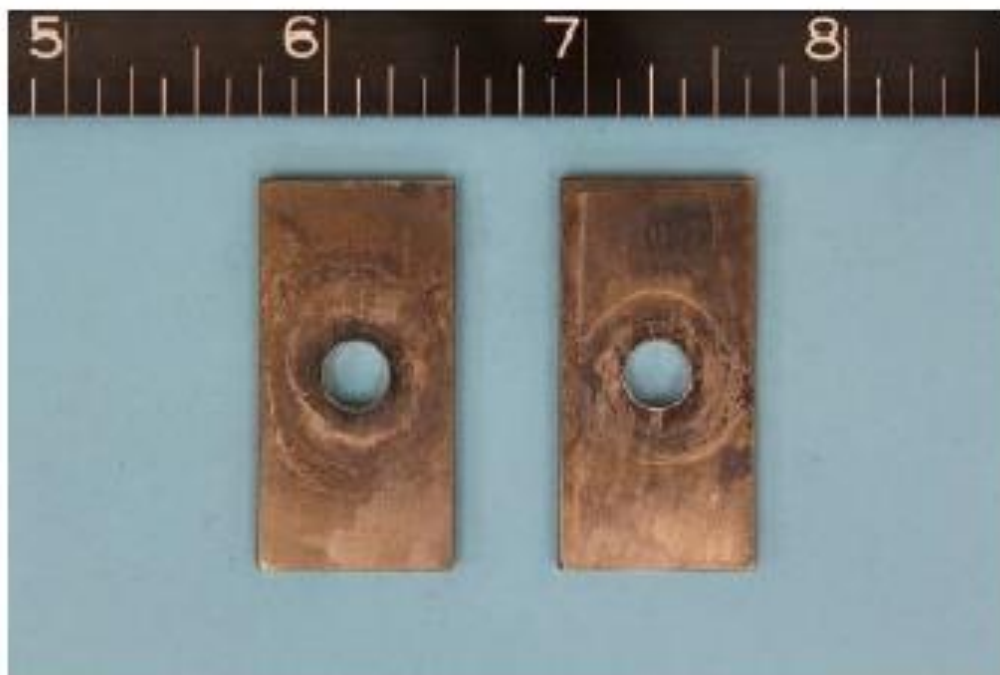


After Cleaning

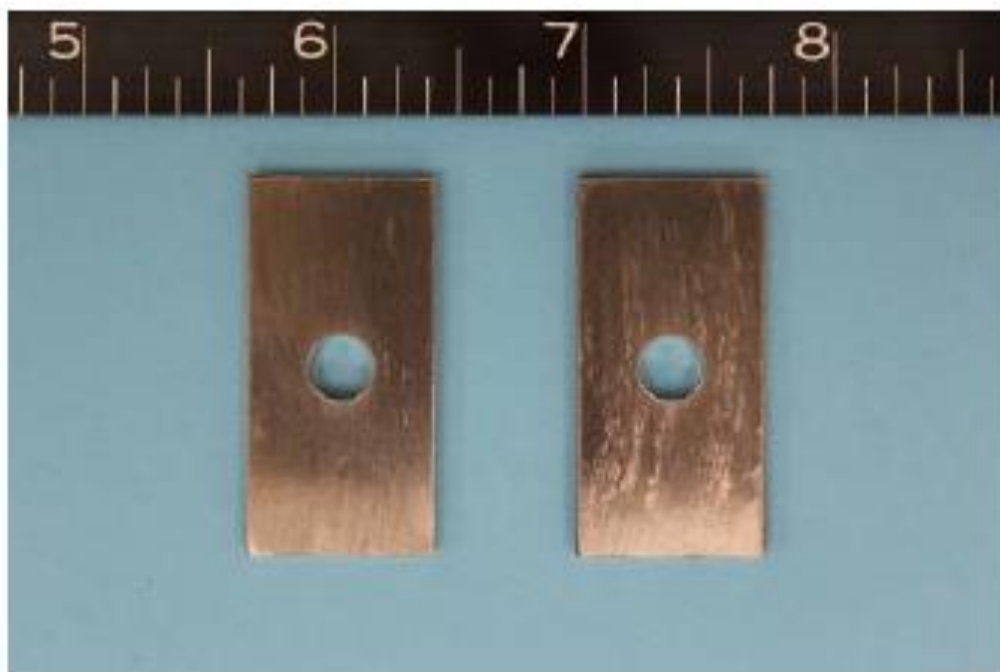
Figure B-3. Alloy 945X Coupons, 12-week exposure

Final Report No. TS3333PH Rev2

Extended Duration Corrosion Testing of Five Ni-base
Corrosion Resistant Alloys at 15,000 psig and 350°F



Before Cleaning

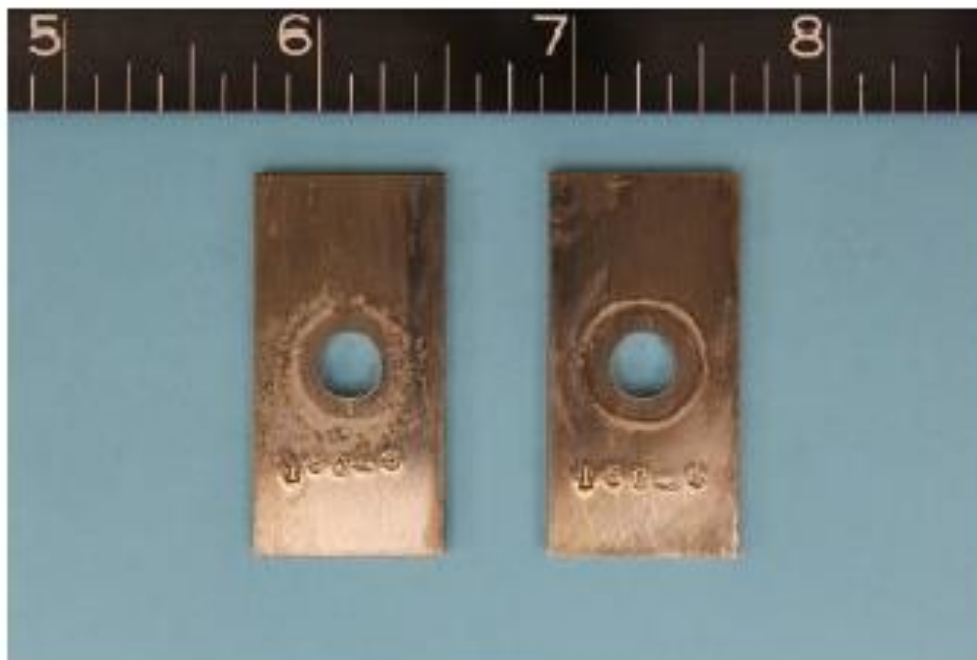


After Cleaning

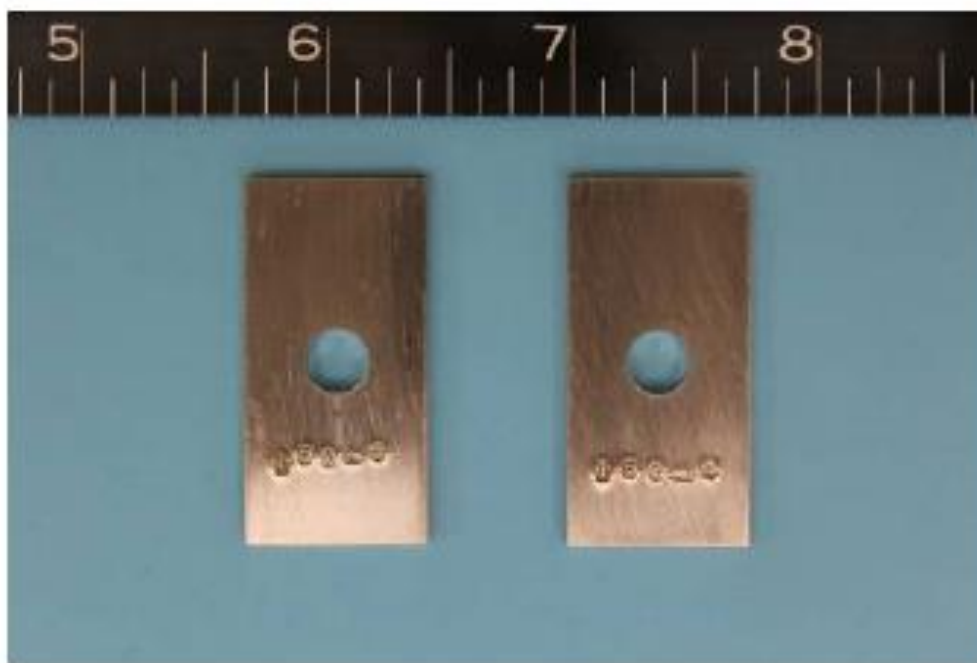
Figure B-4. Alloy 955 Coupons, 12-week exposure

Final Report No. TS3333PH Rev2

Extended Duration Corrosion Testing of Five Ni-base
Corrosion Resistant Alloys at 15,000 psig and 350°F



Before Cleaning

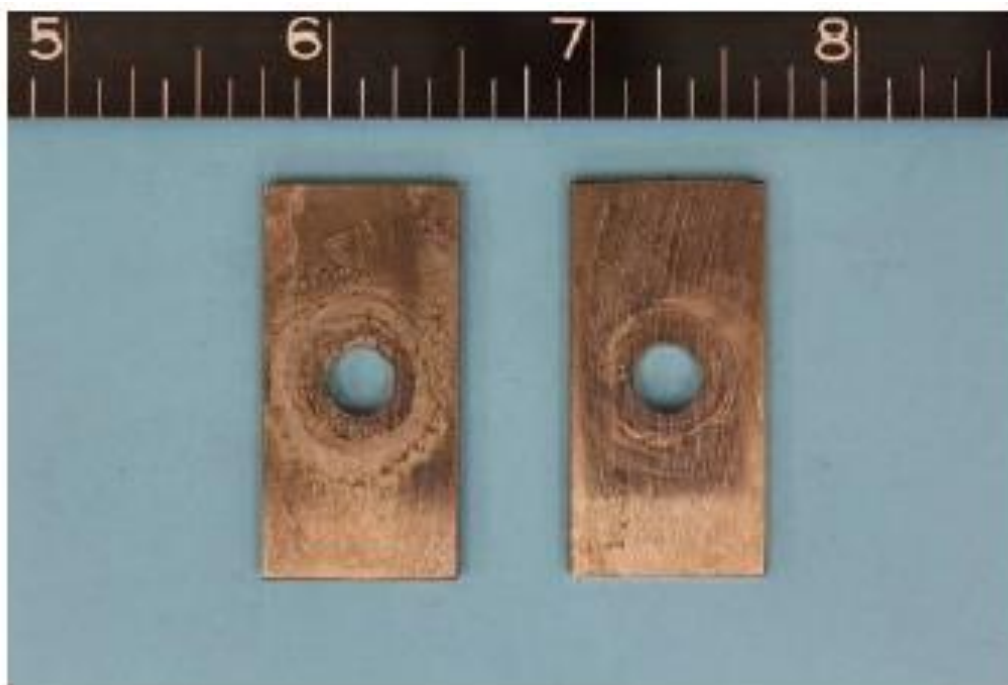


After Cleaning

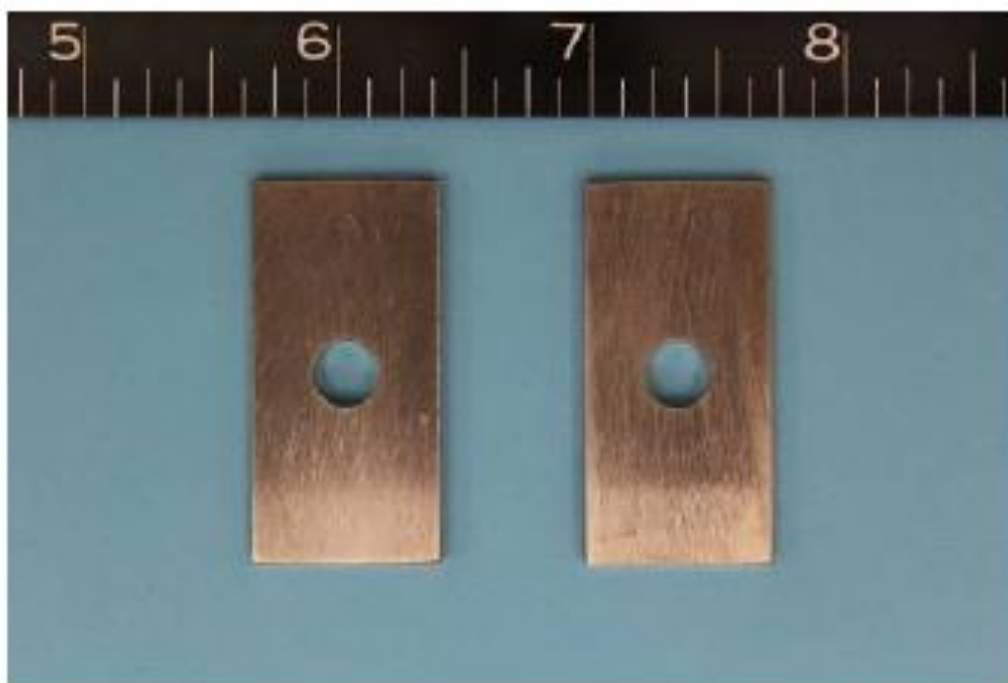
Figure B-5. Alloy C-22HS coupons, 12-week exposure

Final Report No. TS3333PH Rev2

Extended Duration Corrosion Testing of Five Ni-base
Corrosion Resistant Alloys at 15,000 psig and 350°F



Before Cleaning

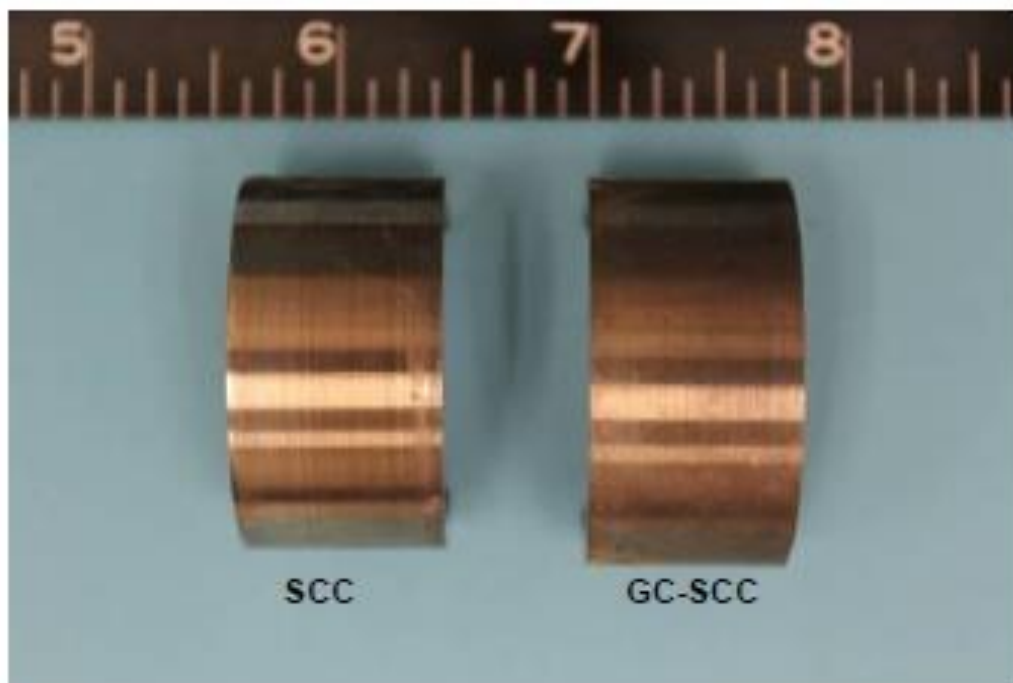


After Cleaning

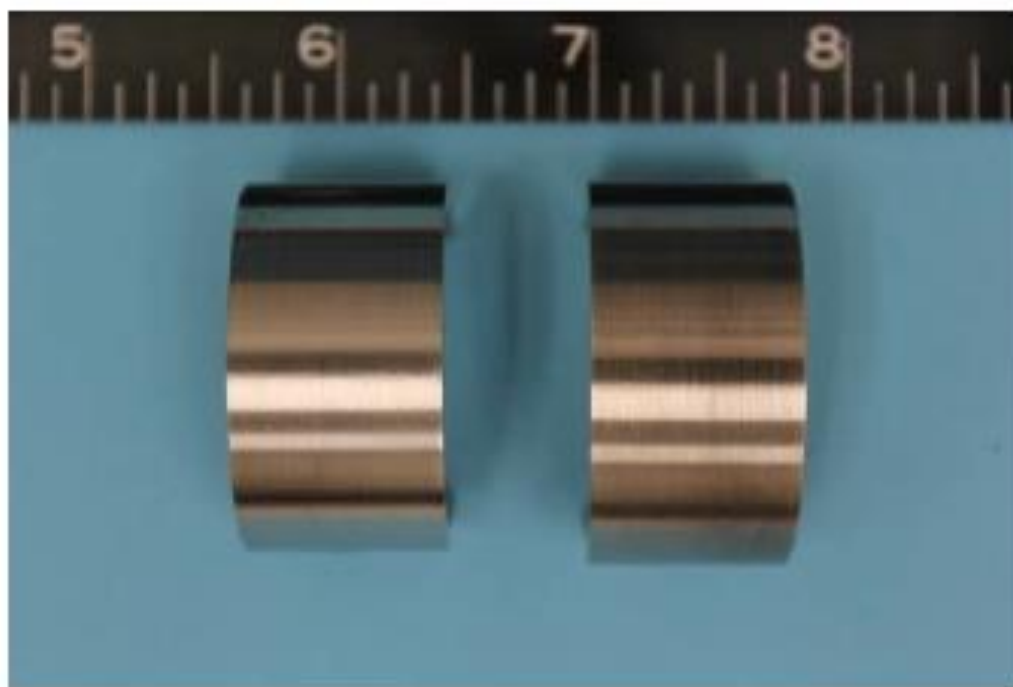
Figure B 6. Alloy 825 coupons, 12-week exposure

Final Report No. TS3333PH Rev2

Extended Duration Corrosion Testing of Five Ni-base
Corrosion Resistant Alloys at 15,000 psig and 350°F



Before Cleaning

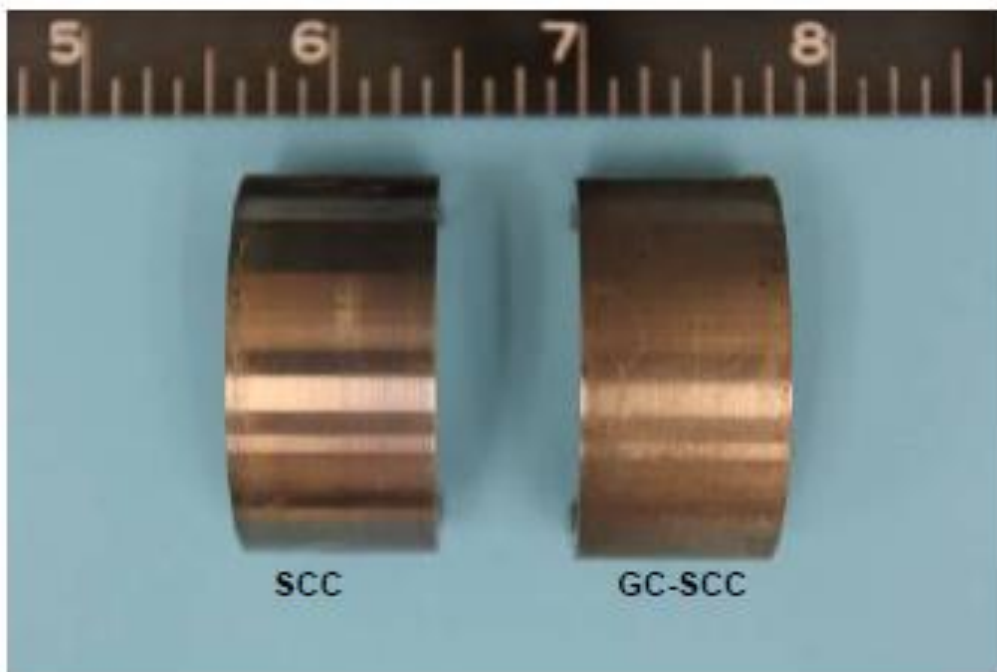


After Cleaning

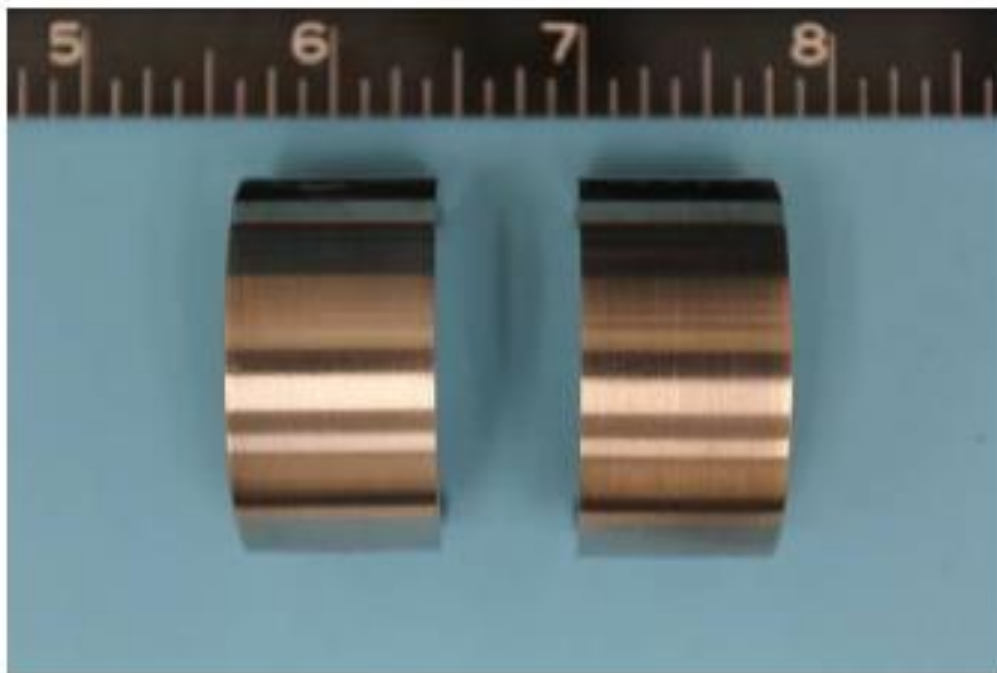
Figure B-7. Alloy 725 C-rings, 12-week exposure

Final Report No. TS3333PH Rev2

Extended Duration Corrosion Testing of Five Ni-base
Corrosion Resistant Alloys at 15,000 psig and 350°F



Before Cleaning

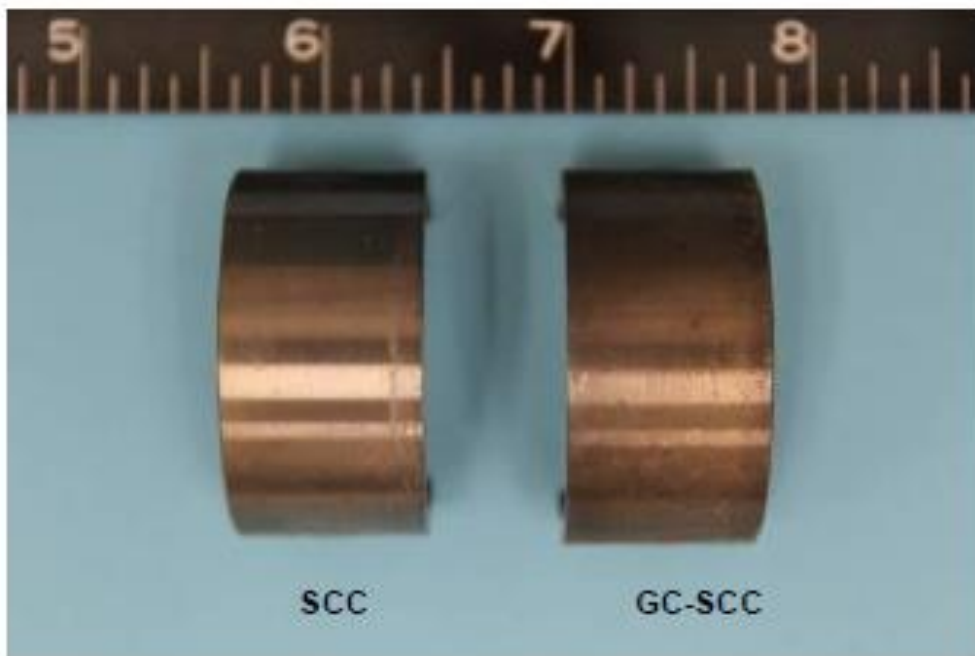


After Cleaning

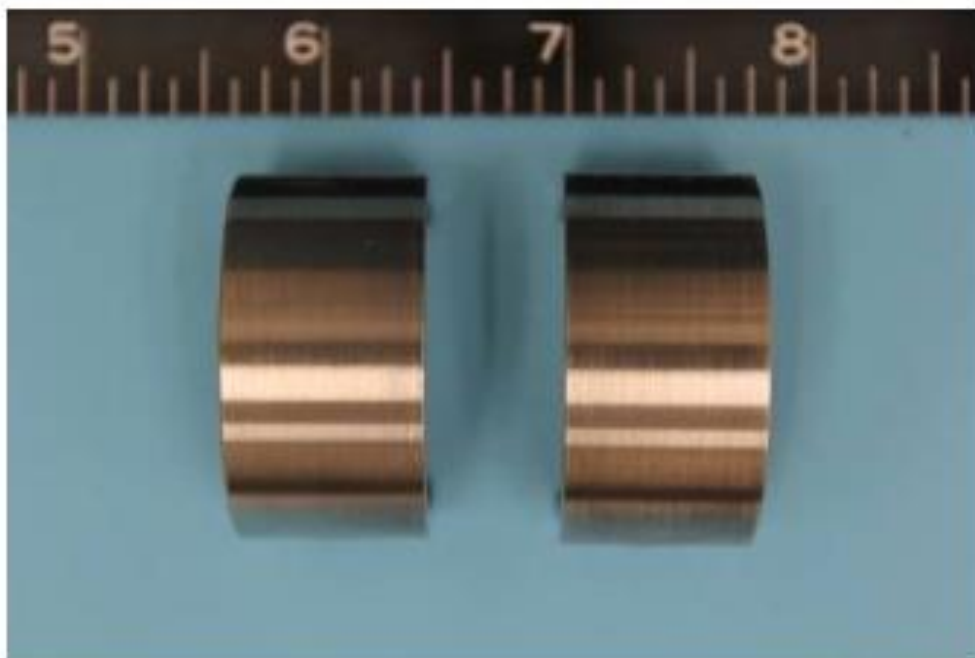
Figure B-8. Alloy 945X C-rings, 12-week exposure

Final Report No. TS3333PH Rev2

Extended Duration Corrosion Testing of Five Ni-base
Corrosion Resistant Alloys at 15,000 psig and 350°F



Before Cleaning

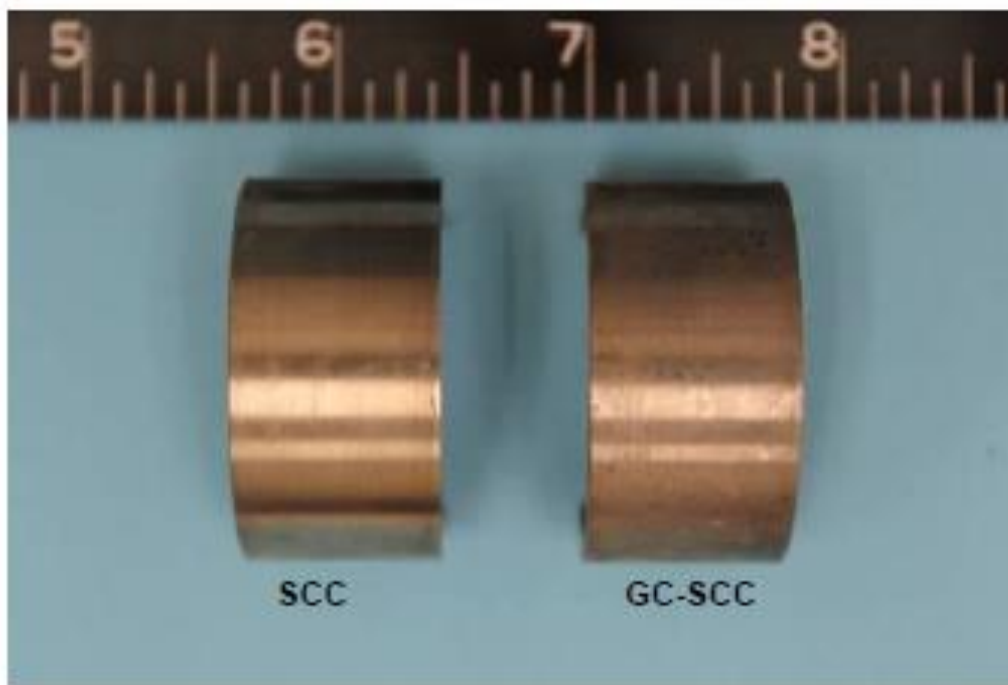


After Cleaning

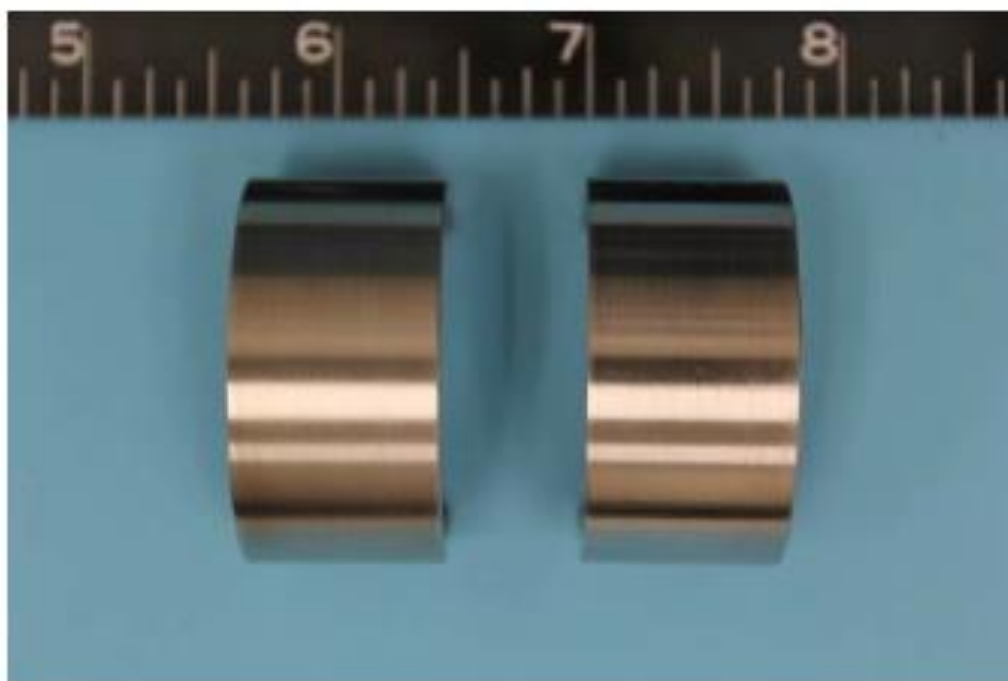
Figure B-9. Alloy 955 C-rings, 12-week exposure

Final Report No. TS3333PH Rev2

Extended Duration Corrosion Testing of Five Ni-base
Corrosion Resistant Alloys at 15,000 psig and 350°F



Before Cleaning



After Cleaning

Figure B-8. Alloy C-22HS C-rings, 12-week exposure

Final Report No. TS3333PH Rev2

Extended Duration Corrosion Testing of Five Ni-base

Corrosion Resistant Alloys at 15,000 psig and 350°F

Appendix C

Eighteen-Week Exposure Post-Exposure Specimen Photographs

Note:

The 18-week post-exposure "before cleaning" specimen photographs were inadvertently not taken.

Final Report No. TS3333PH Rev2

Extended Duration Corrosion Testing of Five Ni-base

Corrosion Resistant Alloys at 15,000 psig and 350°F

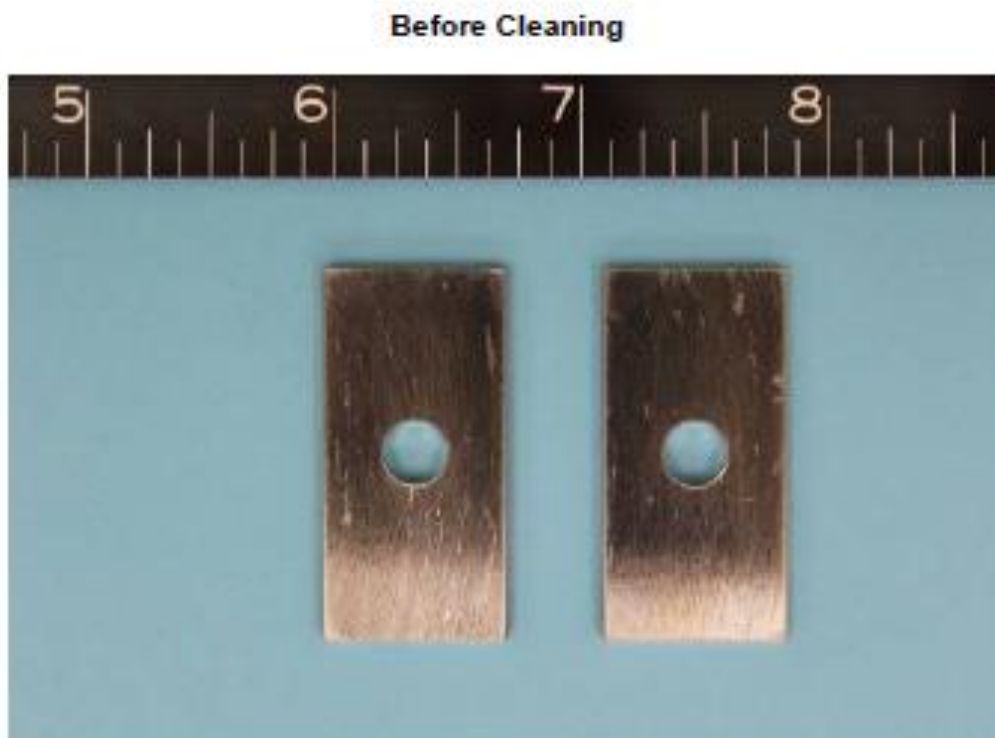


Figure C-1. Alloy 725 Coupons after 18-week exposure and cleaning, pitting not observed.

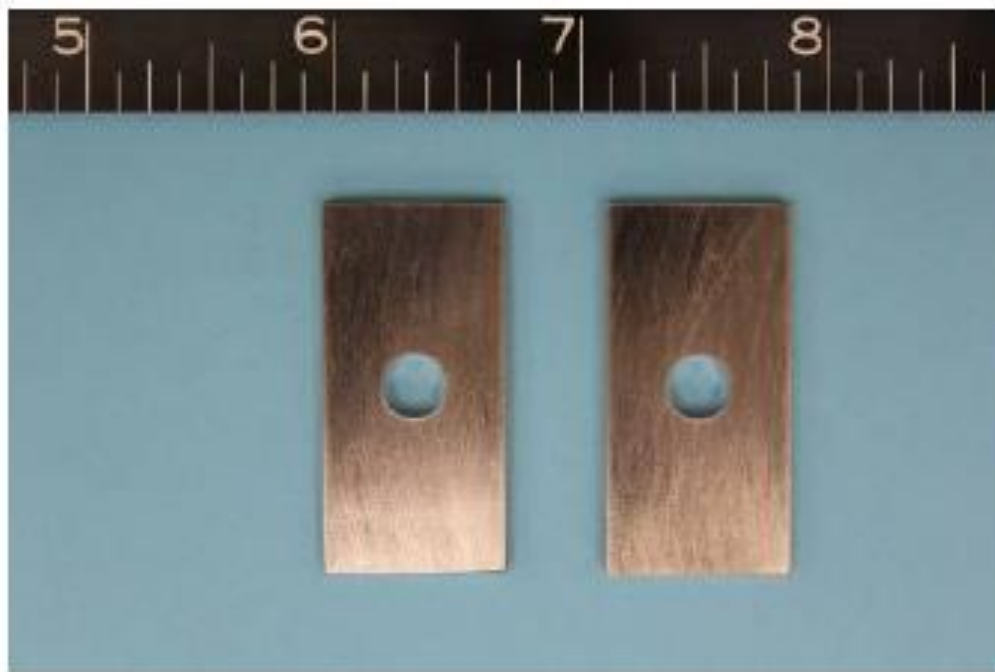


Figure C-2. Alloy 945X Coupons after 18-week exposure and cleaning, pitting not observed.

Final Report No. TS3333PH Rev2

Extended Duration Corrosion Testing of Five Ni-base
Corrosion Resistant Alloys at 15,000 psig and 350°F

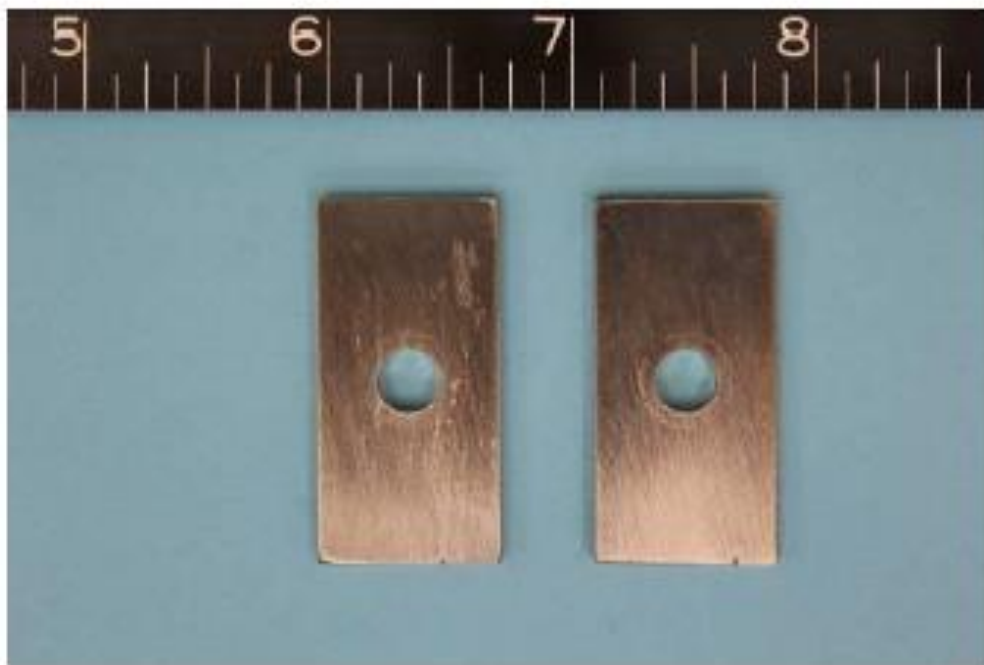


Figure C-3. Alloy 955 Coupons after 18-week exposure and cleaning, pitting not observed.

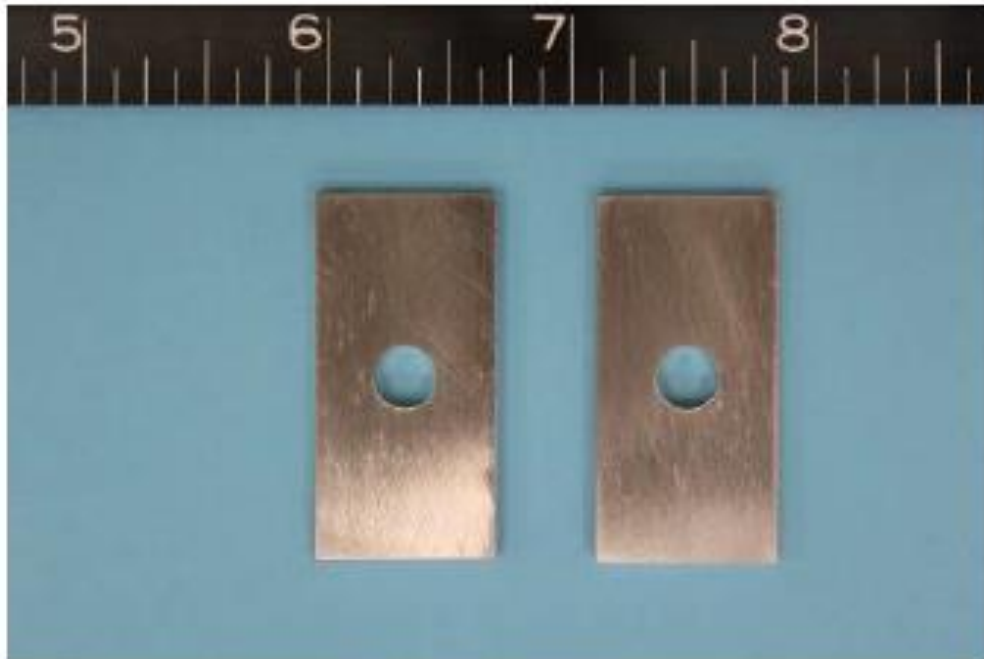
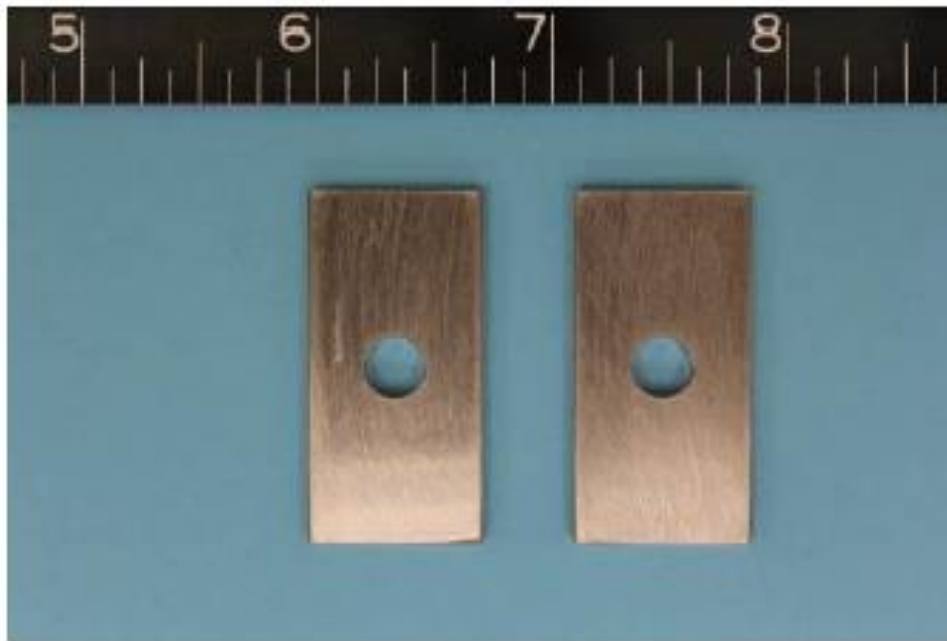


Figure C-4. Alloy C-22HS Coupons after 18-week exposure and cleaning, no pitting observed.

Final Report No. TS3333PH Rev2

Extended Duration Corrosion Testing of Five Ni-base
Corrosion Resistant Alloys at 15,000 psig and 350°F



After Cleaning

Figure C 5. Alloy 825 Coupons after 18-week exposure and cleaning, no pitting observed.

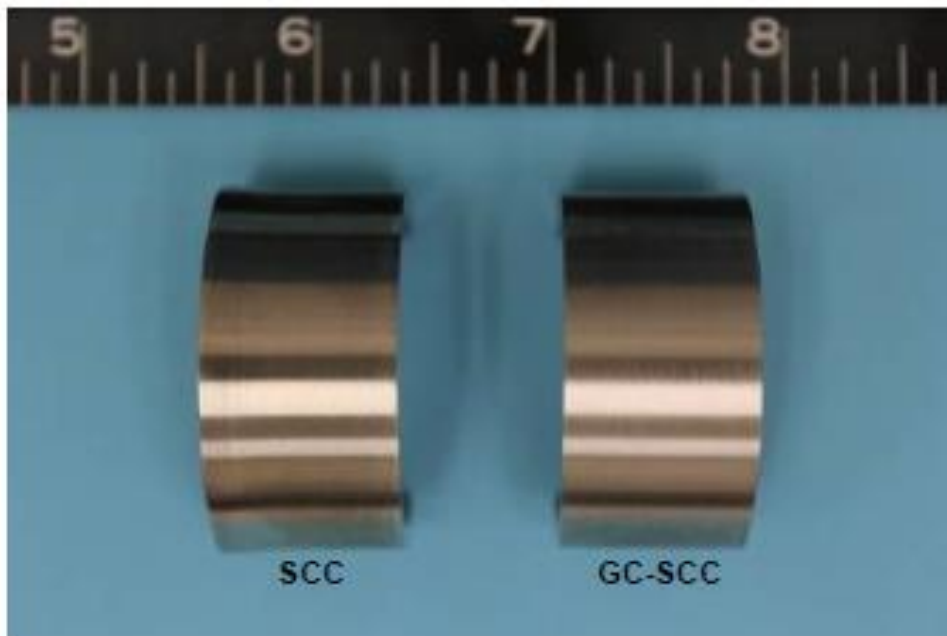


Figure C-6. Alloy 725 C-rings after 18-week exposure and cleaning, no evidence of cracking.

Final Report No. TS3333PH Rev2

Extended Duration Corrosion Testing of Five Ni-base
Corrosion Resistant Alloys at 15,000 psig and 350°F

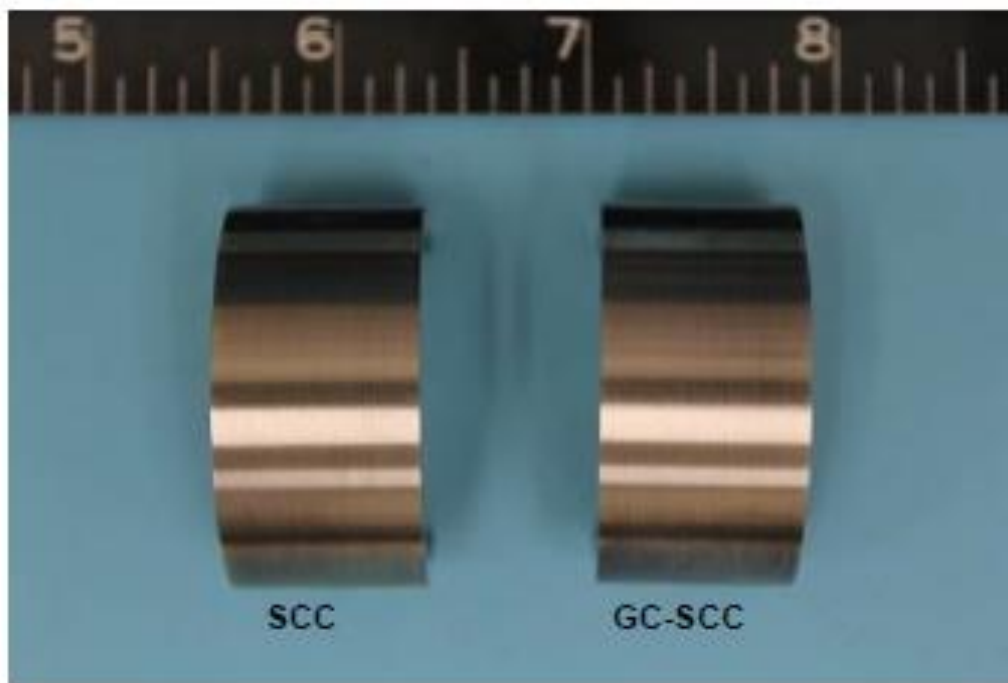


Figure C-7. Alloy 945X C-rings after 18-week exposure and cleaning, no evidence of cracking.

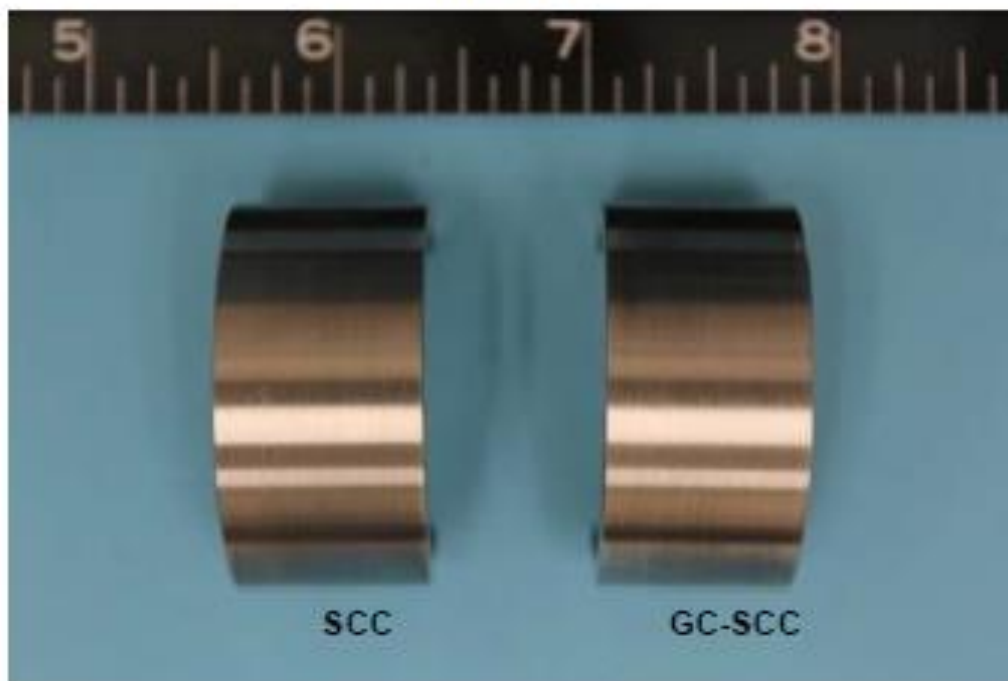


Figure C-8. Alloy 955X C-rings after 18-week exposure and cleaning, no evidence of cracking.

Final Report No. TS3333PH Rev2

Extended Duration Corrosion Testing of Five Ni-base
Corrosion Resistant Alloys at 15,000 psig and 350°F

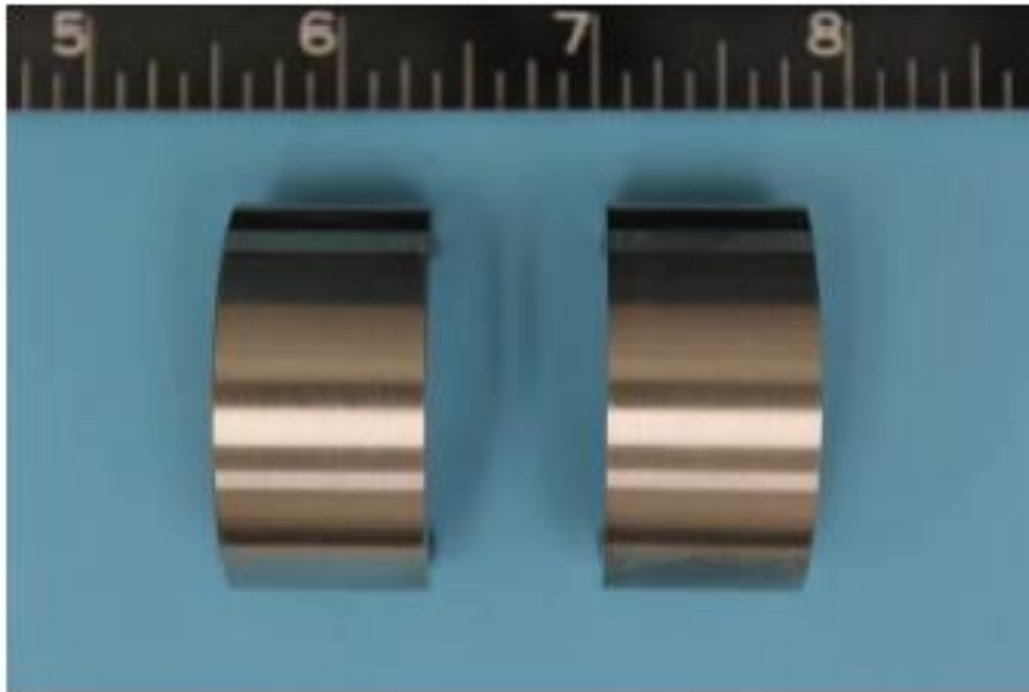


Figure C-9. Alloy C-22HS C-rings after 18-week exposure and cleaning, no evidence of cracking.

Final Report No. TS3333PH *Rev2*

Extended Duration Corrosion Testing of Five Ni-base

Corrosion Resistant Alloys at 15,000 psig and 350°F

Appendix D

Test IV

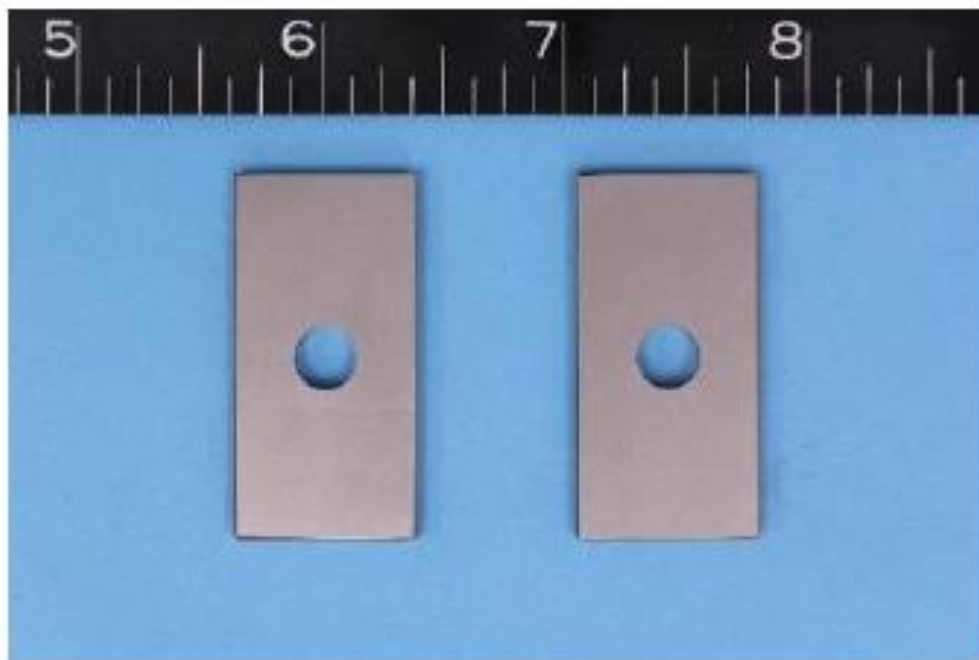
Post-Exposure Specimen Photographs

Final Report No. TS3333PH Rev2

Extended Duration Corrosion Testing of Five Ni-base
Corrosion Resistant Alloys at 15,000 psig and 350°F



Before Cleaning

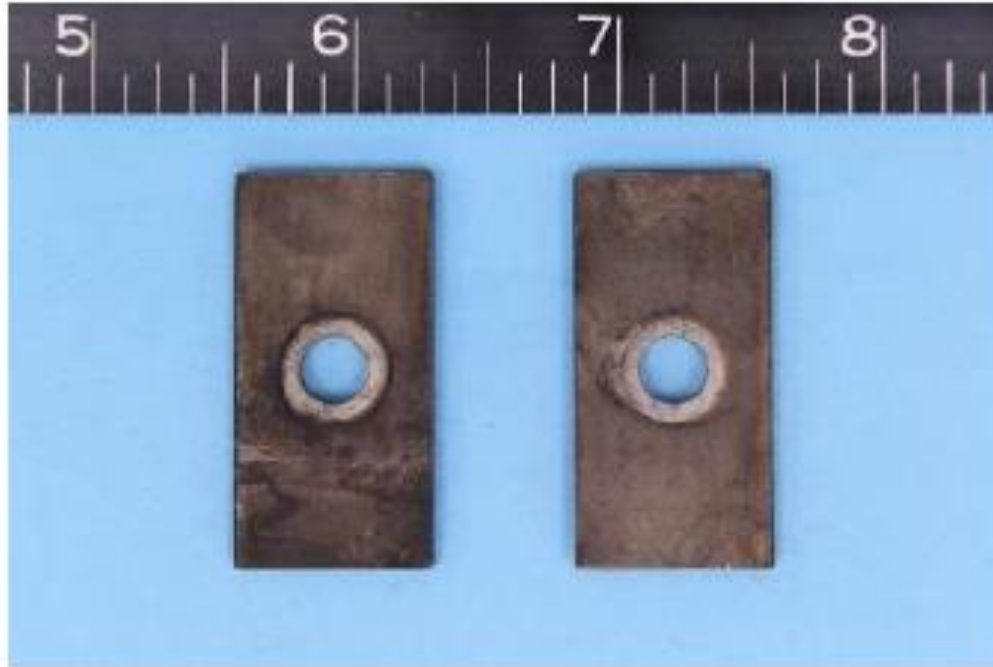


After Cleaning

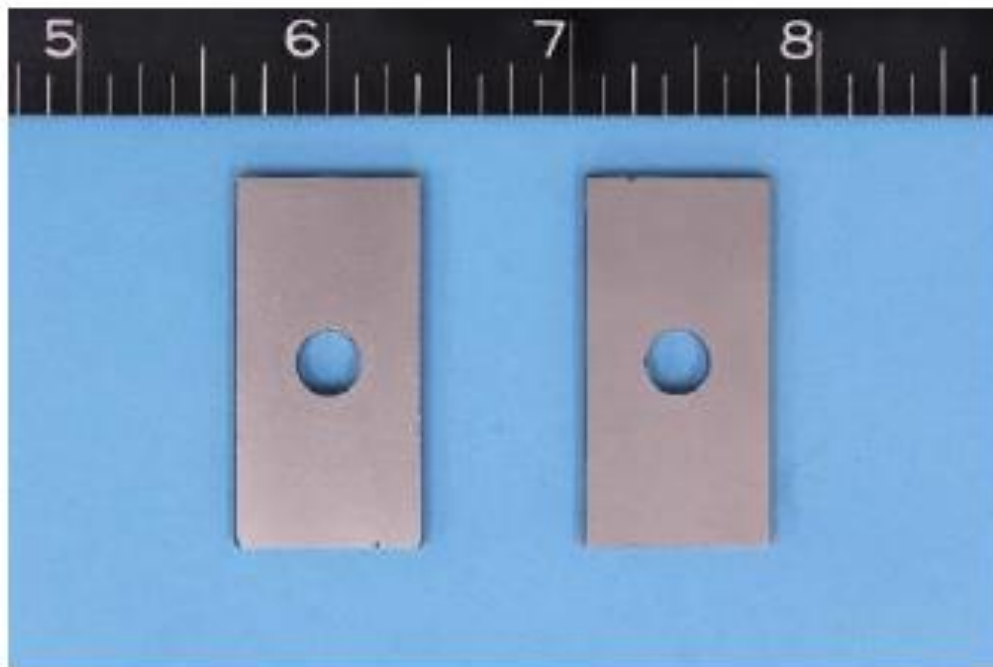
Figure D-1. Alloy 725 coupons, 48- week exposure, no pitting detected.

Final Report No. TS3333PH Rev2

Extended Duration Corrosion Testing of Five Ni-base
Corrosion Resistant Alloys at 15,000 psig and 350°F



Before Cleaning

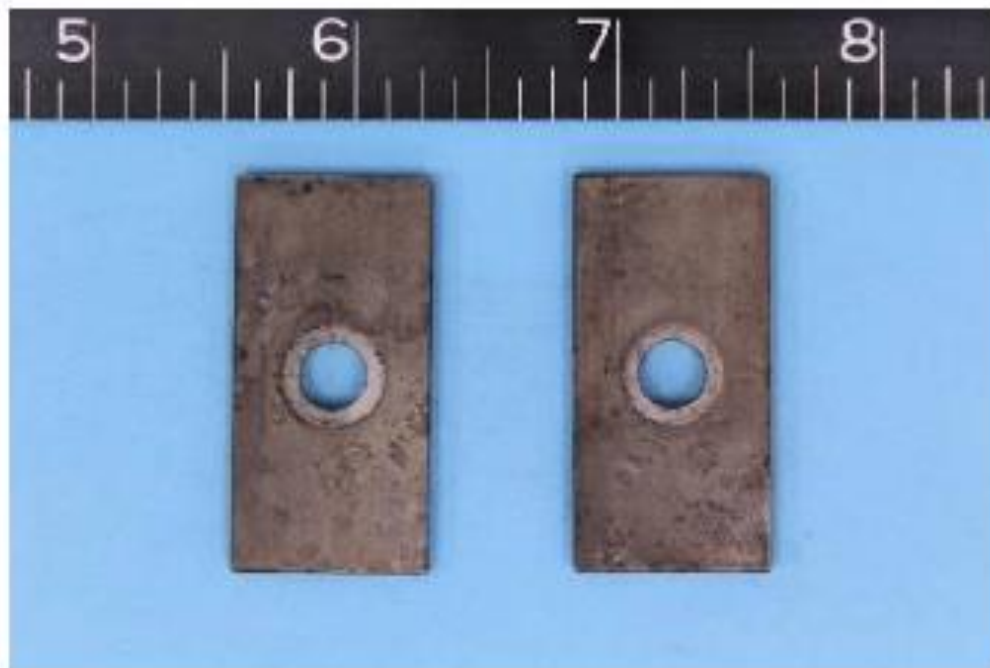


After Cleaning

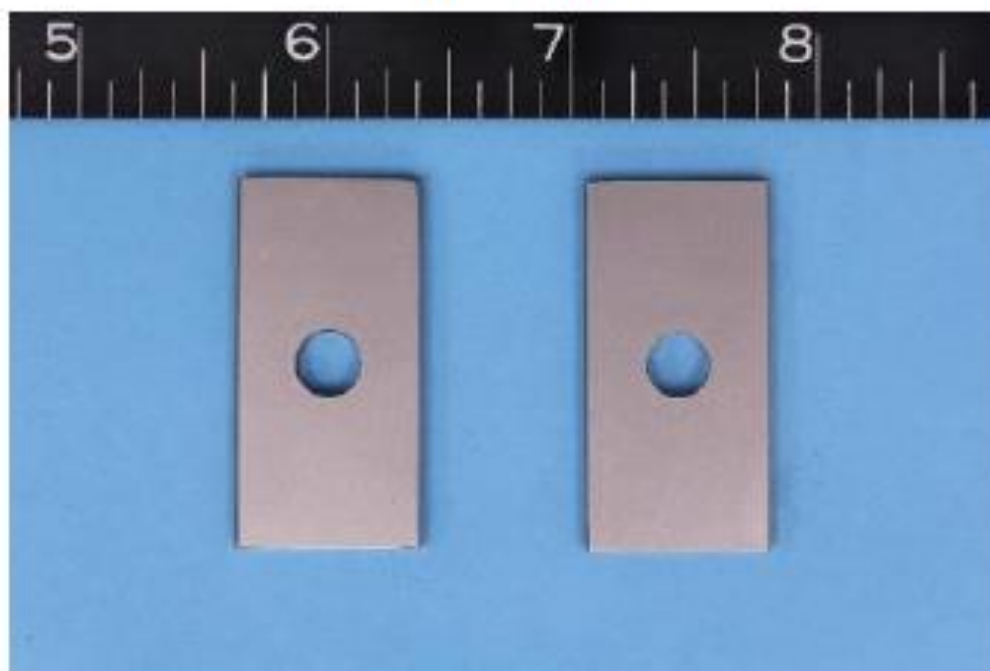
Figure D-2. Alloy 945X Coupons, 48-week exposure, no pitting detected.

Final Report No. TS3333PH Rev2

Extended Duration Corrosion Testing of Five Ni-base
Corrosion Resistant Alloys at 15,000 psig and 350°F



Before Cleaning

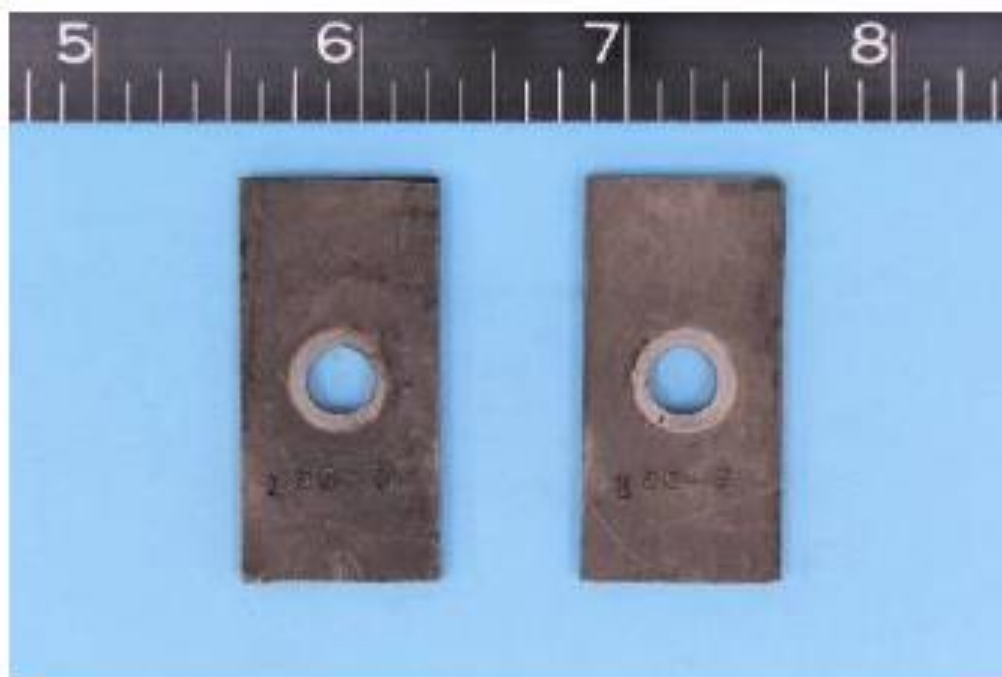


After Cleaning

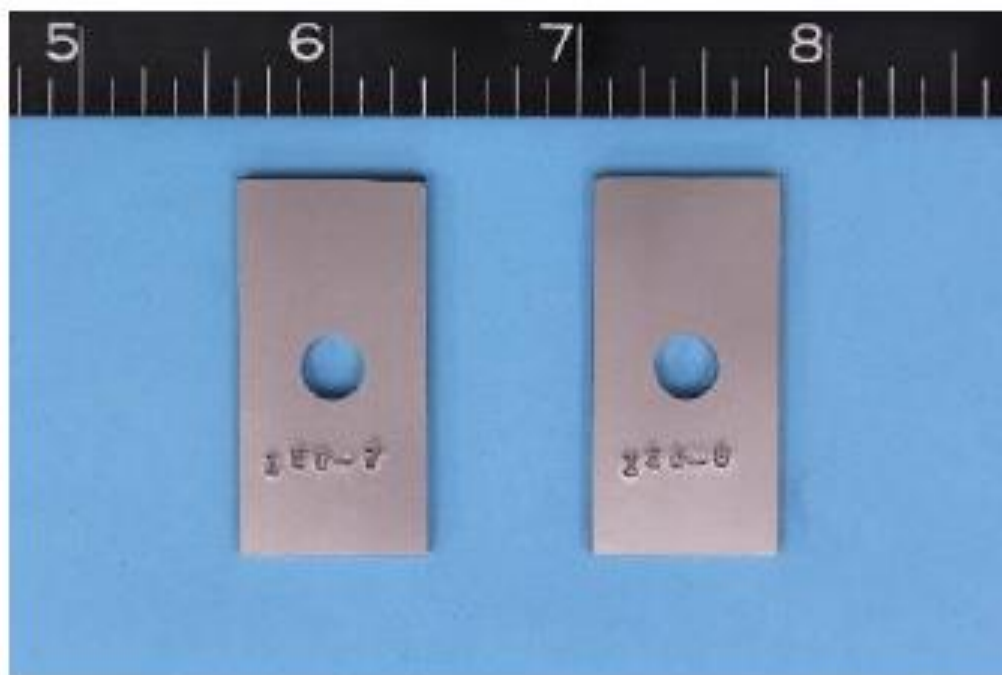
Figure D-3. Alloy 955 Coupons, 48-week exposure, no pitting detected.

Final Report No. TS3333PH Rev2

Extended Duration Corrosion Testing of Five Ni-base
Corrosion Resistant Alloys at 15,000 psig and 350°F



Before Cleaning

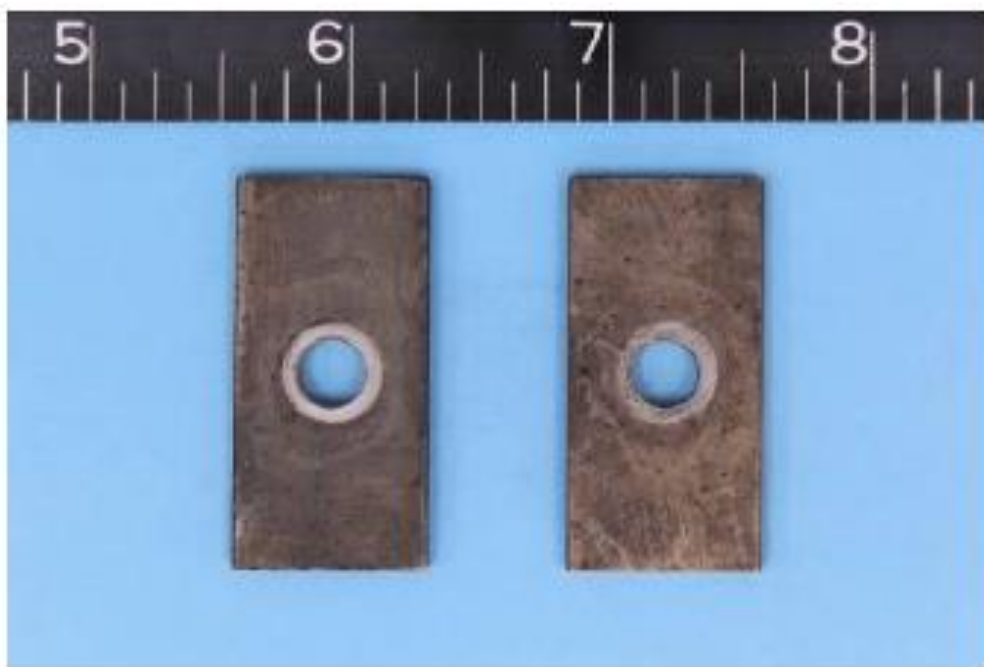


After Cleaning

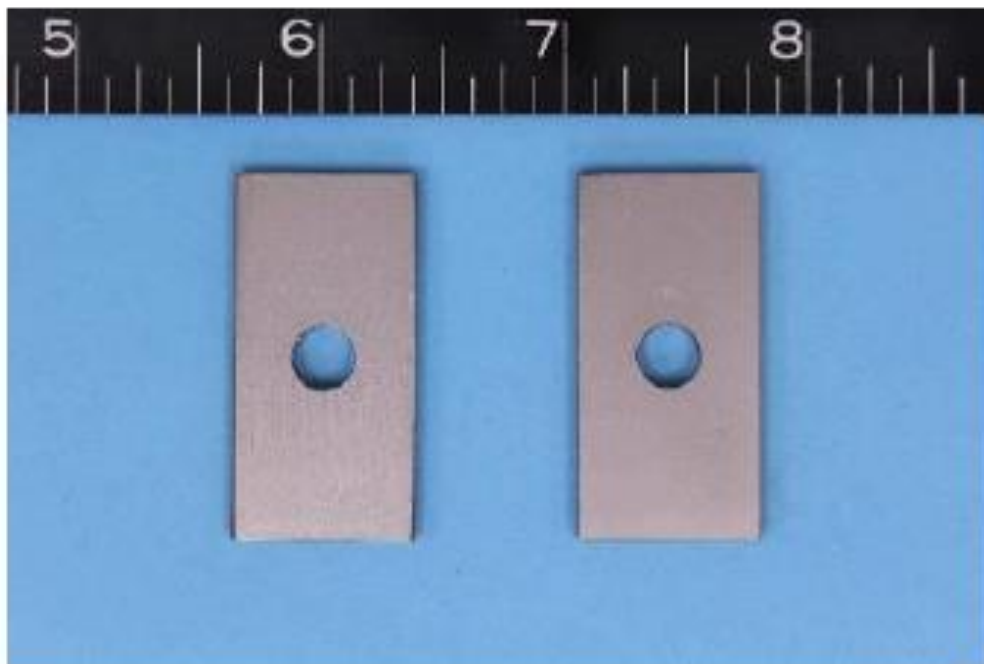
Figure D-4. Alloy C-22HS coupons, 48-week exposure, no pitting detected.

Final Report No. TS3333PH Rev2

Extended Duration Corrosion Testing of Five Ni-base
Corrosion Resistant Alloys at 15,000 psig and 350°F



Before Cleaning

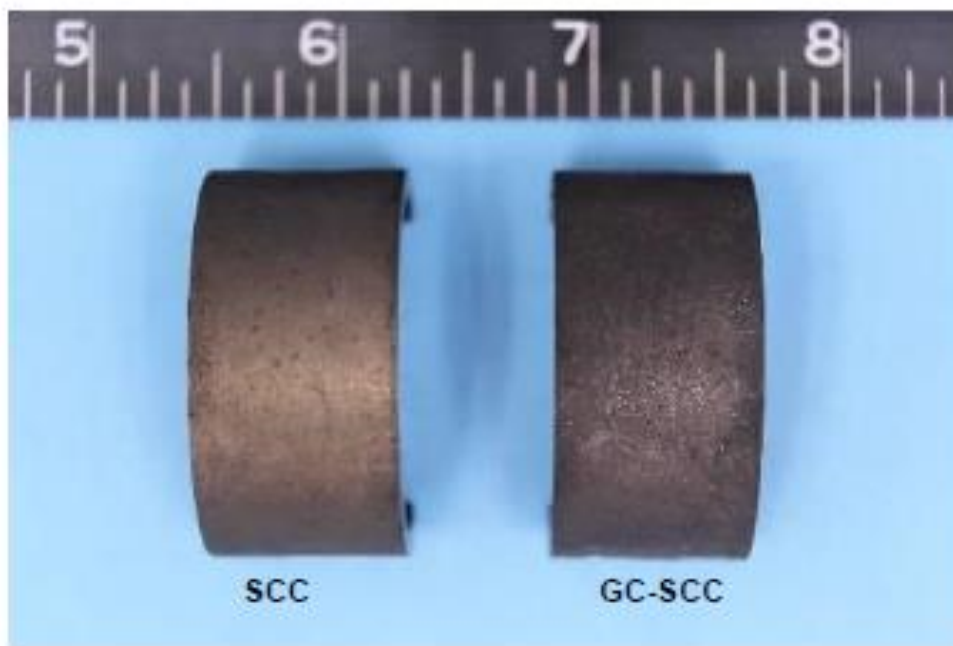


After Cleaning

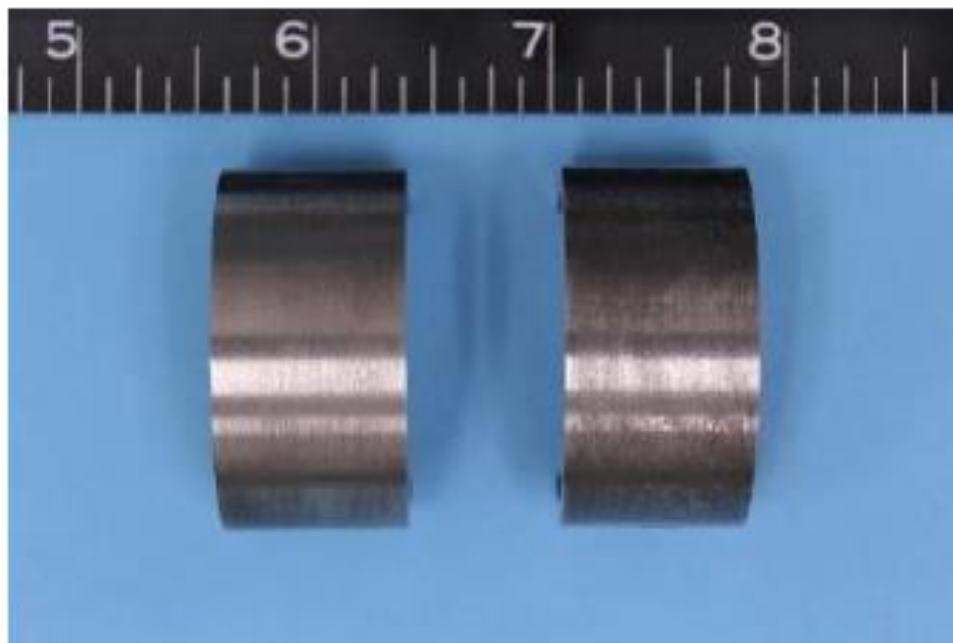
Figure D 5. Alloy 825 coupons, 48-week exposure, no pitting detected.

Final Report No. TS3333PH Rev2

Extended Duration Corrosion Testing of Five Ni-base
Corrosion Resistant Alloys at 15,000 psig and 350°F



Before Cleaning

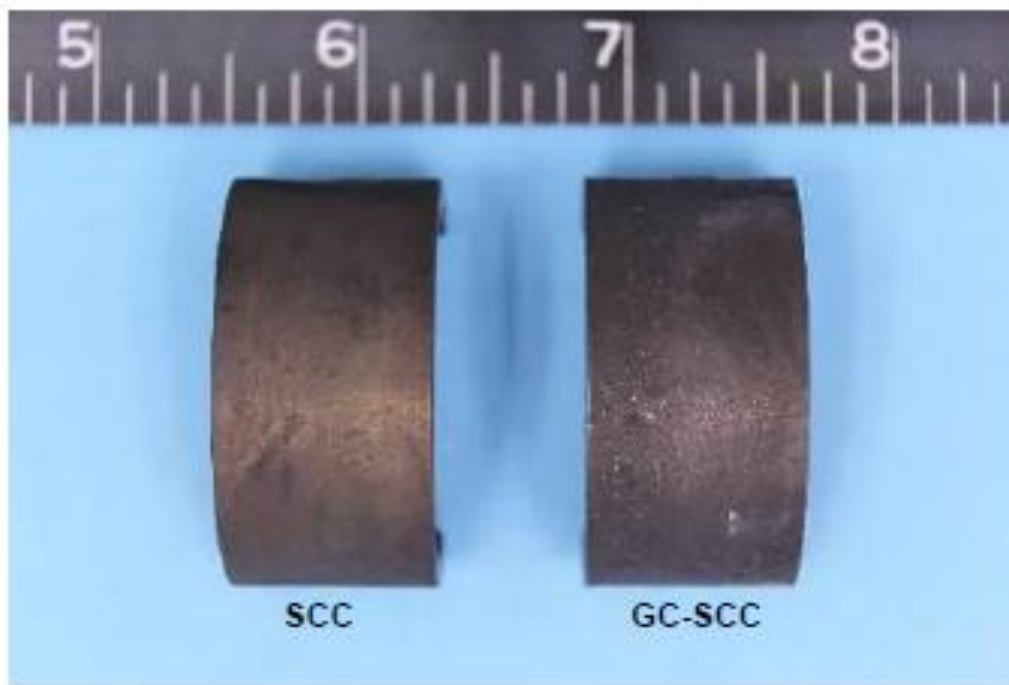


After Cleaning

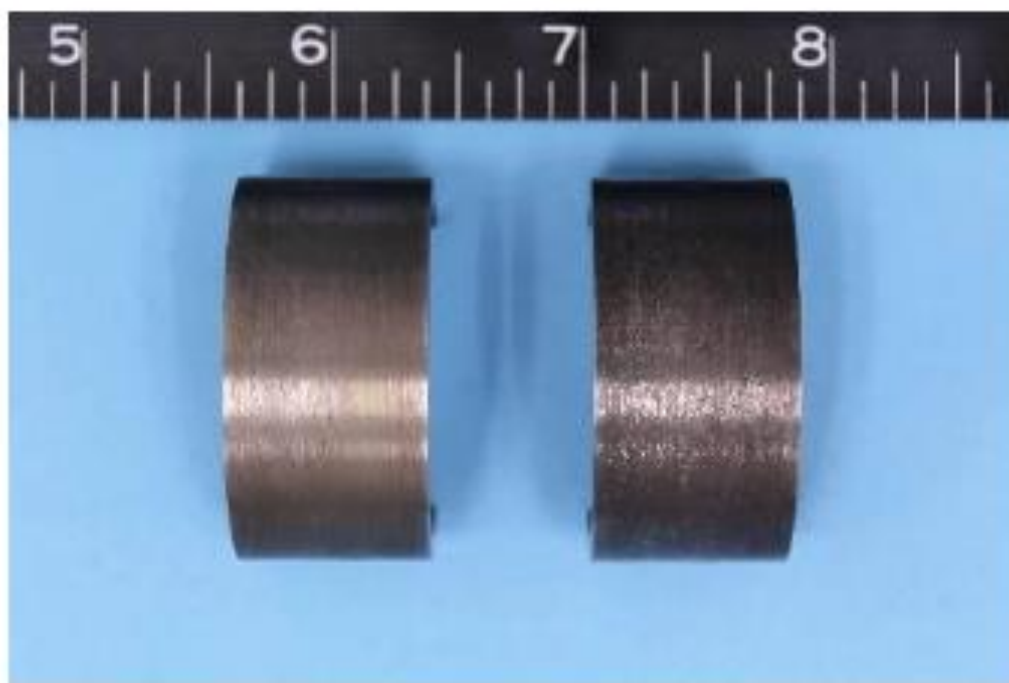
Figure D-6. Alloy 725 C-rings, 48-week exposure, no cracking detected.

Final Report No. TS3333PH Rev2

Extended Duration Corrosion Testing of Five Ni-base
Corrosion Resistant Alloys at 15,000 psig and 350°F



Before Cleaning

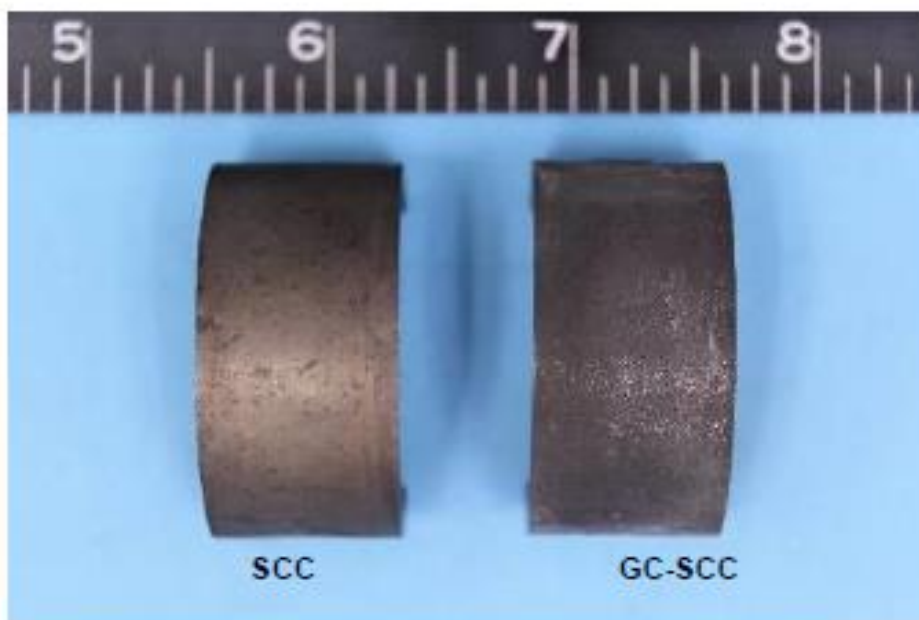


After Cleaning

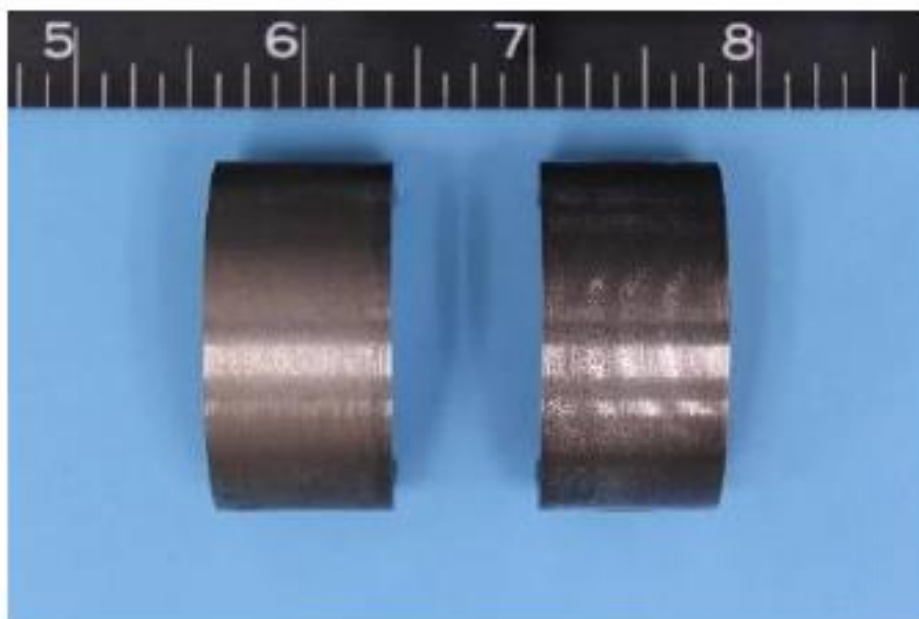
Figure D-7. Alloy 945X C-rings, 48-week exposure, no cracking detected.

Final Report No. TS3333PH Rev2

Extended Duration Corrosion Testing of Five Ni-base
Corrosion Resistant Alloys at 15,000 psig and 350°F



Before Cleaning



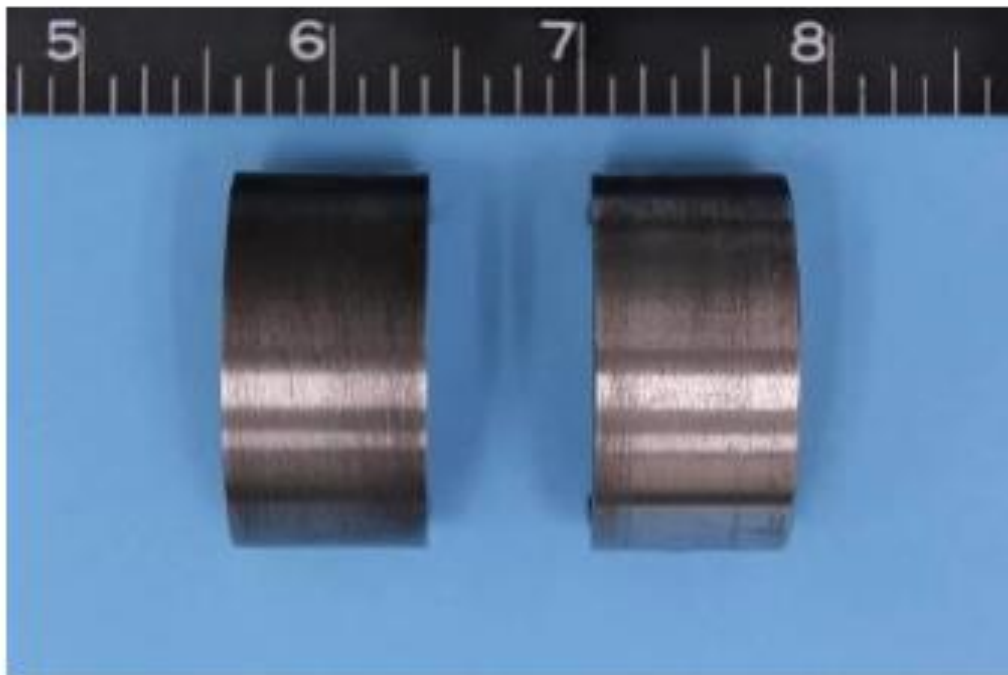
After Cleaning

Figure D-8. Alloy 955 C-rings, 48-week exposure, no cracking detected.

Final Report No. TS3333PH Rev2
Extended Duration Corrosion Testing of Five Ni-base
Corrosion Resistant Alloys at 15,000 psig and 350°F



Before Cleaning



After Cleaning

Figure D-9. Alloy C-22HS C-rings, 48-week exposure, no cracking detected.

This page intentionally left blank.

"THIS INFORMATION IS DISTRIBUTED SOLELY FOR THE PURPOSE OF PRE-DISSEMINATION PEER REVIEW UNDER APPLICABLE INFORMATION QUALITY GUIDELINES. IT HAS NOT BEEN FORMALLY DISSEMINATED BY THE BSEE. IT DOES NOT REPRESENT AND SHOULD NOT BE CONSTRUED TO REPRESENT ANY AGENCY DETERMINATION OR POLICY."



Energy Systems Division

Argonne National Laboratory
9700 South Cass Avenue, Bldg. 362
Argonne, IL 60439

www.anl.gov



Argonne National Laboratory is a U.S. Department of Energy
laboratory managed by UChicago Argonne, LLC